NASA Contractor Report 195358

STOVL Control Integration Program

C. Weiss
Pratt & Whitney
West Palm Beach, Florida

P. McDowell
McDonnell Douglas Aerospace East
St. Louis, Missouri

and

S. Watts
Pratt & Whitney
West Palm Beach, Florida

July 1994

Prepared for
Lewis Research Center
Under Contract NAS3–25194

National Aeronautics and
Space Administration

TABLE OF CONTENTS

TABLE OF CONTENTS (Con't)

LIST OF FIGURES

LIST OF FIGURES (Con't)

LIST OF FIGURES (Con't)

LIST OF FIGURES (Con't)

LIST OF FIGURES (Con't)

LIST OF FIGURES (Con't)

LIST OF FIGURES (Conc'ld)

LIST OF TABLES

Acknowledgments:

Many individuals contributed to the results documented in this report. While it is not practical to recognize them all, the authors wish to single out a few whose direct efforts or technical guidance supported the success of the program.

Mr. W. R. Lambert preceded P. McDowell as the principal investigator of the SCIP efforts at McDonnell Douglas and contributed to the planning as well as the early technical progress of the program.

Dr. J. A. Franklin of NASA Ames provided both technical and programmatic guidance throughout the 5 1/2 years duration of the program.

Technical guidance for this NASA Lewis funded program was provided by three of the Research Center's engineers: Mr. J. Milhaloew was the initial technical contract monitor and after his retirement he was succeeded by Mr. P. Ouzts and then Dr. S. Garg.

STOVL CONTROL INTEGRATION PROGRAM
(SCIP)
FINAL REPORT

1. INTRODUCTION & SUMMARY

1.1. Scope of Report

This report documents all activities completed under task orders 1, 7 and 10 of contract NAS3-25194. This is a NASA Lewis contract awarded to Pratt & Whitney titled "Supersonic STOVL Definition, Modification, Test". Task order No. 1 is titled "Planning, Modeling and Preliminary Control System Design for a Vectored Thrust Concept STOVL Aircraft". Task order No. 7 is titled "Control Logic and Simulation Development and Simulation Validation for a Vectored Thrust Concept STOVL Aircraft." Task Order No. 10 is titled "Control Logic and Simulation Delivery and Piloted Simulation Evaluation Support for a STOVL Aircraft". Together, these three task orders are more commonly referred to as the "STOVL Control Integration Program" or "SCIP" and when it is desirable to distinguish among the task orders, they are referred to as SCIP1, SCIP2, and SCIP3. This is therefore the STOVL Control Integration Program final report and documents the activities completed between the start of SCIP1 in February 1988 and the conclusion of SCIP3 in the summer of 1993.

1.2. Problem Statement

Flight and propulsion control integration on most aircraft is a pilot function. On those aircraft which do employ an Integrated Flight/Propulsion Control (IFPC), it is usually a performance enhancement feature that is not critical to vehicle operation. For many advanced STOVL concepts though, the IFPC will be critical to the success of the aircraft as they would be unflyable otherwise. They will rely on digital electronics and advanced algorithms to a much greater extent than in any existing aircraft to make for an acceptable pilot work load through the various mission segments and under widely differing operating conditions.

The objective of SCIP is to develop IFPC technologies and processes for advanced STOVL applications. This was achieved by designing an IFPC for a representative STOVL aircraft, developing the integrated designs and processes along the way. To validate the IFPC, a piloted simulation at NASA Ames occurred as the culmination of the program. To make this possible SCIP developed and delivered aircraft and engine models in addition to the IFPC.

1.3. Program Background

Advanced supersonic STOVL concepts couple the operation of the propulsion system and the airframe in ways too complex for the pilot to be the sole systems integrator. Integration of the flight and propulsion controls is therefore a requirement for these concepts, and the success of these concepts will greatly depend how successful this integration is carried out. Recognizing this challenge, NASA initiated SCIP to investigate IFPC design for an advanced vectored thrust STOVL aircraft.

Pratt & Whitney was awarded this contract with McDonnell Douglas as a subcontractor. This reversal of hierarchy in the normal airframe manufacturer / engine manufacturer relationship was intentional. NASA recognized the criticality of the propulsion control in hover and transition flight modes and that the best way to make the engine manufacturers understand the problem was to make them responsible for it in a technology program.

SCIP was awarded as three separate task orders on a single contract. A funding hiatus occurred at the end of SCIP1 and when work was resumed at the beginning of SCIP2 it was decided to build upon the model and control law development of the PROLIFIC program instead of SCIP1 because at that time it was much further advanced.

PROLIFIC is an Air Force program, that was originally planned as a companion, but independent, program examining IFPC technology for advanced STOVL aircraft. Unlike SCIP, PROLIFIC was planned to test a STOVL IFPC in electronic control hardware rather than on a host computer and the manned simulation was planned for a McDonnell Douglas simulator instead of the NASA Ames simulator. Since PROLIFIC started a year later than SCIP1, it modelled a more up-to-date version of both the McDonnell Douglas Mixed Flow Vectored Thrust (MFVT) aircraft and the Pratt & Whitney engine configured for this concept. When SCIP2 started up, the Air Force had redirected PROLIFIC towards other IFPC applications.

In SCIP1 an initial simulation model was developed and delivered to NASA. The PROLIFIC program updated the aircraft model from SCIP1 and added flight control laws for conventional wingborne flight. It also updated the propulsion model for a cycle tailored to the STOVL aircraft concept and generated the propulsion control laws. In SCIP2 and SCIP3 the aircraft model from PROLIFIC was updated to include STOVL jet effects and STOVL hover and transition control laws. Also the propulsion model was simplified and tailored for realtime operation at NASA Ames.

In hindsight, program timing was rather serendipitious in that the original delay in start of the PROLIFIC program let PROLIFIC benefit from the work completed under SCIP1, while the delay in starting SCIP2 let it benefit from the work completed under PROLIFIC.

References to PROLIFIC in this report refer to STOVL efforts conducted under the Air Force program before its redirection to other IFPC applications and upon which much of the later SCIP efforts were based.

Over the five and one-half years SCIP progressed, many changes have taken place. There have been changes in personnel working the program, changes in the NASA technical contract monitor, changes in the preferred STOVL concepts, changes in propulsion and propulsion control technology, and changes in the airframe and engine manufacturer teams that may build the next production STOVL aircraft. Despite all these changes, one is surprised at how well SCIP met the intentions of those who started on the program over half a decade ago. The basic purpose of SCIP was to advance the state-of-the-art in STOVL IFPC design so as to reduce risk in a flight demonstrator program, and in this, it definitely succeeded. The control design approach proposed at the beginning of the program and which then appeared to us at Pratt & Whitney as such a great challenge, is now our basic approach to all complex IFPC problems and would be the foundation to any succeeding flight test program.

1.4. Principal Findings

The technical accomplishments of SCIP are detailed fully in this report, but, it is also important to highlight the top lessons learned with respect to IFPC development.

First, much of the success of SCIP came from the very free and open communication between the flight control designers and the propulsion control designers. Through this communication came an understanding of the other designers' challenges and concerns, and this understanding was the first step in the path to resolving those issues. Most of our design hacks were traced back to poor communication and not to any individual's mistake in analysis. Probably the best approach to an integrated design is to locate all the designers in the same room. This is usually not possible and must be compensated for by making communication as easy as possible.

Second, the Generalized Actuator Model (GAM) employed in SCIP is a very useful tool in developing an IFPC. The GAM is a much simplified engine model, but with all the I/O of the full model, given to the airframer early in the development of the IFPC to simulate predicted engine and propulsion control performance. It let the flight control designer know upfront what performance could be expected from the propulsion system so that he could begin his design. It also acted as the performance specification for the propulsion control designer. This proved more useful than a typical performance specification and let many issues be resolved early in the program when the cost of making changes is small.

Lastly, piloted simulations were again demonstrated as a necessary tool in IFPC development. Despite all the technical preparations there were many surprises in how the different control modes acted that would not have been uncovered without either a simulator or the prohibitive cost and expense of a flight demonstrator. A high fidelity piloted simulation is critical to developing a successful ASTOVL IFPC.

1.5. Report Organization

This report is divided into four sections. It opens with a short introduction section which is followed by a section which describes the activities performed in SCIP1. This second section is further divided into subsections defining the configuration, the control modes, the control requirements and the control system architecture. The third section describes the activities performed in SCIP2 and SCIP3. This section is further divided into subsections defining the airframe and ground effects model, the propulsion model and the IFPC logic design. Also included are subsections detailing the transition envelope sensitivity and control power analysis and another subsection presenting the simulation test results. A short summary and conclusion section completes the report.

2. SCIP1 - PLANNING, REQUIREMENTS, AND DEFINITIONS

2.1. Baseline Configuration Definition

The aircraft configuration used in the SCIP Program evolved from the MDA ASTOVL Mixed Flow Vector Thrust (MFVT, Figure 1) aircraft developed in the US/UK ASTOVL Program (Reference 1). In SCIP1, this aircraft was resized to fit some other design missions, and used as the study aircraft for the rest of that phase. Also in SCIP1, a trade study was performed to select between several options on the type of propulsive control effectors. Then, in the USAF PROLIFIC Program (Reference 2), another version of the MFVT aircraft was redesigned and redrawn to fit a USAF air superiority mission (it was one of the SCIP1 missions), and used as the study aircraft for that program. In PROLIFIC, a six degree of freedom simulation model of that aircraft was developed by modifying the simulation model that was developed in SCIP1. Since this model was the most mature existing at the time the remaining phases of SCIP began, since the aircraft it represented was very close to the original SCIP aircraft, and since the aircraft fit one of the SCIP design missions, the new variant was used as the study aircraft for the remainder of the SCIP Program.

2.1.1. SCIP1 Initial Definition

The process by which a baseline STOVL configuration was initially chosen for SCIP is shown in Figure 2. The MFVT concept aircraft (Figure 1) developed in the US/UK program (Reference 1) was chosen as the study aircraft for this program. The configuration was initially sized to the US/UK ASTOVL air superiority mission, (Reference 1), using the SE550 PW5000 derivative engine (Figure 3), and designated by MDA as the MFVT Model 4629E. As shown in Figure 2, an analysis was done to resize the aircraft's wing area and fuel capacity to fit the requirements of three other missions that were considered in this study: a USMC deck launched intercept mission (Figure 4), a USMC close air support mission (Figure 5), and a USAF air superiority mission (Figure 6). The resulting configuration used for study in SCIP1 was a variant of the MFVT Model 4629 with slightly more fuel and a slightly larger TOGW than the US/UK variant. The SCIP1 study aircraft is referred to in this report as the ASTOVL MFVT Model 4629.

Six variants of the 4629 were studied in SCIP1, representing different control configurations for the propulsive control effectors, as shown in Figure 7. Variant I (Figure 8) is the baseline 4629 configuration with main lift nozzle splay vectoring and compressor bleed RCS. Variant II (Figure 9) is the same as Variant I, except that mixed flow is used to drive the RCS instead of compressor flow. Variant III, (Figure 10), eliminates th RCS system, and adds lateral vectoring to the ventral nozzle. All Variants I, II, and III employ main lift nozzle variable splay vectoring. Variants IV, V, and VI, are similar to I, II, and III, respectively, except that the variable splay on the main lift nozzles is replaced with a pitch vectoring capability (Figure 11).

Analyses were performed to determine the variant to be used in the remaining Phases of SCIP. These analyses (discussed in Section 2.3.1) resulted in Variant VI being chosen as the preferred control configuration, although the compressor bleed RCS system was retained on the aircraft so that the technical issues between RCS versus nozzle vectoring could be studied in more detail in the rest of the program.

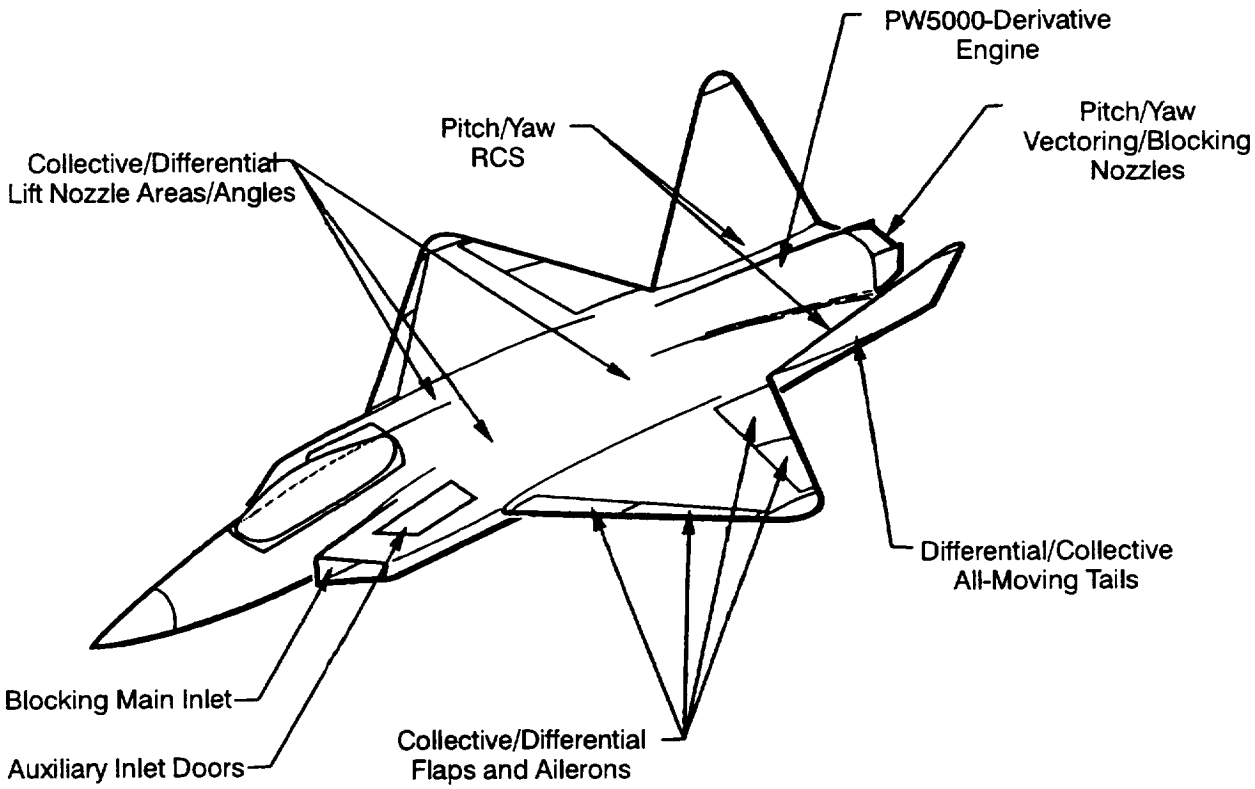

Figure 1. Mixed Flow Vectored Thrust Model 4629E

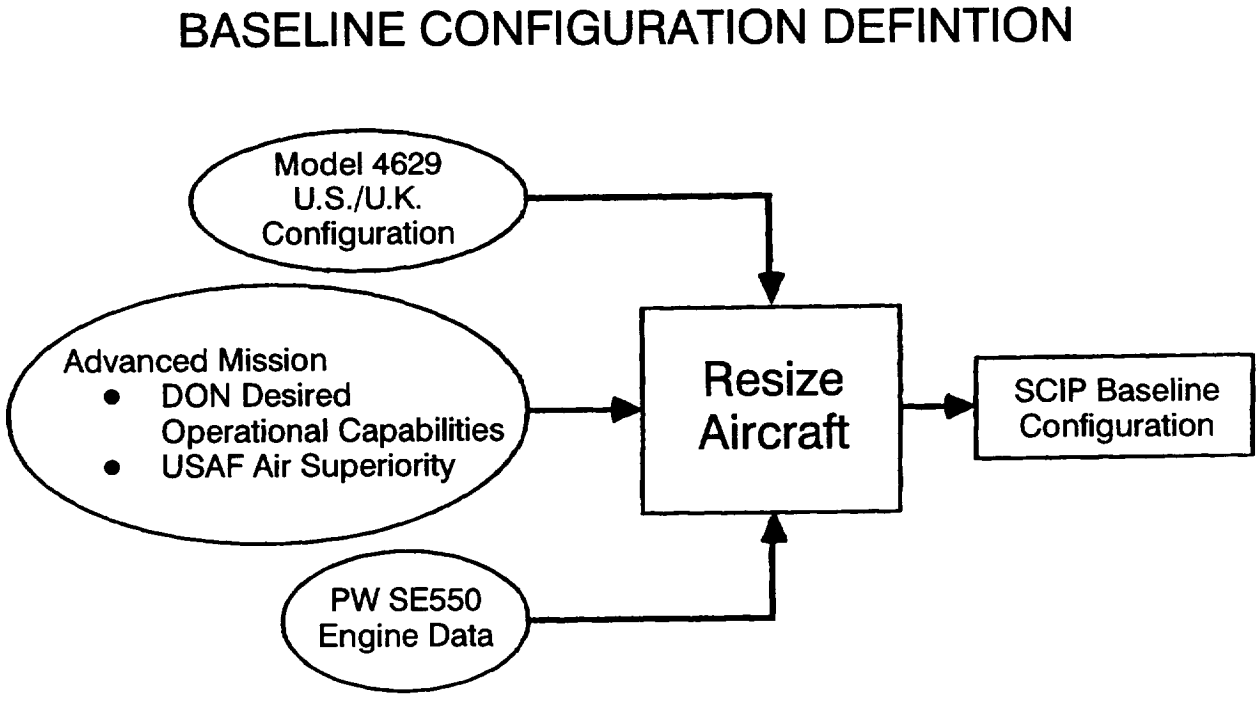

Figure 2. Initial SCIP Configuration Definition

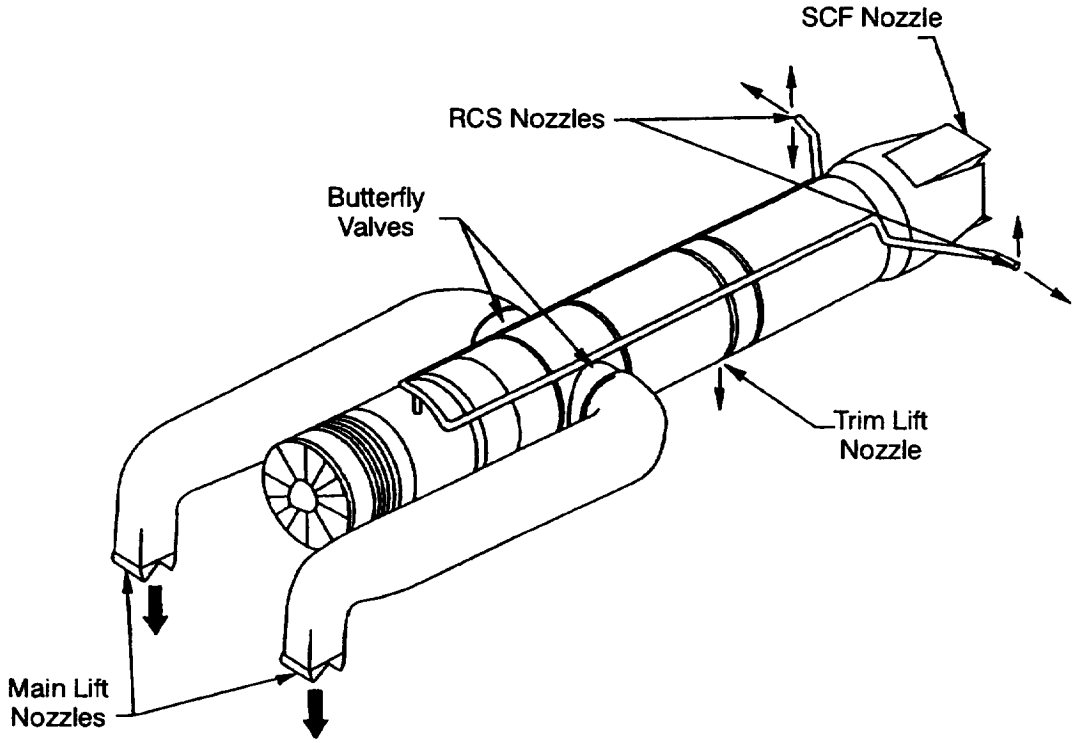

Figure 3. Mixed Flow Vectored Thrust Propulsion Concept

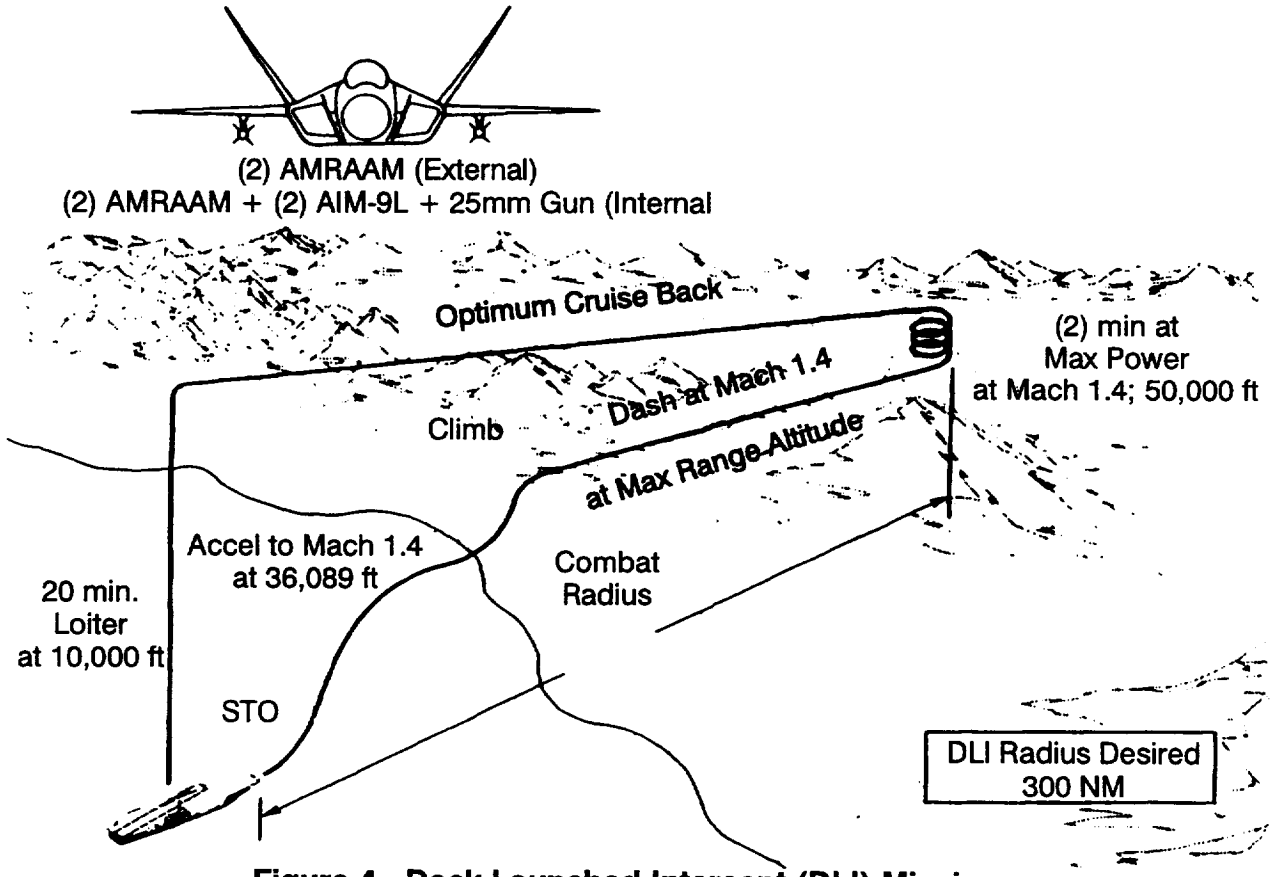

Figure 4. Deck Launched Intercept (DLI) Mission

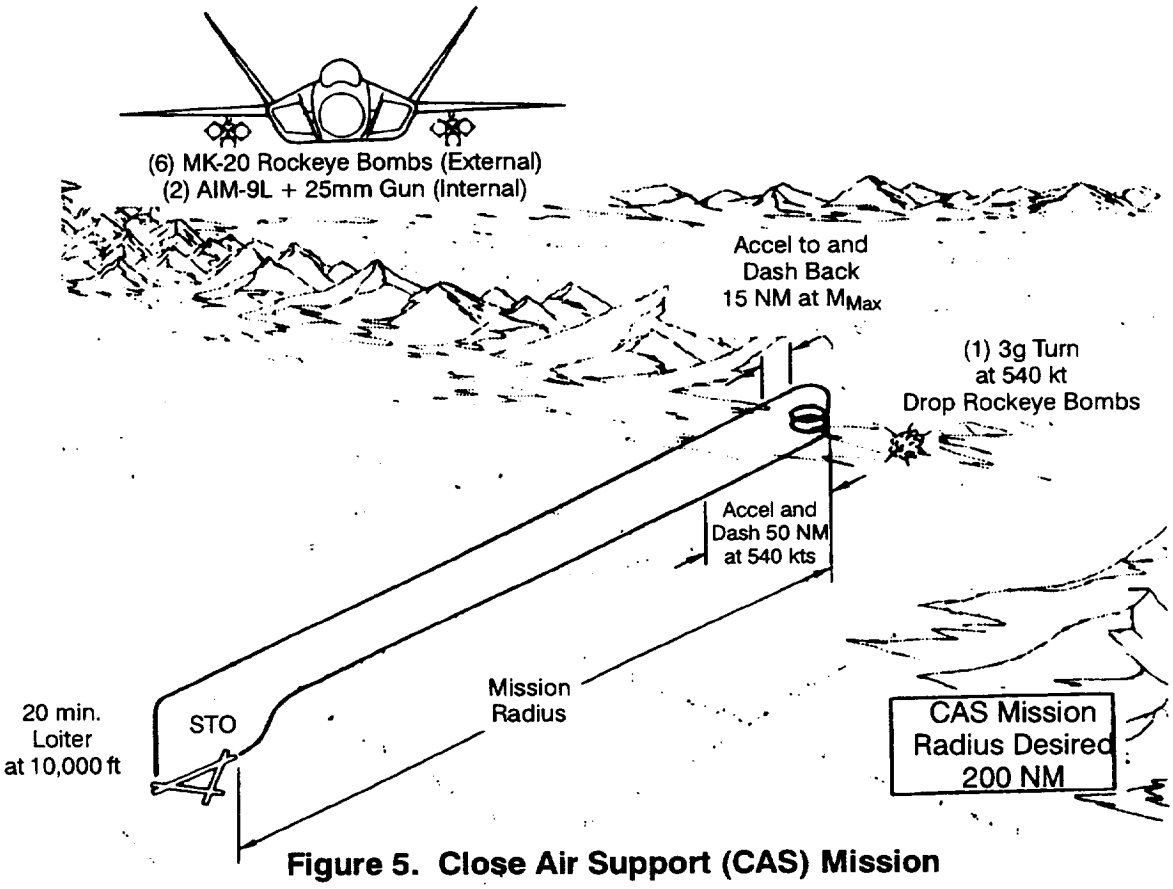

Figure 5. Close Air Support (CAS) Mission

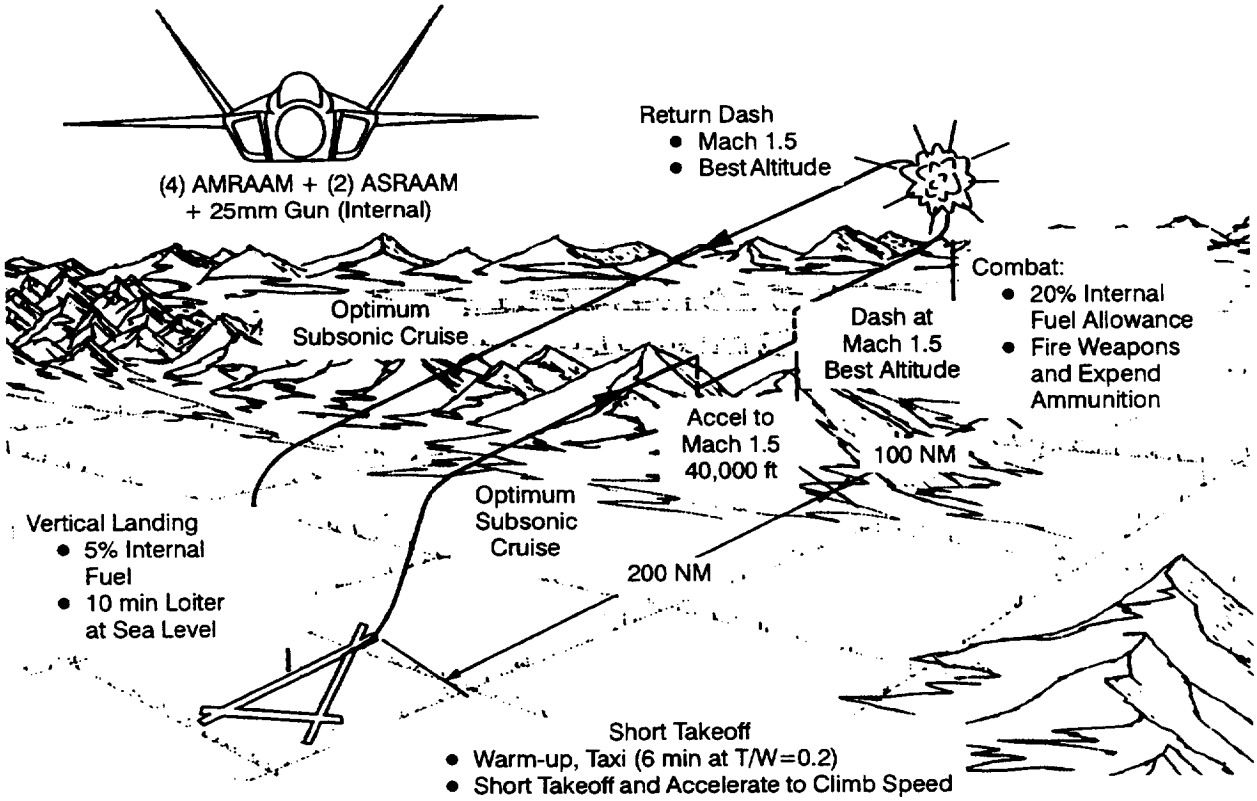

Figure 6. USAF Air Superiority Mission

MAIN LIFT NOZZLE OPTIONS → / RCS OPTIONS ↓	VARIABLE SPLAY AND FIXED VECTOR ANGLE FORWARD NOZZLES	FIXED SPRAY AND LIMITED VECTORING FORWARD NOZZLES
COMPRESSOR BLEED RCS	Variant I (Baseline)	Variant IV
MIXED FLOW RCS	Variant II	Variant V
YAW NOZZLE - NO RCS	Variant III	Variant VI

Figure 7. Six Variants of the Mixed Flow Vectored Thrust Concept

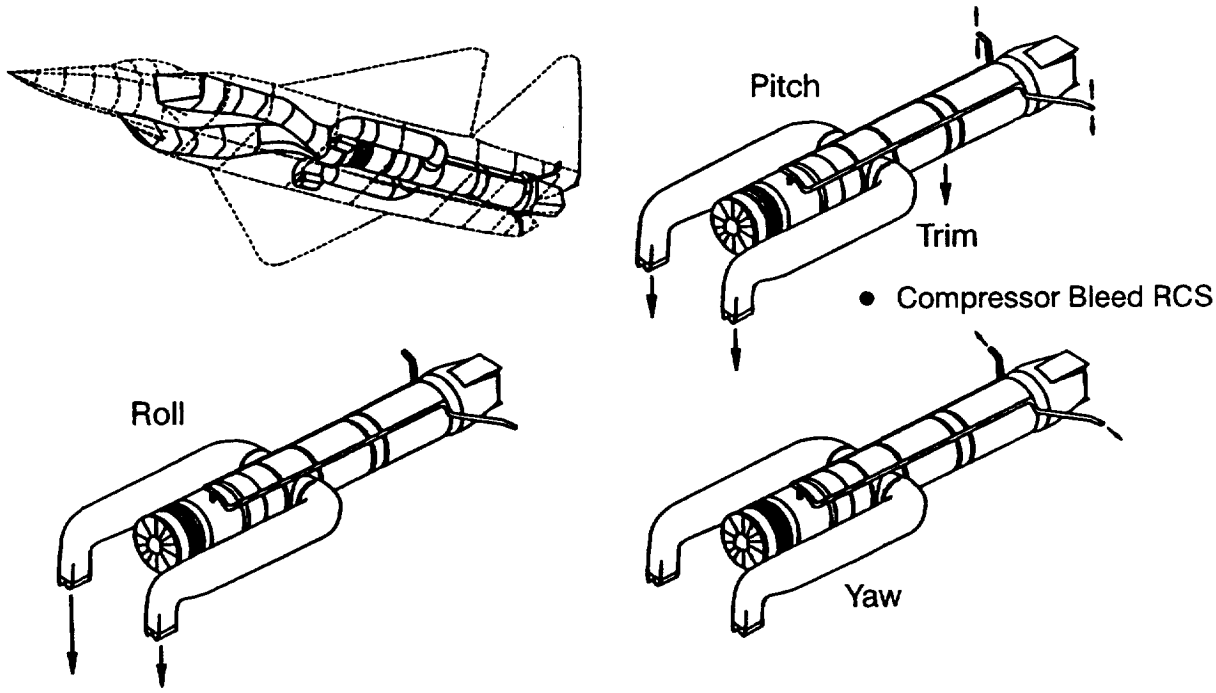

Figure 8. MFVT Variant I Control Effectors

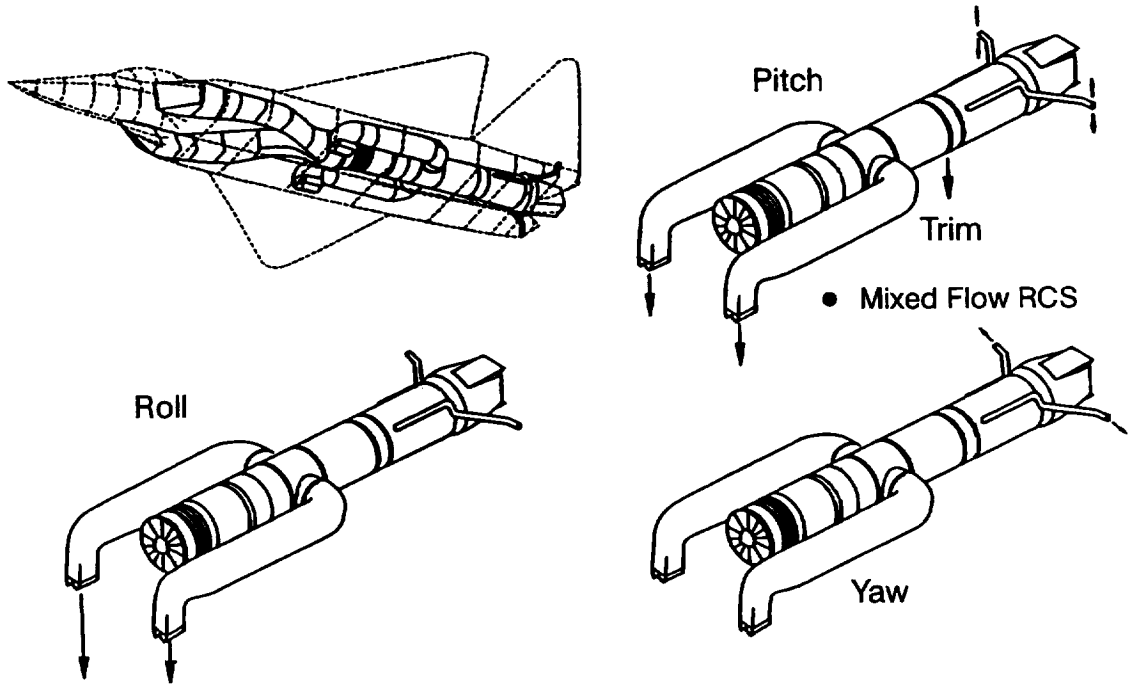

Figure 9. MFVT Variant II Control Effectors

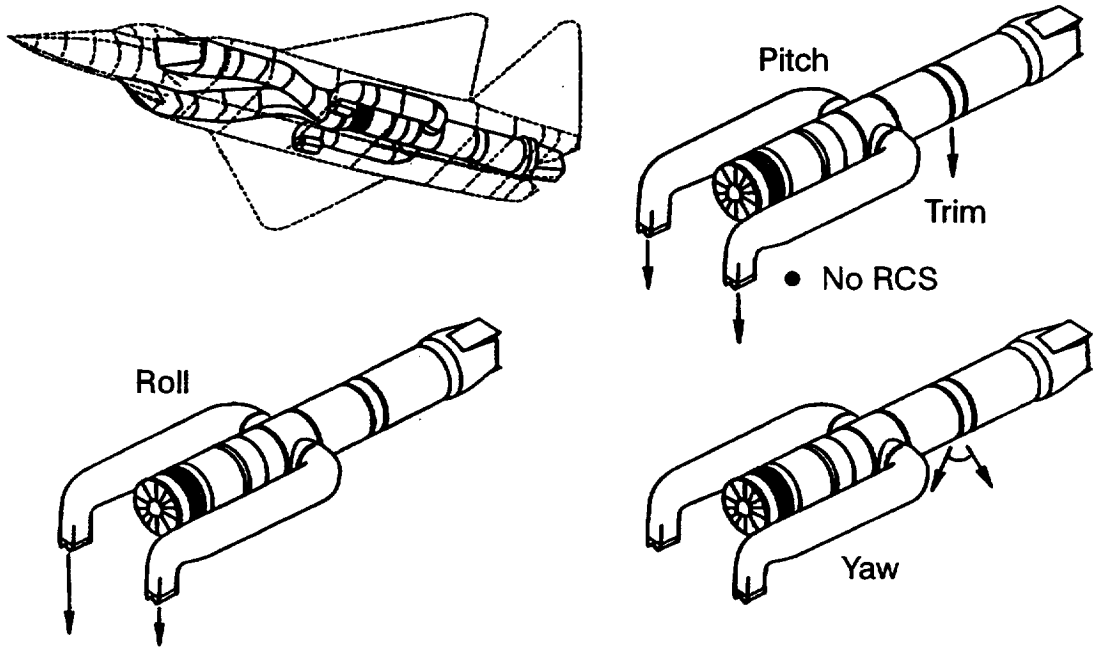

Figure 10. MFVT Variant III Control Effectors

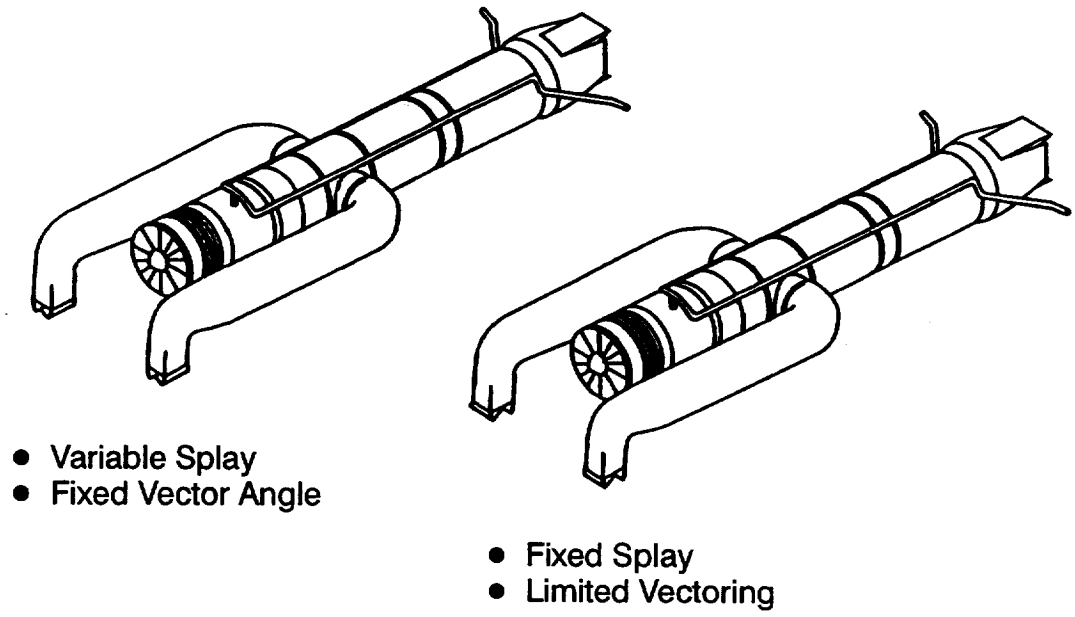

Figure 11. Splay Vectoring versus Pitch Vectoring

2.1.2. PROLIFIC Configuration Definition

The 4629 Variant VI was used as a starting point in the development of the study aircraft for PROLIFIC. The US/UK ASTOVL Model 4629E was redesigned to fit the USAF Air Superiority mission as part of the USAF ATEGG study, and designated by MDA as the ASTOVL MFVT Model 4636. An overview of the derivation of the 4636 is shown in Figure 12.

The initial step to resizing the Model 4629 was to incorporate the Air Force requirements into the Computerized Aircraft Design Assessment (CADE) program. The CADE program resized the fuel to meet the 300 NM radius requirements, and resized the wing area and engine thrust to meet the maneuvering point performance. The required maneuvering point performance is 90 percent of the 1984 Tactical Air Command Statement Of Need (TAC SON) point performance.

The CADE representation of the aircraft included weight and performance increments for Low Observable (LO) requirements. Although the Model 4629 development had no LO requirements, the basic aircraft was conceived with fundamental aircraft shaping and internal weapons carriage that would be feasible for add on LO provisions. In parallel with the NASA Ames US/UK ASTOVL activity, an Air Force Addendum contract was awarded to MCAIR for the design and evaluation of an LO variant of the Model 4629 MFVT concept. That study provides a direct breakout of weight and performance increments that, when applied to the Model 4629 aircraft, produces the same aircraft size and performance as the LO variant. These increments were added to the CADE representation of the Model 4629 concept. The addition of these increments allows for the consideration of LO requirements in the MFVT aircraft without requiring additional security restrictions on the aircraft design.

The next step in establishing the MFVT aircraft was to redraw the configuration. The performance of the redrawn configuration was then evaluated. The preliminary sized aircraft achieved a Take Off Gross Weight (TOGW) of less than 35,000 lb. while meeting the Air Force requirements.

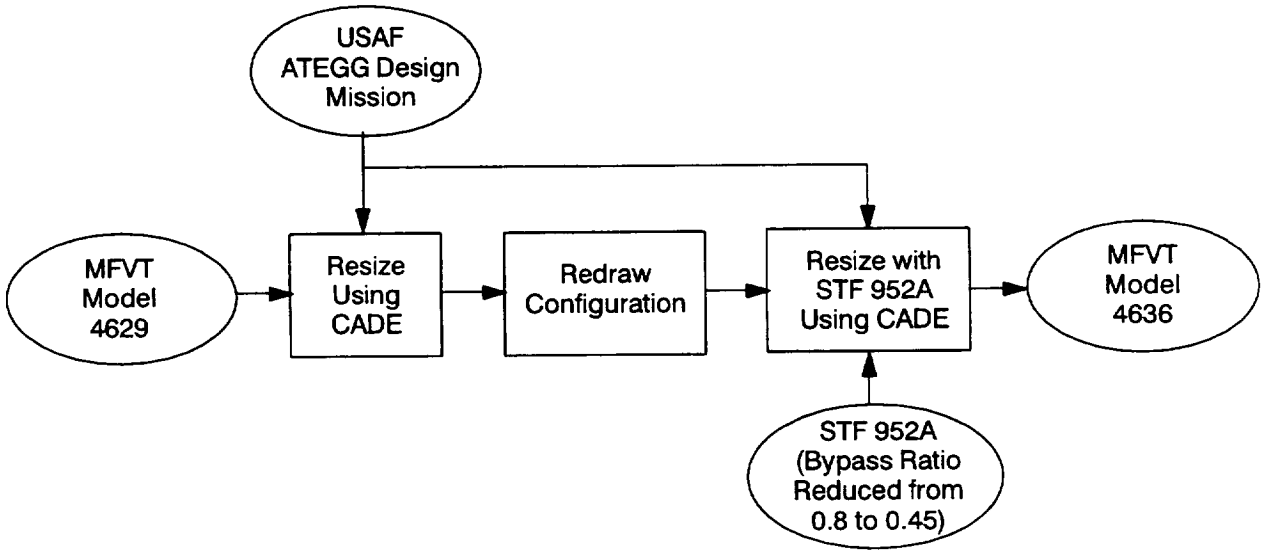

Figure 12. Mixed Flow Vectored Thrust Model 4636 Development

The final step involved selection of the engine. An engine cycle optimization was performed by Pratt & Whitney which reduced the bypass ratio of the STF 868A (the engine in the original aircraft) from 0.8 to 0.45, and increased the dry power thrust relative to maximum power. The new engine was designated STF 952A. This engine was incorporated into the CADE representation of the aircraft and resized to the Air Force mission. This final configuration was designated Model 4636 and is lighter than the Model 4629.

As part of the PROLIFIC program, the SCIP1 Variant VI propulsion control effectors were also included with this configuration. The MFVT 4636 with the Variant VI control effectors was chosen as the study aircraft for the PROLIFIC and for SCIP2 and SCIP3. This study aircraft is referred to as the ASTOVL MFVT Model 4636.

2.1.3. Configuration Description

The resulting MFVT Model 4636, shown in Figure 13, is a supersonic, single seat, blended body configuration. The vehicle has a mid-mounted wing, canted tails, and internal weapons bays for low drag carriage of four AMRAAMS and two ASRAAMS. A 20 MM gun with 500 rounds of ammunition is also carried internally. Hard points are provided in the wing for external store stations which allow carriage of additional air-to-air weapons, air-to-ground weapons, and external fuel tanks.

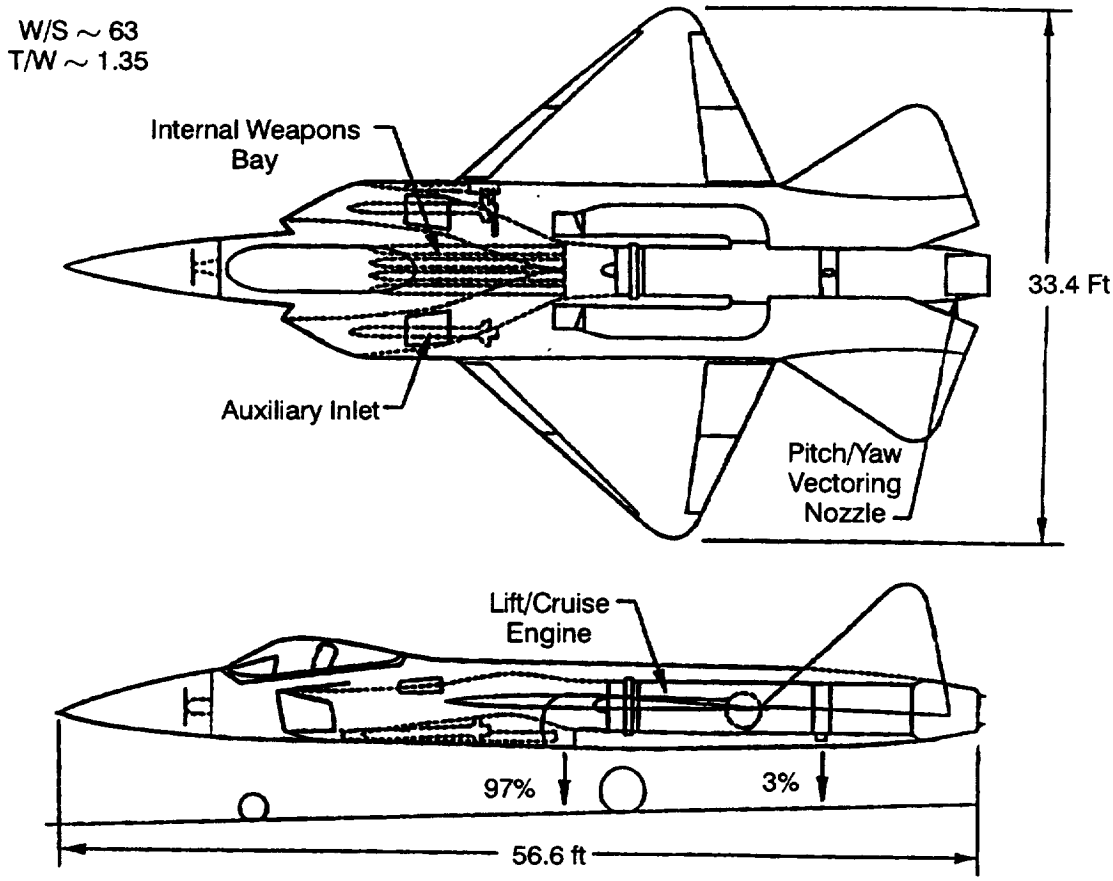

Figure 13. Model 4636 Mixed Flow Vectored Thrust Concept

Fuel tanks are located in the airframe to minimize fuel system vulnerability and to maintain a desired narrow center of gravity travel for inflight and STOVL operations. None of the tanks are located over or around hot sections of the cruise engine.

The cruise engine inlet system consists of twin, side mounted, fixed geometry, seven degree, single ramp, two-dimensional inlets and bifurcated subsonic diffusers. For STOVL operation, two large top located auxiliary inlets, sized to two times the throat area of the main inlet, are installed in the inlet diffusers. The auxiliary inlets provide predicted inlet recovery ratios as high as 0.962 in the static STOVL hover mode with the main inlets blocked. The main inlet blocking doors provide necessary control of hot gas ingestion from cruise engine lift nozzles as well as protection from ingestion of foreign objects into the inlet system during STOVL operations.

Lift Improvement Devices (LIDs) are located on the underside of the fuselage. The LIDs are retractable fences which form a box to capture the jet fountain upwash in the vertical landing mode of operation. Capturing the fountain increases lift and also controls the hot gas flows to reduce hot gas ingestion.

The Pratt & Whitney STF 952A engine is shown in Figure 14.

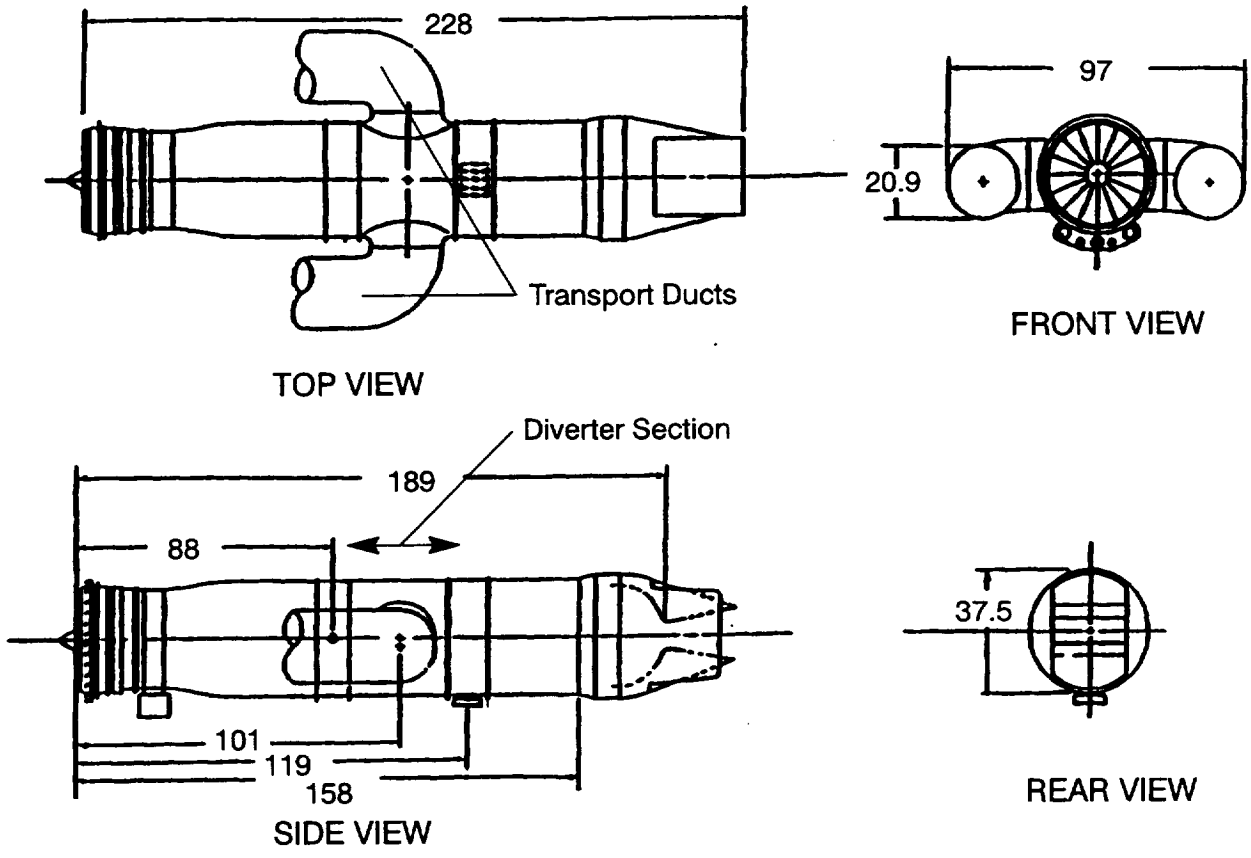

Figure 14. STF 952A MVFT STOVL Engine

The diverter section to the transport ducts consists of two laterally positioned offtake ports located just aft of the turbine exit. Each port has a two position (open or closed) valve. The transport duct consists of dual integral elbows connecting the diverter ports to dual remote lift nozzles, located forward of the aircraft center of gravity. The lift nozzles are installed with eight degrees aft fixed thrust angle. The angle matches the eight degree nose up attitude during aircraft hover. The nozzles have variable area control, providing vertical thrust modulation for hover roll control and are blocked (valve closed at the diverter and the lift nozzle closed) for conventional up and away engine operations. The lift nozzles also have ±20 degree vectoring, providing increased deceleration in transition to hover, increased maneuverability in hover, and reduced pitch reaction control bleed requirements. The lift nozzles are completely enclosed within the airframe behind actuated doors. A trim nozzle, Figure 3, is also provided for pitch control and cam vector laterally for yaw control.

The STF 952A also provides for rear compressor stage bleed air extraction. The Reaction Control System (RCS) bleed acts as another control effector to provide for added pitch, roll and yaw control. Additionally, the STF 952A is equipped with a two dimensional, convergent-divergent main cruise nozzle. This nozzle is a Spherical Convergent Flap (SCF) design with partial and full blockage capability for flow diversion to the lift nozzles. The nozzle also has ±20 degrees pitch, Figure 15, and ±20 degrees yaw, Figure 16, thrust vectoring capability without power setting restrictions.

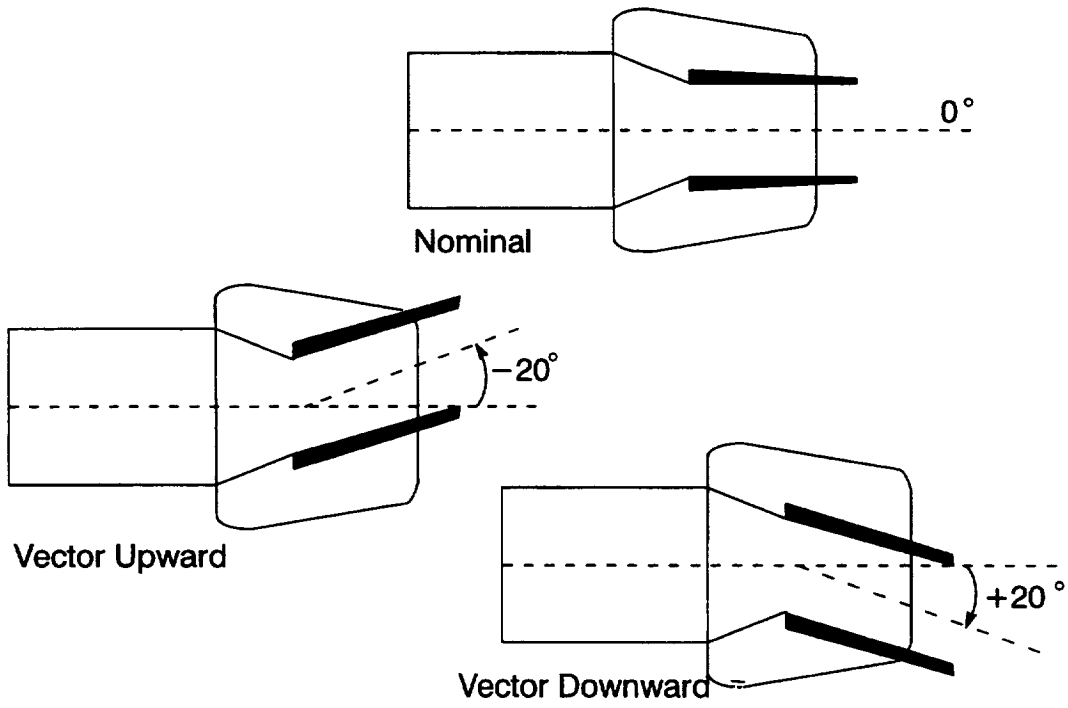

Figure 15. SCF Nozzle Pitch Vectoring (Side View)

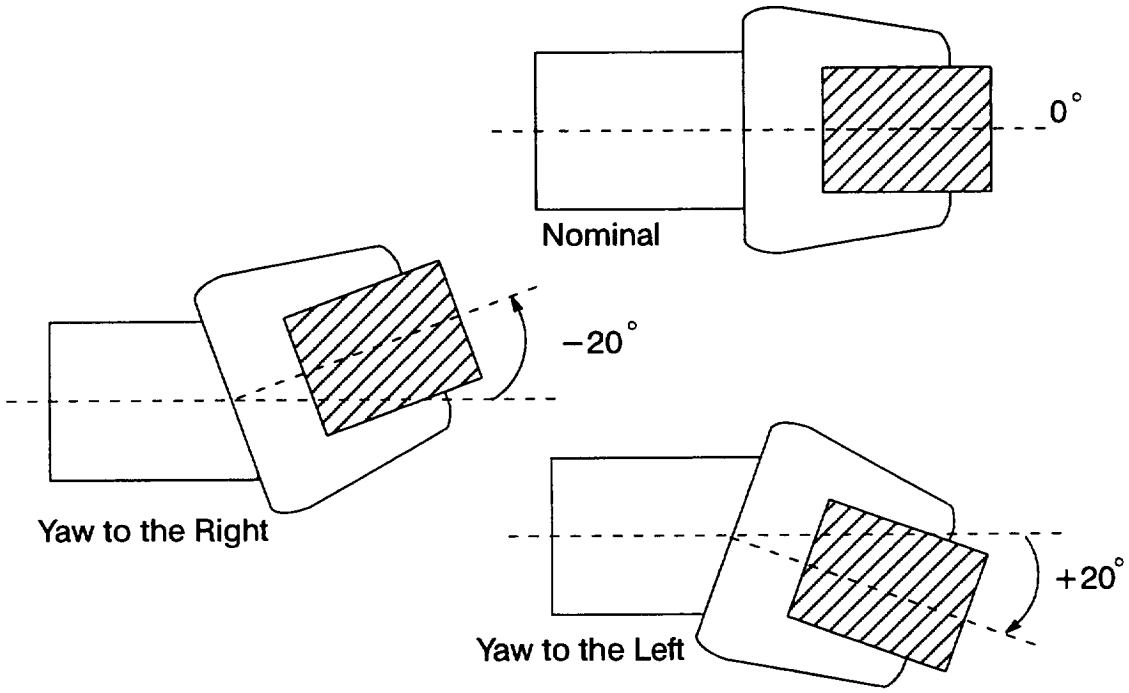

Figure 16. SCF Nozzle Yaw Vectoring (Top View)

2.2. Control Mode Definition

The process used for determining the control modes for this study is shown in NO TAG. First, the available sources of information on STOVL control modes and handling qualities were reviewed to determine several candidate control modes. These candidate modes were then implemented in MDA's Generic Aircraft (GENAIR) simulation for STO and Hover tasks. Simulation testing was performed to establish preferred control modes and to study handling qualities for each mode. An analytical evaluation was done for the transition task.

2.2.1. Candidate Control Modes

The candidate control modes were determined by dividing the missions into specific segments, and defining the piloting tasks required to perform each mission segment. Focus was drawn to three segments where STOVL operation is required: STO, transition, and hover.

As a source for information on candidate control modes, we drew upon our experience on existing aircraft, including the AV-8B and S/MTD. Information on the operational aspects of these aircraft relative to STO, transition, and hover tasks was obtained by interviewing pilots experienced with these aircraft. Experts knowledgeable on the control systems for these aircraft were also interviewed.

Other sources of information were simulation studies performed at MDA (References 3-6), and at NASA-ARC (References 7-9). Both of these sources provide data on translational rate command systems in hovering flight. The referenced NASA-ARC simulations also provide much information on different control concepts for transition flight.

Various other sources available in the literature were also drawn upon, including earlier Navy (References 10, 11) and Air Force (References 12-14) studies. Also, UK experiments were reviewed to include control concepts being studied by RAE. The US and UK military specifications, MIL-F-83300 and proposed revision and AGARD 577 (References 15-18), were also reviewed.

This study effort produced the candidate control modes shown in NO TAG. For the STO task two modes were defined. The manual rotation mode is a fairly conventional thrust vectoring STO where the pilot is given a cue on the Head-Up Display (HUD) to rotate the aircraft to liftoff attitude at a particular groundspeed. In the automatic rotation mode, the IFPC rotates the aircraft to a pretrimmed attitude at the correct groundspeed, providing a potential improvement in the repeatability of the take-off distances achieved.

For the transition task, three candidate control modes were defined. The first is a manual mode where the pilot directly controls engine power and equivalent thrust vector angle. This mode is similar to the Harrier, and would provide the highest safety for a technology demonstrator aircraft because of pilot familiarity. However, more highly augmented modes in transition have a great potential for decreasing pilot workload and enabling operation in more severe environments.

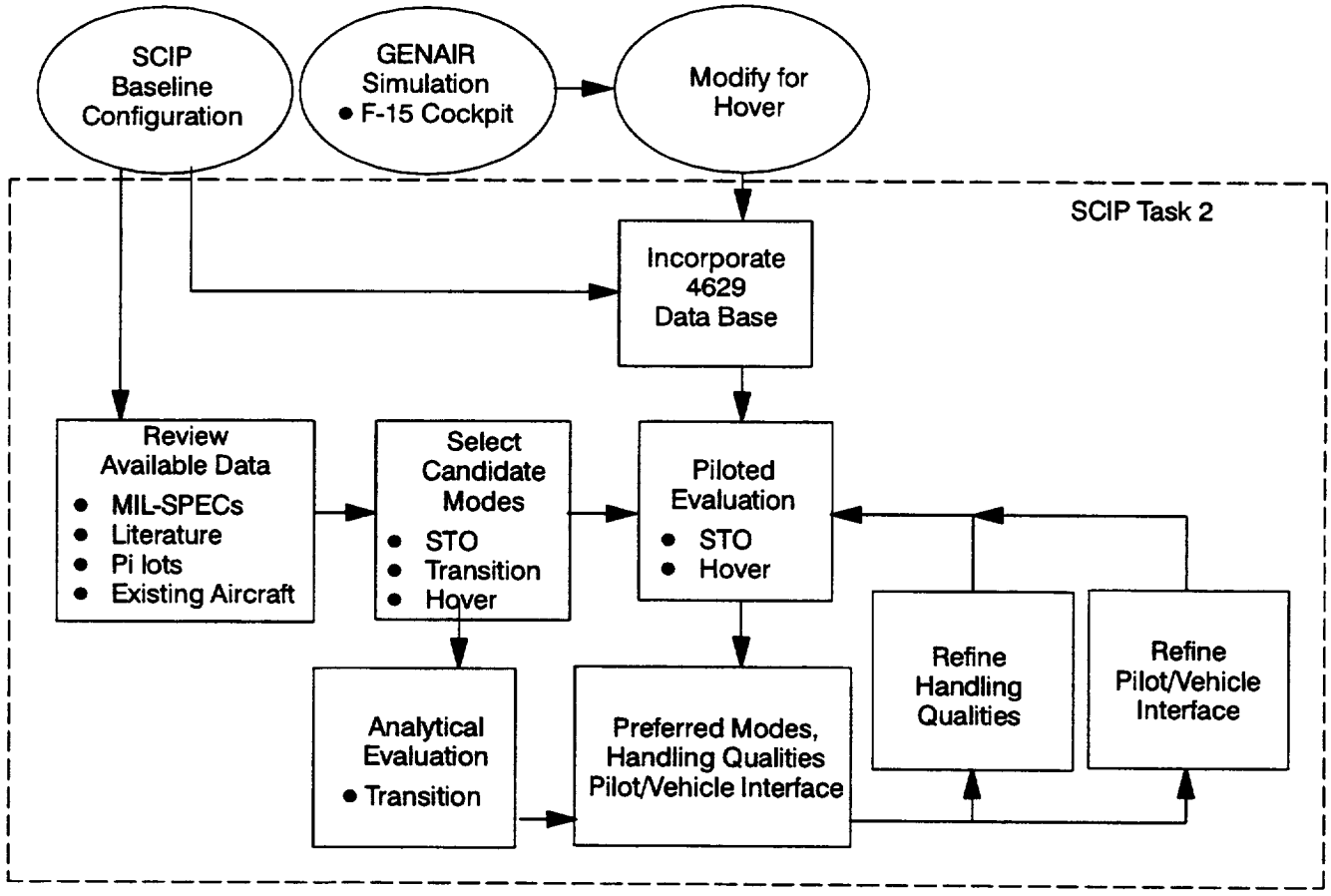

Figure 17. Control Mode Definition Process

Task	Mode	Merits
STO	Manual Rotation	Conventional Takeoff Simpler to Mechanize No Uncommanded Motion
	Automatic Rotation	Hi-g Takeoff Procedure Precise Rotation Control Similar to F-18 Catapult Launch
Transition	Manual	Similar to Harrier Pilot Controls Thrust and Thrust Angle Directly
	Velocity/Flight Path	Similar to F-15 S/MTD Applicable to Slow Landing
	Acceleration/Flight Path	Similar to NASA VSRA and RAE VAAC Experiments Lowest Workload for Approach to Hover
Hover	Rate	Similar to Harrier
	Attitude	Lower Workload Than Rate Command Better Damping
	Velocity-Fixed Nozzles	Simplest Nozzle Design
	Velocity-Vectoring Nozzles	Decoupled Velocity and Attitude Better Visibility
		} Lowest Workload Stable Hands-Off

Figure 18. Candidate Control Modes

One candidate is a mode where control of aircraft speed is provided on a speed control lever (such as the Harrier nozzle lever), with an autothrottle providing control of aircraft flight path. This mode decouples the aircraft's response in the speed and flight path axes, relieving the pilot from having to manually control speed and flight path through management of the thrust and thrust vector. This mode is especially suitable for slow or rolling landings where the pilot wishes to capture a particular approach speed for landing.

Another candidate mode is similar to that being studied at NASA-ARC on the referenced simulation, and being implemented on the V/STOL Research Aircraft (VSRA), for eventual flight test. This mode provides control of acceleration on a thumbwheel (with speed hold), with an autothrottle providing decoupled control of flightpath. This mode is especially suitable for precisely tracking an approach profile to capture a particular hover position.

Several candidate control modes for the hover task were defined as shown in NO TAG. In all modes, the throttle controls altitude rate and rudder pedals control heading rate. Therefore, each of the modes differ in the stick control characteristics. One mode provides control of pitch and roll rate with attitude hold and is similar to the response of the Harrier to stick inputs. The second mode provides direct control of pitch and roll attitude, potentially reducing pilot workload especially during shipboard landing tasks where precise control of aircraft attitude is required. The third mode provides control of horizontal translation rate on the stick, with the IFPC commanding changes in aircraft attitude to achieve the translation. This Translation Rate Command (TRC) system exhibits the greatest potential for reducing pilot workload. The fourth mode is the same as the third, except that longitudinal translations are achieved through vectoring the main lift nozzles;

thus pitch attitude changes are not required to translate, potentially improving aircraft handling.

The two candidate control modes for the STO task, and the four candidate modes for the hover task were implemented in the GENAIR simulation and evaluated by four different pilots over 87 flights. The simulation test and results are discussed in the following sections. The GENAIR simulation was not capable of simulating transition flight. As a result, the transition modes were only analyzed for pros and cons by a panel of IFPC experts and pilots experienced in V/STOL flight. Also, all three candidate transition modes were retained as modes to be tested in the final SCIP manned simulation.

2.2.2. GENAIR Description

GENAIR is a simple, flexible, low cost simulation developed by MDA to design and evaluate aircraft performance, flying characteristics, and cockpit controls and displays. The GENAIR simulation model provides realistic aircraft response characteristics with a minimum of required aerodynamic data.

The rotational dynamics of the GENAIR aircraft are modeled using a transfer function approach. Thus the user can specify the handling qualities to be tested by using frequency and damping parameters in an equivalent system response. These parameters can then be programmed directly into the GENAIR model's transfer functions to simulate an aircraft with the specified equivalent system response.

The linear acceleration dynamics of the GENAIR aircraft are determined using a straightforward calculation of the forces resulting from the angular responses and thrust.

Thrust forces are generated by the use of a transfer function model of the engine dynamics and output level. Thus vertical or axial dynamics can also be specified by the user in terms of equivalent system parameters and directly incorporated into the GENAIR aircraft model.

2.2.3. GENAIR Test Description

The GENAIR simulation was performed in MDA's Manned Aircraft Combat Simulator number 3 (MACS3). MACS3 is a 40 ft domed simulator facility with reprogrammable head–up (HUD) and head down displays to allow flexibility to study different display formats.

The main objective of the GENAIR simulation was to make a preliminary assessment of pilot preference between the candidate control modes for the STO and hover tasks. One secondary objective was to investigate variations in the closed loop dynamics of the aircraft response in the various hover control modes to establish good flying qualities goals for the SCIP simulation control law design. Another objective was to evaluate new HUD display concepts for the hover task.

For the STO task, both the manual and automatic rotation modes were implemented in the GENAIR simulation. The STO task that the pilots performed to evaluate the modes is shown in Figure 19. The pilot presets the pitch trim to 12° angle of attack, throttles up, and releases the brakes to start the groundroll. In the manual rotation mode, the pilot

rotates the aircraft to the pretrimmed 12° attitude at 60 knots, with liftoff occurring at about 120 knots. In the automatic rotation mode, the IFPC rotates the aircraft at the proper velocity, resulting in essentially a "hands-off" STO.

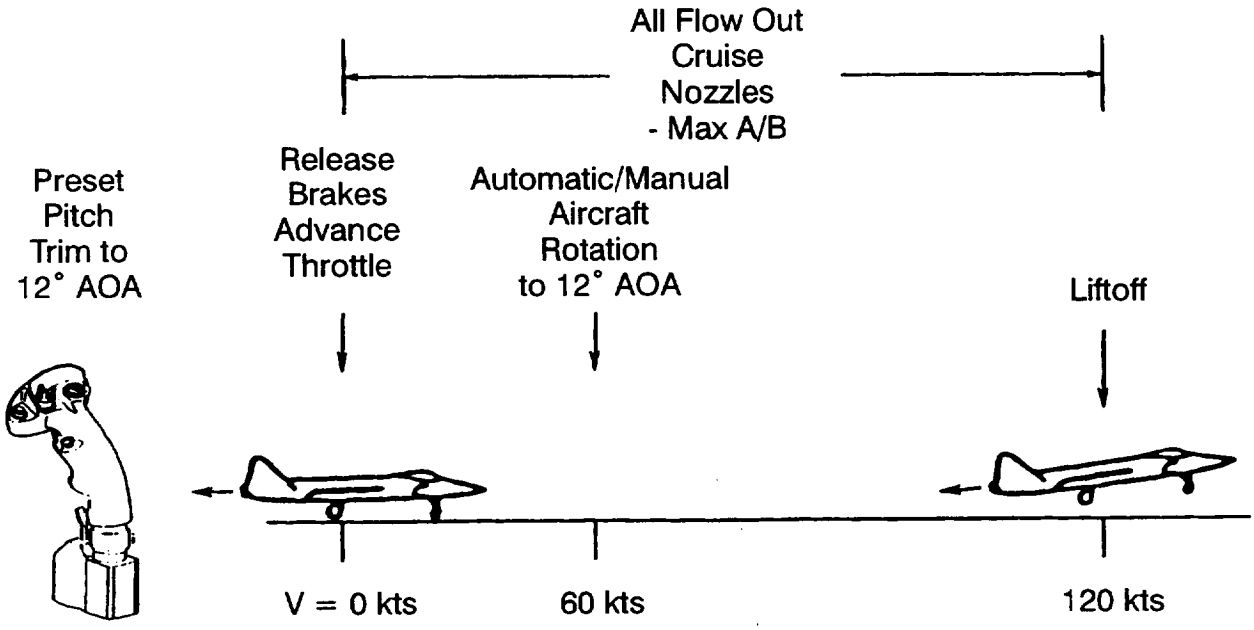

Figure 19. GENAIR STO Evaluation Task

For the hover task, all four candidate modes were implemented in the GENAIR simulation. The task the pilots performed to evaluate the modes is shown in Figure 20. The task segment starts at 100 feet of altitude and 100 feet south and east of the hover landing pad. The pilot performed a lateral translation to the proper cross range followed by a longitudinal translation to the hover pad. Then a 360° pedal turn was performed to evaluate directional characteristics, followed by a vertical landing.

A HUD display was developed in the SCIP program for use in the hover task, Figure 21. This display contains some of the features of a HUD being developed by NASA-ARC (Reference 19). NASA's hover HUD display is currently being flight tested on the NASA-ARC VSRA. The major new features that were included in the GENAIR hover HUD are symbology that superimposes both horizontal and vertical situation information. These include a trident representing the aircraft position relative to both a vertical landing pad symbol and a horizontal landing pad location symbol represented by a cross that is centered in a circle. Also, a circle representing a commanded velocity is included in the display, with a symbol emanating from the trident as shown in Figure 21, to represent the velocity response of the aircraft. Off to the right of the display is a caret next to a reference line which indicates vertical closure rate to the hover pad.

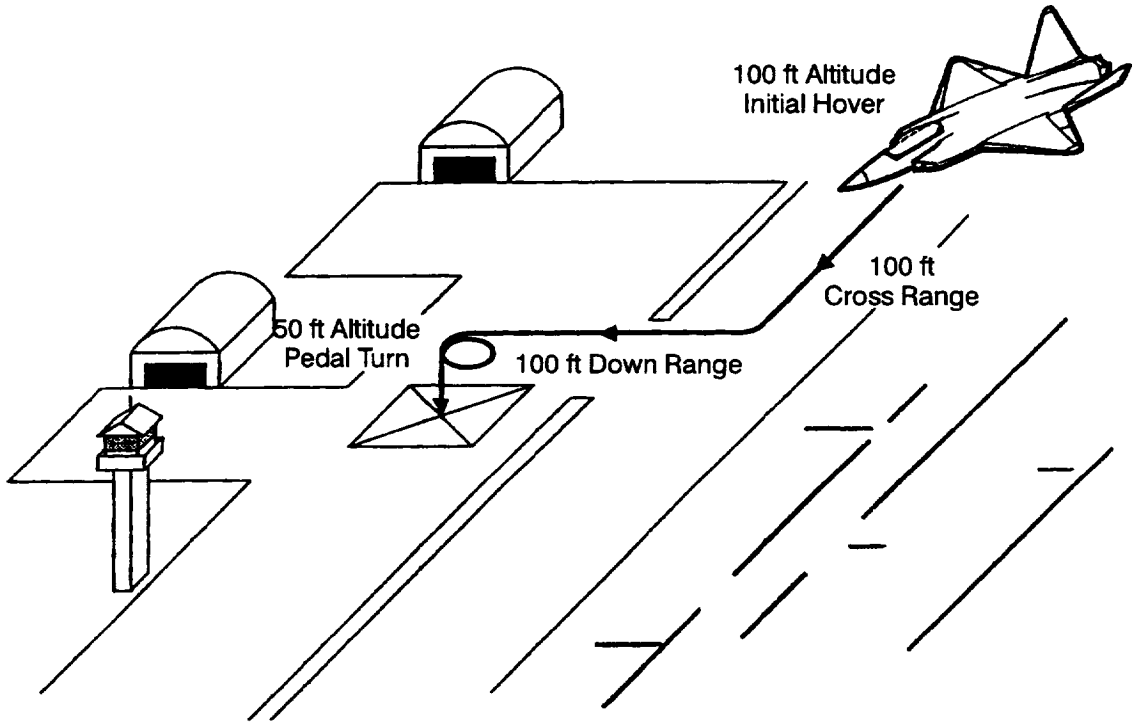

Figure 20. GENAIR Hover Evaluation Task

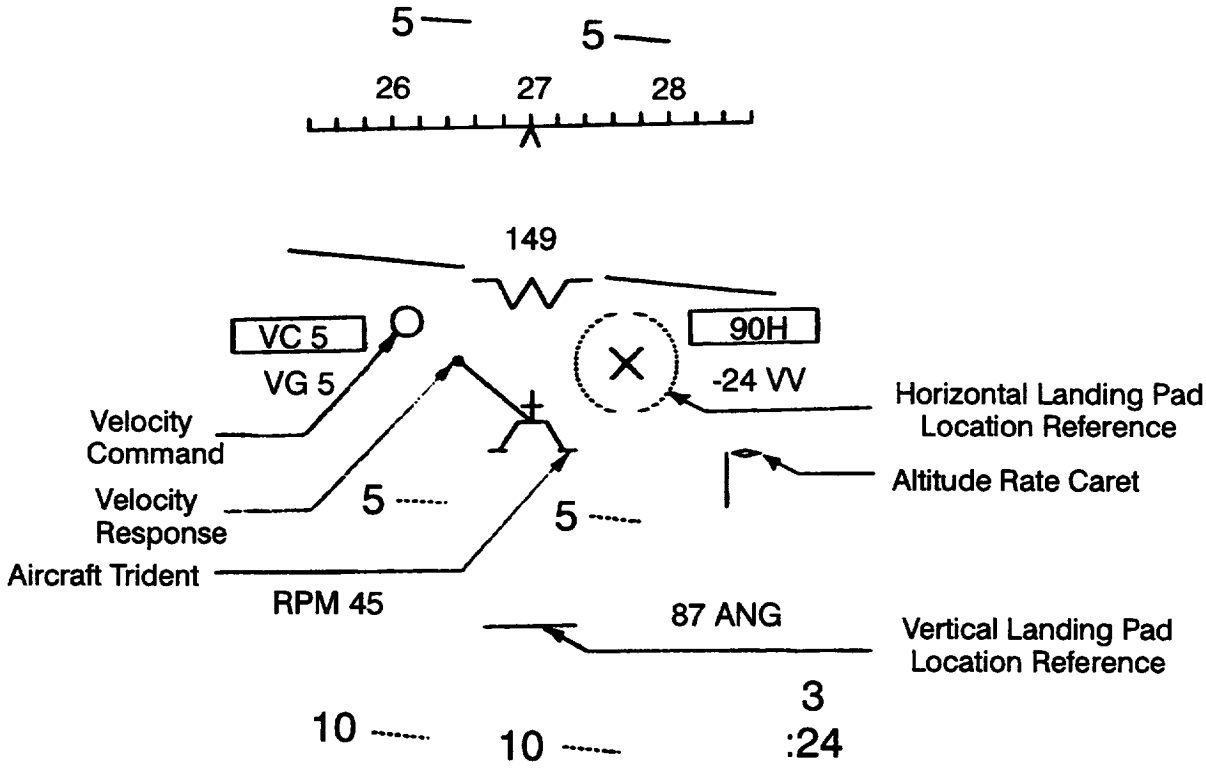

Figure 21. GENAIR Hover Head-Up Display (HUD)

2.2.4. GENAIR Test Results

The two candidate control modes for the STO task, and the four candidate modes for the hover task were evaluated by four different pilots over 87 flights. Most of the flights were spent in the hover modes experimenting with different dynamical characteristics for the stick responses. As a result, only a limited number of evaluations for each mode in hover could be compared with evaluations in other hover modes. Therefore only qualitative data could be extracted to rank the pilot preferences between the various modes.

The results of the rankings are shown in Figure 22, where the modes for both the STO and hover tasks are listed in ascending order of preference. Sample pilot comments on each mode are also included. For the STO task, the autorotation mode was seen as providing a lower pilot workload and a more repeatable task. For the hover tasks, the pilot preferences confirmed results seen in previous simulations and flight tests, with the TRC system providing the greatest relief in pilot workload, while also providing a system which could be flown very aggressively in severe conditions. The TRC using nozzle vectoring for longitudinal translations was slightly preferred because pitch attitude changes were not needed to translate.

Task	Mode	Pilot Comments
STO	Manual Rotation	"Requires Large Stick Displacements to Start Rotation and Capture AOA After Liftoff"
	Automatic Rotation	"Easier Than Manual, Rotates You to 12° Climbout Angle,...Reduces the Pitch Rate to Zero, Hands You the Airplane in a Very Nice Place. Fairly Comfortable".
Hover	Rate (no attitude hold)	"High Workload...Won't Stay Put...Have to Constantly Readjust".
	Attitude	"Very Precise...Acceptable Workload, More Work Than Velocity Command, but More 'Airplane Like' Response...Safe and Controllable, but Sensitivity Too Low, and Response Too Slow for Large Corrections".
	Velocity • Fixed Nozzles	"Absolutely Accurate...Responsive...Acceptable for Fine Tracking...Very Stable in Trimmed Hover".
	Velocity •Vectoring Nozzles	"Takes a Little Getting Used to but You Can Do Some Pretty Neat Stuff With It. Can Make a Very Precise Landing".

Figure 22. Control Mode Rankings

2.2.5. Control Modes for the SCIP Manned Flight Simulation

The transition control modes were analyzed by a panel of IFPC experts and pilots experienced with V/STOL operations. A summary is provided in Figure 23. The manual throttle/nozzle lever mode requires the pilot to integrate the throttle and nozzle lever responses to control speed and flight path, and represents the highest workload control mode of the three candidates. The velocity/flightpath mode provides decoupled control of speed and flightpath, but requires that the pilot frequently switch his left hand between the throttle and speed lever when acquiring the hover point. The acceleration/flightpath system also decouples speed and flightpath control, accommodates constant speed tasks such as slow landings or rolling vertical landings, and does not require the pilot to switch his hands between controls.

Mode	Factors
Attitude Power Thrust Angle	• Pilot Integrates Propulsion and Flight Control Systems • High Workload and Control Activity
Velocity Flight Path/Altitude Rate	• Decoupled Operation • Good Conventional Approach Characteristics • High Control Activity for Approach to Hover
Acceleration Flight Path/Altitude Rate	• Consistent With STOVL Operation • Minimizes Control Operation • Accommodates Constant Velocity Operation for Slow Landing • Decoupled Operation for Low Pilot Workload

Figure 23. Transition Control Mode Evaluation

The results of the analytical studies and the GENAIR simulation were used to define the control modes to be implemented in the SCIP3 simulation. They are:

Task Segment	Control Mode
STO	• Manual Rotation
Transition	• Manual Throttle/Nozzle Lever • Velocity/Flightpath • Acceleration/Flightpath
Hover	• Attitude Command • TRC by Attitude

The STO auto rotation mode was not implemented because programming the autorotation so that the rotation occurs at the appropriate velocity for all aircraft configurations and flight conditions would have required an extensive analysis of many flight conditions to find the correct rotation schedules. Therefore, the autorotation mode was eliminated so that more program resources could be concentrated on the transition and hover modes. All three transition modes were implemented in the SCIP3 simulation. Two of the hover modes, the attitude and TRC modes were implemented. The TRC by nozzle vectoring was not implemented because the Variant VI control effectors use the nozzle vectoring differentially to control yaw, and the control power on the nozzle vectoring was not adequate for simultaneously vectoring for both yaw control and longitudinal control.

The control modes are described in more detail in Section 3.3.1.

2.3. Control System Requirements Definition

The control system requirements defined in this section are the aircraft actuator response requirements and the propulsion system response requirements. In SCIP1, initial trade studies investigated the Variant I-VI control configurations, (refer to Figures 8 through 11). The propulsive control power of each variant was compared relative to the US/UK Concept Evaluation Model (CEM) requirements, and a preferred control configuration was selected for use throughout the rest of the program, Section 2.3.1. Two subsequent control power analyses were performed on the preferred control configuration, Section 2.3.2, before the final propulsive system response requirements were determined, Section 2.3.3. The aircraft actuator response requirements were determined in the US/UK Program, Reference 1 and Section 2.3.4.

2.3.1. Vectoring vs. RCS Trade Studies

In SCIP1, the six variant control configurations were analyzed in a trade study to determine the most promising candidate. Variant I (Figure 8) is the baseline US/UK 4629 control configuration, and employs compressor bleed RCS. Thrust split between the main lift nozzles and the ventral nozzle is used as a slow rate control effector to trim pitching moment, while the pitch RCS system provides fast dynamic response for pitch control. Thrust split between the main lift nozzles is used for roll control, and yaw control is achieved through the yaw RCS system. Control power for this variant meets the US/UK CEM

requirements, Reference 1, but employs compressor bleed RCS to provide adequate pitch and yaw control.

Since the compressor bleed RCS system inflicts large performance penalties for the engine, mixed flow RCS was investigated as an alternative RCS bleed system. A mixed flow RCS system was designed with the same exit valve type and locations as the compressor bleed system, and with the ducts and valves sized to provide the same control authority. The resulting duct sizes were large and could not be easily integrated into the 4629 configuration.

Variant III attempts to remove the requirement for compressor bleed RCS by increasing the rate requirement for modulating thrust split between the main lift nozzles and the ventral nozzle to provide adequate pitch control without the pitch RCS. Also, ventral nozzle vectoring was added to provide a yaw control effector to replace the yaw RCS. Figure 24 presents the yaw control power produced by the ventral nozzle for various ventral nozzle vectoring limits. This figure shows that ventral nozzle vectoring alone does not provide the 0.2 rad/sec^2 required by the CEM.

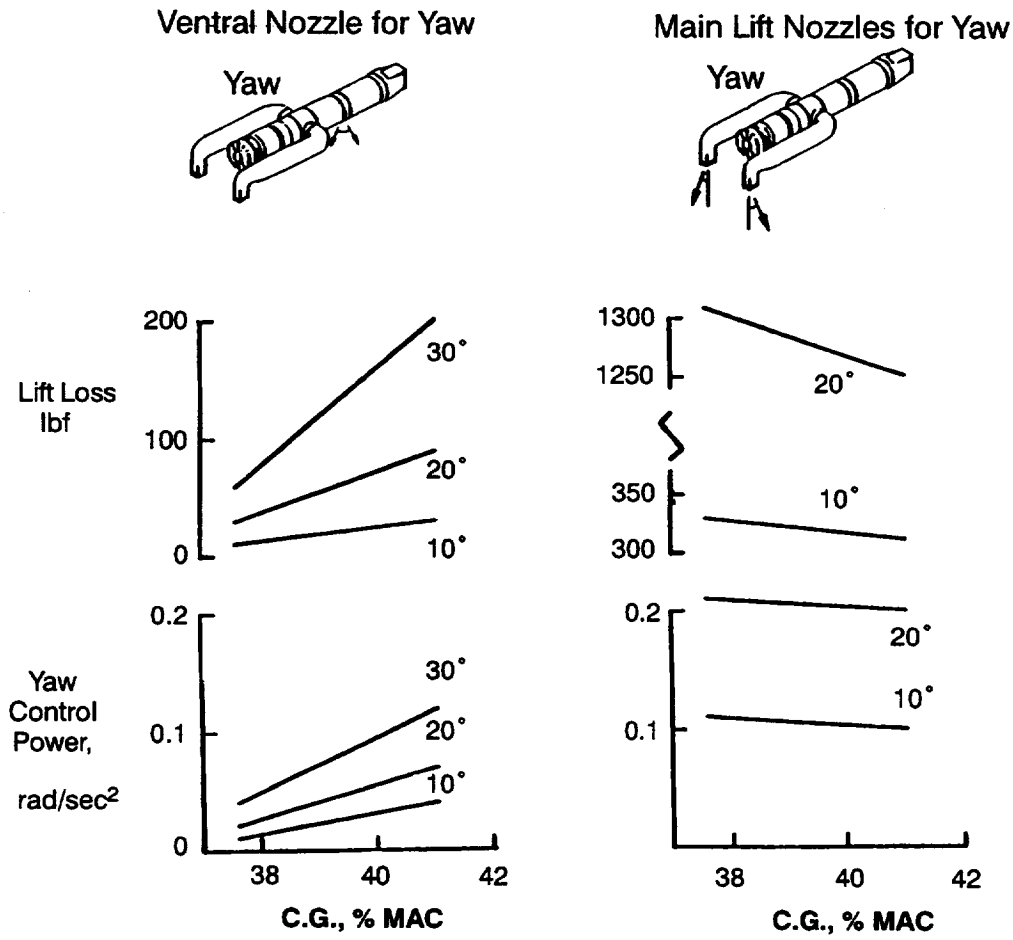

Figure 24. Yaw Control Authority from Lift Nozzle Vectoring

Variants IV and V add main lift nozzle vectoring to the Variant I and II configurations, respectively. Vectoring the equivalent thrust vector angle using lift nozzle vectoring is more efficient than thrust vectoring using thrust split between the main lift nozzles and the cruise nozzle (Figure 25), thus increasing the aircraft's acceleration capability in transition, Figure 26. Also, the forward vectoring capability of the main lift nozzles improves decelerations during transition into hover, Figure 26. The main lift nozzle vectoring provides increased yaw control power, Figure 24, however the yaw control power provided by main lift nozzle vectoring alone only barely meets the CEM requirement.

The variant VI control configuration employs both main lift nozzle vectoring and ventral nozzle vectoring. This nozzle vectoring combination provides adequate yaw control relative to the CEM requirements. As with the Variant III configuration, the rate requirement for modulating thrust split between the main lift nozzles and the ventral nozzle was increased to provide adequate pitch control without the pitch RCS. Therefore, the Variant VI control configuration provides adequate control power without the use of RCS, and was selected as the preferred control configuration.

The control configuration selected for use in the rest of the program is shown in Figure 27. In the rest of this report, this control configuration is referred to as the SCIP control configuration.

Although, Variant VI was chosen as the preferred configuration, the compressor bleed RCS was retained so that the technical issues between using RCS versus nozzle vectoring could be studied in more detail during the rest of the program. As shown in Figure 27, pitch control is achieved by modulating the thrust split between the main lift nozzles and the ventral nozzle. Pitch control authority is supplemented with the RCS system by collectively modulating the vertical thrust component of the left and right aft RCS valves. Modulation of the thrust split between the left and right main lift nozzles provides roll control. Additional roll control authority is provided through the RCS by commanding thrust in the dorsal direction on one side and commanding thrust in the ventral direction on the opposite side. Yaw control authority is provided through differential vectoring of the main lift nozzles and lateral vectoring of the ventral nozzle. Yaw control power is supplemented by side to side thrust commands to the RCS.

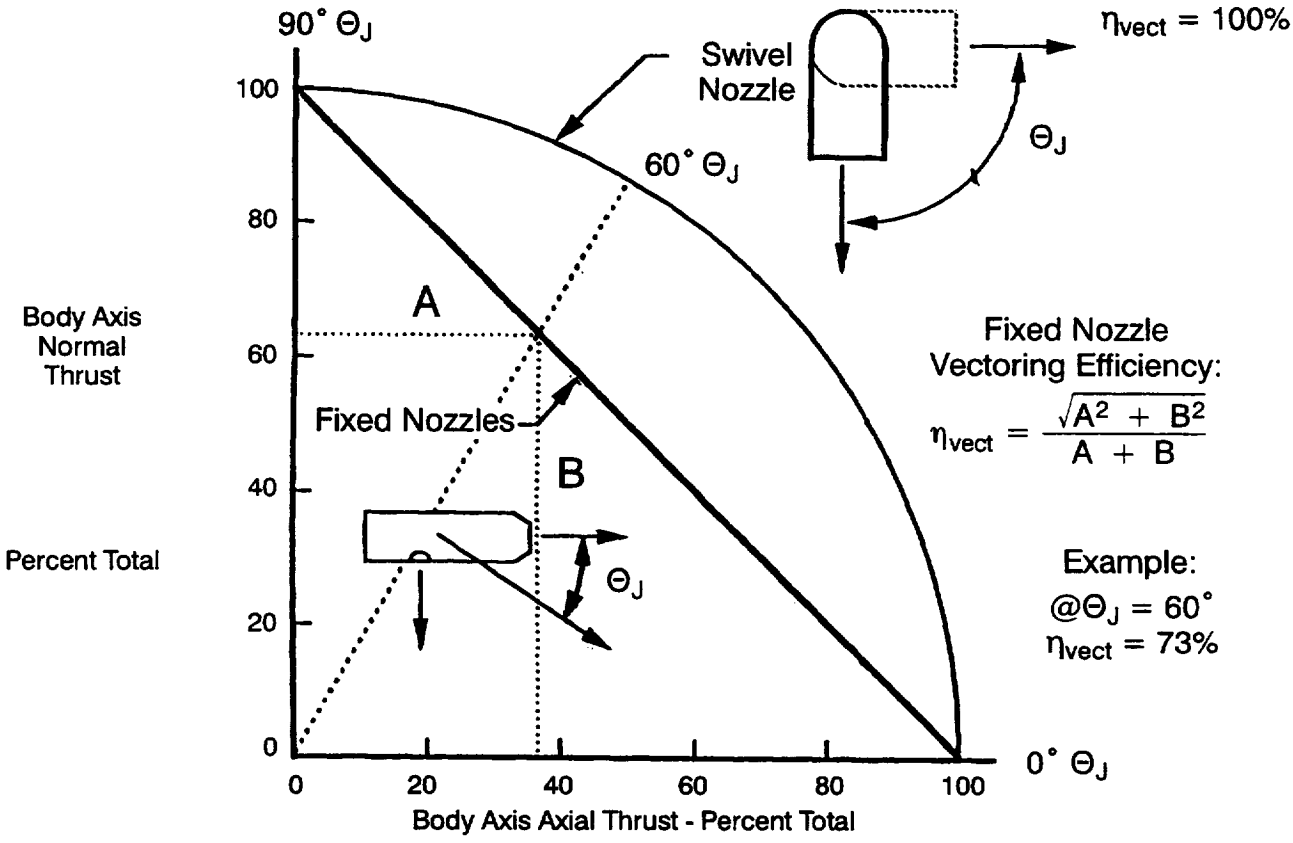

Figure 25. Vector Angle Efficiency

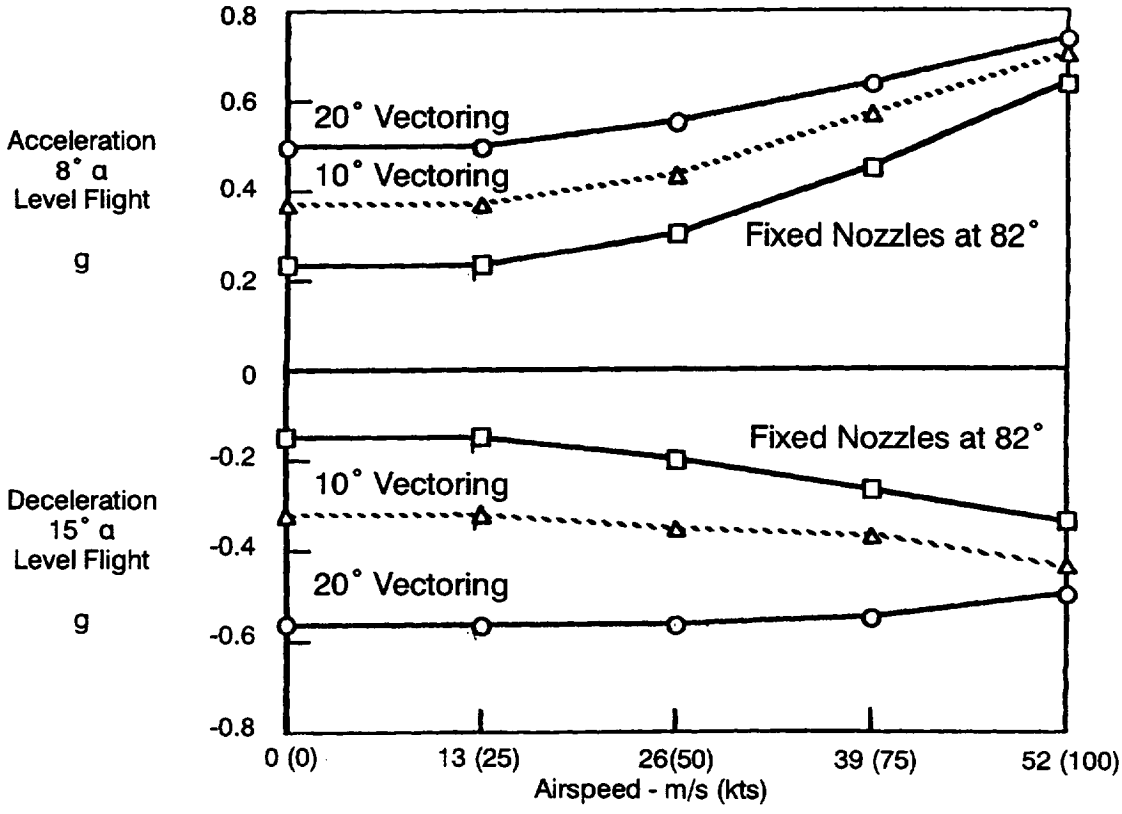

Figure 26. Acceleration/Deceleration During Transition

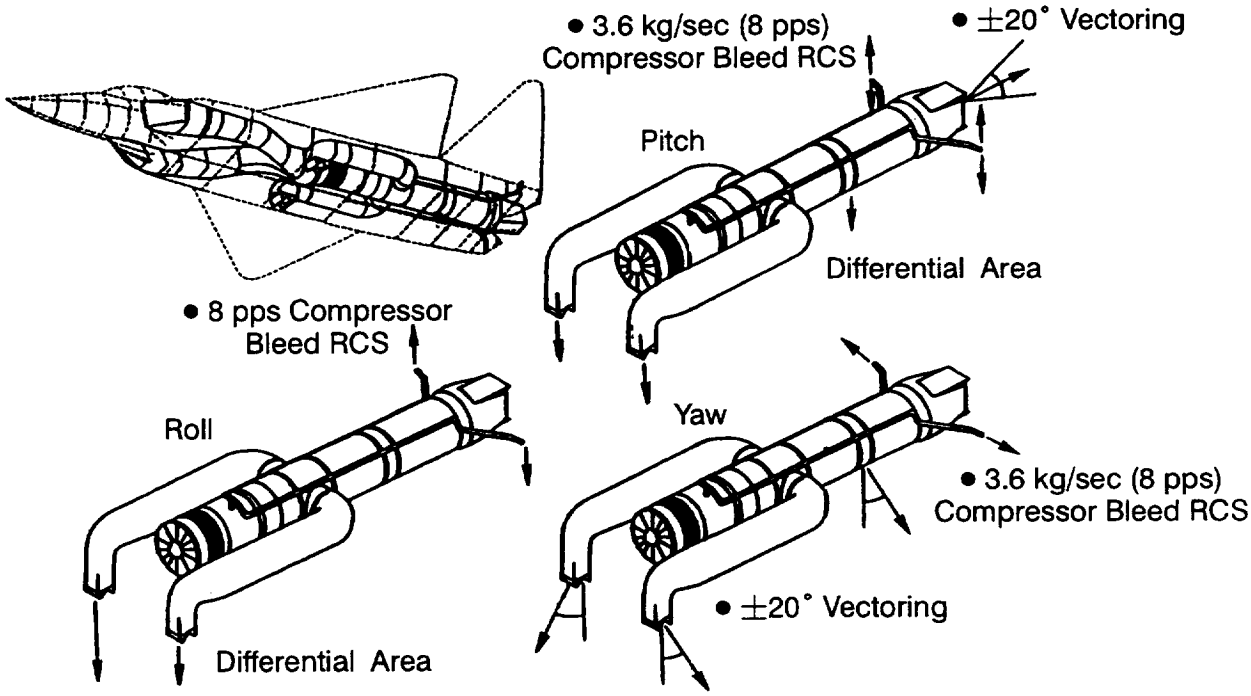

Figure 27. SCIP Control Configuration

2.3.2. Summary of SCIP and PROLIFIC Control Power Requirements Studies

In SCIP1, control power was computed analytically and compared to the CEM requirements, MIL-SPEC requirements, and MDA derived requirements based on AV-8B experience. During the SCIP1 trade studies, time histories of the GENAIR simulation runs were used to determine the pitch, roll, and yaw control actually used during the flights. A model of the aircraft was used to back out time histories of the control effector positions and rates that were required to generate the aircraft responses recorded in the GENAIR simulations. These results were used to refine the aircraft response requirements in pitch, roll, and yaw, and also to refine the actuator rate and dynamic response requirements.

In PROLIFIC Task 1, the analysis performed in SCIP1 was repeated for the 4636 with the SCIP control configuration, including both the analytical control power studies and the GENAIR time history studies. The results are presented in Reference 2. However, the results from the GENAIR simulation runs were of limited value, because a complete set of maneuvers could not be generated from the limited number of simulation runs.

Therefore, in PROLIFIC Task 2, a complete set of maneuvers was generated using a non-real time program developed in PROLIFIC Task 2. This program used rate limited transfer function representations of the desired equivalent system response of the aircraft in the pitch, roll, yaw, vertical and axial axes. Time histories were generated by inputting commands through the equivalent system transfer functions to generate time histories of the required aircraft motions. A model of the aircraft (including induced aerodynamic and jet effects) was used to back out the forces and moments that the propulsive control

effectors must generate to produce the aircraft motion given by the time histories. Then time histories of the individual nozzle thrusts and vector angles were generated from physical models of the nozzles. From these time histories, the dynamic response requirements, the required maximum rates, and the required maximum travels of the nozzle thrusts and vector angles were computed.

2.3.3. Propulsion System Response Requirements

All of the studies described in Sections 2.3.1 and 2.3.2 were used to generate requirements on the propulsion system, Figure 28. The nozzle vectoring position limits were driven by the results of Figure 24, which shows that 20° vectoring of both the main lift nozzles and the ventral nozzle is required to achieve adequate margin above the CEM requirement of 0.2 rad/sec^2 yaw acceleration. The vectoring rate requirements were derived from the results of the PROLIFIC Task 2 studies which showed that 80 deg/sec of vectoring was required to eliminate the need for yaw RCS. The nozzle thrust split rate requirements were driven by pitch and roll control authority requirements. The pitch and yaw vectoring requirements of the SCF nozzle were set to meet the rate requirements of the aerodynamic tail surfaces.

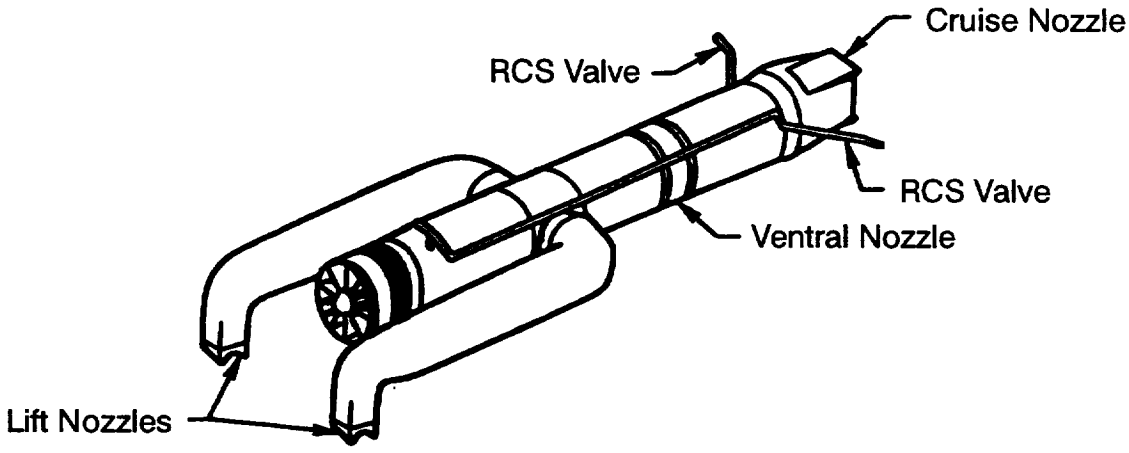

Propulsive Control Effector	Vectoring Sign Convention	Deflection Limits		No Load Rate Limits
Cruise Nozzle Pitch Vector	+Ventral	-20.0°	20.0°	60.0 deg/sec
Cruise Nozzle Yaw Vector	+Port	-20.0°	20.0°	60.0 deg/sec
Left Lift Nozzle Pitch Vector	+Forward	-20.0°	20.0°	80.0 deg/sec
Right Lift Nozzle Pitch Vector	+Forward	-20.0°	20.0°	80.0 deg/sec
Ventral Nozzle Lateral Vector	+Port	-20.0°	20.0°	80.0 deg/sec
(Left Lift Thrust)/(Left + Right Lift Thrust	-	0.35	0.65	100%/sec
(Ventral Thrust)/Left + Right + Ventral Thrust)	-	0.00	0.37	100%/sec
RCS Valves	-	0.0 sq in	8.0 sq in	8.0 sq in/sec

Figure 28. Propulsive Control Effectors

2.3.4. Aircraft Actuator Response Requirements

The requirements for the aerodynamic surfaces are shown in Figure 29. The control deflection limits of the 4629's aerodynamic control surfaces were designed in the US/UK Program (Reference 1) to meet 90% of the 1984 TAC SON point performance requirements for a supersonic fighter aircraft. Since the 4636 aircraft is nearly the same size and weight as the 4629, these same requirements were used for the aerodynamic surfaces on the 4636.

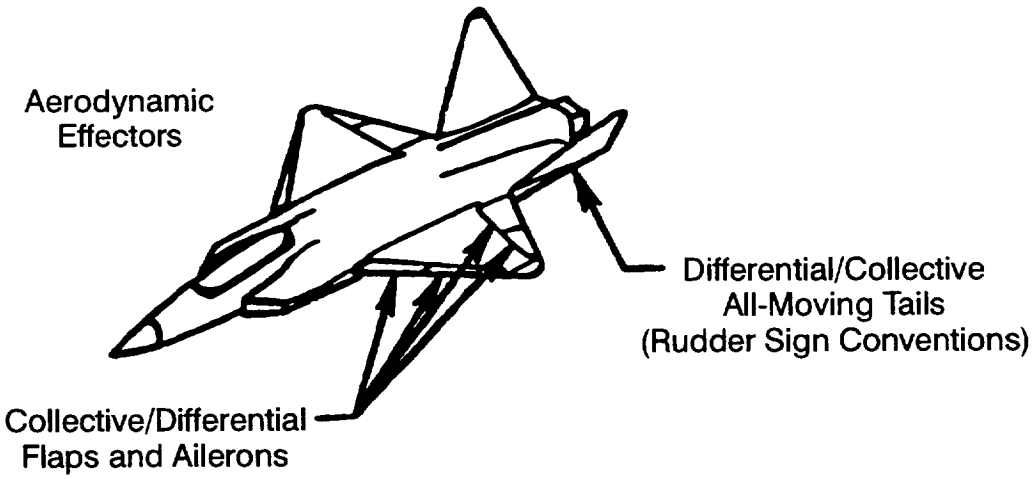

Surface	Description	Sign [1] Convention	Deflection Limits (deg)		No Load Rate Limits (deg/sec)
TAILL	Left Tail	+TEL	-30	30	60
TAILR	Right Tail	+TEL	-30	30	60
AILL	Left Aileron	+TED	-30	30	100
AILR	Right Aileron	+TED	-30	30	100
TEFL	Left Trailing Edge Flap	+TED	-30	40	80
TEFR	Right Trailing Edge Flap	+TED	-30	40	80
LEFOL	Left Outboard Leading Edge Flap	+LED	0	30	20
LEFOR	Right Outboard Leading Edge Flap	+LED	0	30	20
LEFIL	Left Inboard Leading Edge Flap	+LED	0	30	20
LEFIR	Right Inboard Leading Edge Flap	+LED	0	30	20

[1] TEL=Trailing Edge Left, TED=Trailing Edge Down, LED=Leading Edge down

Figure 29. Aerodynamic Control Surfaces

The rate response requirements were determined from the handling qualities requirements of the aircraft using an MDA developed advanced design software tool called VECTOR.

This program defines multiple aerodynamic surface requirements for a number of different aircraft handling qualities requirements. Specific handling qualities goals are defined and VECTOR computes the aerodynamic deflections and rates required to achieve these goals. Specific inputs to the VECTOR program are aerodynamic data,

geometry data, handling qualities data, and thrust data. VECTOR calculates the rates and deflections required to trim the aircraft, augment the aircraft to desired dynamics, negate inertial coupling effects, and to coordinate a stability axis roll.

The specific handling qualities goals input into VECTOR are the steady state roll rate or time to a given bank angle, the roll mode time constant, the short period frequency and damping, and the dutch roll frequency and damping. These data were input into VECTOR, and control rates were determined at several points of Mach number and altitude covering the flight envelope (including ranges in angle of attack up to 20 degrees at each point). The results output from VECTOR were rate requirements for the tails, ailerons, and trailing edge flaps as a function of angle of attack for each Mach and altitude considered. These rate requirements define an overall rate requirement for each of these surfaces, (Figure 29). The vectoring requirements of the SCF pitch/yaw vectoring were not investigated with the VECTOR program, instead the rate requirements were set equal to the aerodynamic tail surfaces' rate requirements.

2.4. Control System Architecture Definition

The architecture definition for the SCIP Program began in SCIP1, where a DMICS (Reference 20) type of methodology was used to partition control functions based on mission level requirements.

The ASTOVL MFVT aircraft has a high degree of interaction between the aerodynamic and propulsion control effectors. In wingborn flight the aircraft motion is primarily controlled by the aerodynamic surfaces. While hovering, the aircraft motion is controlled entirely by the propulsion system. During the transition from wingborn flight to jetborn flight, both the aerodynamic controls and the propulsion controls must be coordinated to a high degree to achieve a smooth and controlled transition. To define the IFPC requirements, a DMICS type methodology was used to determine the functional responsibilities and the control law requirements of the aircraft and propulsion systems for each aircraft.

In SCIP1, a model of the MFVT Model 4629 was developed, and a mathematical partitioning of the global aircraft/propulsion system was performed to determine a division of the control functions required of the aircraft and propulsion systems. This partitioning was performed for low speed wingborn flight, transitional flight to hover, and in jetborn flight. Since the control variables and aircraft model are very similar to the MFVT Model 4636, the results of this study were used to define a preliminary partitioning of the control functions. The partitioning resulted in an IFPC design where the engine controller directly controls anything that affects engine stability and performance while responding to flight control nozzle vector and thrust requests. As such, the flight controller commands the control action which is required to achieve the pilot commanded motion and has direct control over all nonpropulsion subsystem actuators. This partitioning is described below.

The process of subsystem partitioning was performed as follows:

1. Create a global model of the aircraft and propulsion system.
2. Normalize the aircraft model states, inputs, and outputs.

3. Analyze the interactions of states, inputs, and outputs using modal analyses, control power analyses, and observability analyses.

4. Divide the aircraft into functional subsystems.

The first task was to create a global model of the aircraft and propulsion system. This was done by developing a nonlinear model of the MFVT Model 4629 in the MCAIR Modular Six-Degree-of-Freedom (MODSDF) nonreal-time simulation package. The airframe model included the basic aerodynamics and equations of motion of the aircraft. The engine model consisted of a state variable model of the Pratt & Whitney STF 868A cruise engine with the SCF nozzle. Models of the inlets, cactus ducts, lift nozzles, trimmer nozzle, and reaction control ducts and valves, were integrated with the engine and aircraft models. Other effects, including ram drag, jet induced lift loss, and jet induced pitching moment, were also integrated into the model. Once the nonlinear aircraft model was developed, a MODSDF routine was written to trim the aircraft. This trim routine calculates 1-g equilibrium points for the aircraft for different mach numbers and altitudes. The variables used for trimming the aircraft are shown in Figure 30. Next, a MODSDF routine was written which defines small perturbations of states, inputs and outputs about the trim points, and computes a linear state variable model of the global aircraft and propulsion system for a particular flight condition. These states, inputs, and outputs are shown in Figure 31, Figure 32 and Figure 33, respectively.

Trim Variable	Jetborn	Semi-Jetborn Transition	Wingborn
Normal Force	Power Lever Angle	Switch Between PLA and Pitch Angle at 45 Degrees Effective Thrust Angle	Pitch Angle
Longitudinal Force	Total Effective Thrust Angle	Switch Between Effective Thrust Angle and PLA at 45 Degrees Effective Thrust Angle	PLA
Side Force	Relative Wind Angle	Relative Wind Angle	Relative Wind Angle
Pitching Moment	Differential Between Lift Nozzle Areas and Ventral Nozzle Area	Blend Differential Lift/Ventral Nozzle Areas and Differential Tail	Differential Tail (Rudder Sign Convention)
Rolling Moment	Differential Between Lift Nozzle Areas	Blend Differential Lift Nozzle Areas and Differential Aileron	Differential Aileron
Yawing Moment	Yaw Reaction Control Force	Blend Yaw RCS and Collective Tail	Collective Tail (Rudder Sign Convention)

Figure 30. Trim Routine

Variable	Description	Units
U	- x body axis velocity component	(ft/sec)
V	- y body axis velocity component	(ft/sec)
W	- z body axis velocity component	(ft/sec)
P	- x body axis rotational component	(rad/sec)
PHI	- roll attitude	(rad)
Q	- y body axis rotational component	(rad/sec)
THETA	- pitch attitude	(rad)
R	- z body axis rotational component	(rad/sec)
PSI	- heading	(rad)
NL	- low rotor physical speed	(rpm)
NH	- high rotor physical speed	(rpm)
TBT	- high pressure turbine blade metal temperature	(deg R)

Figure 31. Global Aircraft/Propulsion States

Variable	Description	Units
DTAIL	- differential vertical tail	(deg)
CTAIL	- collective vertical tail	(deg)
DFAIL	- differential aileron	(deg)
DRAIL	- aileron "droop"	(deg)
DFTEF	- differential trailing edge flap	(deg)
DRTEF	- collective trailing edge flap	(deg)
DFLEI	- differential inboard leading edge flap	(deg)
DRTEI	- collective inboard leading edge flap	(deg)
DFLEO	- differential outboard leading edge flap	(deg)
DRLEO	- collective outboard leading edge flap	(deg)
PLA	- power lever angle	(%)
CVV	- compressor variable vane	(deg)
FVV	- fan variable vane	(deg)
A8TC	- cruise nozzle area request	(in**2)
PV	- cruise nozzle pitch angle	(deg)
YV	- cruise nozzle yaw angle	(deg)
DLNV	- differential lift vs. ventral area	(in**2)
DLN	- differential main lift area	(in**2)
CLNT	- collective lift nozzle angle	(deg)
DLNT	- differential lift nozzle angle	(deg)
CPRCS	- collective pitch rcs area	(in**2)
DPRCS	- differential pitch rcs area	(in**2)
YRCS	- yaw rcs area	(in**2)

Figure 32. Global Aircraft/Propulsion Inputs

Variable	Description	Units
U	- x body axis velocity component	(ft/sec)
V	- y body axis velocity component	(ft/sec)
W	- z body axis velocity component	(ft/sec)
P	- x body axis rotational component	(rad/sec)
PHI	- roll attitude	(rad)
Q	- y body axis rotational component	(rad/sec)
THETA	- pitch attitude	(rad)
R	- z body axis rotational component	(rad/sec)
PSI	- heading	(rad)
NXCG	- axial load factor	(g)
NYCG	- lateral load factor	(g)
NZCG	- normal load factor	(g)
P2	- total pressure at engine face	(psi)
T2	- total temperature at engine face	(deg R)
NL	- low rotor physical speed	(rpm)
NH	- high rotor physical speed	(rpm)
TBT	- high pressure turbine blade metal temperature	(deg R)
P4	- main burner exit total pressure	(psi)
WFE	- main burner fuel flow	(lbm/hr)
P6	- total pressure at augmentor face	(psi)
T6	- total temperature at augmentor face	(deg R)

Figure 33. Global Aircraft/Propulsion Outputs

The second task was to normalize the units of the states, inputs, and outputs of the state variable model so that they have the same relative effect on the dynamics of the overall system. The small perturbation engine states and outputs were normalized so that the units were in terms of a percent of their nominal values. The small perturbation aircraft states and outputs were scaled relative to the forward body velocity, in such a way that the energy required to achieve a unit change in the linear or rotational rate in any axis was the same. The units of the aircraft and engine inputs were scaled to equal percentages of their maximum range.

The third task was to partition the global aircraft into subsystems. The partitioning tools were developed in the SCIP program and are listed in Figure 34. The state, input, and output modal analyses were done by first transforming the state coordinates of the model so that the new state coordinates represent states that are the actual modes which correspond to the characteristic value of the dynamic model. Afterwards, the transformation matrix is studied to determine the relative effect each state and input has on a particular mode. The controllability analysis was done by examining the controllability grammian for each input to determine the relative controllability of each input to each state. The observability analysis was done by examining the output matrix (the C matrix of the normalized (A, B, C, D) state variable quadruple). The steady state coupling analysis was performed by examining the relative steady state values of the transfer function matrix elements of the output responses to the inputs. The high frequency coupling analysis was done by examining the relative values of the direct feedthrough terms of the state variable model (the D matrix of the normalized (A, B, C, D) state variable quadruple).

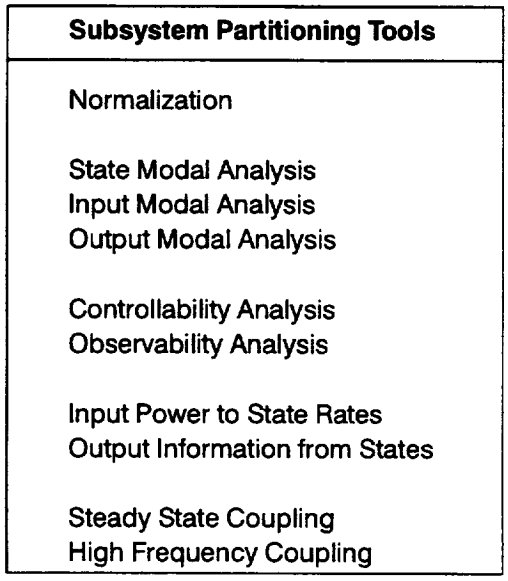

Figure 34. Partitioning Tools

The final task was to divide the aircraft model into functional subsystems. The results of the analyses were combined to define the overall interactions of the states, inputs, and outputs. Groups of states, inputs, and outputs were defined for which the relative interactions of states, inputs and outputs between the groups was much less than the interactions of the states, inputs, and outputs within each group. This partitioning was performed for the flight conditions shown in Figure 35, and include wingborn, jetborn, and semi-jetborn conditions. The results of the 90-knt semi-jetborn condition are shown in Figure 36. The aircraft was divided into three subsystems: longitudinal aircraft, lateral/directional aircraft, and engine. The partitioning for jetborn and wingborn flight were also divisible into these three subsystems, although the controls and sensed outputs are only a subset of those shown in Figure 36.

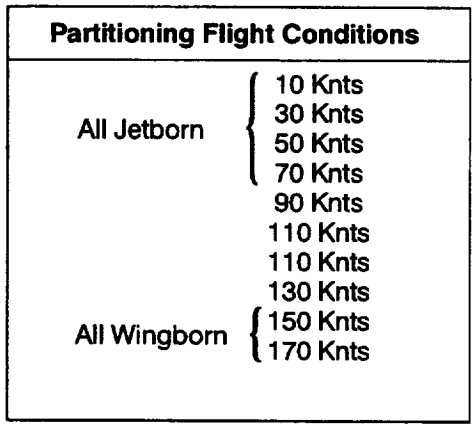

Figure 35. Flight Conditions (250 ft)

Subsystem	States	Inputs	Sensors	Request to Other Subsystems
Longitudinal	u, w, q, $\ominus$	DTAIL DRAIL DPRCS	u, w, q, $\ominus$, nx, nz	PLA A8TC PV YV DLN DLNV
Lateral/ Directional	v, p, Φ, r, Ψ	CTAIL DFAIL DPRCS YRCS	v, p, Φ, r, Ψ, ny	PLA YV DLN
Engine	NL, NH, TBT	PLA A8TC PV YV CVV FVV DLNV DLN CLNT DLNT	NL, NH, TBT, P2, T2, P4, WFE, P6, T6, v, w	———

Figure 36. Partition for Low Speed 90 Knts

Based on the results of this mathematical partitioning, the aircraft control responsibility of the MFVT Model 4636 was partitioned between the aircraft and the propulsion systems by giving the propulsion system control over anything that affects engine stability and performance. This responsibility includes control of the engine core processes, as well as control over the SCF nozzle actuators, the lift and ventral nozzle actuators, the diverter doors to the ventral nozzle ducts and the lift nozzle ducts, and the RCS bleed valve. The responsibility of the aircraft system includes actuation of the aerodynamic effectors, the RCS nozzles, and all external doors. The aircraft system will also issue commands to the propulsion system to effect the motion of the aircraft. These commands include the thrust split between the engine nozzles and nozzle vectoring commands.

From this functional partitioning of the control, a basic approach was developed for the design of the IFPC system where the engine and nozzles are controlled by an engine control system, and the motion of the aircraft is controlled by a flight control system. The flight control system will actuate the aerodynamic surfaces and issue commands to the propulsion system. The propulsion system will control the engine process and respond to flight control system requests. The integrated flight and propulsion controls will thus act together to achieve all pilot commands.

This distributed approach to aircraft control also has many advantages from a system integrity point of view. These benefits include:

1. Minimizes loss of control that is due to faults or external damage. Survivability is increased since functions are split between controllers using input voting planes to isolate faults to one controller only.
2. Facilitates aircraft installation as nondistributed controllers tend to become too large with too much wiring.
3. Minimizes the number of items that cross the firewall and the amount of data exchanged between the aircraft and engine.
4. Permits stand alone controller modes to increase survivability and facilitate testing of the IFPC subsystems.
5. Minimizes the complexity of engine and aircraft test equipment through localization of functions

3. SCIP2 AND SCIP3 – LOGIC AND SIMULATION DEVELOPMENT AND TEST

3.1. Airframe and Ground Effects Model Definition

In SCIP1, a six degree of freedom nonlinear model of the 4629 aircraft was developed, including a static Jet Induced Iteractions (JII) model and a static Hot Gas Ingestion (HGI) model. Pratt & Whitney delivered a transient model of the propulsion system to MDA. MDA then integrated the engine model with the aircraft model and delivered the integrated model back to Pratt & Whitney.

Then, in SCIP1, the aircraft model was installed in MDA's Modular Six Degree of Freedom (MODSDF) simulation program. MODSDF is a simulation program used for non–real time nonlinear analysis. This program contains interfaces for input/output and graphics plotting, an interface to a standard set of equations of motion, and interfaces to standard and user defined analyses programs. Then, this model was used to perform the IFPC functional partitioning described in Section 2.4.

Then, in PROLIFIC Task 2, the SCIP MODSDF model was modified to fit the 4636 aircraft geometry, the aerodynamic database was expanded to include the entire flight envelope, new static JII and HGI data were added, and a transient state variable engine model of the STF 952 was integrated with the model.

The aircraft model was completed in SCIP2, where a dynamic JII model was inserted.

The aircraft model was documented in Reference 21, and delivered to Pratt & Whitney, NASA–ARC, and NASA–LeRC. NASA–ARC used Reference 21 to install the aircraft model into the SCIP simulation. The following describes the model sources for the aircraft geometry, the aerodynamic forces and moments, the nozzle forces and moments, the RCS forces and moments, the JII forces and moments, the inlet forces and moments, and the inlet temperature and pressure. The details of the construction of the model are in Reference 21.

3.1.1. Aircraft Geometry

The aircraft geometry model specifies the location of the aircraft's reference center of gravity, center of lift, wing area, and wing span. The model also specifies the aircraft's weight and moments of inertia.

The center of gravity calculation is based on the center of gravity trace for the US/UK air superiority mission from Figure 2–68 in Reference 1. This center of gravity calculation is valid for the wing tanks empty and the feed tank full, covering fuel ranges between 5% and 60% of full internal fuel. The center of gravity is also a function of the stores, and this model proves a simple increment for either a fully loaded configuration or a configuration with all weapons expended. This model also provides an increment for the change in center of gravity due to the gear position.

The moment of inertia model is a linear interpolation between values corresponding to inertias which were calculated at combat weight and landing weight for the US/UK air superiority mission. It includes an increment for gear position.

3.1.2. Aerodynamic Forces and Moments

The aerodynamic forces and moments are defined using standard dimensionalized aerodynamic coefficients. The coefficients were derived from our Advanced Design Wind Tunnel test of the 4.2% scale model of the ASTOVL Model 279–4629E. This test provided nonlinear data for the static coefficients for lift, sideforce, rolling moment, pitching moment, and yawing moment at Mach 0.2. This data was rescaled to fit the slightly larger Model 4636 aircraft. Then, the data was extended to Mach 2.0 using the Woodward Analysis Method, verified on F–15, F/A–18, and Model 279–3 data. Drag data is from linear analysis also verified on F–15, F/A–18, and 279–3 data.

The dynamic coefficients were generated using program DYNAMIC, Reference 22. This program computes the dynamic derivatives using a strip theory approach modified to remove Mach number and angle of attack limitations, and has been verified with F–15 data.

The aerodynamic data was extended down to zero airspeed using predictions from the US/UK Program, which were based on flat plate drag predictions integrated over appropriate cross section areas of the aircraft. The resulting aerodynamic coefficients are blended with the Mach 0.2 aerodynamic data as described in Reference 21.

3.1.3. Nozzle Forces and Moments

The nozzle forces and moments are computed from the nozzle thrusts and thrust vector angles received from the propulsion model and the nozzle thrust center locations relative to the aircraft center of gravity. Also the cruise nozzle boattail drag is computed as part of the nozzle model.

The cruise nozzle boattail drag is computed from three tables which are valid for dry power, minimum afterburner, and maximum afterburner. These tables are a function of Mach number and cruise nozzle pressure ratio. These tables were derived from a database at MCAIR which describes boatail drag data for various types of nozzles. If the afterburner fuel flow is zero, then the nozzle boattail drag coefficient is looked up from the dry power table. If the afterburner fuel flow is not zero, then the boattail drag is computed by linearly interpolating between the maximum afterburner table and the minimum afterburner table as a function of the afterburner fuel flow.

In the nozzle model, the aircraft body axis components of the forces due to the nozzles' thrusts and thrust vector angles are calculated. The displacements of the nozzles from the center of gravity are computed, the forces and moments due to the nozzles' thrusts are computed, and the forces on the aircraft are computed by simply adding the individual components. The moments are computed by summing the body axis components of each nozzle's thrust multiplied by the appropriate moment arm.

3.1.4. Reaction Control System Forces and Moments

The RCS valves' forces and moments are computed from the RCS valves' thrusts from the propulsion model and the RCS valves' locations relative to the aircraft center of gravity.

Each RCS valve assembly is built on the end of the cylindrical pipe used to port the airflow from the RCS bleed valve on the compressor to the valve assembly location, located near the tails. The valve assembly consists of a sleeve valve which rotates around the end of the duct pipe, allowing flow to exit from either the dorsal or the ventral side of the assembly. Also, a cock valve is located on the end of the duct pipe which regulates airflow to either port (for the left RCS assembly) or starboard (for the right RCS assembly).

The RCS valve assembly displacements from the center of gravity are used to compute the moments due to the forces resulting from the RCS valves' thrusts.

3.1.5. Jet Induced Interaction Forces and Moments

The jet induced forces and moments are computed based on static test data from the JII testing of the 6.02% scale jet effects model of the 279–4629E on the MCAIR Jet Induced Test Apparatus. Static test data for jet induced lift and pitching moment were given to NASA–ARC, who then generated dynamic jet induced lift and pitching moment as a function of lift nozzle thrust, lift nozzle vector angle, airspeed, and height above the runway for aircraft configurations with LIDs and without LIDs.

The jet induced lift and pitching moment calculations are computed as a function of airspeed, height above the runway, jet vector angle, jet thrust, and Lift Improvement Device (LID) deployment.

Jet induced rolling moment is computed as a function of the aircraft Euler roll angle. If the magnitude of the roll angle is less than 10 degrees, the coefficient of JII rolling moment is read directly from a table derived from the test data. If the magnitude of the roll angle is greater than 10 degrees, then the roll angle is outside of the region of the test data, and an equation is used to compute the coefficient. This equation is a second order extrapolation of the test data beyond 10 degrees roll angle.

Finally, the jet induced forces and moments are computed by dimensionalizing the coefficients based on the jet thrust and the equivalent nozzle diameter.

3.1.6. Inlet Forces and Moments

The forces and moments due to the inlet include inlet drag and ram drag. The inlet drag includes the additive frictional effects due to the inlet duct cross sectional area being smaller throughout its length than the inlet, and spill and boundary layer effects at the inlet lip. The ram drag is the impulse created by the momentum change due to stagnating the flow at the airmass velocity.

The inlet centroid displacements from the center of gravity are the assumed points at which the ram drag forces are acting. To account for the high suction pressure created by turning the flow in front of the secondary inlets, the ram drag forces at the secondary inlets are assumed to act at a point above the inlet plane. The main inlet ram drag is calculated as a function of inlet airflow and the normalized open area of the main and secondary inlets. The airflow through both of the main inlets is first calculated using the ratio of main inlet area to total inlet area (the secondary inlet area is 1.4 times the main inlet area). Then the airflow is split between the left and right main inlets. The secondary inlet ram drag is calculated similarly to the main inlet ram drag calculations.

The inlet cowl drag is computed using a table look–up that is a function of Mach number, angle of attack, and corrected airflow. This table was derived from a database at MCAIR which describes inlet drag for various types of inlets. Finally, the drag coefficient is dimensionalized and the drag forces are converted to body axes to compute the resultant inlet forces and moments.

3.1.7. Inlet Temperature and Pressure

The inlet temperature and pressure model computes the total temperature and pressure at the fan face. The inlet pressure calculation consists of a pressure recovery factor multiplied to the total pressure. The pressure recovery was derived from a MCAIR database of pressure recovery data for various types of inlets. Pressure distortion data is not available for this engine/inlet combination, and thus is not modeled.

The inlet temperature model computes temperature rise due to hot gas ingestion. This temperature is set equal to the total temperature if the sum of the lift and ventral nozzles' thrusts are less than 80% of the total thrust (an arbitrary threshold). Temperature recovery and distortion are not modeled. When the lift nozzle's thrust exceeds 80% of the total, both near and far field temperature rise due to hot gas ingestion are looked up from tables. These data are based on empirical prediction procedures based on data from tests of the 9.2% model of the 279–3 in the NASA–LeRC 9'X15' wind tunnel performed as part of the MCAIR/NASA–LeRC Hot Gas Ingestion Test Program. Water tank flow visualization testing of the 6% scale model of the 279–4629E aircraft at the McDonnell Douglas Research Labs' Hover Research Facility has shown that the near field component of the hot gas ingestion is eliminated when the main inlet doors are closed. Therefore, the near field component is scaled by the main inlet open area to eliminate that contribution when the main inlet is closed.

3.2. Propulsion Model

The engine which was selected for the SCIP PROGRAM is designated as STF 952A. The STF 952A is a twin spool, mixed flow, afterburning turbofan engine.

The fan for the STF 952A is packaged in three highly loaded stages. Fan size is reduced by increasing airfoil loading via increased rotational speeds. Low aspect ratio airfoils, though heavy, are required for the increased demands. The efficiency penalty introduced by increasing maximum tip speed to 1700 ft/sec is reduced through the use of a 3–D viscous design system and swept blades. To minimize the effect of low aspect ratio airfoils and high rotational speeds on the weight of the fan rotor, hollow fan blades are utilized.

The four stage high pressure compressor incorporates many of the same advanced technologies which were used in the fan. Three–D viscous aerodynamic design allows for high efficiencies with the increased stage loading.

An Axially Staged Triangular Alignment (ASTRAL) combustor is used in the STF 952A. An ASTRAL combustor is significantly shorter in length when compared to a conventional combustor. Improved axial and circumferential zoning allows higher combustor exit temperature and reduced pressure loss without negative impact on smoke, pattern factor, or combustion efficiency. Diffuser pressure loss for this design is reduced using an advanced stepped diffuser design.

The High Pressure Turbine (HPT) and Low Pressure Turbine (LPT) require advanced aerodynamic efficiency with reduced cooling air at high temperatures. Improved cooling effectiveness blades and vanes, improved thermal barrier coatings, advanced blade outer seals, advanced single crystal blades, and high temperature intermetallic vanes each play a part in reducing the STF 952A turbine cooling requirements. Improvements in turbine efficiency will be realized through advanced 3–D viscous unsteady aerodynamic design technique and passive blade tip clearance control. A vaneless, counterrotating, "stage and a half" LPT is an attractive concept for the STF 952 principally because the resulting engine configuration offers size, weight, cost, and performance advantages relative to the more conventional two stage design.

The engine operates as a conventional takeoff and landing mixed flow turbofan engine with all thrust exiting the engine through the Spherical Convergent Flap (SCF) nozzle which is capable of both ± 20 degrees of pitch and yaw vectoring. The SCF also has full blocking capability (ability to go to zero convergent area).

In the transition flight mode, the lift and Reaction Control System (RCS) ducts are pressurized so that thrust may be ported out through combinations of the lift, trim, RCS, or SCF nozzles. The lift and trim nozzles have variable area and vector capability, ± 20 degrees for each, to provide engine pressure ratio control and to provide aircraft pitch and roll control while in transition or vertical flight mode. The lift nozzles are designed to provide both collective and differential roll control.

3.2.1. State Variable Model

The engine is modeled in three sections. The first section (the fan face to the mixing plane) consists of a piece–wise linear representation of the thermodynamic processes involved, based on partial derivatives of engine states about fixed operating points. This is referred to as the State Variable Model (SVM). The second section (downstream of mixing plane) includes performance calculations of the augmentor and nozzles. The last section models the dynamics of the Reaction Control System (RCS) bleed line.

The state variable modeling technique extends the classical linearized dynamic theory, which employs partial derivatives about a single operating point, by including multiple model points. Bivariant interpolation between these model points is used to define a base point which moves with time as engine power changes. Adjustments for non–steady state operation and augmentation provide accurate steady state and transient characteristics of an engine operating between idle and maximum power settings.

The engine is modeled using three types of variables: states, inputs, and outputs. States represent energy storage parameters like speed and metal temperature. Inputs are variables which perturb the systems, such as fuel flow. Outputs are parameters of interest other than the state and input variables.

Dynamically, the SVM is characterized by differential equations relating the time rate of change of the state variables to the state variables themselves and the input parameters. States are obtained transiently by calculating the derivatives and numerically integrating forward in time.

The linearized time rate of change of a state is formed as the sum of partial derivatives with respect to pertinent parameters using the Chain Rule. Using low spool rotor speed (XNL) as an example,

$$\frac{d(XNL)}{dT} = \frac{\partial \dot{XNL}}{\partial XNL}(XNL - XNLb) + \frac{\partial \dot{XNL}}{\partial XNH}(XNH - XNHb) + \frac{\partial \dot{XNL}}{\partial WFE}(WFE - WFEb) + \ldots\ldots$$

XNL = low spool rotor speed
XNH = high spool rotor speed
WFE = main burner fuel flow

and "b" denotes a base operating point.

For convenience, the equation is broken into two parts, one dealing with the partials with respect to states, the other dealing with partials with respect to inputs. The full set of differential equations can then be written in matrix notation as:

$$\dot{X} = A(\Delta X) + B(\Delta U)$$

where:

$\dot{X}$ = Vector of state derivatives.

A = Matrix of partial derivatives relating state derivatives to states.

B = Matrix of partial derivatives relating state derivatives to inputs.

ΔX = Vector of differences between the actual and base point values of the states. The base points are values of the states about which the partial derivatives were defined.

ΔU = The difference between the actual and base point values of the input parameters.

Likewise, outputs are calculated as functions of the states and input parameters. In matrix notation,

$$\Delta Y = C(\Delta X) + D(\Delta U)$$

where:

ΔY = Vector of differences between the actual and base point value of the outputs. The base points are values of the outputs about which the partial derivatives were defined.

C = Matrix of partial derivatives relating outputs to states.

D = Matrix of partial derivatives relating outputs to inputs.

ΔX and ΔU are as defined above.

The partial derivatives (A, B, C and D matrices) that are used in the state variable model are derived from an aerodynamic/thermodynamic model generated using the NASA ROCket Engine Transient Simulation (ROCETS) system, consisting of detailed component representations which accurately characterize transient performance.

The matrices of partial derivatives were generated at a particular flight condition (sea level static). In order to simulate other flight conditions, parameters must be shifted according to corrected parameter theory to the actual flight condition.

The technique employed is to shift the states and inputs from the actual flight condition to the flight condition at which the matrices were generated. The matrix operations are carried out at the base condition and the derivatives and outputs then shifted back to the actual flight condition.

A simplified representation of the state variable model including the states and inputs modeled is shown in Figure 37.

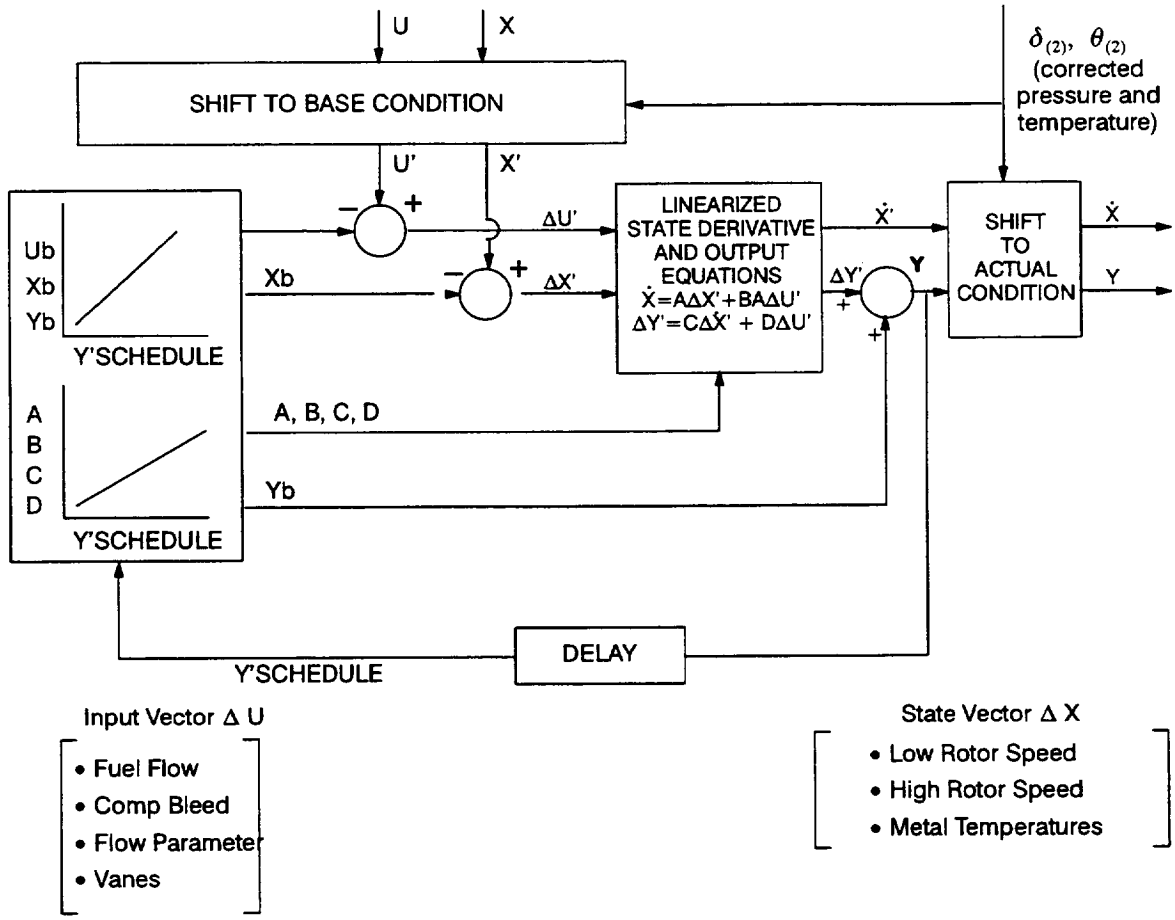

Figure 37. Schematic of Matrix Operations

3.2.2. Mixed Flow Model

The mixed flow model represents the augmentor volume dynamics, the lift duct volume dynamics, the lift duct valve pressure losses, augmentor, and nozzles, Figure 38. The model uses mixing plane (station 61) total pressure & temperature from the state variable model. The augmentor pressure and the list duct pressure are dynamic states which are used to calculate the nozzle flows. The nozzle flows are summed and used in calculating the flow parameter which is an input for the state variable model. The flow parameter is the feedback variable which allows the mixed flow model to communicate with the state variable model.

3.2.3. RCS Model

The dynamics of the RCS bleed line and nozzle are characterized by two transfer functions, Figure 39. The RCS Nozzle areas, the RCS shutoff valve position, and the HPC exit total pressure & temperature are used to calculated the steady state RCS shutoff valve flow and the steady state RCS nozzle total pressure. The transfer functions are then applied to the steady state values. Thrust for each of the RCS is then calculated. The transfer functions were developed from a detailed model of the RCS bleed line. The transfer function approach was used because the detailed model is too computationally intensive for simulator application.

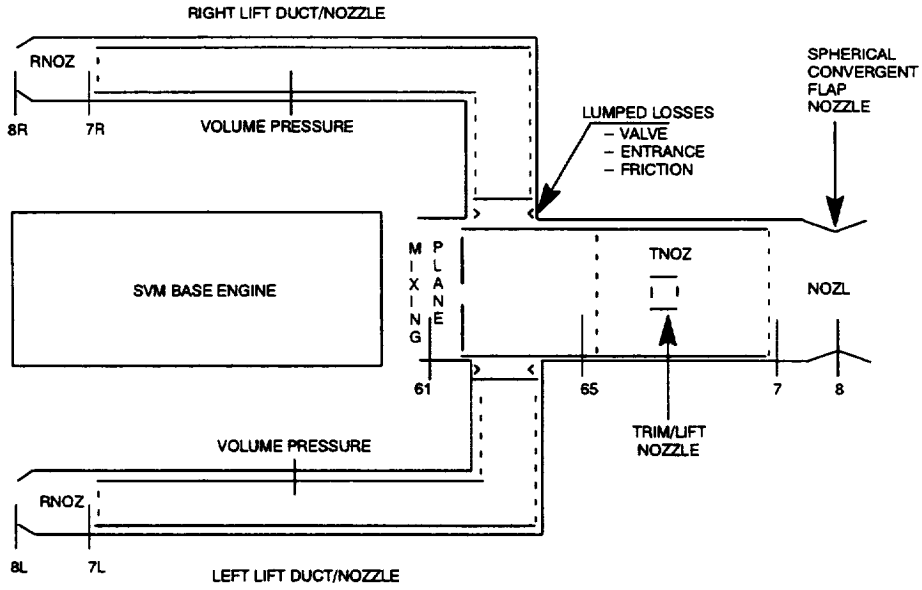

Figure 38. Schematic of Mixed Flow Model

3.3. IFPC Control Logic Design

This section describes the SCIP flight control laws. A description of the control modes that were implemented in the SCIP simulation is followed by a description of the control logic which implements the control modes.

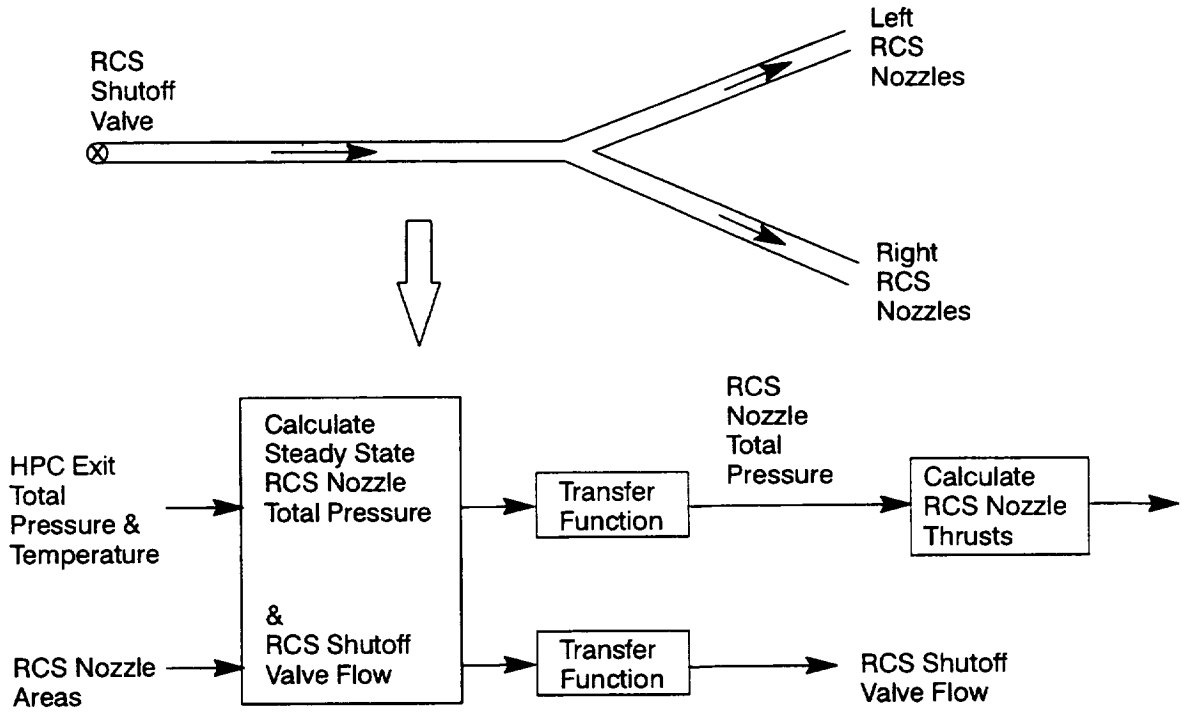

Figure 39. Schematic of RCS Bleed Line Model

3.3.1. Control Modes

The control modes for the SCIP simulation were chosen as described in Section 2.2. These modes also include two conventional modes, one for maneuvering flight (a flaps up mode) and the other for a conventional approach and landing (a flaps down mode). The STOVL control modes include one STO mode, three transition modes, and two hover modes. Two additional transition modes were added during the simulation. The final control laws implemented two conventional modes (these do not use the propulsive lift system), and five transition modes, as listed below (STO–MR ended up being exactly the same as TRAN–RCAH):

Conventional Modes:

CONV	Conventional Up & Away (Flaps Up)
LAND	Conventional Landing (Flaps Down)

STO Mode:

STO–MR	STO – Manual Rotation

Transition Modes:

TRAN	Transition
TRAN–RCAH	Transition with Rate Command/Attitude Hold
ACT–MT	Acceleration Transition – Manual Throttle
ACT–AT	Acceleration Transition – Autothrottle
VET	Velocity Transition

Each transition mode smoothly blends to the hover mode with pitch and roll attitude command on the stick. In each transition mode, Translational Rate Command (TRC) systems,

TRC–MT	Translational Rate Command – Manual Throttle
TRC–AT	Translational Rate Command – Autothrottle

are pilot selectable below 80 knots airspeed by pressing a mode switch button on the stick. TRC switches the pitch and roll attitude on the stick to groundtrack and crosstrack velocity commands.

During the simulation, a transition mode was set by the flight simulation engineers. The pilot could select from the conventional mode to the transition mode by lowering the gear handle. This action also lowers the flaps and the gears.

The cockpit controls included McFadden stick and rudder pedals set to AV–8 type force gradients, and an AV–8 type throttle/nozzle lever quadrant from the Kestral aircraft. Thumbwheels for the ACT–MT and ACT–AT modes were available on either the stick or the throttle.

The conventional modes are described in more detail in Section 3.3.1.1, the transition modes in 3.3.1.2, and the TRC mode in Section 3.3.1.3.

3.3.1.1. Conventional Modes

CONV	Conventional Up & Away (Flaps Up)

The conventional mode is normally entered from a flaps down mode (Conventional Landing, STO, or Transition) by raising the gear handle. The nozzle lever must be in the zero degree stop for the mode switch to occur. In conventional mode, the longitudinal stick commands pitch rate, with a steady stick input holding a constant normal acceleration above corner speed (320 KCAS for the 4629E). Below four tenths corner speed (128 knots), a steady stick input holds the angle of attack. In between, a steady stick input controls a blend of normal acceleration and angle of attack. The lateral stick commands stability axis roll rate. The throttle controls engine power. The nozzle lever is not used, being inactive even if it is accidentally pushed over the zero degree stop.

LAND	Conventional Landing (Flaps Down)

The conventional landing mode is selected from the conventional mode by lowering the gear handle. The controls operate similar to the conventional mode, with some changes to the handling qualities in that a pitch rate feedback is blended with the angle of attack feedback to improve the pitch response to airspeed excursions.

3.3.1.2. Transition Modes

The transition modes are illustrated in Figure 40. During the simulation the control mode corresponding to the gear down position on the gear handle was set by a flight simulation engineer, and the mode was selected during the flight by the pilot using the gear handle. Each mode is described below.

TRAN Transition

The command systems for TRAN mode are shown in Figure 40. This mode is similar to the AV–8B with improved handling qualities. The longitudinal stick response is the same as LAND mode, but blending from angle of attack command in transition to pitch attitude command in hover as a function of airspeed. Lateral stick commands roll rate in transition blending to roll attitude along the same airspeed schedule. The rudder pedals command sideslip/turn coordination in transition blending to heading rate command in hover.

The throttle commands the effective thrust vector magnitude, with maximum thrust occurring at the MIL power detent setting. The A/B settings are disabled by the mode switch to transition, commanding the same thrust as if the lever was in the MIL power detent. An altitude rate damping feedback is added to the throttle, blending in as a function of airspeed to improve height response in hover. The nozzle lever commands effective thrust vector angle.

TRAN–RCAH Transition with Rate Command/Attitude Hold

This mode is the same as TRAN, except that the stick control laws are replaced with a pitch/roll rate with pitch/roll attitude hold command system in transition, blending to pitch/roll attitude command in hover along the same airspeed schedule as TRAN mode.

	TRAN	TRAN–RCAH	ACT–MT	ACT–AT	VET	TRC
Longitudinal Stick	Angle of Attack	Pitch Rate Attitude Hold	Pitch Rate Attitude Hold	Pitch Rate Attitude Hold	Pitch Rate Attitude Add	
	Blending to	Blending to	Blending to	Blending to	Blending to	
	Pitch Attitude	Pitch Attitude	Pitch Attitude	Pitch Attitude	Pitch Attitude	Ground track velocity
Lateral Stick	Roll Rate	Roll Rate Attitude Hold	Roll Rate Attitude Hold	Roll Rate Attitude Hold	Roll Rate Attitude Hold	
	Blending to	Blending to	Blending to	Blending to	Blending to	
	Roll Attitude	Roll Attitude	Roll Attitude	Roll Attitude	Roll Attitude	Cross-track Velocity
Rudder Pedals	Sideslip & Turn Coordination	Sideslip & Turn Coordination	Sideslip & Turn Coordination	Sideslip & Turn Coordination	Sideslip & Turn Coordination	
	Blending to	Blending to	Blending to	Blending to	Blending to	
	Heading Rate	Heading Rate	Heading Rate	Heading Rate	Heading Rate	Heading Rate
Throttle	ETVM	ETVM	ETVM	Flight Path Angle	Flight Path Angle	
				Blending to	Blending to	
	ETVM with Altitude Rate Damper	ETVM with Altitude Rate Damper	ETVM with Altitude Rate Damper	Altitude Rate	Altitude Rate	Same as current mode
Nozzle Lever	ETVA	ETVA	Not used	Not used	Airspeed	
					Blending to	
	ETVA	ETVA	Not used	Not used	Groundspeed	Not used
Thumbwheel	Not used	Not used	Groundtrack Acceleration	Groundtrack Acceleration	Not used	
	Not used	Not used	Groundtrack Acceleration	Groundtrack Acceleration	Not used	Not used

(1) ETVM – Equivalent Thrust Vector Magnitude
(2) ETVA – Equivalent Thrust Vector Angle

Figure 40. Transition Command Systems

ACT–MT Acceleration Transition – Manual Throttle

This mode is the same as TRAN–RCAH, except control of the equivalent thrust vector angle is removed from the nozzle lever. Instead, a thumbwheel commands groundtrack acceleration through a control law that commands the equivalent thrust vector angle to achieve the desired acceleration response.

ACT–AT Acceleration Transition – Autothrottle

This mode is the same as ACT–MT, except that control of the equivalent thrust vector magnitude on the throttle is replaced by an automatic throttle which becomes a maximum AOA/flightpath/thrust consent control as shown in Figure 41. The operation of the autothrottle control is described in the following example.

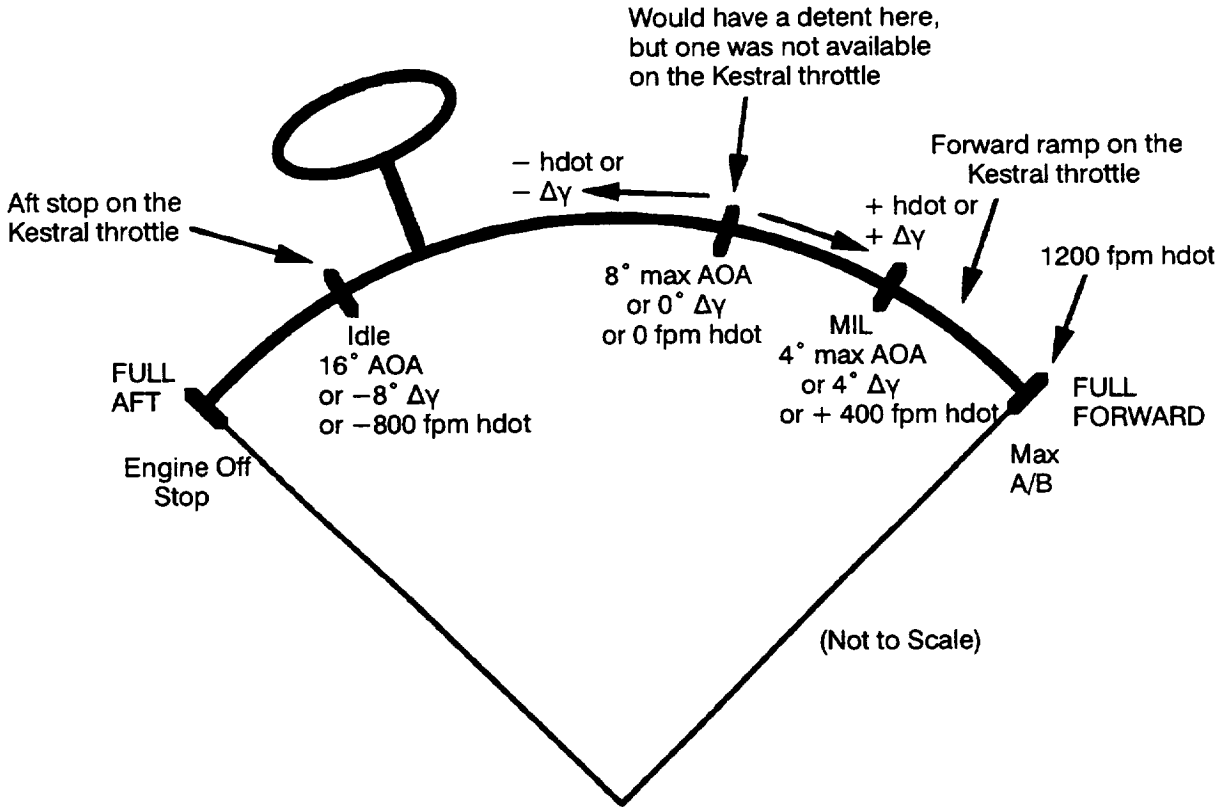

Figure 41. Autothrottle as Max AOA/Flightpath/Attitude Rate Control

With the aircraft in transition mode at steady level flight at 200 knots, the pilot selects a 0.1g deceleration with the thumbwheel. The aircraft initially decelerates by vectoring forward and by reducing power along a deceleration schedule chosen by the IFPC. The throttle now indicates a maximum AOA, and would indicate a maximum AOA somewhere between 10 and 16 degrees with the throttle left at the setting it was at for power–for–level–flight. If there is a zero stick input the aircraft will begin to descend. The pilot controls his desired flight path with the stick as in conventional flight, eventually reaching the maximum AOA indicated on the throttle control as the aircraft continues to slow.

As the aircraft continues to slow, the angle of attack is held by the IFPC to that indicated on the throttle. The pilot sets the desired glide slope with pitch stick commands, and the IFPC drives the inertial flight path vector to the attitude symbol offset by an amount, $\Delta\gamma$, determined by the throttle position (i.e. $\Delta\gamma$ = 8 degrees minus the AOA indicated on the throttle), resulting in a constant angle of attack approach. Thus the throttle can also be thought of as a $\Delta\gamma$ control, since the flight path can also be controlled by holding a constant attitude with the stick and resetting the AOA with the throttle.

Under normal conditions, after setting the speed control the pilot would set the throttle to 8 degrees max AOA, the nominal optimum AOA for transition. If increased thrust margin is desired, the throttle can also act as a thrust consent control, since the thrust needed at a constant airspeed and flight path varies with the AOA. As shown in Figure 42, for a 25,000 lb. aircraft weight, the thrust margin varies by 20 percent as the maximum AOA chosen by the throttle control varies from 8 to 17 degrees. The pilot can increase the thrust margin by setting a higher maximum AOA or by backing off on the deceleration command.

If the aircraft is wingborne and decelerating in response to the thumbwheel and the pilot moves the throttle forward to a maximum AOA below the current AOA, then the IFPC will couple the thrust vectoring to follow the new maximum AOA profile set by the throttle. If the pilot increases the maximum AOA, the IFPC will increase the AOA until either that value of AOA is reached or until the thrust vector limits to 0 degrees, in which case the IFPC will decouple the thrust vectoring, and the flight path is controlled by pitch stick inputs as in conventional flight. The aircraft continues the deceleration in response to the thumbwheel, and will recouple the thrust vectoring when the new max AOA is reached.

As the speed decreases through 56 knots the throttle blends to an altitude rate command with the 8 degree maximum AOA setting corresponding to zero ft/sec altitude rate, so that the throttle commands zero altitude rate when it is set at the optimum AOA for transition.

VET Velocity Transition

The VET mode is the same as ACT–AT except that control of deceleration is removed from the thumbwheel. Instead, the nozzle lever commands airspeed in transition, blending to groundspeed in hover, using a control law which commands the equivalent thrust vector angle to achieve the desired response.

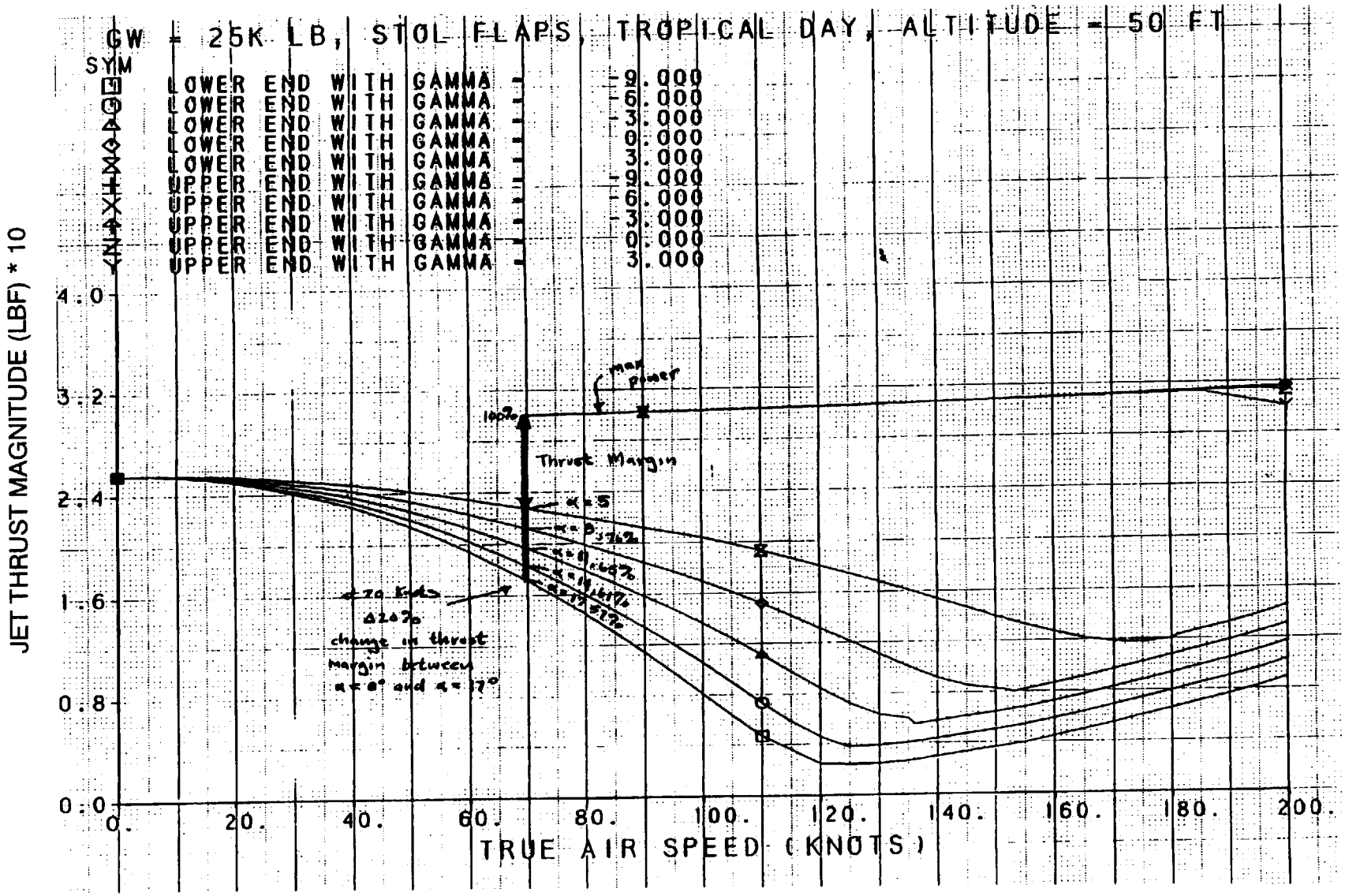

Figure 42. M4636 Transition Corridor Dependence on Flight Path

3.3.1.3. Hover Modes

The transition modes described in the previous section generally blend to the same pitch attitude/roll attitude/yaw rate command system in hovering flight. However, there are some differences in hovering flight, due to the level of augmentation provided in the thrust axes. These differences are described in this section. Also the TRC control mode in hovering flight is described in this section.

TRAN and TRAN–RCAH

These two modes have identical control laws in hovering flight. Horizontal translations are achieved through control of aircraft attitude. Forward/aft translations can also be commanded using the nozzle lever to control thrust vector angle. Height control is achieved by commanding engine power using the throttle. The throttle has a limited authority altitude rate damper, thus for small inputs, the throttle acts as an altitude rate controller.

ACT–MT

Although longitudinal stick commands pitch attitude, in this mode, the groundtrack velocity response to attitude changes is held to zero by the thumbwheel control laws, which close the loop on groundtrack acceleration. Thus horizontal translations are achieved by coordinating thumbwheel inputs with lateral stick inputs. Forward/aft translations are achieved with no pitch attitude changes, instead the pitch attitude is set for proper gear contact at touchdown.

ACT–AT

The hovering command systems for this mode is the same as ACT–AT except that a full authority altitude rate command system employing proportional plus integral control is on the throttle. As was seen in the simulation testing, this throttle control law provided better control of sink rate in ground effect.

VET

The VET mode has the same throttle control law as ACT–AT. As in the ACT modes, pitch attitude is decoupled from groundtrack velocity by the nozzle lever control laws which close the loop on groundtrack velocity. Again, forward/aft translations are achieved with no pitch attitude changes.

TRC–MT and TRC–AT

In all of the transition control modes, a TRC mode may be engaged below 80 knots using a button on the stick. When TRC is engaged, the stick controls groundtrack and crosstrack velocity. The pilot translates by pointing the stick in the direction of desired travel, the velocity in that direction is proportional to the stick travel. In the ACT modes this mode switch disables the thumbwheel. Also in VET mode, this mode switch disables the nozzle lever.

The only difference in the modes with TRC engaged is the autothrottle. Thus, for TRAN, TRAN–RCAH, and ACT–MT, the TRC control laws are identical and use the manual throttle with the height damper. This TRC mode is referred to as TRC–MT. For ACT–AT

and VET modes, the TRC control laws are also identical and use the autothrottle with proportional plus integral altitude rate control. This TRC mode is referred to as TRC–AT.

3.3.2. Control Law Description

The IFPC Logic was designed assuming that the control functions are partitioned between the propulsion control and the flight control as determined in the mathematical partitioning performed in SCIP1. The flight control receives pilot commands and aircraft sensor information, processing them to produce commands to the aircraft actuators and requests to the propulsion control system. The propulsion controller actuates the nozzles' thrust magnitudes and angles in response to requests from the flight control.

The flight control logic is divided into two modules, termed the Core Control Laws and the Control Mixer, as shown in Figure 43. The Core Control Laws process the pilot commands and sensor information, and compute aircraft motion requests, passing them to the Control Mixer in terms of commanded aircraft axial, normal, pitch, roll, and yaw accelerations. The Control Mixer transforms the requested aircraft accelerations to aircraft surface actuator commands and propulsion system nozzle thrust magnitude and angle requests. This approach has the advantage that the structure of the Core Control Laws is mostly independent of the propulsion system control configuration, so that modifications required for different types of propulsion systems are confined to the Control Mixer.

The design methodology for the Core Control Laws is based on experience gained from the AV–8B, F/A–18, S/MTD, and YF–23 Programs. Nonlinear feedbacks are utilized to negate inertial cross–coupling and gravity vector position effects to decouple the aircraft axes. Additional feedback gains scheduled with flight condition deaugment the aircraft to a neutrally stable airframe. Primary feedbacks are used to reaugment the aircraft to provide the desired flying qualities and stability margins.

3.3.2.1. Longitudinal Axis Core Control Laws

The longitudinal axis control laws compute the Control Mixer command, PCMD, based on the longitudinal stick position. First, nonlinear feedbacks are used which deaugment and decouple the longitudinal axis to provide a neutrally stable deaugmented aircraft longitudinal axis. The control laws then use feedback to reaugment the aircraft according to the control mode selected by the pilot. The conventional landing (LAND) and the baseline transition (TRAN) control laws are shown in Figure 44. During the simulation testing, the landing mode for a particular run was preset at the simulation engineer's console. The pilot switches from CONV mode to a landing mode with the gear/flap handle, which also selects gears/flaps down. The LAND mode control laws shown in Figure 44 execute with $K_\theta = 0$, always. The LAND mode provides the equivalent system closed loop dynamics as shown in Figure 44.

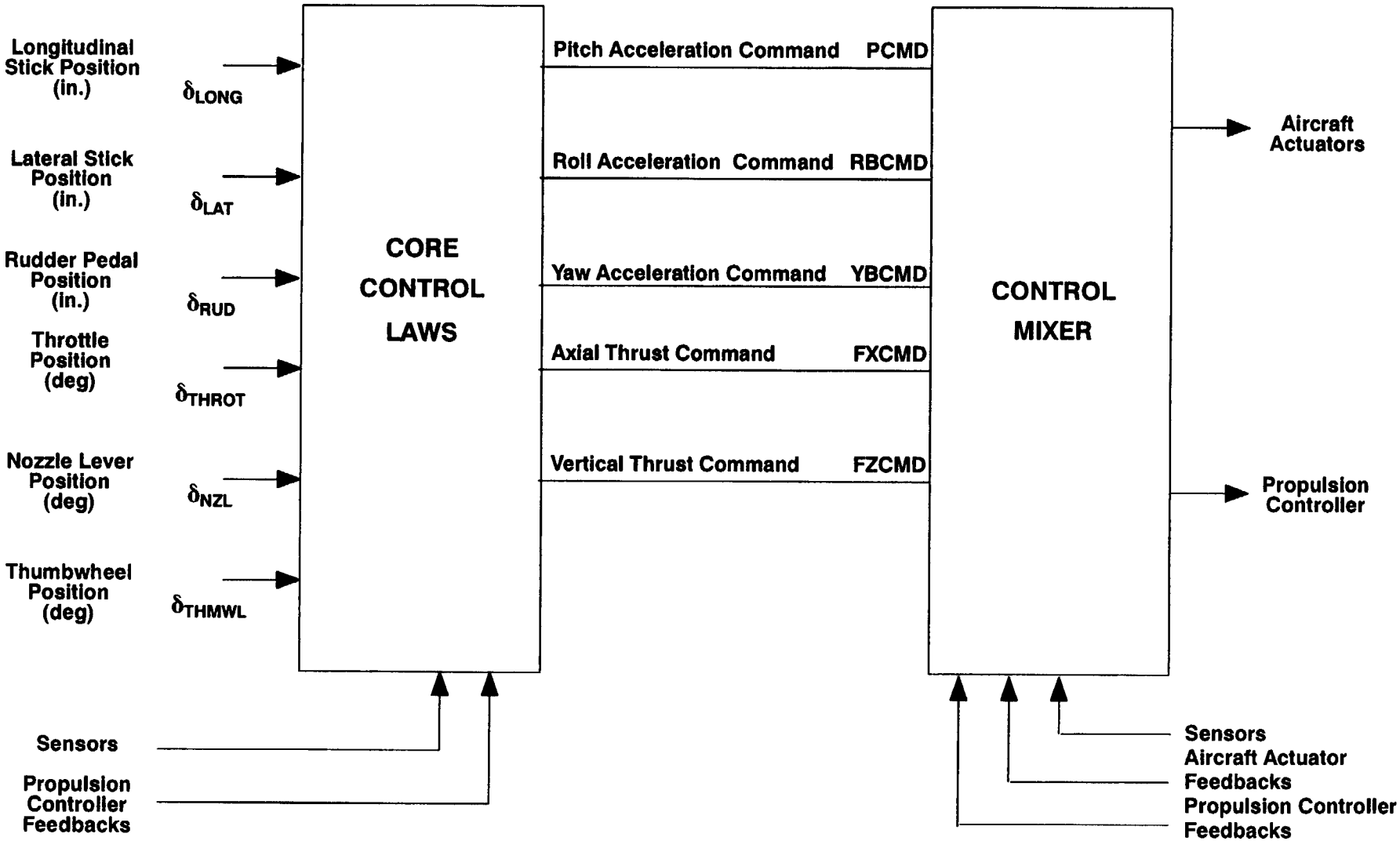

Figure 43. Control Law Structure

When landing in TRAN mode, lowering the gear/flap handle activates the powered lift system and switches the control laws. During the propulsion system's transition to powered lift mode, the outer skin doors are opened, the lift nozzles are repositioned, and the inner diverter doors are opened to pressurize the transport ducts. In the TRAN mode, Figure 44, the control laws use a pitch attitude feedback blended in as a function of airspeed using the K_θ schedule, Figure 45. At the same time, the angle of attack feedback is blended out using the same schedule. This feedback scheme provides the equivalent system responses shown in Figure 44, where the resulting equivalent systems show that the stick command blends from a pitch rate command to a pitch attitude command in a natural manner by augmenting the pitch attitude pole to the bare airframe L_α value as the pitch attitude gain varies from zero to one.

All other landing modes use a RCAH command system in the longitudinal axis. The RCAH control laws use the landing mode control laws from Figure 44 as an inner loop, with the K_θ schedule set to 1 at all airspeeds, as shown in Figure 46. A pitch RCAH command system is generated by adding a proportional plus integral filter in the forward loop, Figure 47, and provides a typical second order short period pitch rate response to stick inputs. Attitude hold is provided, as the output of the integrator loads up to the proper attitude command to hold altitude. A blend to an attitude command system is achieved by scheduling the integrator gain to zero as a function of airspeed using the schedule in Figure 45.

When below 80 knots airspeed, a precision hover mode switch is enabled which allows the pilot to select to TRC system. The translational rate control laws for the pitch axis also use the attitude control laws from Figure 46 as an inner loop. As shown in Figure 48, the TRC control laws are implemented as an outer loop driving the attitude command system control laws. The resulting equivalent systems dynamics, Figure 48, show that the velocity damping is augmented by these control laws so that the stick commands inertial groundtrack velocity. Integral control is provided so that the same trimmed stick position commands the same groundtrack velocity in all flight conditions.

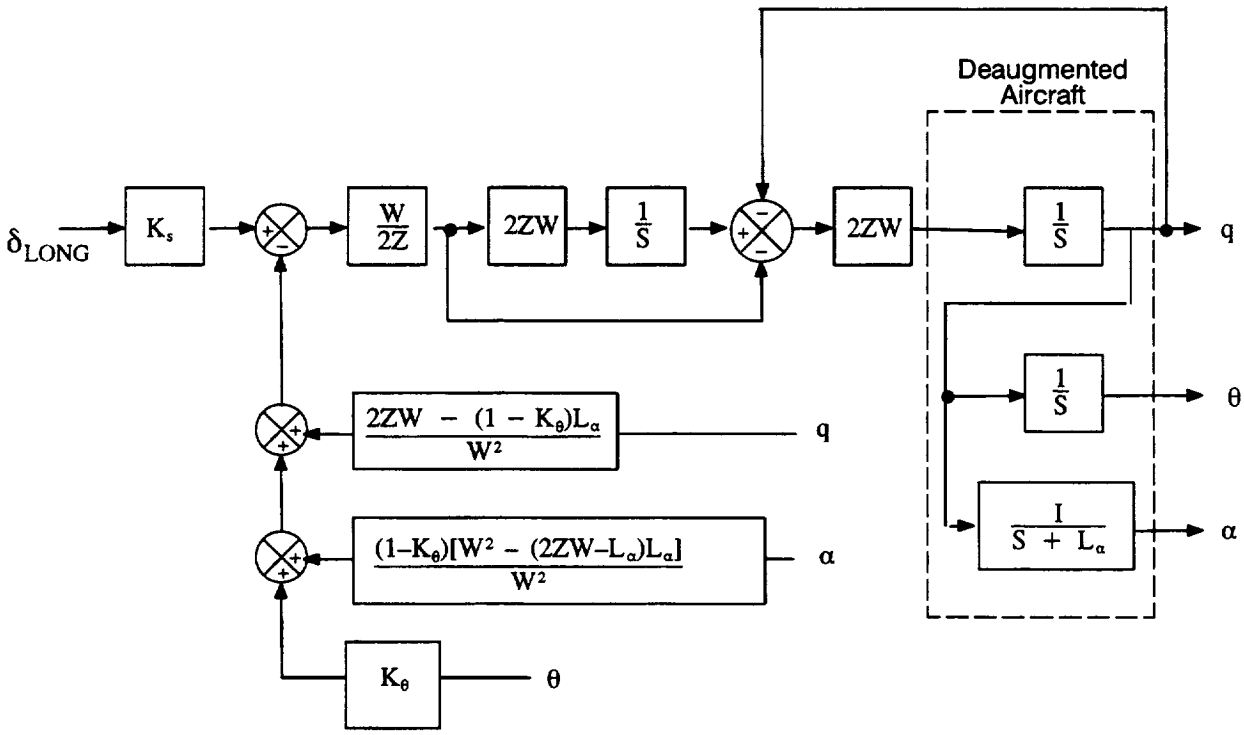

$$\frac{q}{\delta_{LONG}} = \frac{K_s W^2(S + L_\alpha)}{(S^2 + 2ZWS + W^2)} \quad \frac{q}{\delta_{LONG}} = \frac{K_s W^2(S + L_\alpha)S}{(S^2 + 2ZWS + W^2)(S + K_\theta L_\alpha)} \quad \frac{q}{\delta_{LONG}} = \frac{K_s W^2 S}{(S^2 + 2ZWS + W^2)}$$

$$\frac{\alpha}{\delta_{LONG}} = \frac{K_s W^2}{(S^2 + 2ZWS + W^2)} \quad \frac{\alpha}{\delta_{LONG}} = \frac{K_s W^2 S}{(S^2 + 2ZWS + W^2)(S + K_\theta L_\alpha)} \quad \frac{\alpha}{\delta_{LONG}} = \frac{K_s W^2 S}{(S^2 + 2ZWS + W^2)(S + L_\alpha)}$$

$$\frac{\theta}{\delta_{LONG}} = \frac{K_s W^2(S + L_\alpha)}{(S^2 + 2ZWS + W^2)S} \quad \frac{\theta}{\delta_{LONG}} = \frac{K_s W^2(S + L_\alpha)}{(S^2 + 2ZWS + W^2)(S + K_\theta L_\alpha)} \quad \frac{\theta}{\delta_{LONG}} = \frac{K_s W^2}{(S^2 + 2ZWS + W^2)}$$

Figure 44. LAND and TRAN Mode Longitudinal Control Laws and Equivalent Systems

LAND Mode:

$K_\theta = 0.0$

TRAN Mode and RCAH Modes:

$K_\theta = F111$

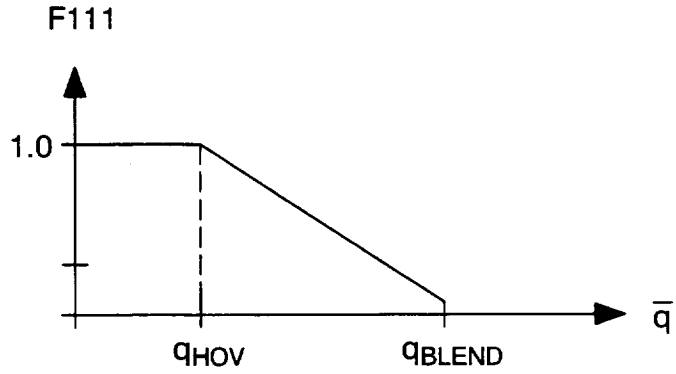

$q_{HOV} = \bar{q} @ V_{KEAS} = 35$ knots

$q_{BLEND} = \bar{q} @ V_{KEAS} = 70$ knots

Figure 45. Transition/Hover Feedback Blending Schedules

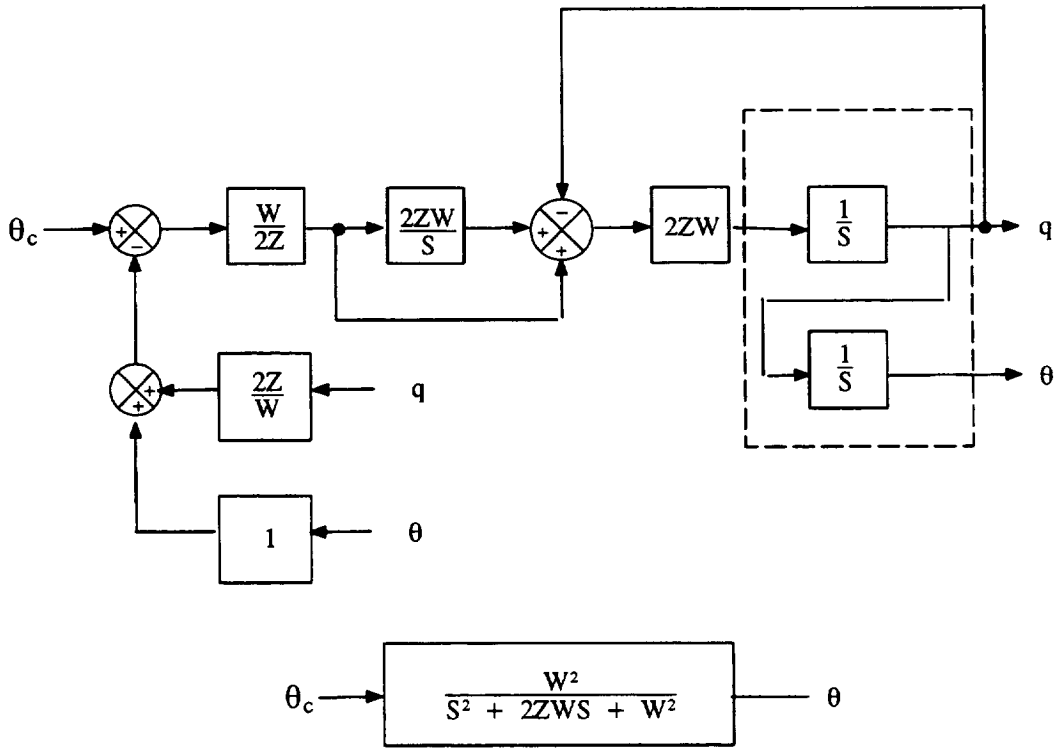

Figure 46. Pitch Attitude Command Control Laws and Equivalent System

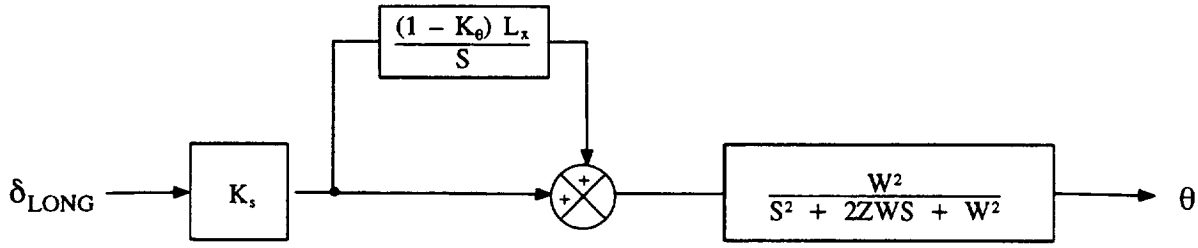

RCAH ($K_\theta = 0$) | Blend to Attitude Command ($0 < K_\theta < 1$) | Attitude Command ($K_\theta = 1$)

$$\frac{q}{\delta_{LONG}} = \frac{K_s W^2 (S + L_\alpha)}{(S^2 + 2ZWS + W^2)} \qquad \frac{q}{\delta_{LONG}} = \frac{K_s W^2 [S + (1 - K_\theta) L_\alpha]}{(S^2 + 2ZWS + W^2)} \qquad \frac{q}{\delta_{LONG}} = \frac{K_s W^2 S}{(S^2 + 2ZWS + W^2)}$$

$$\frac{\theta}{\delta_{LONG}} = \frac{K_s W^2 (S + L_\alpha)}{(S^2 + 2ZWS + W^2) S} \qquad \frac{\theta}{\delta_{LONG}} = \frac{K_s W^2 [S + (1 - K_\theta) L_\alpha]}{(S^2 + 2ZWS + W^2)} \qquad \frac{\theta}{\delta_{LONG}} = \frac{K_s W^2}{(S^2 + 2ZWS + W^2)}$$

Figure 47. Longitudinal RCAH Control Laws and Equivalent Systems TRAN–RCAH, ACT–MT, ACT–AT, VET Modes

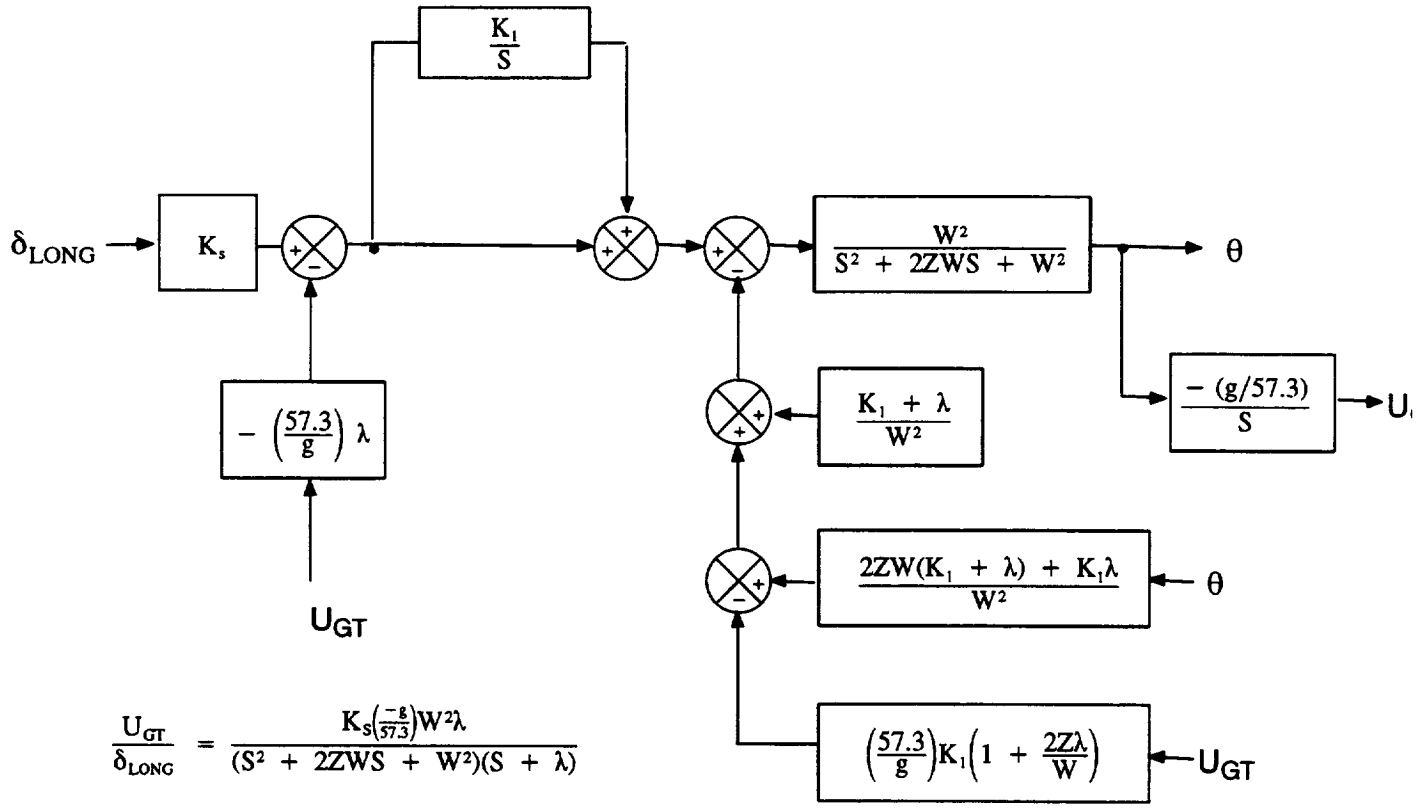

$$\frac{U_{GT}}{\delta_{LONG}} = \frac{K_s\left(\frac{-g}{57.3}\right)W^2\lambda}{(S^2 + 2ZWS + W^2)(S + \lambda)}$$

Figure 48. Longitudinal TRC Mode Control Laws and Equivalent System

Lateral/Directional Core Control Laws

The lateral/directional control laws also utilize nonlinear decoupling and deaugmenting feedbacks, as shown in Figure 230. These feedbacks provide the control laws with commands for stability axis roll and yaw acceleration for which the aircraft's response is approximately the integral of the respective command variable. Feedbacks are then used to reaugment the aircraft for proper flying qualities for the directional axis.

Lateral Axis Core Control Laws

The lateral axis control laws compute the Control Mixer command, RBCMD, based on the lateral stick position.

Figure 49 shows the CONV mode lateral control laws, consisting of a simple roll rate feedback with a gain to set the equivalent system roll rate damping. The equivalent system damping, shown in Figure 50, is set proportional to the airspeed. In LAND mode, the lateral control laws are the same as in CONV mode.

The TRAN mode control laws are shown in Figure 51. The control laws blend from a rate to an attitude command system along the same schedule used in the pitch axis, Figure 45. A proportional plus integral gain is used to stabilize the aircraft when hovering in ground effect. This instability is caused by a positive L_ϕ derivative of roll acceleration due to roll angle that occurs with asymmetric suckdown on one wing coupled with the fountain upwash on the opposite wing for nonzero roll angles. The L_ϕ derivative is a function of gear height, an integrator gain of about 3 is sufficient to stabilize the aircraft at all gear heights.

All other landing modes use a RCAH command system in the lateral axis. The RCAH control laws use the landing mode control laws from Figure 51 as an inner loop, with the K_θ schedule set to 1 at all airspeeds, as shown in Figure 52. This inner loop structure provides an attitude command system which is used to build a roll RCAH command system by adding a proportional plus integral filter in the forward loop, Figure 53, and provides a typical first order roll rate response at higher airspeeds. Attitude hold is provided, as the output of the integrator loads up to the proper attitude command to hold attitude. A blend to an attitude command system is achieved by scheduling the integrator gain to zero as a function of airspeed using the schedule in Figure 45. The feedback gains are also scheduled with airspeed to provide a second order attitude response in hover.

When below 80 knots airspeed, a precision hover mode switch is enabled which allows the pilot to select to TRC system. The translational rate control laws for the roll axis also use the attitude control laws from Figure 52 as an inner loop. As shown in Figure 54, the TRC control laws are implemented as an outer loop driving the attitude command system control laws. The resulting equivalent systems dynamics, Figure 54, show that the velocity damping is augmented by these control laws so that the lateral stick commands inertial crosstrack velocity. Integral control is provided so that the same trimmed stick position commands the same crosstrack velocity in all flight conditions.

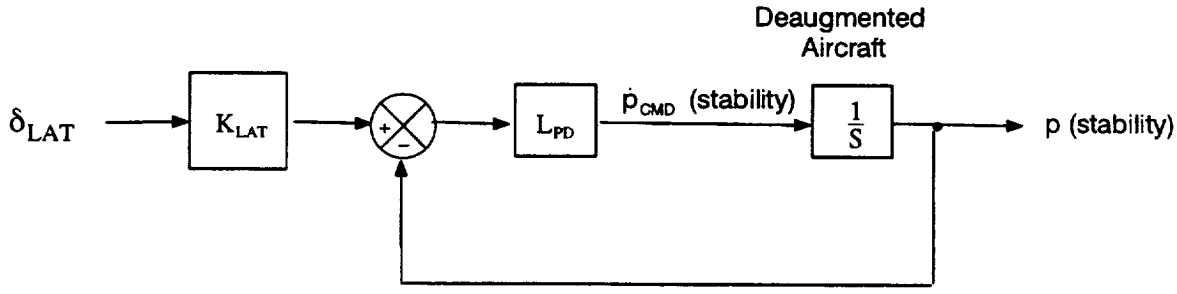

$$\frac{p}{\delta_{LAT}} = \frac{K_{LAT}L_{PD}}{S + L_{PD}}$$

Figure 49. CONV and LAND Mode Lateral Control Laws and Equivalent System

$$\frac{p}{\delta_{LAT}} = \frac{K_{LAT}L_{PD}}{S + L_{PD}}$$

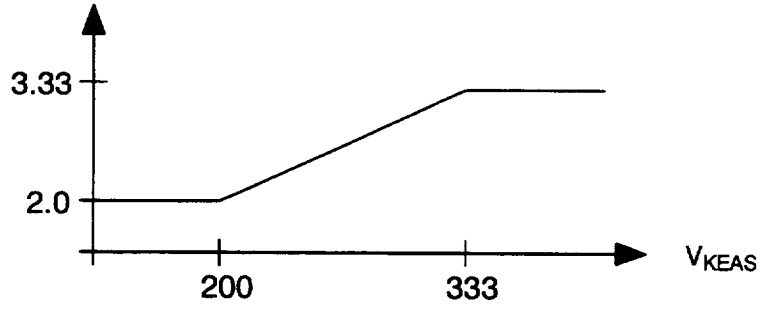

Use Roll Damping = $\frac{V_{KEAS}}{100} = L_{PD}$

Upper Limit = 3.33 $\tau_R = 0.3$

Lower Limit = 2.0 $\tau_R = 0.5$

Figure 50. Roll Damping

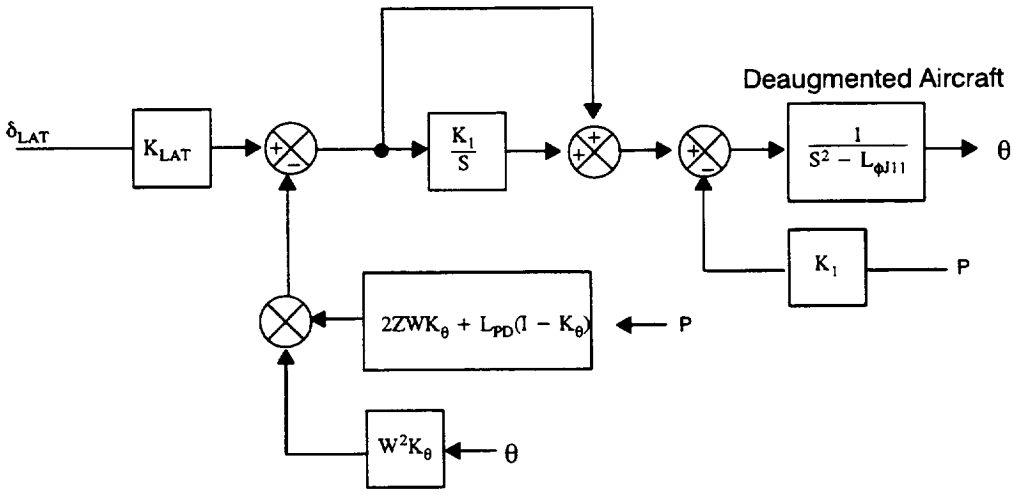

Rate Command ($K_\theta = 0$)

Blend to Attitude Command ($0 < K_\theta < 1$)

Attitude Command ($K_\theta = 1$)

$$\frac{p}{\delta_{LAT}} = \frac{K_{LAT}}{S + L_{PD}} \qquad \frac{P}{\delta_{LAT}} = \frac{K_{LAT}S}{S^2 + [2ZWK_\theta + L_{PD}(1-K_\theta)]S + W^2K_\theta} \qquad \frac{p}{\delta_{LAT}} = \frac{K_{LAT}S}{S^2 + 2ZWS + W^2}$$

$$\frac{\phi}{\delta_{LAT}} = \frac{K_{LAT}}{S(S + L_{PD})} \qquad \frac{\phi}{\delta_{LAT}} = \frac{K_{LAT}}{S^2 + [2ZWK_\theta + L_{PD}(1 - K_\theta)]S + W^2K_\theta} \qquad \frac{\phi}{\delta_{LAT}} = \frac{K_{LAT}}{S^2 + 2ZWS + W^2}$$

Figure 51. TRAN Mode Lateral Control Laws and Equivalent Systems ($2ZWK_1 >> L\phi J1_1$)

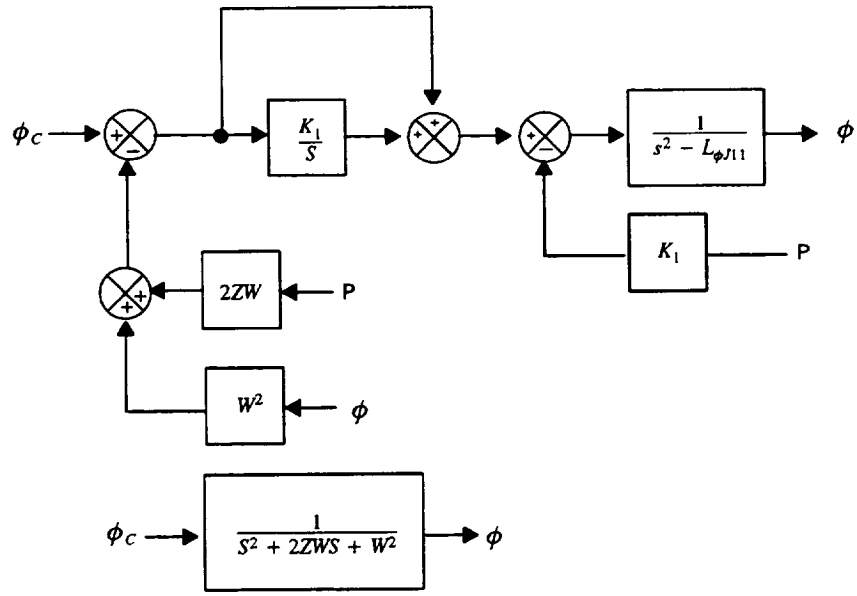

Figure 52. Roll Attitude Control Laws and Equivalent System ($2ZWK_1 >> L_{\Phi J11}$)

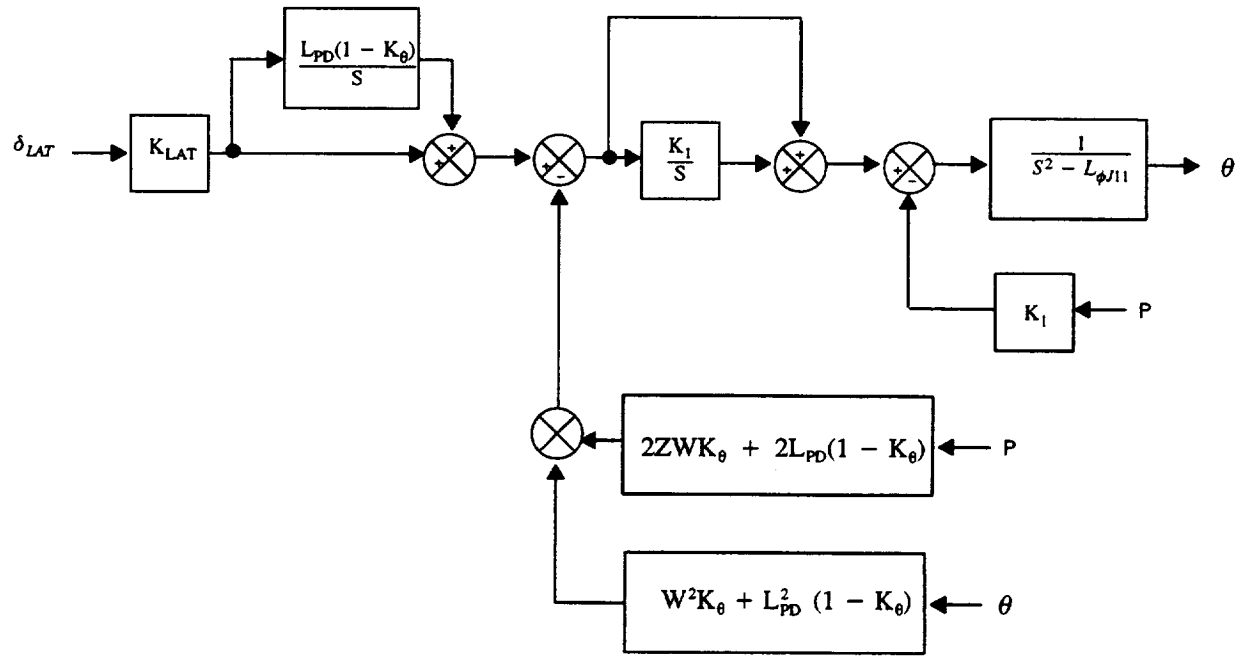

RCAH ($K_\theta = 0$)

$$\frac{p}{\delta_{LAT}} = \frac{K_{LAT}}{S + L_{PD}} \qquad \frac{\phi}{\delta_{LAT}} = \frac{K_{LAT}}{s(s + L_{PD})}$$

Blending to Attitude Command ($0 < K_\theta < 1$)

$$\frac{p}{\delta_{LAT}} = \frac{K_{LAT}[S + L_{PD}(1 - K_\theta)]}{[S^2 + [2ZWK_\theta + 2L_{PD}(1 - K_\theta)]S + [W^2K_\theta + L_{PD}^2(1 - K_\theta)]]}$$

$$\frac{\phi}{\delta_{LAT}} = \frac{K_{LAT}[S + L_{PD}(1 - K_\theta)]}{S[S^2 + [2ZWK_\theta + 2L_{PD}(1 - K_\theta)]S + [W^2K_\theta + L_{PD}^2(1 - K_\theta)]]}$$

Attitude Command ($K_\theta = 1$)

$$\frac{p}{\delta_{LAT}} = \frac{K_{LAT}S}{S^2 + 2ZWS + W^2} \qquad \frac{\phi}{\delta_{LAT}} = \frac{K_{LAT}}{S^2 + 2ZWS + W^2}$$

Figure 53. Lateral RCAH Control Laws and Equivalent Systems TRAN–RCAH, ACT–MT, ACT–AT, VET ($2ZWK_1 >> L_{\Phi J11}$)

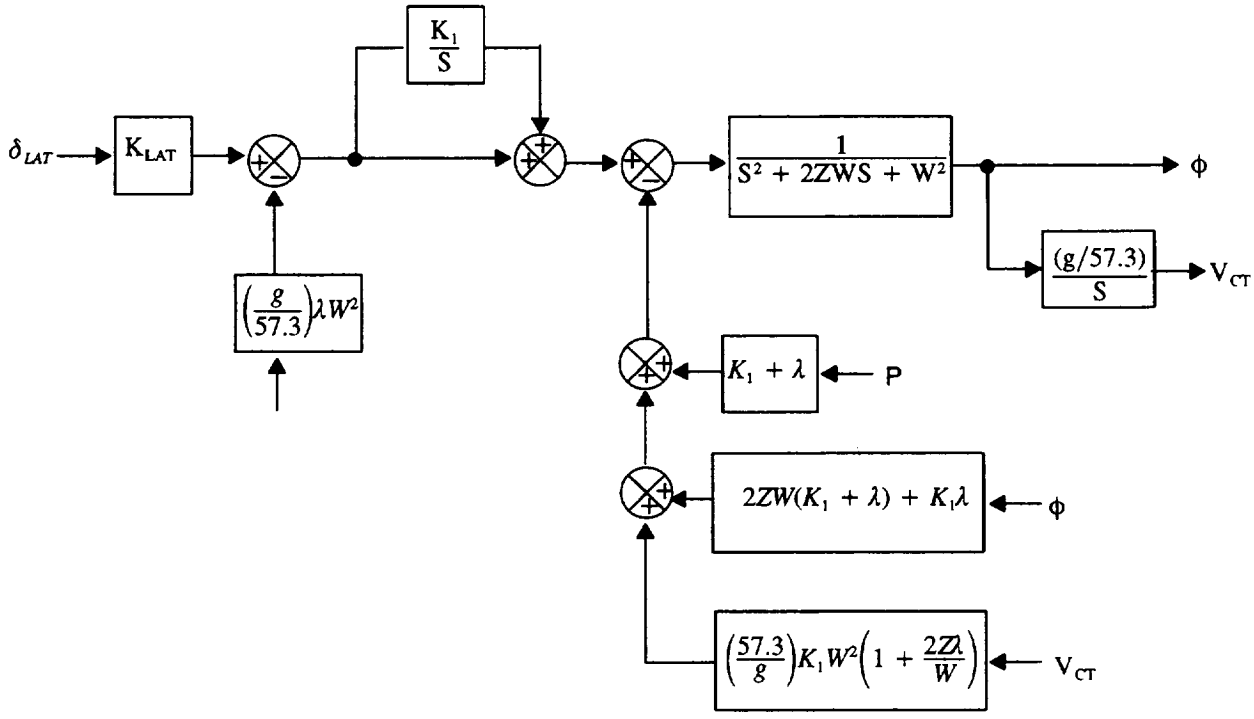

$$\frac{V_{CT}}{\delta_{LAT}} = \frac{\left(\frac{g}{57.3}\right)K_{LAT}}{(S^2 + 2ZWS + W^2)(S + \lambda)}$$

Figure 54. Lateral TRC Mode Control Laws and Equivalent System

Directional Axis Core Control Laws

The directional axis control laws compute the Control Mixer command, YBCMD, based on the rudder pedal position.

The directional control laws are shown in Figure 55, with the sideslip and yaw rate equivalent system closed loop responses. In CONV mode, the control system commands stability axis yaw acceleration with a sideslip error for turn coordination and sideslip rate to improve dutch roll damping. The yaw rate feedback is set to zero. The equivalent system dutch roll frequency is specified by computing the control power from the tails available for augmentation, and is specified proportional to airspeed. The control laws for LAND mode are the same as CONV.

The directional axis control laws for all of the powered lift modes use the structure shown in Figure 55, where the sideslip and sideslip rate feedbacks are scheduled down to zero as airspeed decreases, as shown in Figure 56. Along a complementary schedule, the yaw rate feedback is increased from zero to its proper value in hover, as shown in Figure 56. This scheduling provides a blend from a sideslip/turn coordination command system at higher airspeeds to a yaw rate command system in hovering flight.

Thrust Axis Core Control Laws

The thrust axis control laws compute the Control Mixer commands, FXCMD and FZCMD, from the throttle position and either the nozzle lever position or the thumbwheel position, depending on the control mode.

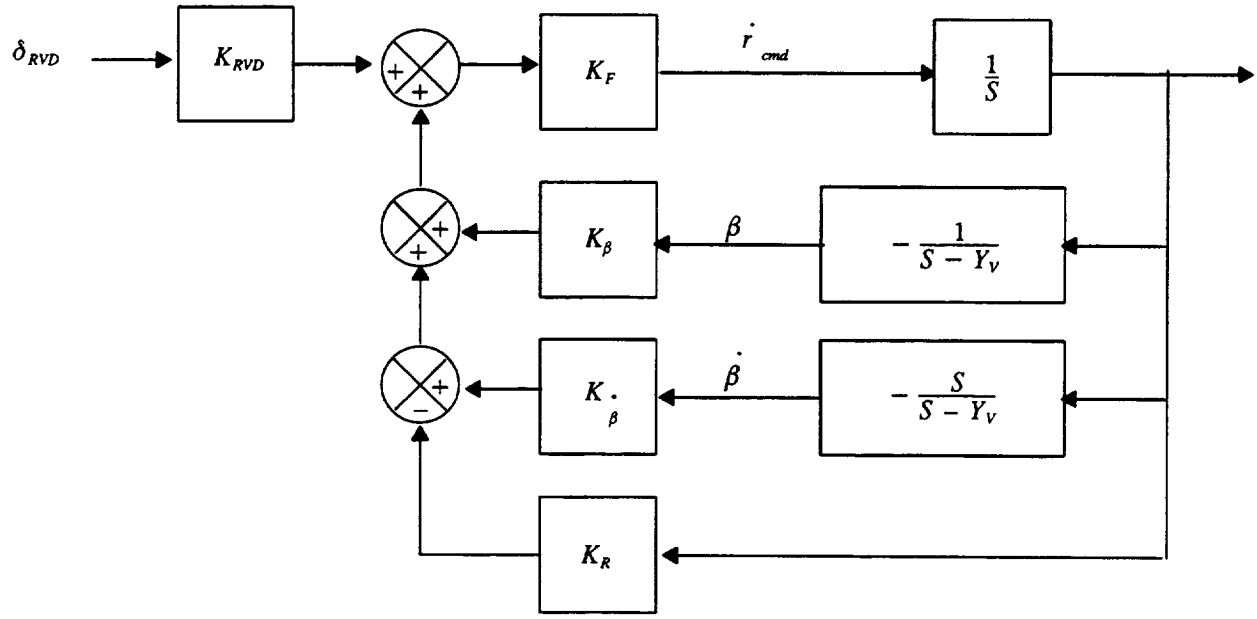

$$\frac{r}{\delta_{RUD}} \cong \frac{K_{RUD}\, K_F S}{S_2 + K_F(K_\beta + K_r)S + K_F K_\beta)}$$

$$\frac{\beta}{\delta_{RVD}} \cong \frac{-\,K_{RUD}\, K_F}{S_2 + K_F(K_\beta + K_r)S + K_F K_\beta)}$$

Figure 55. Directional Axis Control Laws and Equivalent Systems All Modes

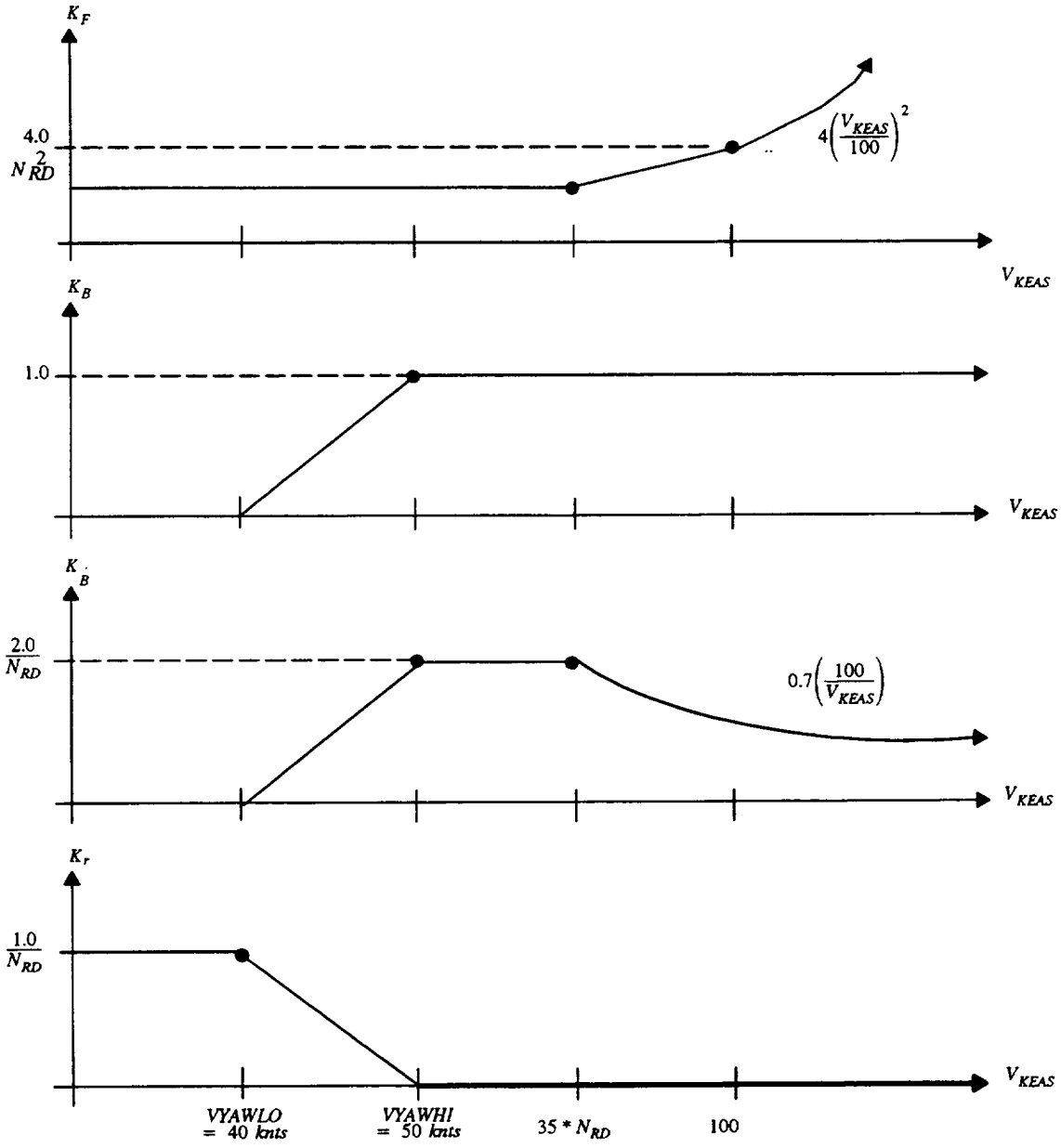

$V_{KEAS} > 100$

$$\frac{\beta}{\delta_{RUD}} = \frac{-K_{RUD}W^2}{S^2 + 2ZWS + W^2}$$

$$\frac{r}{\delta_{RUD}} = \frac{-K_{RUD}W^2S}{S^2 + 2ZWS + W^2}$$

$Z = 0.7$ and $W = 2\left(\frac{V_{KEAS}}{100}\right)$

$V_{KEAS} < VYAWLO$

$$\frac{\beta}{\delta_{RUD}} = \frac{-K_{RUD}N^2_{RD}}{(S + N_{RD})}$$

$$\frac{r}{\delta_{RUD}} = \frac{K_{RUD}N^2_{RD}}{(S + N_{RD})}$$

$N_{RD} = 2.0$

Figure 56. Directional Axis Gains and Equivalent Systems

CONV and LAND Modes

When one of these modes is engaged, the powered lift system is off and the nozzle lever and the thumbwheel are inactive. The throttle lever position sets PLA according to the schedule in Figure 57. The core control laws set FZCMD to zero, and computes FXCMD by multiplying a rate limited PLA command by the maximum available thrust (a feedback from the propulsion control), Figure 58.

TRAN and TRAN–RCAH Modes

When one of these modes is engaged, the powered lift system is active, and the thrust vector angle is commanded by the nozzle lever, Figure 59. The throttle commands PLA along the same schedule as the CONV and LAND modes, Figure 57.

The thrust axis core control laws are shown in Figure 60. Above 80 knots airspeed, the throttle and nozzle lever positions are converted to thrust and thrust vector commands, which are then converted to FXCMD and FZCMD commands through a simple polar to Cartesian transformation. Below 80 knots, a height damping feedback is blended in to improve altitude rate response to the throttle in hovering flight.

Thrust Axis Deaugmentation

For the other STOVL modes, ACT–MT, ACT–AT, and VET, the core control laws use a design procedure whereby deaugmentation feedbacks are used to provide the control laws with a command variable which is approximately the integral of the controlled variable.

A wind referenced deaugmentation network for the thrust axis is shown in Figure 61. Using standard equations of motion for path velocity, $V_P = V_T \cos\beta$, and angle of attack, α, and neglecting engine dynamics, it can be shown that the path velocity and angle of attack are approximately proportional to the integrals of the command variables, δ_{NL}, and δ_{TL}.

A similar ground referenced deaugmentation network for the thrust axis is shown in Figure 62. Here, the groundtrack velocity and the altitude rate are approximately the integrals of the command variables, δ_{NL}, and δ_{TL}.

In the autothrottle control modes, ACT–AT and VET, the throttle controls angle of attack at higher transition speeds, and altitude rate at lower speeds. Thus these two deaugmentation networks are blended together along the same airspeed schedule as the control laws, using the pitch axis rate to attitude command blending schedule, as shown in Figure 63.

ACT–MT Mode

In this mode the throttle control laws are the same as TRAN and TRAN–RCAH. The nozzle lever is made inactive, and a thumbwheel controls inertial groundtrack acceleration. Figure 64 shows the command schedule, with a maximum thumbwheel deflection of ±100 degrees (+ is forward and – is aft) commanding 10 ft/sec^2 of groundtrack acceleration.

The thumbwheel control laws, Figure 65, are taken from Reference 9. The thumbwheel commands grountrack acceleration with a zero thumbwheel input holding the current velocity.

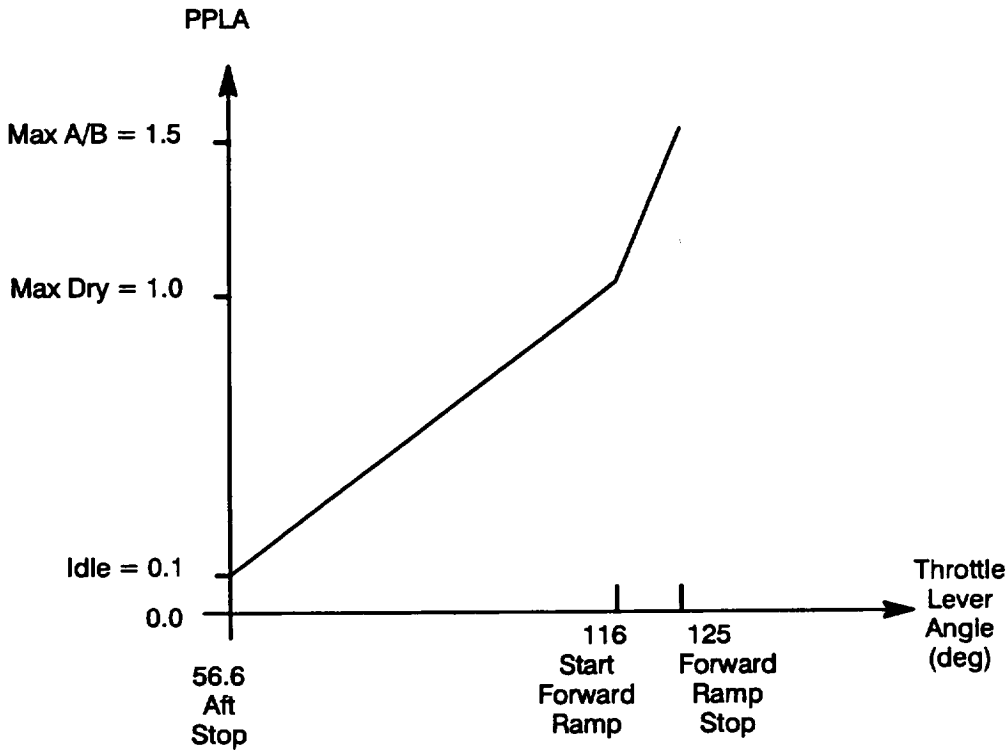

Figure 57. Throttle Lever to PLA Command CONV, LAND, TRAN, TRAN–RCAH, ACT–MT

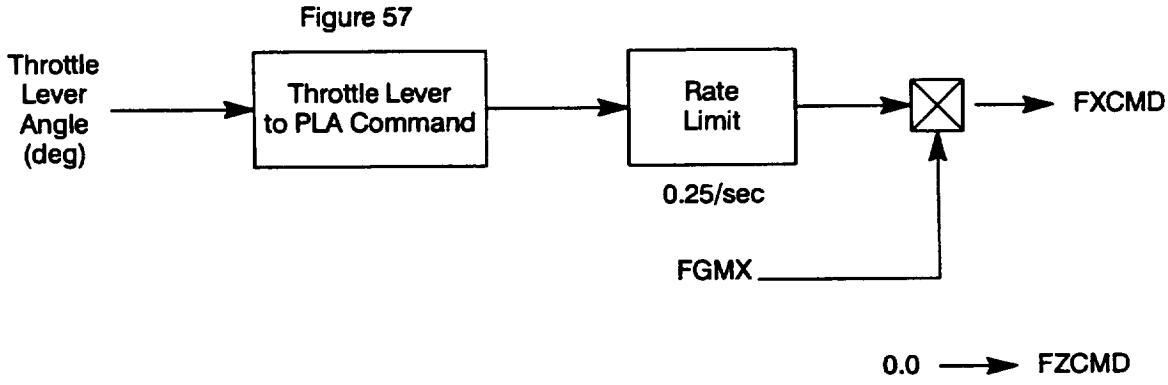

Figure 58. Thrust Axis Control Laws CONV, LAND Modes

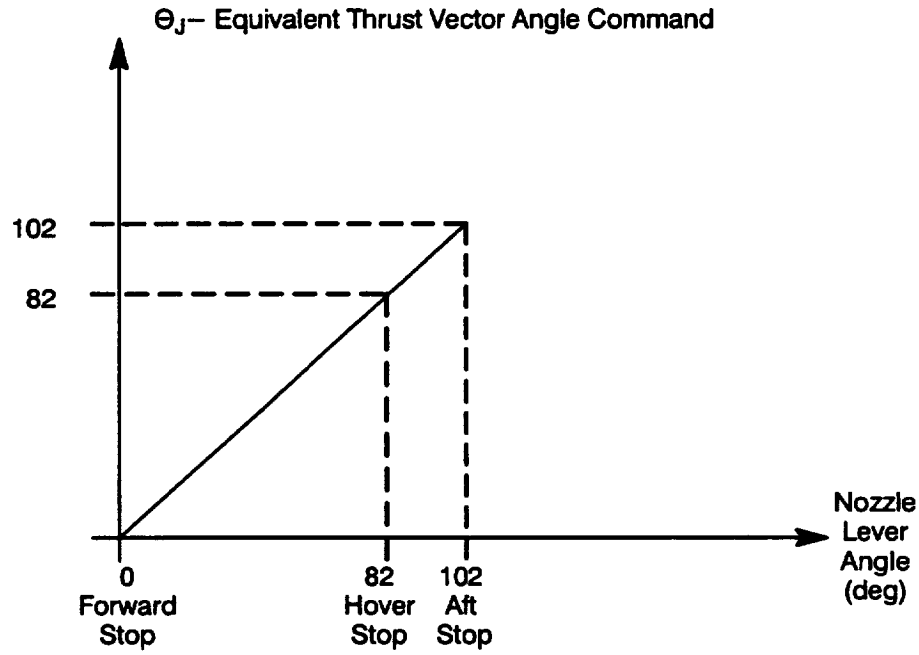

Figure 59. Nozzle Lever to Jet Angle Command TRAN, TRAN–RCAH

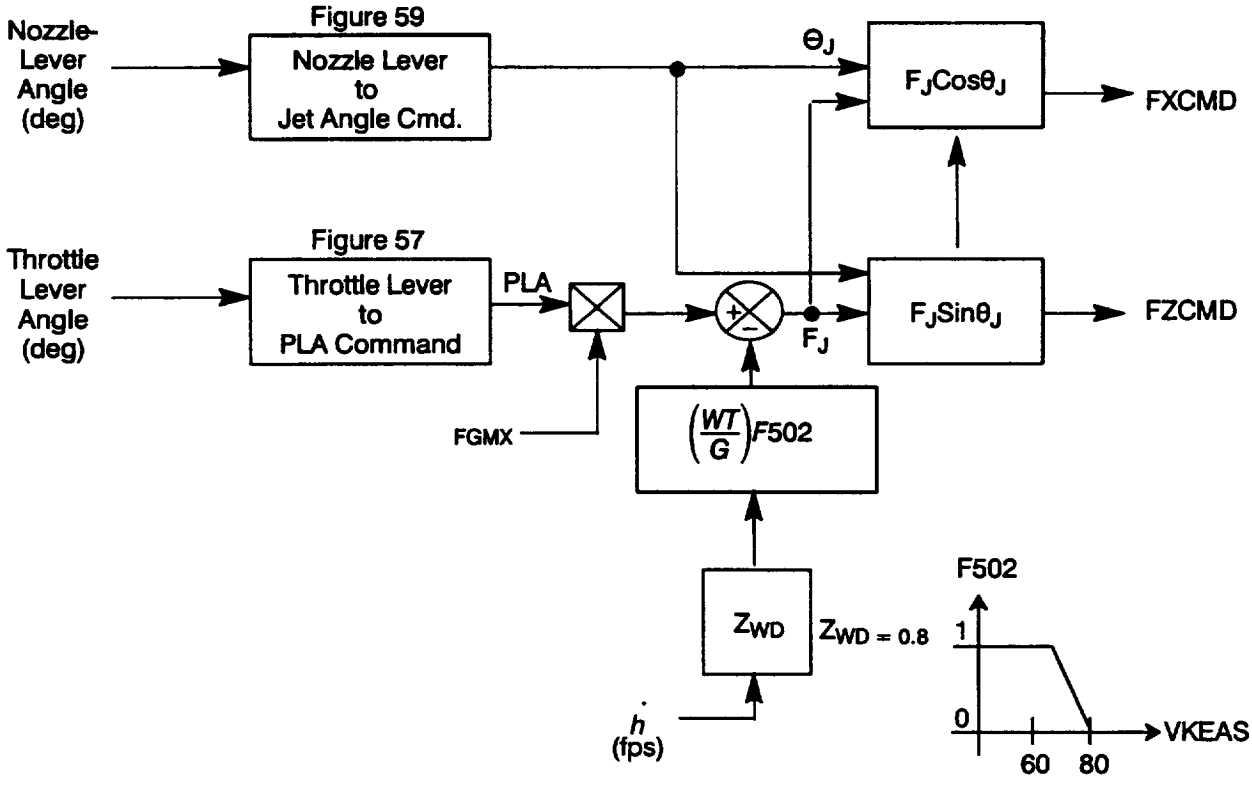

Figure 60. Thrust Axis Control Laws TRAN, TRAN–RCAH Modes

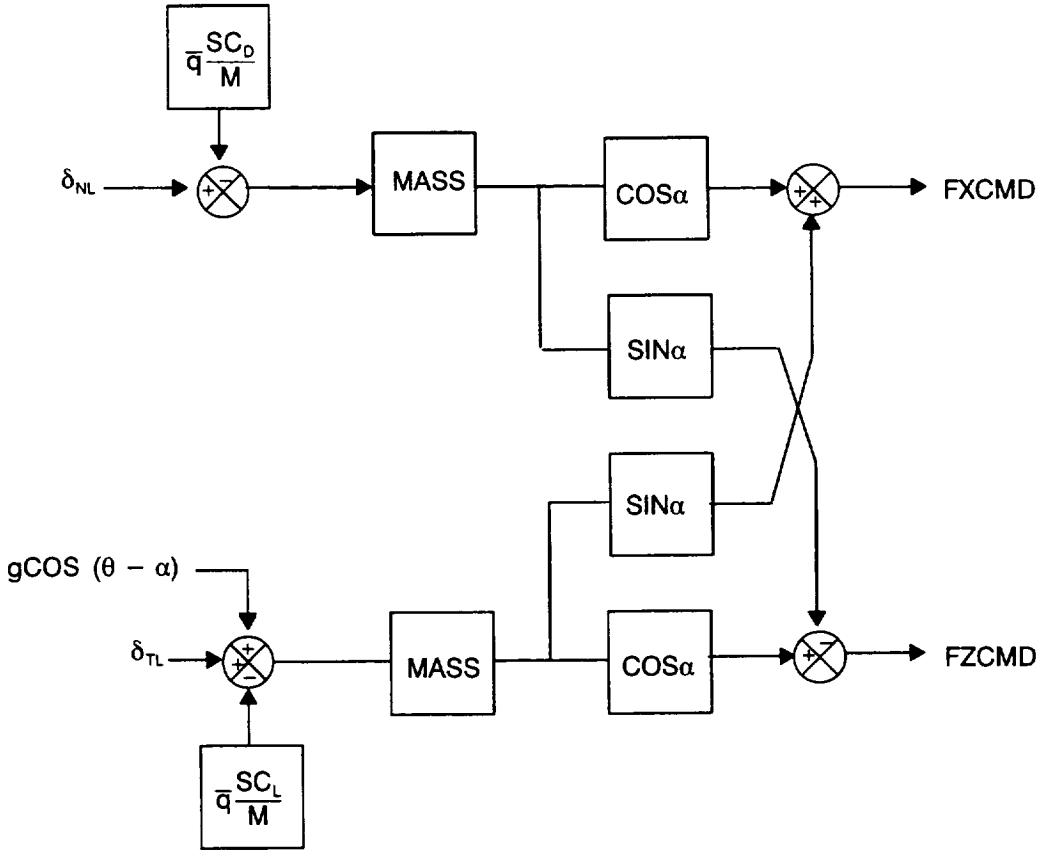

$V_P = V_T COS\beta$

$$\frac{Vp}{\delta_{NL}} = \frac{1}{S}$$

$$\frac{\alpha}{\delta_{TL}} = \frac{-V}{S}$$

Figure 61. Transition Deaugmentation – Wind Referenced

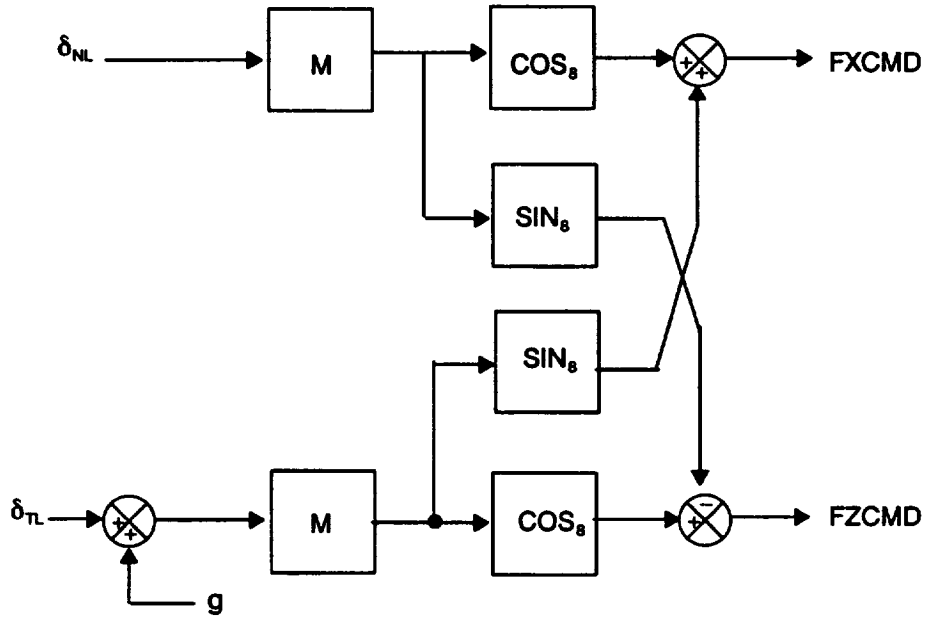

$$\frac{u_{GT}}{\delta_{NL}} = \frac{1}{S}$$

$$\frac{\dot{h}}{\delta_{TL}} = \frac{1}{S}$$

Figure 62. Transition Deaugmentation – Inertially Referenced

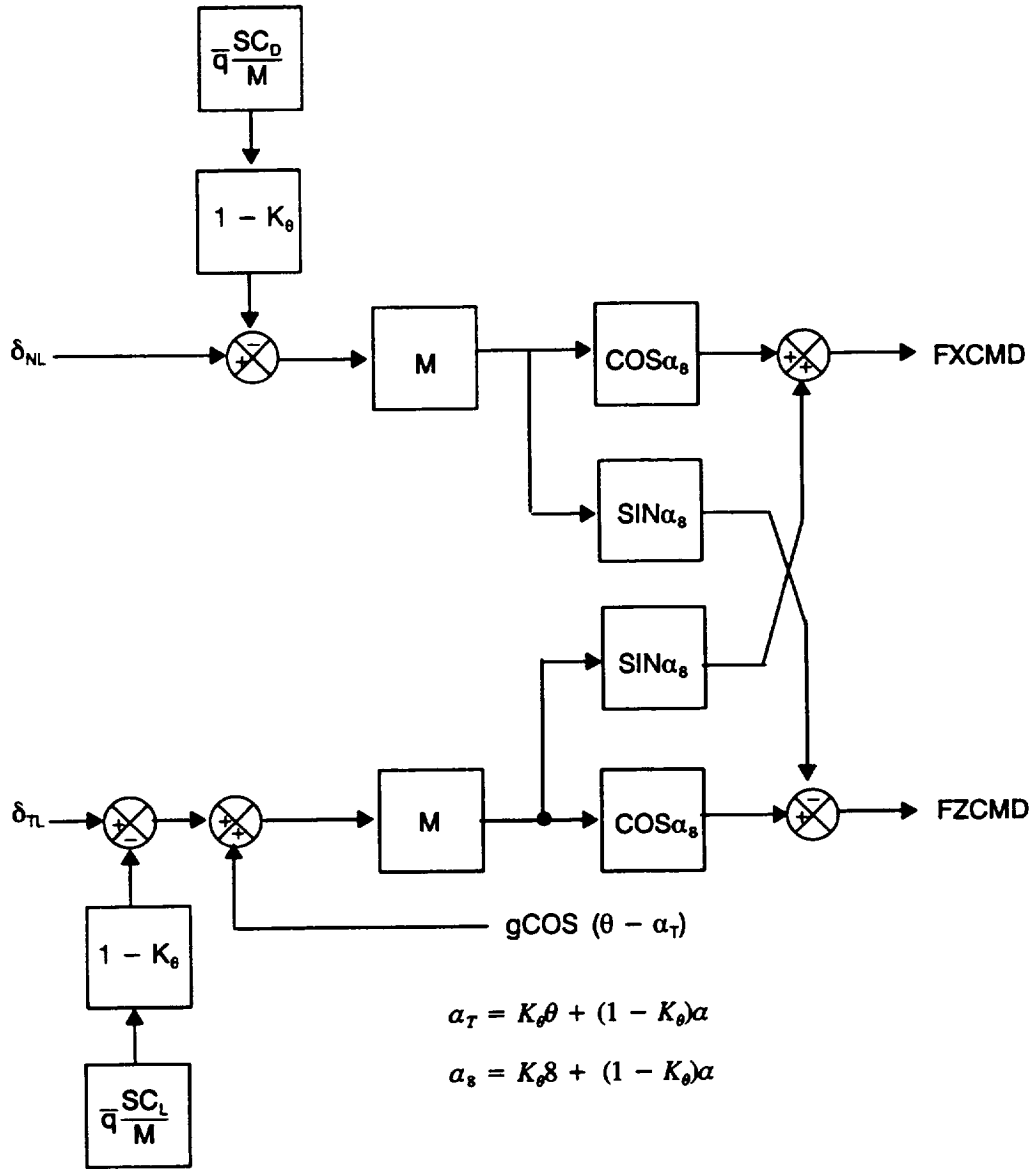

Figure 63. Thrust Axis Deaugmentation

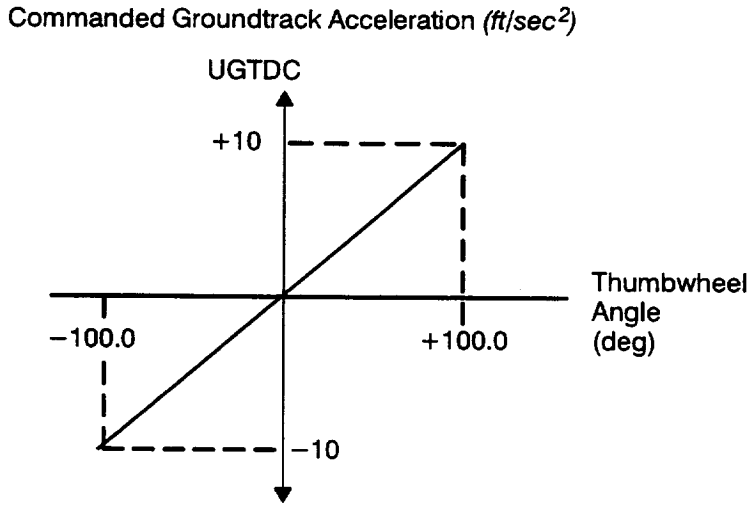

Figure 64. Thumbwheel Angle to Acceleration Command ACT−MT, ACT−AT Modes

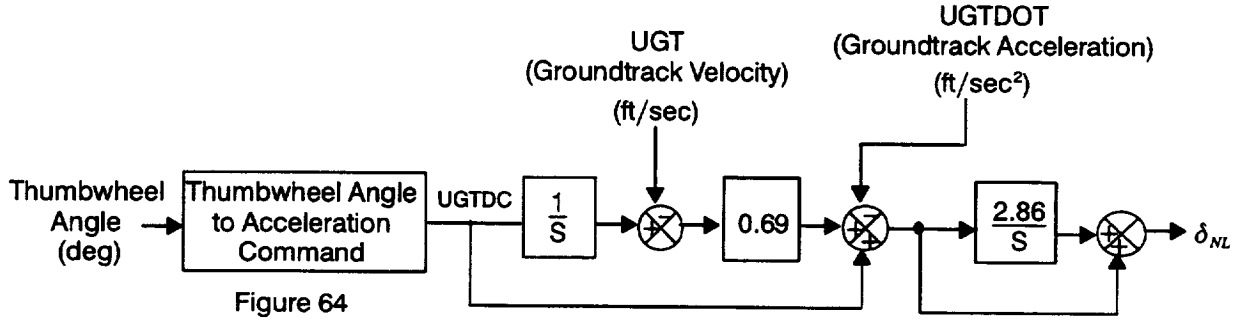

Figure 64

Figure 65. Thumbwheel Control Laws & Equivalent System Dynamics ACT−MT, ACT−AT

The complete thrust axis control laws are in Figure 66. The throttle control laws are similar to Figure 60, except the output of the polar to cartesian conversion is passed through the deaugmentation network. The thumbwheel command is deaugmented and converted to an equivalent thrust vector command before being passed to the polar to cartesian conversion.

ACT–AT Mode

The ACT–AT mode uses the thumbwheel control laws from Figure 65. Thus the ACT–AT Mode is the same as ACT–MT except for the throttle control laws. ACT–AT employs an autothrottle that controls the aircraft's approach angle of attack at higher transition airspeeds, and altitude rate at lower airspeeds. Figure 67 illustrates the conversion of the throttle lever position to commanded angle of attack and altitude rate.

At higher airspeeds the throttle controls angle of attack referenced to 8 degrees. The control laws shown in Figure 68 result in a first order angle of attack response with a natural frequency proportional to airspeed. This result can be derived through straightforward calculation by assuming that the angle of attack response is approximately the integral of the command, δ_{TL}. The inertially referenced control laws in Figure 69 are similar to those in Figure 68, providing a first order altitude rate response to throttle inputs.

The complete autothrottle control laws are shown in Figure 70, where the wind referenced control laws are blended with the inertially referenced control laws between 60 and 80 knots airspeed.

VET Mode

The VET mode employs the same autothrottle control laws as the ACT–AT mode. The thumbwheel is made inactive and replaced with the nozzle lever, which commands aircraft's speed (instead of thrust vector angle). The nozzle lever to speed command schedule, Figure 71, has a 6 degree deadband at the forward stop. When the mode is engaged, the nozzle lever is in the deadband. The control laws sample the current speed, and holds that speed until the nozzle lever is moved out of the deadband. Six degrees nozzle lever position indicates 180 knots, the hover stop at 82 degrees commands zero speed. The nozzle lever may be moved over the hover stop to the braking stop, which commands −47 knots aft speed.

At high transition speeds the nozzle lever controls path velocity, using the control laws in Figure 72, which provide a first order airspeed response to nozzle lever position as shown in Figure 72. At low transition speeds, the nozzle lever commands groundtrack velocity, Figure 73, using control laws similar to Figure 72. These control laws are blended together, Figure 74, using the pitch axis rate/attitude command blending schedule.

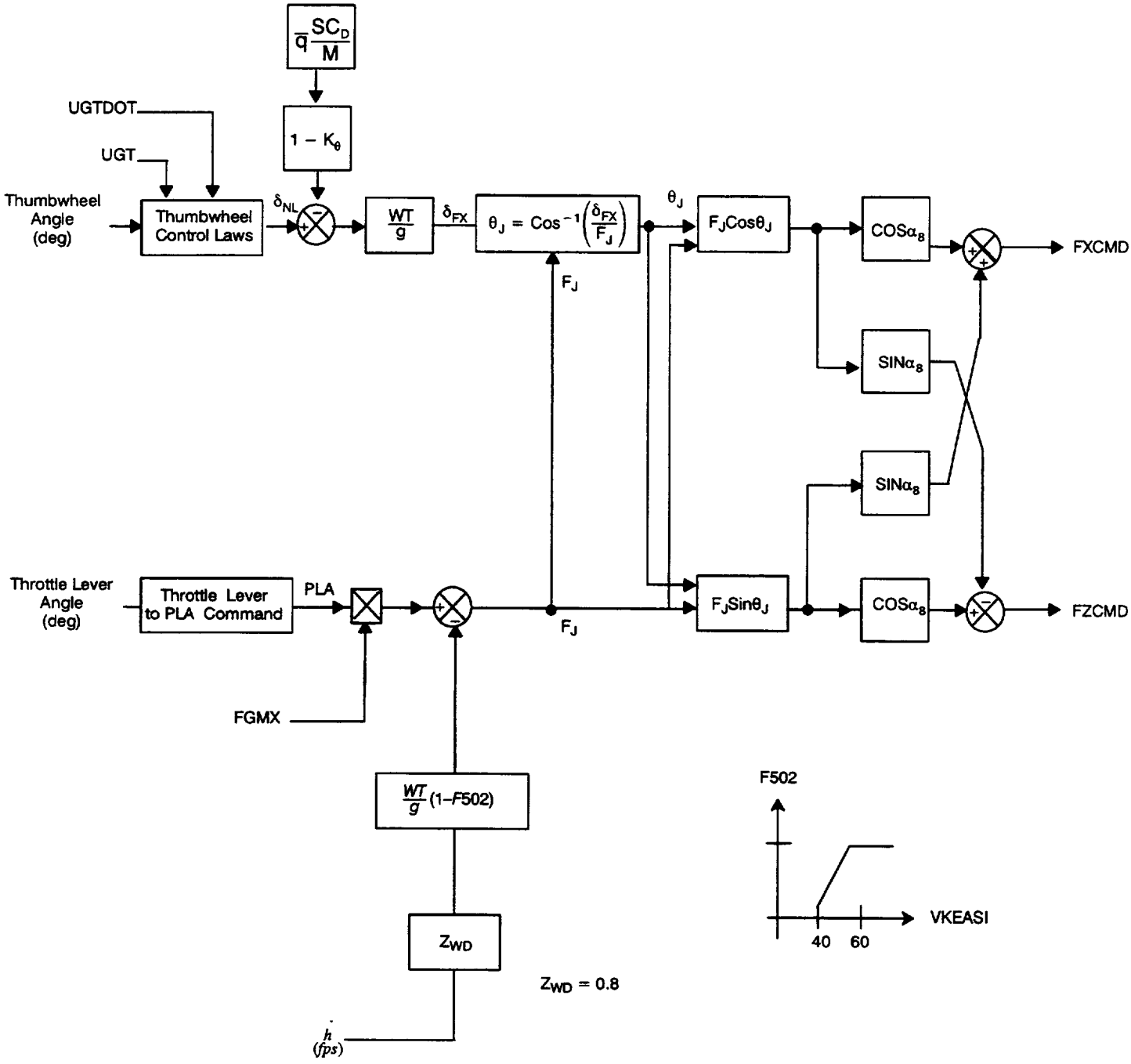

Figure 66. Thrust Axis Control Laws

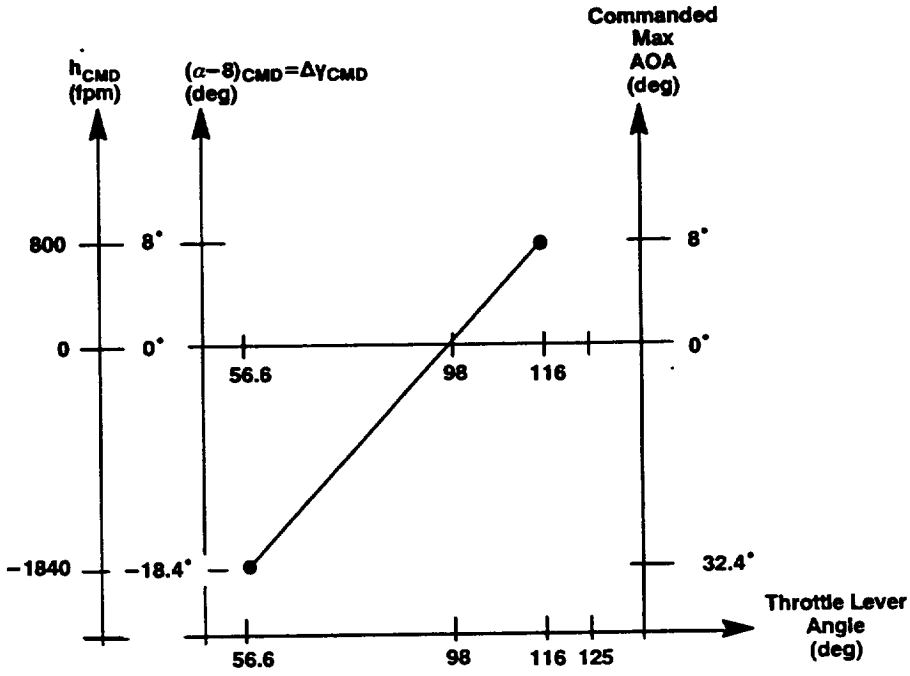

Figure 67. Throttle Angle Schedule for Computing $(\alpha-8)_{CMD}$

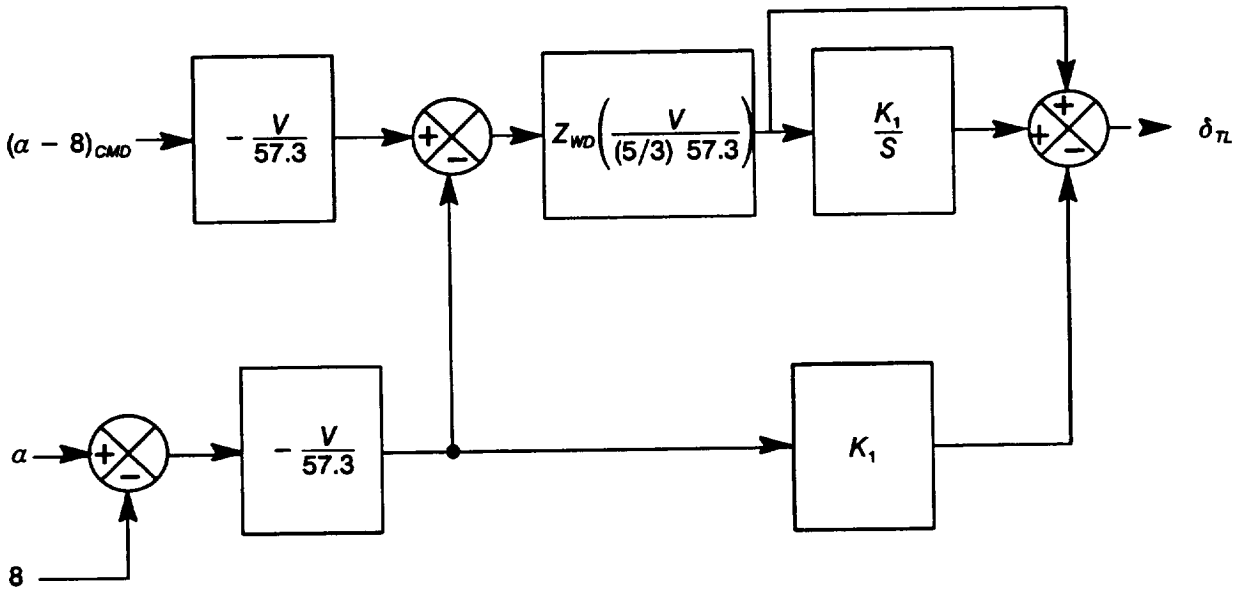

$$\frac{(\alpha - 8)}{(\alpha - 8)_{CMD}} = \frac{Z_{WD}\left(\frac{V}{5/3\ 57.3}\right)}{S + Z_{WD}\left(\frac{V}{5/3\ 57.3}\right)} \qquad Z_{WD} = 0.8$$

Figure 68. Autothrottle Control Laws – Wind Referenced

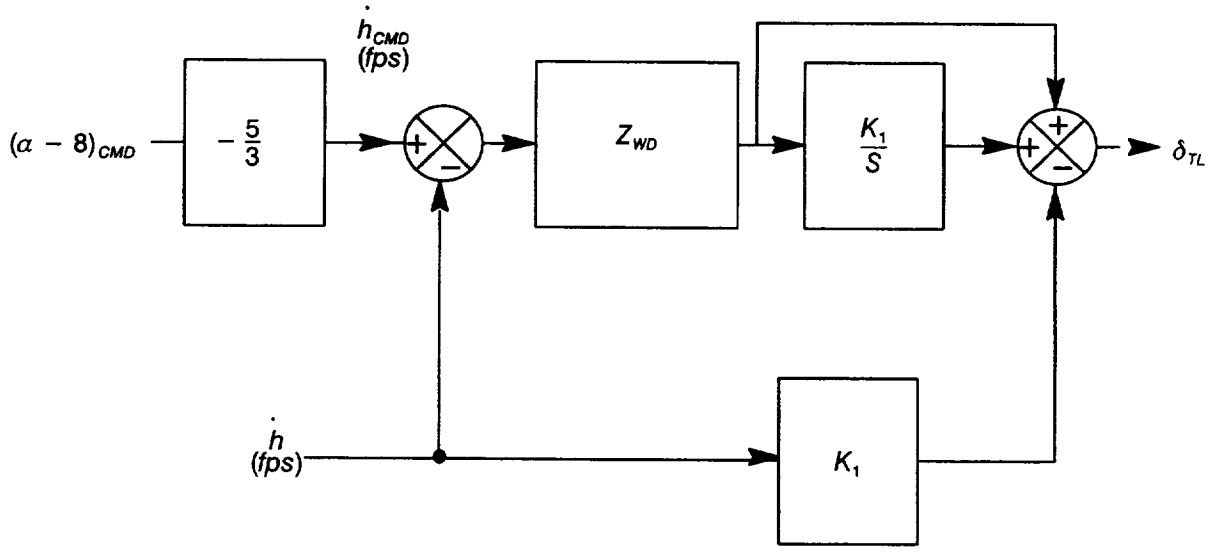

$$\frac{\dot{h}}{\dot{h}_{CMD}} = \frac{Z_{WD}}{S + Z_{WD}} \quad Z_{WD} = 0.8$$

Figure 69. Autothrottle Control Laws– Inertially Referenced ACT–AT, VET

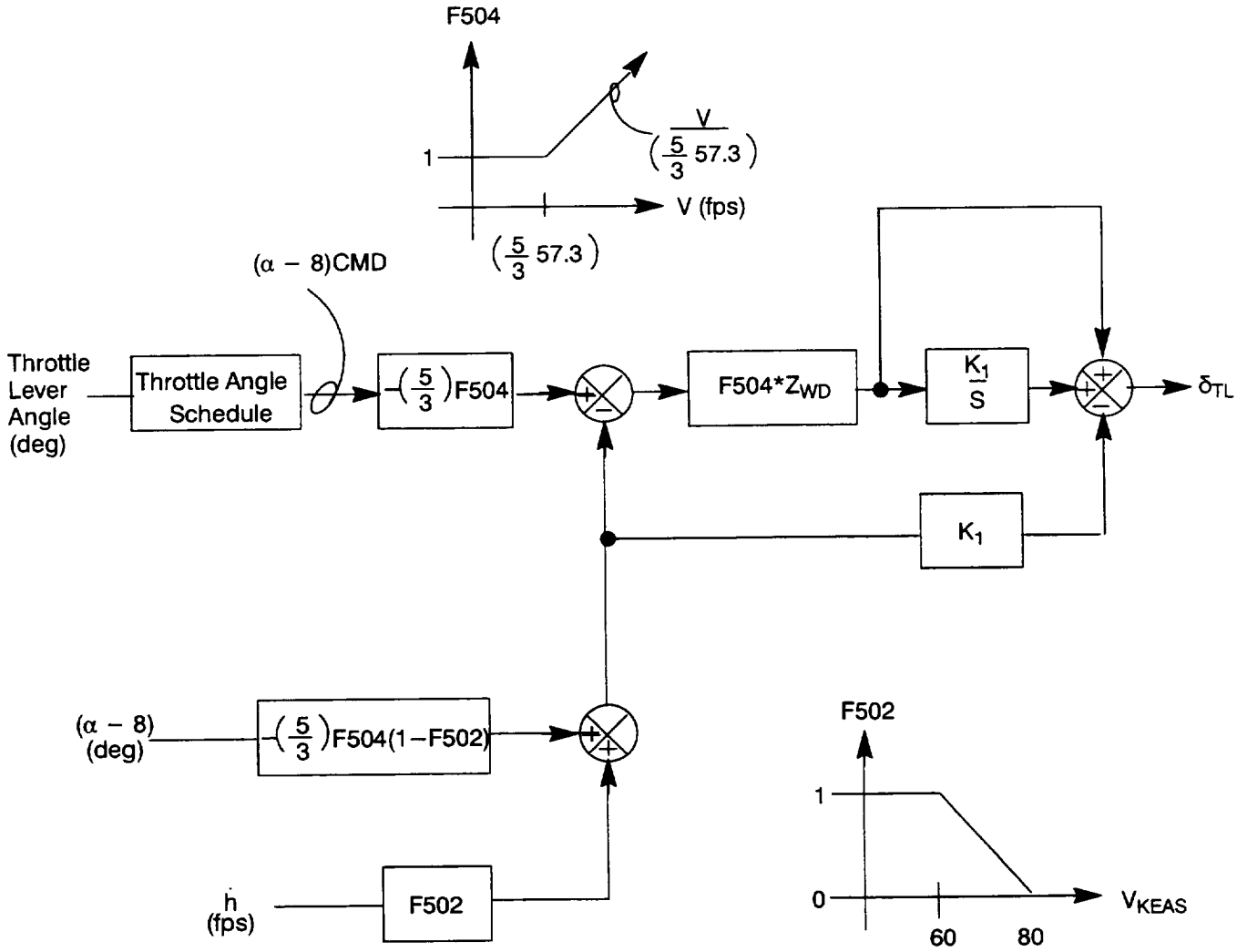

Figure 70. Thrust Axis Control Laws–Autothrottle ACT–AT,VET

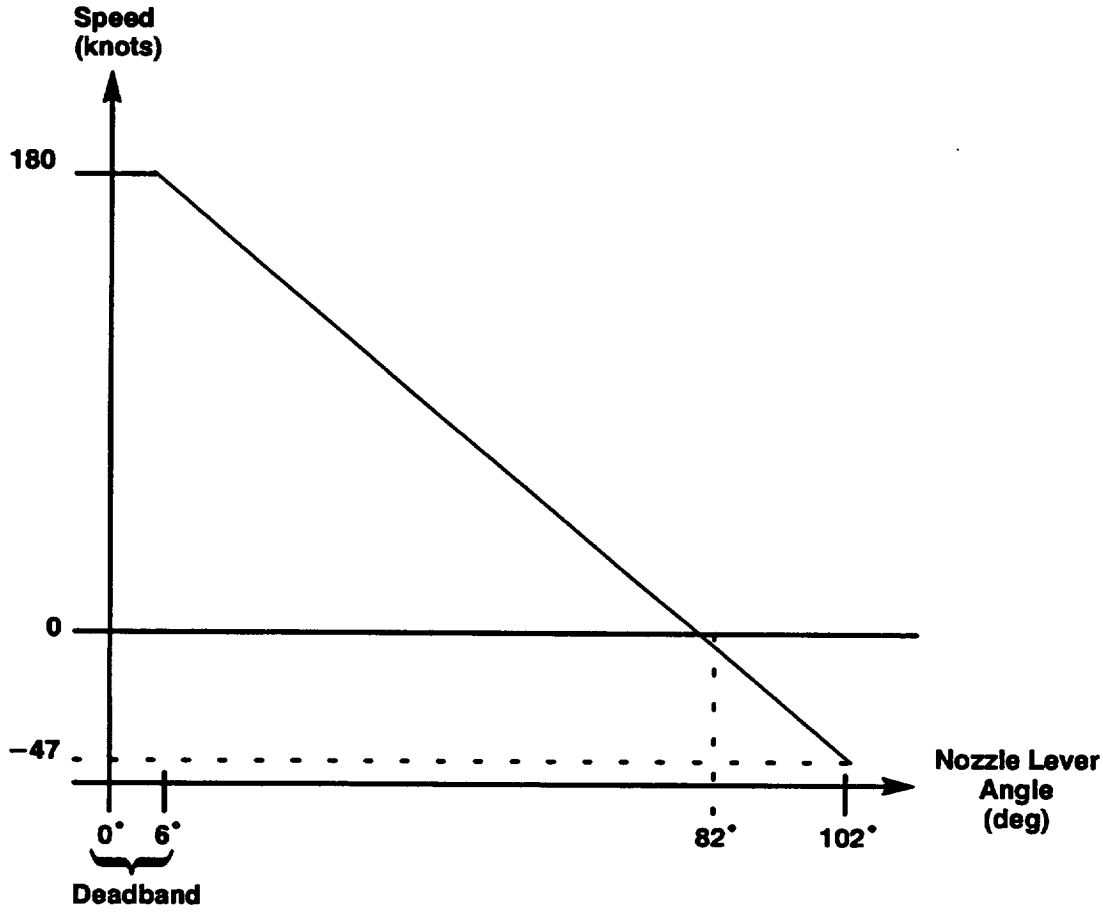

Figure 71. Nozzle Lever Angle to Velocity Command Schedule VET Mode

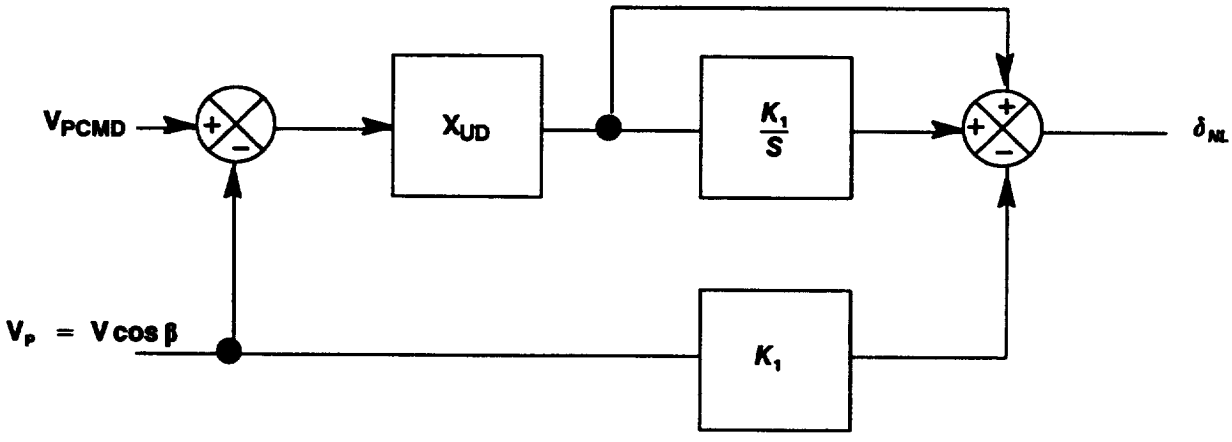

$$\frac{V_P}{V_{PCMD}} = \frac{X_{UD}}{S + X_{UD}}, \quad X_{UD} = 0.5$$

Figure 72. Nozzle Lever Control Laws – Wind Referenced VET Mode

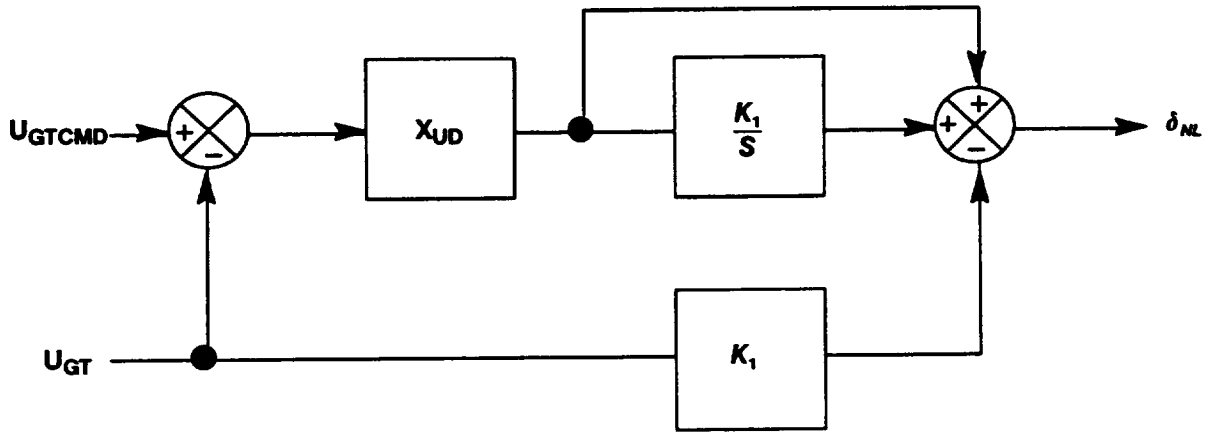

$$\frac{U_{GT}}{U_{GTCMD}} = \frac{X_{UD}}{S + X_{UD}} \qquad X_{UD} = 0.5$$

Figure 73. Nozzle Lever Control Laws – Inertially Referenced VET Mode

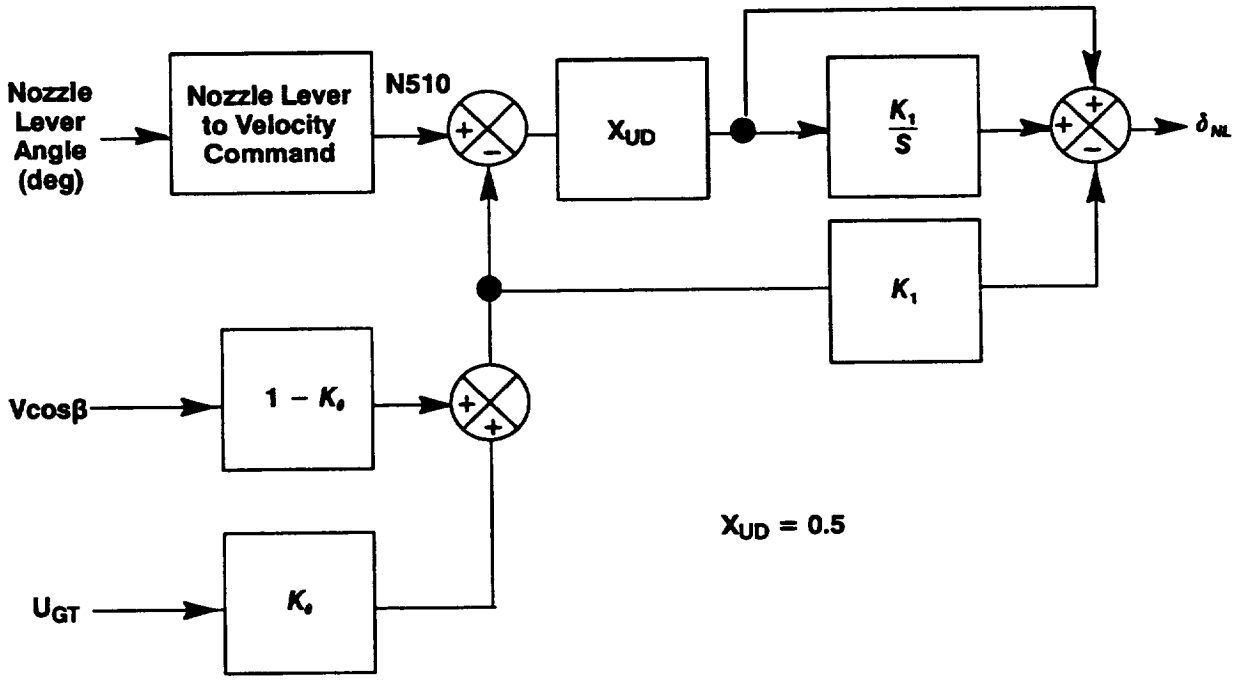

Figure 74. Nozzle Lever Control Laws VET Mode

3.3.2.2. Control Mixer

The control mixer computes the aircraft surface actuator commands, RCS actuator commands, and the thrust magnitude and thrust vector angle commands to the propulsion controller. These commands are computed using the commands received from the core control laws, PCMD, RBCMD, YBCMD, FXCMD, FZCMD. The mixing schedules also depend on the maximum available thrust and nozzle vector angles received as feedbacks from the propulsion controller, and some surface position feedbacks from the actuators.

The control mixer uses the basic mixer scheduling logic shown in Figure 75. In this pitch axis example, the control power of each control, $M_{\delta 1}$, and $M_{\delta 2}$, are computed. The command is then partitioned between the two controls using the gain schedules K_1, and K_2. Ignoring actuator dynamics, the resulting pitch acceleration on the aircraft is approximately equal to the pitch acceleration commanded by the core control laws.

This basic mixer logic is used in three different ways:

1. Commands are scheduled to redundant effectors using the gains K_1 and K_2, with K_1 corresponding to the maximum deflection of the first effector and K_2 corresponding to the maximum deflection of the second effector. This schedule causes both effectors to limit out at the same time, and provides maximum control power at maximum control command.

2. Commands are scheduled between aerodynamic and powered lift control effectors as a function of airspeed by multiplying K_1 by another gain, K_v, with $0 < K_v < 1$, and the other gain, K_2, by $(1-K_v)$. When $K = 1$ the aerodynamic control are used exclusively, when $K = 0$ the propulsive lift controls are used exclusively, in between both aero and propulsive controls are used.

3. The control effectors are reconfigured using multipliers on the gains K_1 and K_2. Setting the multiplier to zero removes the control effector from the command and readjusts the other gains to the other effectors to compensate, so that essentially the core control laws do not see a change in the gain from PCMD to the aircraft's pitch acceleration. This procedure was used in the SCIP simulation to turn the RCS system off and on simply by setting a gain to 0 or 1, respectively.

Longitudinal Axis Mixer Logic

From the command signal, PCMD, the longitudinal axis mixer logic computes commands to differential tail, cruise nozzle pitch vector, collective RCS sleeve valves, and ventral nozzle thrust, as shown in Figure 76. PCMD is converted to a pitching moment command. The pitching moment due to flaps (when flaps are down for takeoff and landing) is subtracted off, producing a signal representing the pitching moment needed from the rest of the controls. The pitching moment command is then partitioned between the controls using the logic in Figure 75. F160 is the aero/prop blending schedule. The cruise nozzle pitch vectoring is not used in powered lift mode. The command to the RCS is washed out so that no RCS is commanded in the steady state, preventing long term down blowing of the RCS for achieving pitch trim. The table in Figure 76 shows the gain values for turning the pitch RCS off and on.

Lateral Axis Mixer Logic

From the command signal, RBCMD, the lateral axis mixer logic computes commands to differential aileron, differential trailing edge flaps, differential lift nozzle thrust, and differential RCS sleeve valve area, Figure 77. RBCMD is first converted to a rolling moment command. The rolling moment due to directional control effector commands are subtracted off, producing a signal representing the rolling moment needed from the roll controls. The rolling moment command is then partitioned to the control effectors. The table in Figure 77 shows the gain settings for turning the RCS or lift nozzle vectoring off and on.

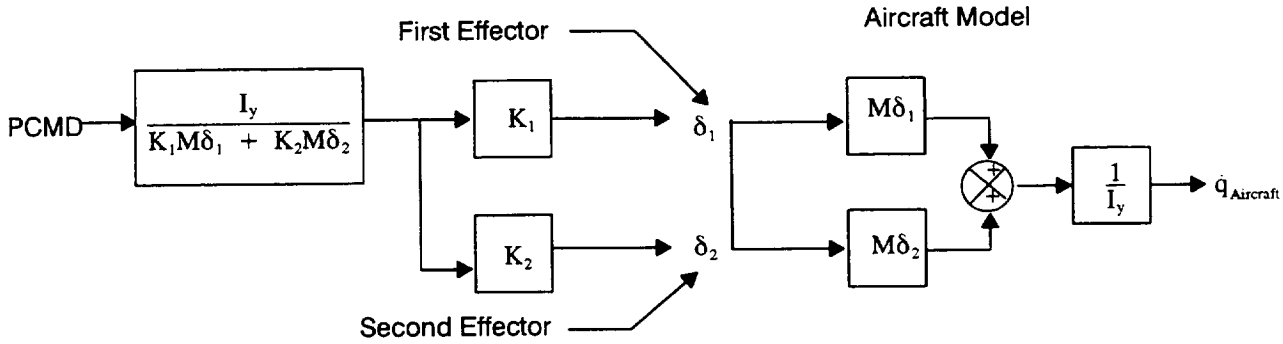

$$\dot{q}_{Aircraft} = PCMD$$

$$\delta_1 = \frac{K_1 I_y}{K_1 M\delta_1 + K_2 M\delta_2} PCMD$$

$$\delta_2 = \frac{K_2 I_y}{K_1 M\delta_1 + K_2 M\delta_2} PCMD$$

Figure 75. Basic Mixer Scheduling Logic – Pitch Axis Generic Example

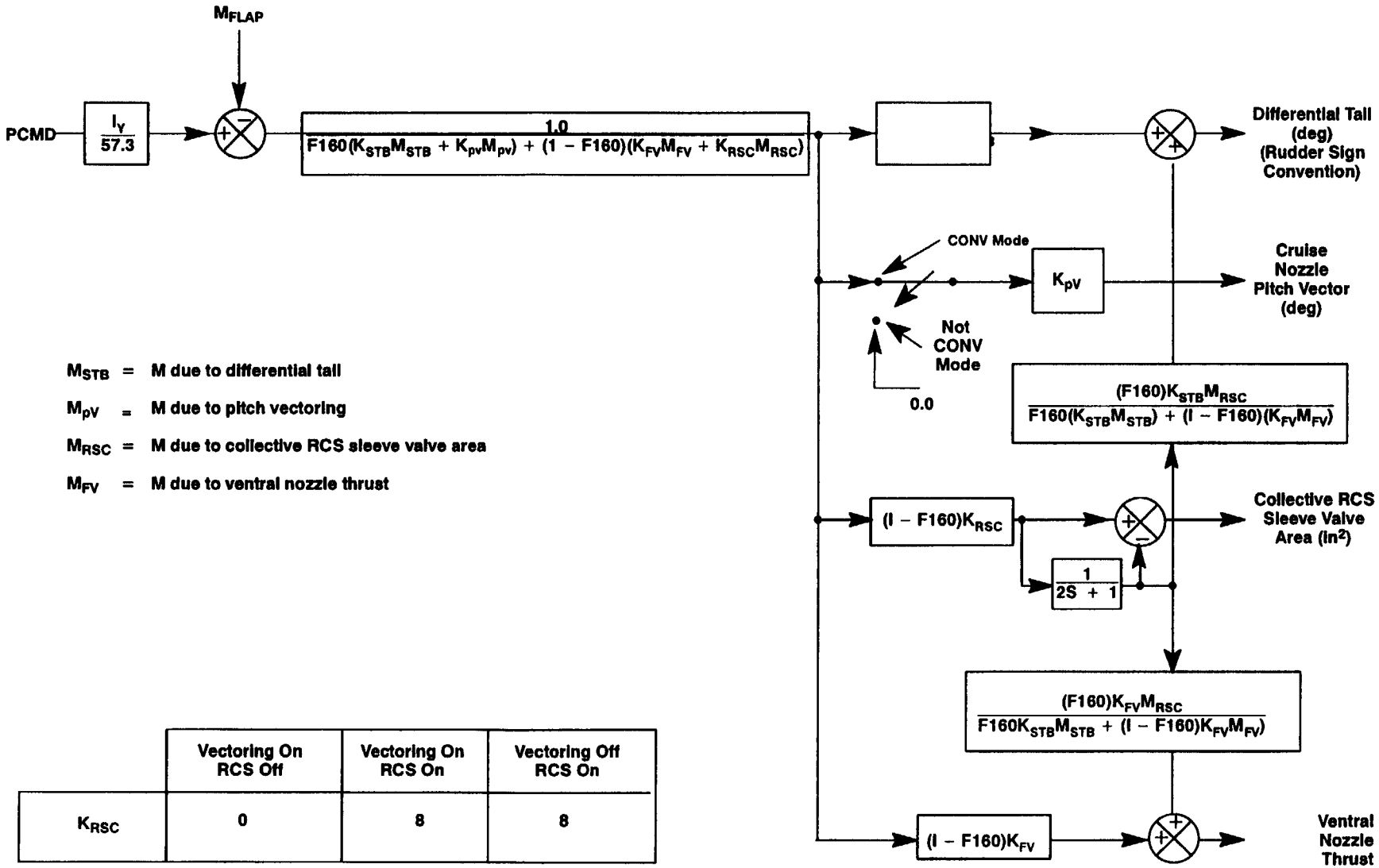

M_{STB} = M due to differential tail

M_{pV} = M due to pitch vectoring

M_{RSC} = M due to collective RCS sleeve valve area

M_{FV} = M due to ventral nozzle thrust

	Vectoring On RCS Off	Vectoring On RCS On	Vectoring Off RCS On
K_{RSC}	0	8	8

Figure 76. Longitudinal Axis Mixer Logic

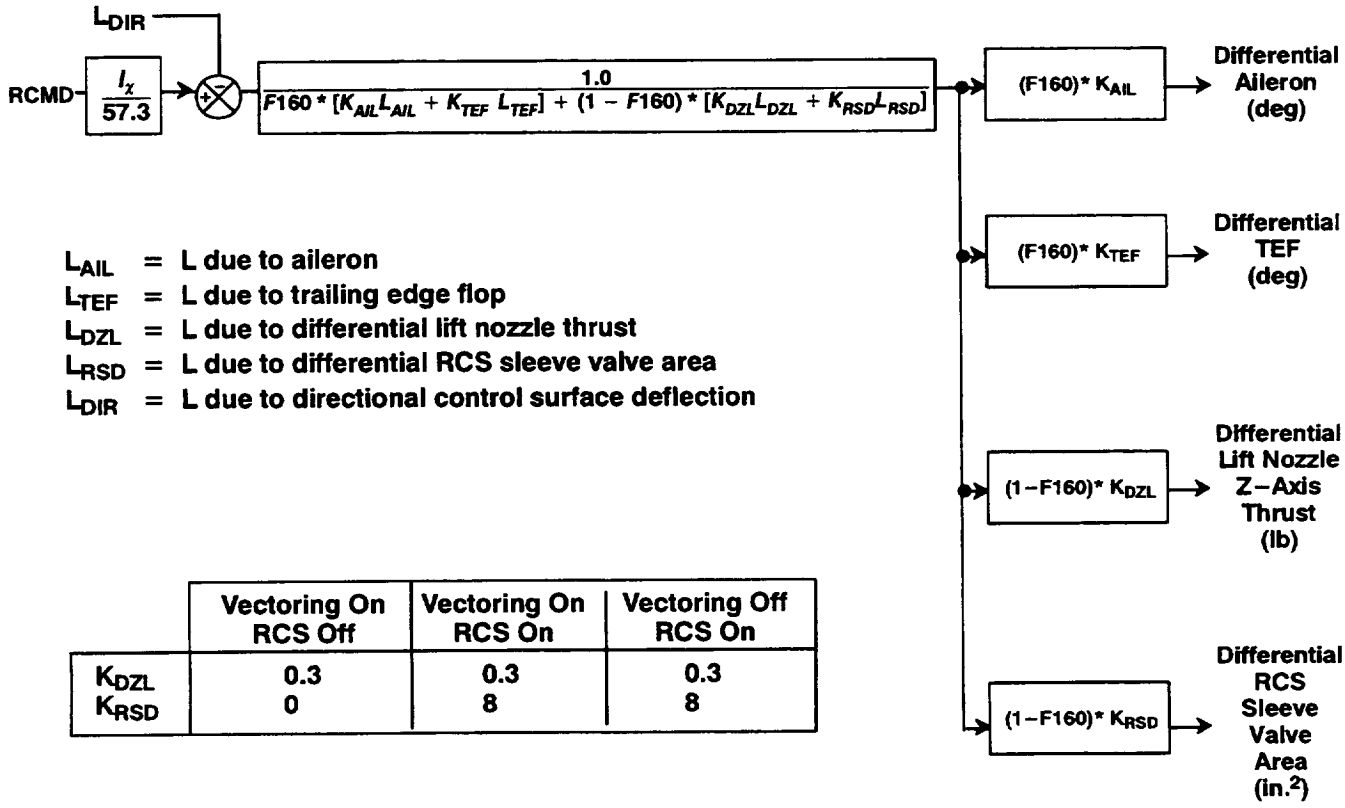

	Vectoring On RCS Off	Vectoring On RCS On	Vectoring Off RCS On
K_{DZL}	0.3	0.3	0.3
K_{RSD}	0	8	8

Figure 77. Lateral Axis Mixer Logic

Directional Axis Mixer Logic

From the command signal, YBCMD, the directional axis mixer logic computes commands to collective tail, cruise nozzle yaw vector, differential lift nozzle pitch vector, ventral nozzle lateral vector, and RCS cock valve area, Figure 78. YBCMD is first converted to a yawing moment command, producing a signal representing the yawing moment needed from the directional controls. The yawing moment command is then partitioned to the control effectors. The cruise nozzle yaw vectoring is not used in powered lift mode. The table in Figure 78 shows the gain settings for turning the RCS or lift nozzle vectoring off and on.

Thrust Axis Mixer Logic

From the command signals, FXCMD and FZCMD, the thrust axis mixer logic computes the collective lift nozzle thrusts, the collective lift nozzle vector angles, and the cruise nozzle thrust. The basic thrust vectoring schedule, Figure 79, uses all lift nozzle thrust between vector angles between 68 and 102 degrees (as measure from the aft waterline), achieving the vectoring through collective vectoring of the lift nozzle pitch vector angles. Some ventral nozzle thrust is also commanded to balance pitching moment. Below 68 degrees, the resultant vector angle is achieved by partially porting thrust through the lift nozzles and partially through the cruise nozzles. The logic in Figure 79 converts FXCMD and FZCMD into commanded axial thrust to the cruise nozzle (FXCCMD), axial thrust to the lift nozzles (FXLCMD, effectively commanding collective pitch vectoring), and vertical thrust from the lift nozzles (FXLCMD). In Figure 80, the axial and vertical thrust commands to the lift nozzles are summed with differential thrust commands from the lateral and directional axes, and converted to thrust and pitch vector commands using a simple rectangular to polar conversion.

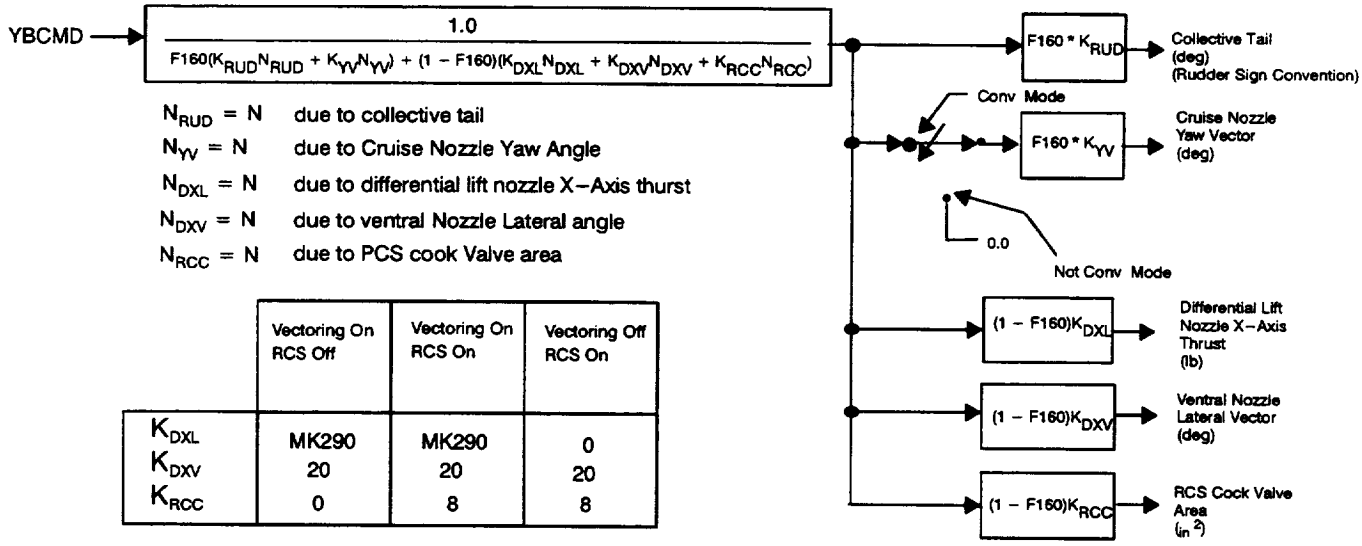

	Vectoring On RCS Off	Vectoring On RCS On	Vectoring Off RCS On
K_{DXL}	MK290	MK290	0
K_{DXV}	20	20	20
K_{RCC}	0	8	8

Figure 78. Directional Axis Mixer Logic

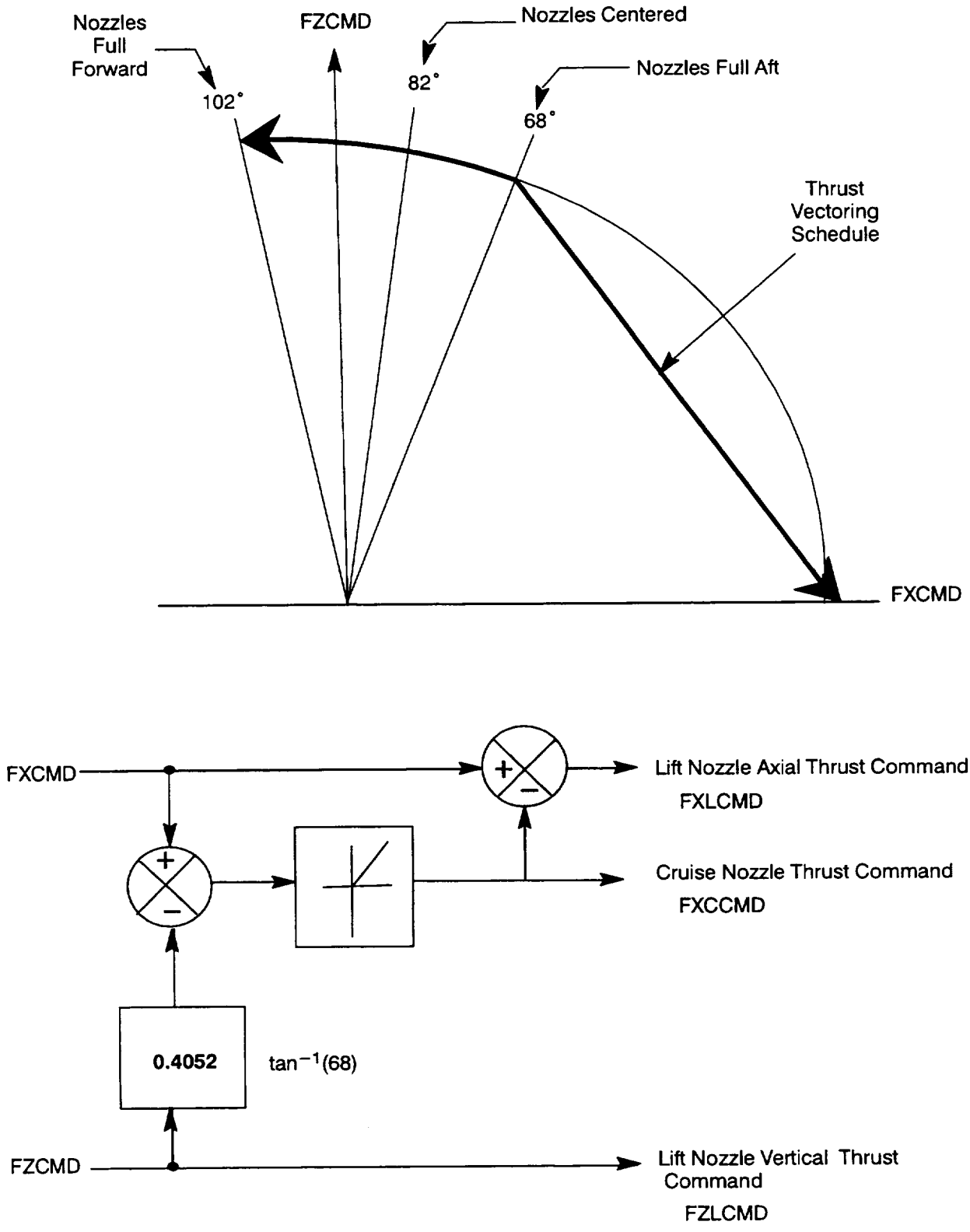

Figure 79. Thrust Axis Mixer Logic
Resolution of Thrust Commands to Lift and Cruise Nozzles

C-2.

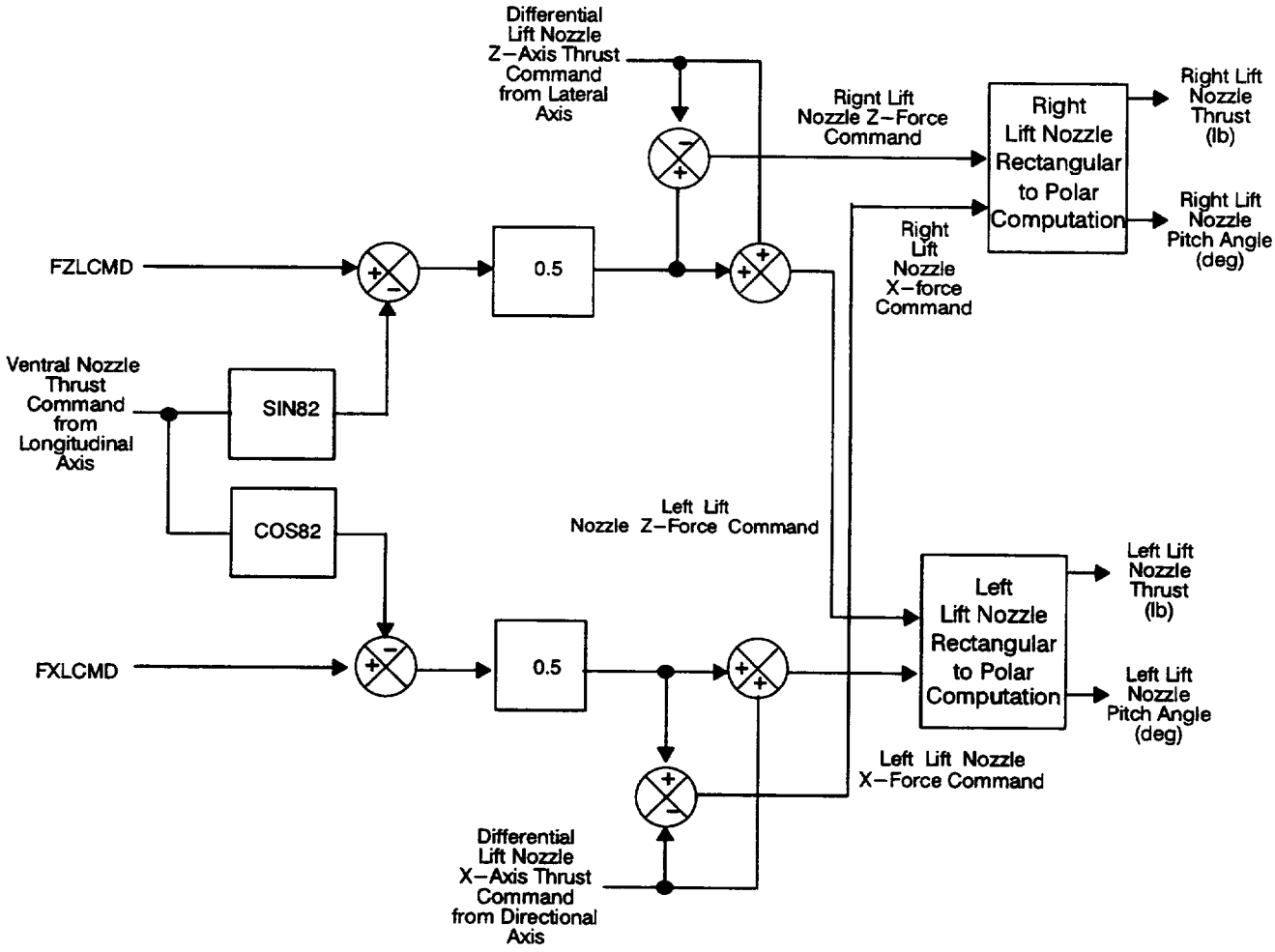

Figure 80. Thrust Axis Mixer Logic – Lift Nozzle Commands

3.3.3. Propulsion Control System Requirements

The results of the DMICS program suggests that each partitioned subsystem be initially treated as "General Actuators". The General Actuator Model (GAM) for the propulsion system is a simplified model that predicts the gross steady state and transient characteristics of the propulsion system. The general actuator model describes the basic propulsion system requirements as defined by the aircraft as well as the propulsion systems dynamic response characteristics. Thus, the GAM serves two very useful purposes. It provides the flight control designer with a propulsion system performance specification for use in the initial stages of flight control design as well as providing the propulsion control designer with precise requirements specification. Initial general actuator model requirements are defined through airframe and propulsion system designers negotiations. After preliminary review of propulsion system response characteristics, iterations on the general actuator model fine tune the propulsion system requirements specification.

The general actuator model developed for SCIP consists of simplified dynamic representations of three propulsion subsystems: the engine, exhaust nozzles system, and the reaction control system (RCS). Each piece of the General Actuator Model provides distinct functions. The Engine model provides an estimate of steady state thrust capability and small signal closed loop thrust response of 10 (radians/second.) Gross transient response is defined from the rate limited acceleration and deceleration requirements. The engine outputs required by the nozzle model and the reaction control system model are proved from correlation's with thrust levels. The Nozzle model provides the basic exhaust nozzle system dynamics and calculates the thrust splits between the spherical convergent flap main nozzle, left and right lift nozzles and trim flap nozzle based upon the available thrust provided from the engine model and the exhaust nozzle system geometry. The reaction control system model calculates the RCS forces from the compressor discharge characteristics provided from the engine model.

An overview of the General Actuator Model is shown in Figure 81. Preliminary evaluations of the general actuator model performed in the PROLIFIC indicated that if the propulsion system responded as a 10 radian/second lag, with thrust acceleration rates of 25 percent maximum dry power thrust/second acceleration capability, vehicle control system performance was acceptable. Thrust deceleration rates as high as 100 percent maximum dry power thrust/sec were found desirable to minimize landing bounce. Additional testing performed at NASA Ames also found that the propulsion system thrust response requirement should be minimum of 5 radians/second and a minimum propulsion system thrust acceleration/deceleration rates of 15 percent/second provided acceptable system response.

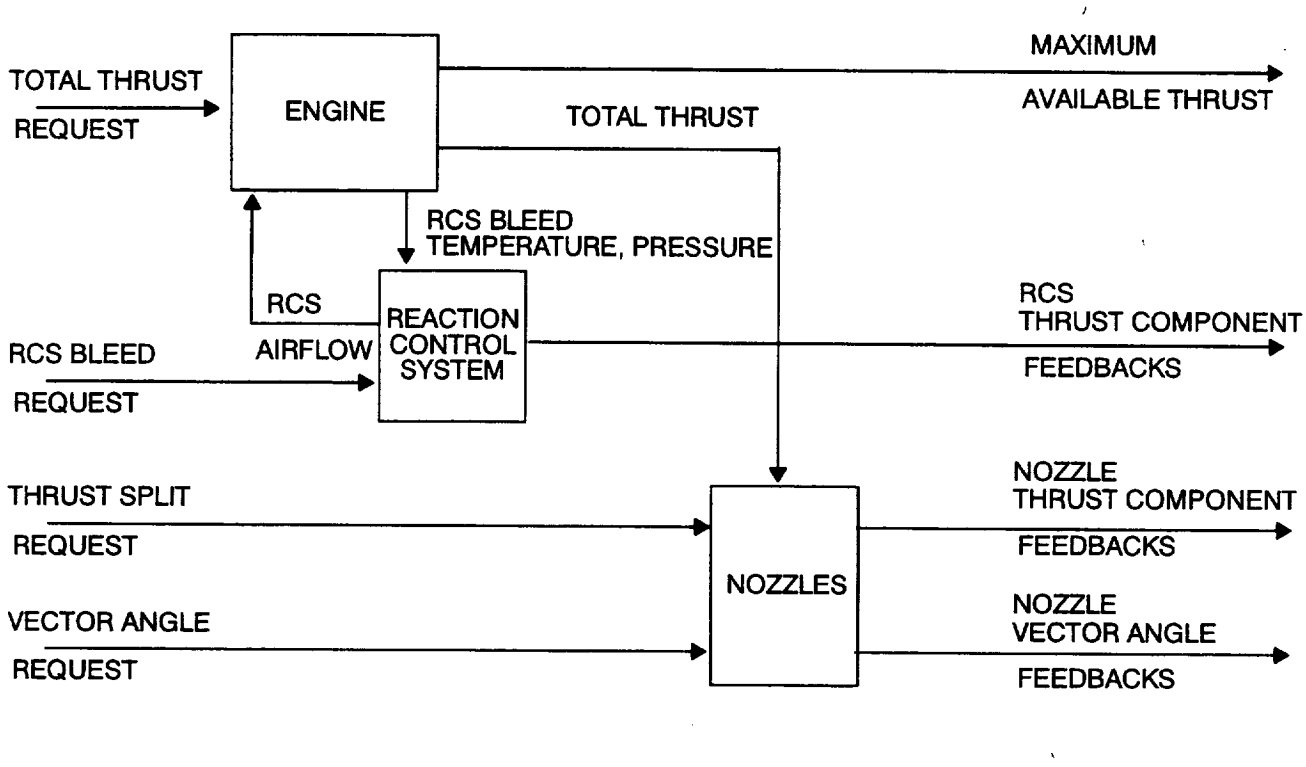

Figure 81. General Actuator Model

The requirement to minimize thrust fluctuations during RCS bleed transients creates a dynamic disturbance rejection requirement for the propulsion system control design. RCS bleed usage was not well defined during the infancy of the flight control design. Therefore, AV–8B Harrier data was chosen to provide typical RCS bleed time histories for both total magnitude and spectral content. Review of the AV–8B data RCS time histories provides the basis of the 20 radian/second compression system response requirement.

The propulsion system control design requirements are the culmination of numerous airframe studies, some of which utilize the general actuator model, and propulsion system design practices. The propulsion system control design requirements, source and approach are shown in Table I.

TABLE I – SCIP/PROLIFIC Propulsion Control Requirements

REQUIREMENT	SOURCE	APPROACH
• 10 radian/second thrust response	• Transfer function model (SCIP I) • General Actuator engine model	• Thrust request fed–forward to slave regulator
• RCS bleed disturbance rejection	• AV–8B RCS time histories • 8 PPS max. bleed (PROLIFIC)	• Minimize Compressor Operating Line excursions with Overall Pressure Ratio (OPR) slave regulator with 20 radian/second response.
• 10000 Lb/Sec side–to–side thrust	• Control power study (PROLIFIC)	• 200 percent/Sec capability on nozzle flaps give 20000 Lb/Sec thrust redistribution
• ± 20 degrees @ 40 degrees/second Pitch/Yaw axial thrust vectoring	• Control power study (PROLIFIC)	• 200 percent/Sec capability on nozzle actuators
• EPR control during up & away, transition and hover	• Engine stall protection	• Minimize Fan Operating Line excursions with Engine Pressure Ratio (EPR) slave regulator with 20 radian/response.
• Lift and trim thrust vectoring	• Control power study (PROLIFIC)	• Independent scheduling of lift and trim flap posisions
• Control loop stability margins >60° phase margin and 10 dB gain margin	• Design practice	• MVC robustness assessed by singular values
• Thrust magnitude and direction and max. available thrust esimates	• ICD	• On–board model provides estimates

3.3.4. Propulsion Control/Vehicle Control Interface

The partitioned elements of the control system also provide the basis for the interface characteristics document, which defines the required communication paths between the elements. The data exchange between the vehicle and propulsion controllers is outlined in Table II. In general, the vehicle requests an overall thrust level from the propulsion system, as well as thrust distribution between the main nozzle, lift nozzles, and lift trim nozzle. Thrust vector angle requests for each of the nozzles are also given. The engine control returns estimates of thrust and vector angle for each of the nozzles, an estimate of

the maximum dry thrust available, and status flags indicating which mode (axial thrust or propulsive lift) the propulsion system is in, and which modes it is capable of attaining.

TABLE II – Data Exchange Between Vehicle (Airframe) and Propulsion Controls

Vehicle To Propulsion	Propulsion To Vehicle
Gross Thrust Level Request	Gross Thrust Feedback
Thrust Split Request	Nozzle Thrust Split Feebacks
Axial Nozzle Pitch Angle Req.	Lift Nozzle Vector Angles & Trim
Axial Nozzle Yaw Angle Req.	Axial Yaw Feedback
TRM & Lift Nozzle Vector Angle Req.	Maximum Allowable Dry Thrust
Vehicle AOA And Sideslip	Maximum Allowable Thrust Splits
Ambient Pressure	Maximum Allowable Vector Angles
Mach Number	Fault And Status Words
Fault And Status Words	

3.3.5. STOVL Unique Propulsion System Requirements

As seen in the propulsion system requirements specification Table I, operation in a STOVL aircraft places unique requirements on the propulsion system. First, the propulsion system must produce, distribute and vector thrust. Second, the engine must maintain nearly constant thrust despite large, rapid fluctuations in compressor bleed flow to the RCS system. Third, fan stability must be maintained despite aircraft operation at extreme angles of attack, and with far–field hot gas ingestion. Fourth, since the vectored thrust is, in fact, a flight control effector, the engine thrust and vectoring response must be sufficiently rapid to not interfere with flight control dynamics. Control power studies for the MFVT aircraft found that increasing the rate at which thrust could be redistributed from side to side, and the ability to rapidly vector the thrust from the lift and trim nozzles, reduced the amount of RCS bleed which was required. In order to assure adequate propulsive lift during hot day it was desired to keep RCS bleed below 5 percent of core flow. As a result, differential roll thrust rates of at least 10000 lb./second, and lift and trim nozzles vector capability of ±20 degrees at 40 degrees/second were required.

Previous STOVL and missile gas ingestion studies have shown that large, rapid excursions in engine inlet temperature will cause fan stalls, regardless of what actions the control system may take. It is therefore incumbent on the airframe to prevent jet exhaust gas from being directly recirculated to the engine inlet. However, far–field gas and operation at extreme angles of attack and sideslip still present fan stability threats which are worse than those typically encountered in up–and–away operation. It is therefore imperative that the control system have precise control of the compression system operating lines.

3.3.6. Control Approach

Figure 82 shows an overview of the STOVL engine control which was developed under the PROLIFIC program. The propulsion control system requirements, and the approaches taken to meet these requirements are summarized in Table I. A 20 rad/sec. regulator was desired to maintain accurate control of the compression system pressure ratios and provide rapid thrust response. Because of the high degree of coupling between the fan operating line and the compressor operating line inherent to a turbofan engine, and because the dynamic response required, it was decided that multivariable control design techniques would be used for the dynamic design of the control regulator logic. The MVC was designed using traditional Linear Quadratic Gaussion/Loop Transfer Recovery (LOG/LTR) techiques to ensure rapid response and maximum robustness. The multivariable control (MVC) requests fuel flow, compressor vane position and total exhaust jet throat area to regulate Overall Pressure Ratio (OPR), Engine Pressure Ratio (EPR), and High Rotor Speed (N2).

Preliminary propulsion system studies indicated that the percent of total thrust delivered by each nozzle is approximately equal to the nozzle's percentage of the total throat area. The nozzle control (NC) logic then uses the thrust distribution request from the vehicle control to determine the throat area of each of the nozzles. The NC performs fault detection on each of the nozzle actuators and returns status flags to the vehicle control advising which modes of operation are attainable.

It was desired to have estimates of the thrust and vector of each of the nozzles to be fed back to the vehicle. Furthermore, it was desired to have an estimate of the maximum available dry thrust, to prevent the vehicle control from requesting transition to hover when the engine cannot provide sufficient vertical force. In order to provide these estimates, a self–tuning on–board real–time engine model was included into the software.

The presence of the on–board model allows accurate estimates of unmeasured engine variables, such as fan and compressor airflow, thrust turbine inlet temperature, and fan discharge total pressure to be fed to the control laws. The thrust estimate was compared to thrust request to provide closed–loop thrust control.

Figure 83 shows a MIL–IDLE–MIL thrust transient, while Figure 84 and Figure 85 show the fan and compressor pressure ratio excursions during the transients. It can be seen that the acceleration (25 percent/second) and deceleration (100 percent/second) are met, while the compression system pressure ratios operation do not exceed the stall level pressure ratios.

SCIP/PROLIFIC MODEL–BASED CONTROL OVERVIEW

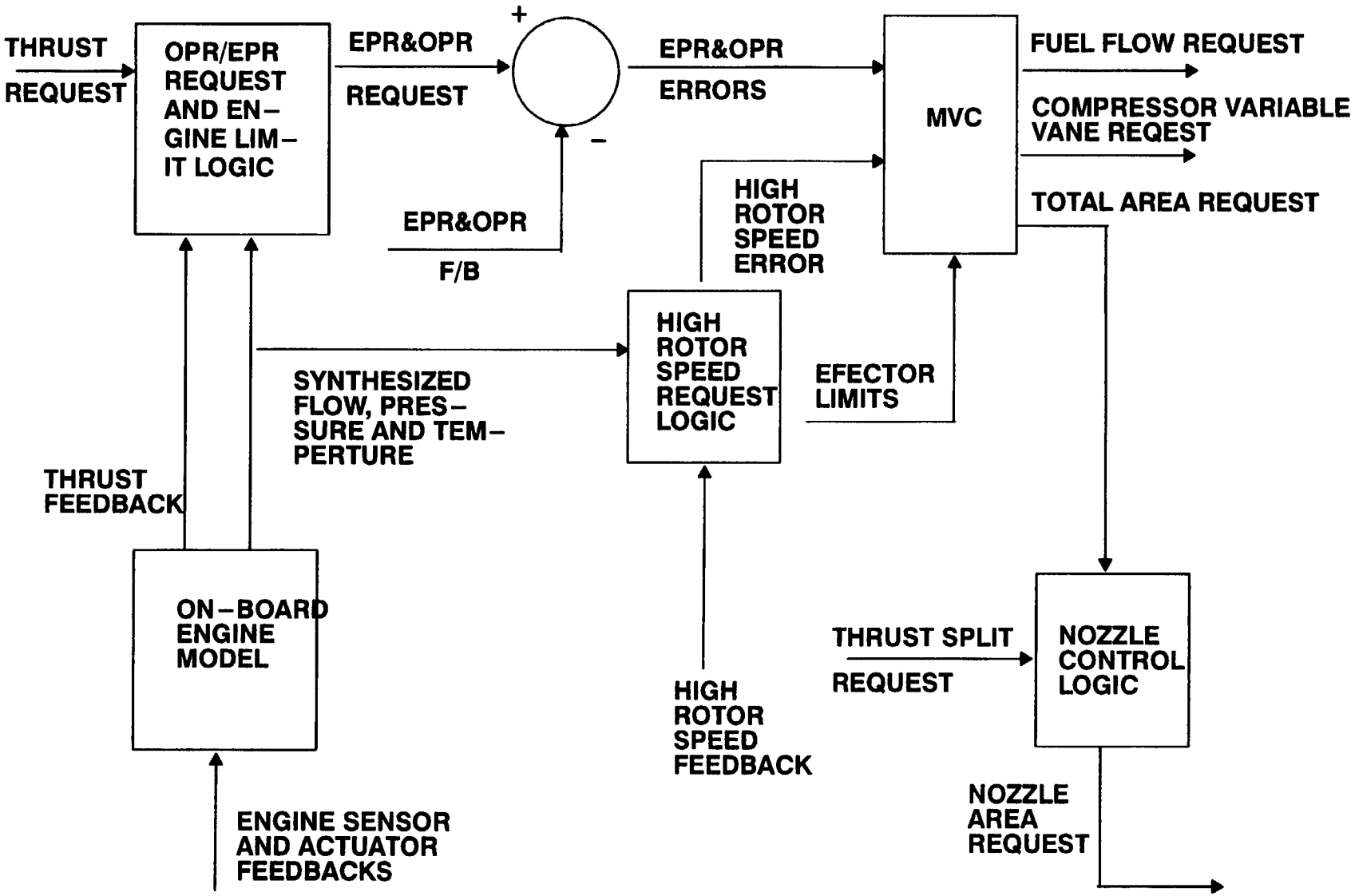

Figure 82. Model Based Control Overview

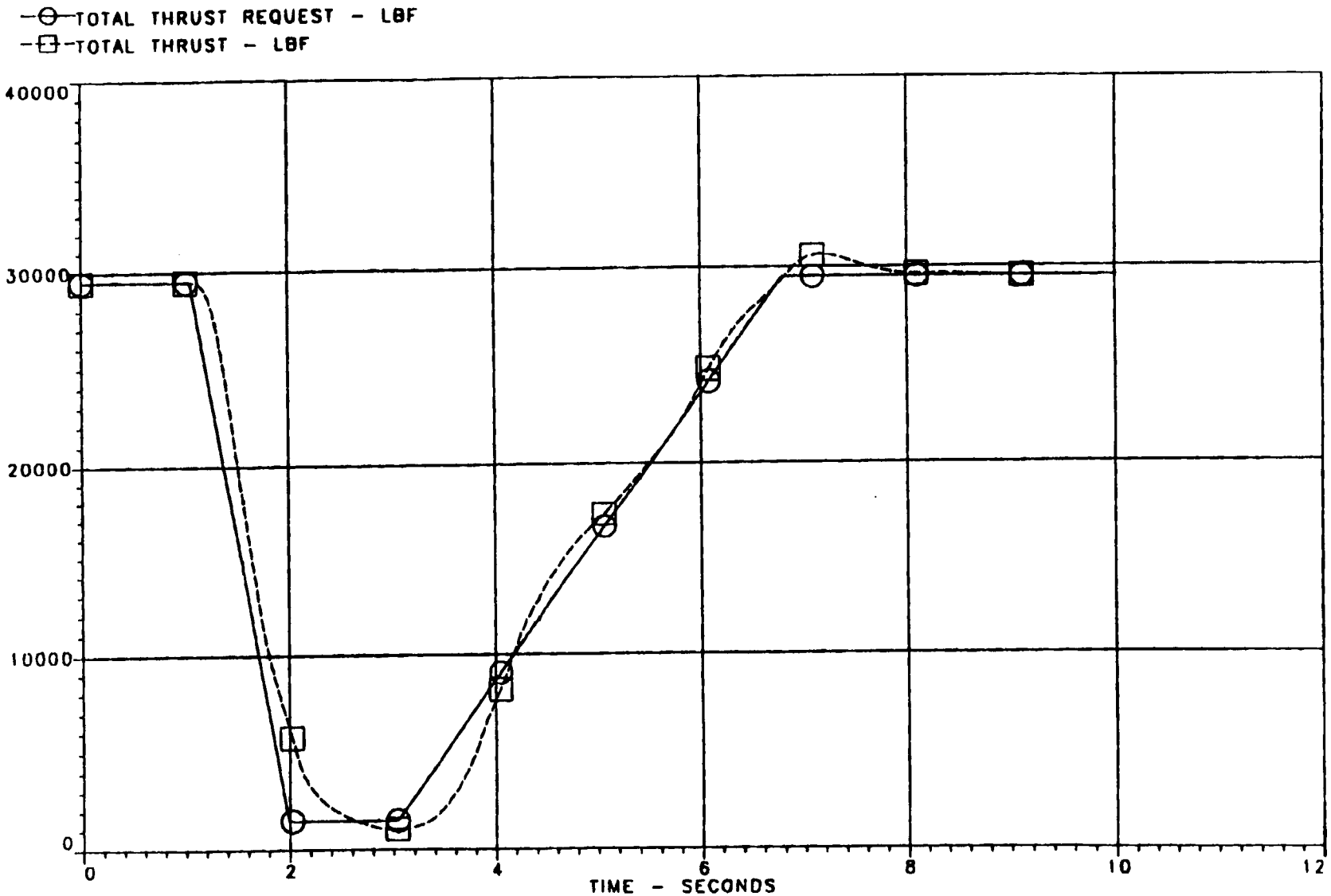

Figure 83. MIL–IDLE–MIL Thrust Transient

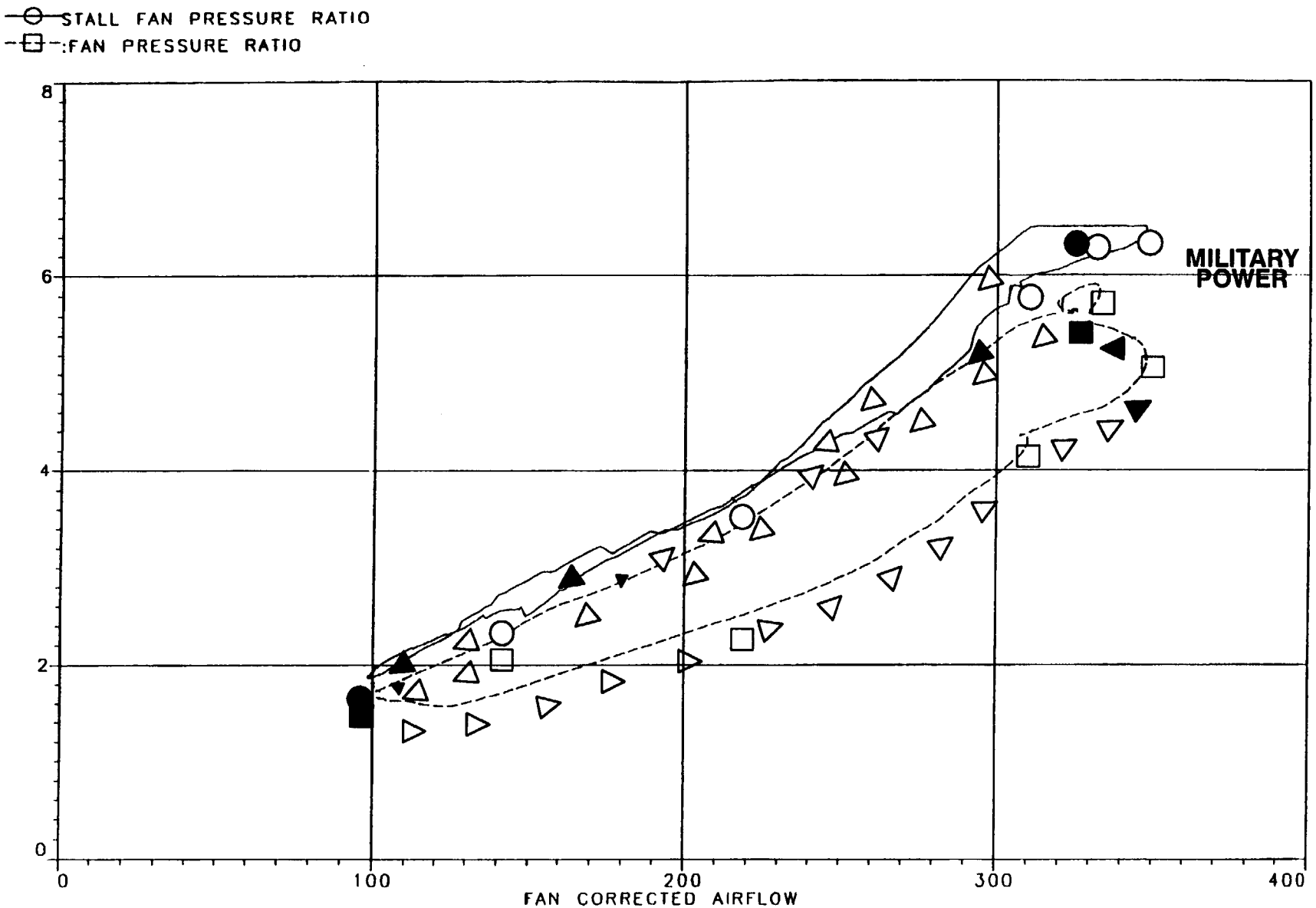

Figure 84. FPR Excursion

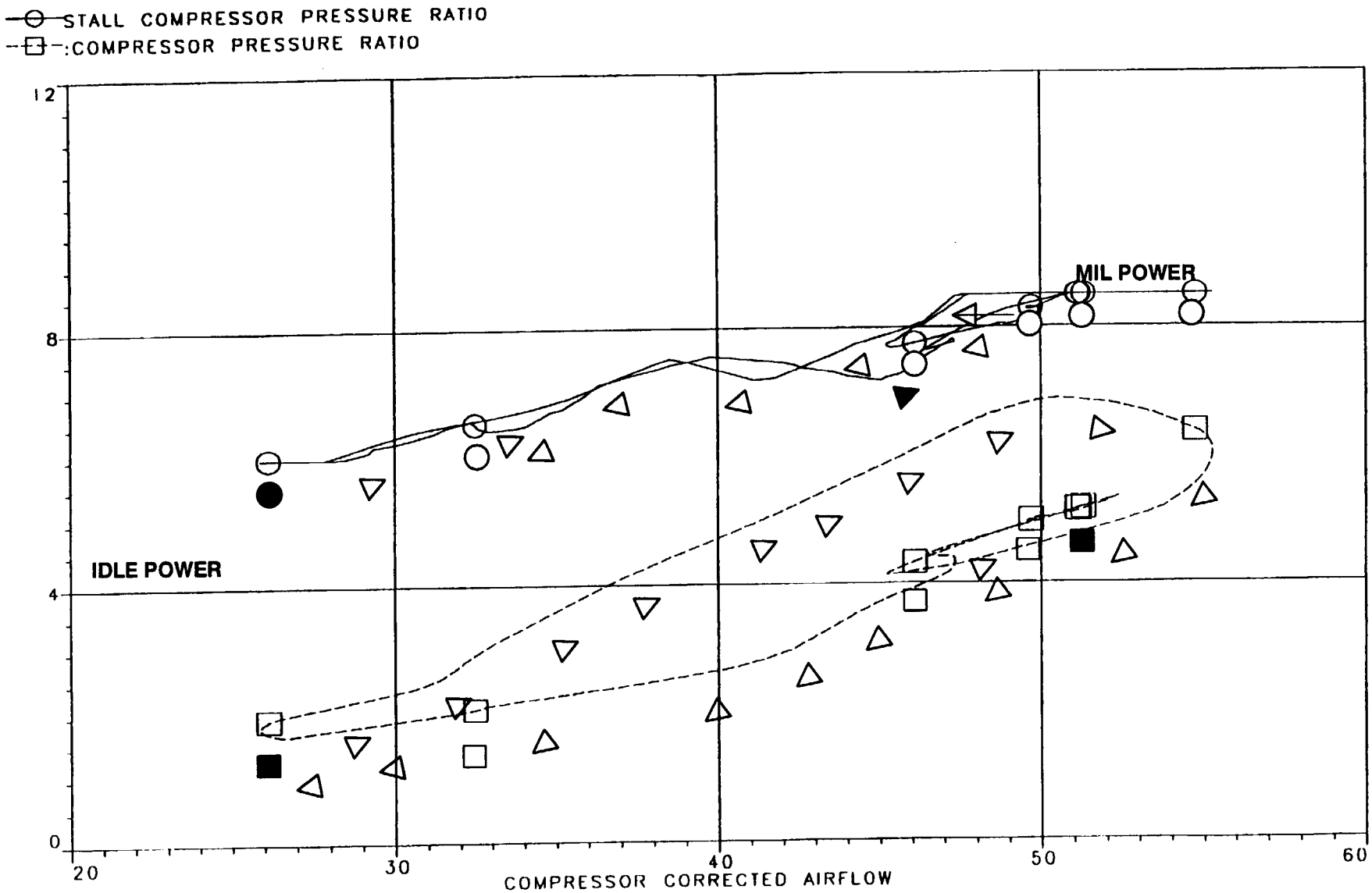

Figure 85. CPR Excursion

3.4. Transition Envelope Sensitivity and Control Power Analyses

In SCIP2, analyses were performed to compute transition envelope sensitivities and the control power available during transition and hovering flight, using the MODSDF model of the 4636 aircraft. The objective of these two tasks was to investigate the envelope of flight conditions for which the aircraft would normally be expected to operate in transition and hover, including the control power available for these flight conditions, and any limitations that may be imposed due to the aircraft state or lack of control power.

MDA's technical approach was in four steps. Step 1 generated computer software modules in MODSDF, called aerodynamic analysis options, which perform trim sweeps. The trim sweeps plot the trimmed aircraft states, surface deflections, nozzle thrusts, and nozzle vector angles, as a function of various flight condition variables. Step 2 defined schedules which blend the actuator commands between aerodynamic and propulsive control effectors as the aircraft transitions between wingborne and jetborne flight. Step 3 analyzed the envelope of operable flight conditions in hover and transition, including the capability of the aircraft to climb or descend, to accelerate and decelerate along the flight path, and to pitch, roll, and yaw.

The results show that the 4636 aircraft has a wide envelope of operable flight conditions in transition and hover with no significant limits imposed by lack of control capability. The control capability meets the US/UK CEM and MIL–STD–83300 control power requirements using nozzle vectoring and thrust modulation alone, and without using the reaction control system.

Section 3.4.1 describes the development of the gain schedules which define the transition of the control effector usage between aerodynamic and propulsive control effectors.

Section 3.4.2 details the transition envelope sensitivity analyses and presents results defining the control capability of the aircraft in transitioning flight. The transition envelope is described using two types of engineering plots. One type is a plot of the envelope of achievable flight path angles as a function of airspeed at a constant value of effective jet angle, and indicates the non– accelerating flight conditions that can be reached. The second type is a plot of the envelope of effective jet angles that can occur (depending on the power setting) as a function of velocity, given a particular aircraft state. This plot is used to show the sensitivity of the transition envelope to various aircraft states, including differing values of flight path angle, of maximum angle of attack (or pitch attitude), of acceleration (or deceleration) along the flight path, and of crosswind velocity.

Each subsection of Section 3.4.2 details the analysis cases which plot aircraft states and control capability for trimmed steady flight and for "trimmed" flight with nonzero steady acceleration along the flight path.

Section 3.4.2.1 describes the transition envelope as the flight path achievable at velocities ranging from 0 to 200 knots at various effective jet angles ranging from 0 to 90 degrees. Envelope limits at maximum angle of attack, and maximum and minimum engine power are shown.

Section 3.4.2.2 describes the sensitivity of the steady level flight transition envelope to maximum allowable pitch attitude, and control power available at the trim points along the

maximum pitch attitude profile. The trim sweep is steady level flight with varying limits on allowable pitch attitude from 6 to 16 degrees.

Section 3.4.2.3 describes the level flight accelerating and decelerating transition envelopes. The trim sweep is level flight along a maximum 8 degree pitch attitude profile with acceleration along the flight path varying between −0.25 and +0.20 g's. A deceleration of −0.21 g's corresponds to the US/UK CEM requirement for a decelerating transition from 200 knots to hover in 50 seconds. Control power available along the 8 degree maximum pitch attitude profile is also described.

Section 3.4.2.4 describes the transition envelope limits in steady ascents and descents. The trim sweeps are steady descents along a maximum 8 degree pitch attitude profile with flight path varying between −9 and 0 degrees, and steady ascents along a maximum 8 degree angle of attack profile with flight path varying between 0 and 12 degrees. Control power available along the maximum pitch attitude descent profiles and the maximum angle of attack ascent profiles are described.

Section 3.4.2.5 describes the steady level flight transition envelopes in crosswinds. The trim sweep is steady level flight along a maximum 8 degree pitch attitude profile in crosswinds ranging from 0 to 20 knots. Control power available in crosswinds along the maximum pitch attitude profile is described.

Section 3.4.2.6 describes the sensitivity of the level flight transition envelope to shifts in center of gravity location. The trim sweep is steady level flight along a maximum 8 degree pitch attitude profile with center of gravity ranging between 37 and 43%. Longitudinal control power variations to these center of gravity shifts are described.

Section 3.4.2.7 describes the sensitivity of the level flight transition envelope to variations in predicted ram drag. The trim sweep is steady level flight along a maximum 8 degree pitch attitude profile with ±20% variation in ram drag.

Section 3.4.2.6 describes the control power available in hovering flight, with the wind velocities up to 40 knots and coming from all directions relative to the aircraft axes.

Table III is a list of variable names and abbreviations used in the figures of this section.

3.4.1. Transition Control Effector Blending Schedules

The control mixer logic contains schedules which blend the control effector actuation from all aerodynamic effectors to all propulsive effectors during the transition from wingborne to jetborne flight. The schedules were developed by analyzing a trim sweep of steady level flight conditions along an 8 degree maximum pitch attitude profile with velocity varying from 0 to 200 knots in 5 knot increments. This profile was chosen since a normal operating attitude of 8 degrees in transition is used on the AV−8 and subsequent analysis showed that this profile is well within the level flight transition corridor, with plenty of margin for generating lift without exceeding the controllable angle of attack, while providing adequate line of sight for the pilot.

The primary aerodynamic and propulsive effectors are described in Figure 1 and Figure 27, respectively. The reaction control system is not used in these analyses since the results indicate that adequate control power exists without the use of the reaction controls.

Table III. Variable Names and Abbreviations

QDTNUT	Total nose up pitch acceleration capability
QDTNUA	Nose up pitch acceleration capability from aerodynamic effectors
QDTNUP	Nose up pitch acceleration capability from propulsive effectors
QDTNDT	Total nose down pitch acceleration capability
QDTNDA	Nose down pitch acceleration capability from aerodyanmic effectors
QDTNDP	Nose down pitch acceleration capability from propulsive effectors
PDTWUT	Total left wing up roll acceleration capability
PDTWUA	Left wing up roll acceleration capability from aerodynamic effectors
PDTWUP	Left wing up roll acceleration capability from propulsive effectors
PDTWDT	Total left wing down roll acceleration capability
PDTWDA	Left wing down roll acceleration capability from aerodynamic effectors
PDTWDP	Left wing down roll acceleration capability from propulsive effectors
RDTNLT	Total nose left yaw acceleration capability
RDTNLA	Nose left yaw acceleration capability from aerodynamic effectors
RDTNLP	Nose left yaw acceleration capability from propulsive effectors
RDTNRT	Total nose right yaw acceleration capability
RDTNRA	Nose right yaw acceleration capability from aerodynamic effectors
RDTNRP	Nose right yaw acceleration capability from propulsive effectors
THETA	Pitch angle in degrees
AXSCMD	Acceleration along the flight path in g's
WL	Aircraft waterline
LWU	Left wing up
LWD	Left wing down
NR	Nose right
AOA	Angle of Attack
GW	Gross Weight
STOL	Short Takeoff & Landing
NTRIMT	Trim Yawing Moment (lb–ft)
LTRIMT	Trim Rolling Moment (lb–ft)
PM	Pitching Moment
YM	Yawing Moment
RM	Rolling Moment
THETAJ	Effective Jet Angle Measured from Aft Waterline
SIGMA	Flight Path Azimuth Angle
VKTAS	Knots True Air Speed
ALT	Altitude
MTRIMT	Trim Pitching Moment
MVENT	Pitching Moment from Ventral Nozzle
MBASCA	Aerodynamic Static Pitching Moment
MBASCP	Propulsive Pitching Moment from Ram Drag, JII, Boattail Drag

The pitch axis schedule blends differential tail with the thrust difference between the lift nozzles and the ventral nozzle. This schedule was developed by studying the differential tail deflection required to trim in transition with the lift and ventral nozzles' thrusts balanced to produce zero pitching moment, using the level flight trim sweep previously described in this section. Figure 86 shows the trimmed effective jet angle as measured from the aft waterline, and the corresponding trimmed pitch attitude as a function of velocity. At velocities from 200 knots down to 154 knots, the aircraft is trimmed in wingborne flight. Below 154 knots, the maximum pitch attitude is reached and the thrust is vectored downward to produce the required additional lift.

In Figure 87, the trimmed differential tail deflections are shown, indicating that the trimmed differential tail deflection is about −10 degrees at wingborne velocities, and reverses through 0 degrees at about 45 knots, as the opposing pitching moment produced by ram drag begins to dominate the basic static aerodynamic pitching moment of the aircraft body. Figure 88 shows the corresponding ratio of the ventral nozzle's thrust to the sum of the lift and ventral nozzles' thrusts which achieves a balance resulting in a net zero pitching moment from these nozzles. Since the trimmed differential tail naturally approaches zero as jetborne velocities are reached, the pitch axis schedule was chosen to command all differential tail during the high end transition, and zero differential tail below 40 knots. Thus this schedule blends the actuator commands from aerodynamic to propulsive effectors along a profile which requires low trimmed pitching moment from propulsive effectors. Subsequent control power analyses (Section 3.4.2) showed that adequate tail power exists above 100 knots, so that the schedule was chosen to command all differential tail above this airspeed. This upper end airspeed value also ensures that the command to propulsive effectors is faded out before a wingborne flight condition is reached (where the ventral nozzle thrust is zero).

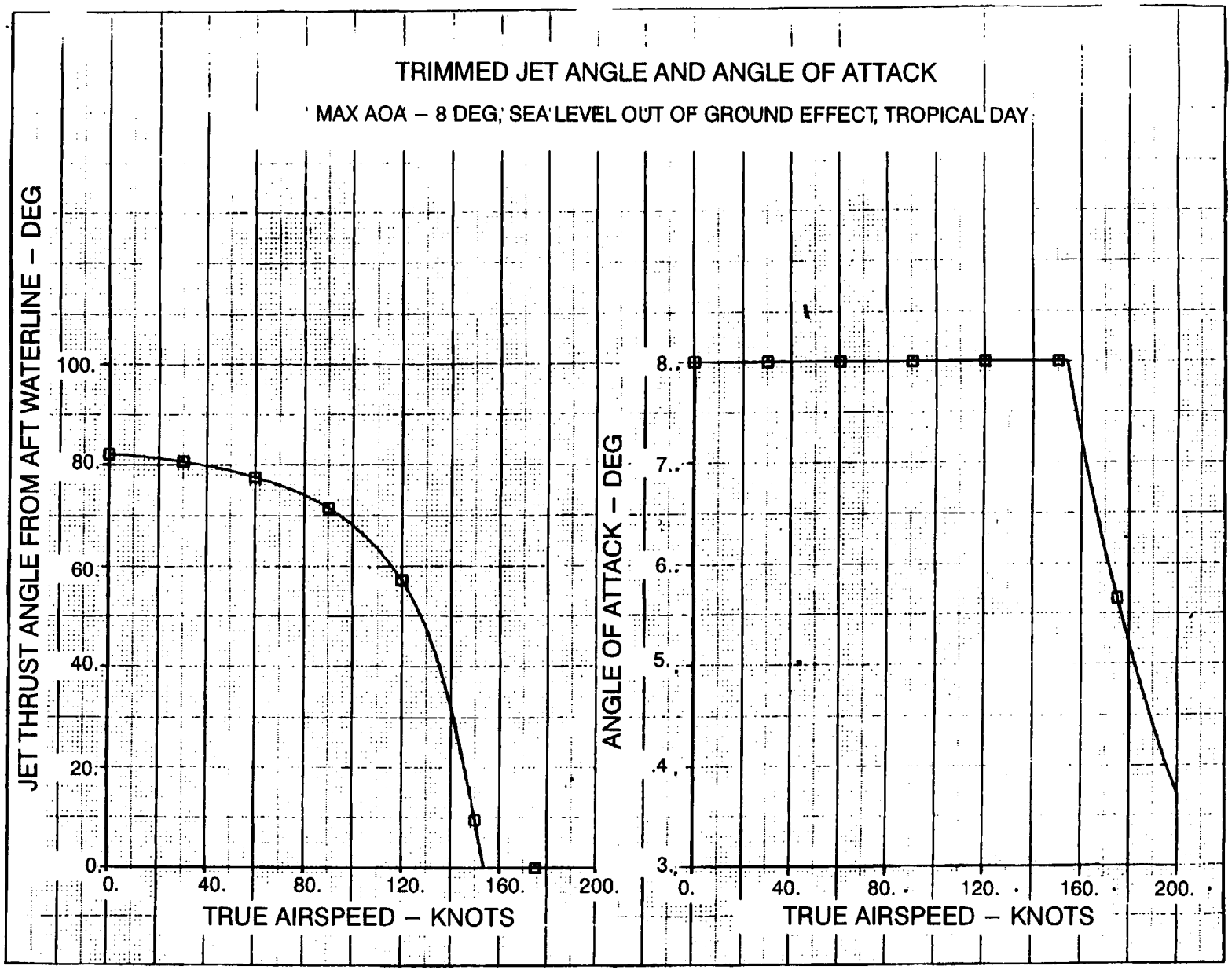

Figure 86. Trimmed Effective Jet Angle

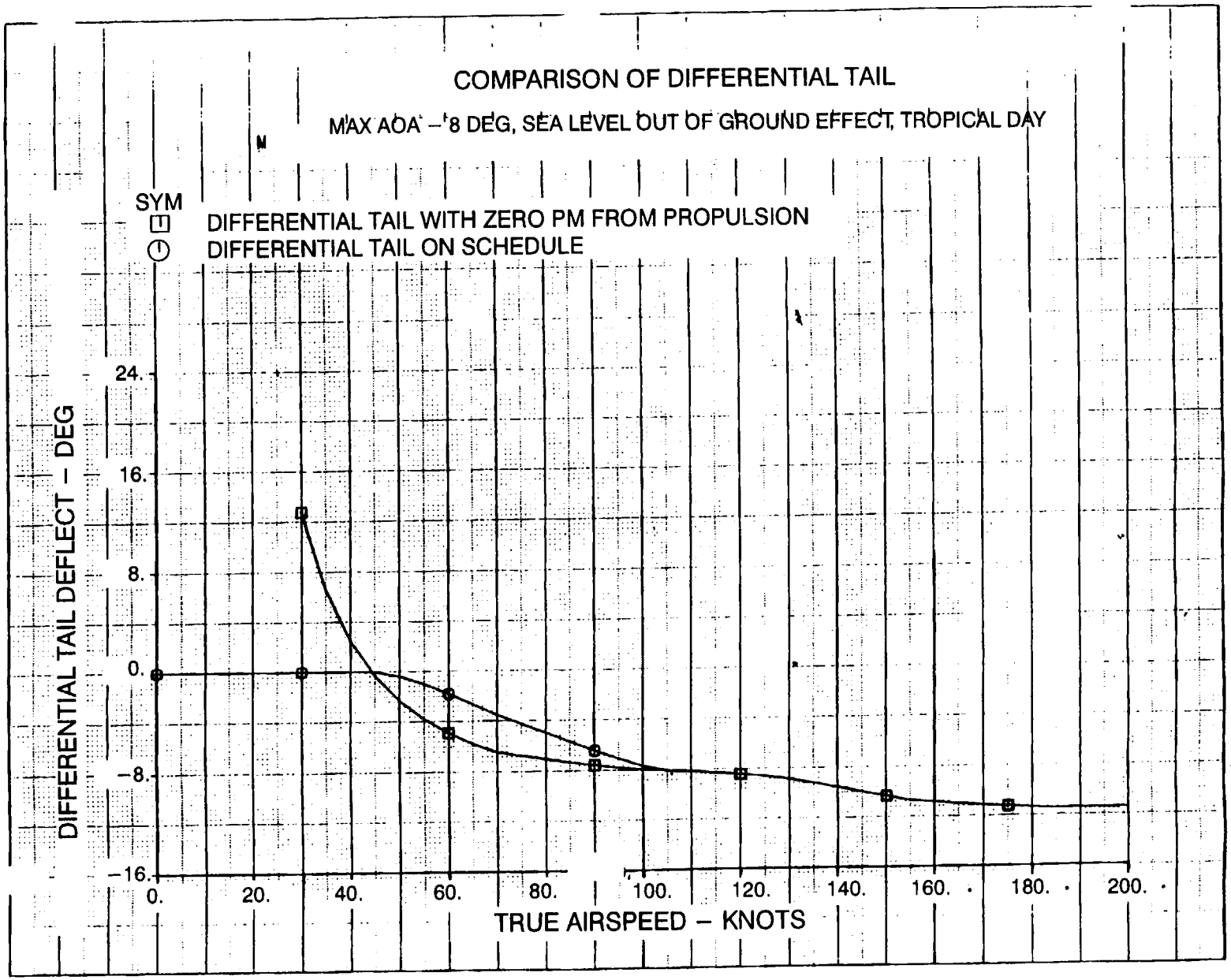

Figure 87. Comparison of Differential Tail

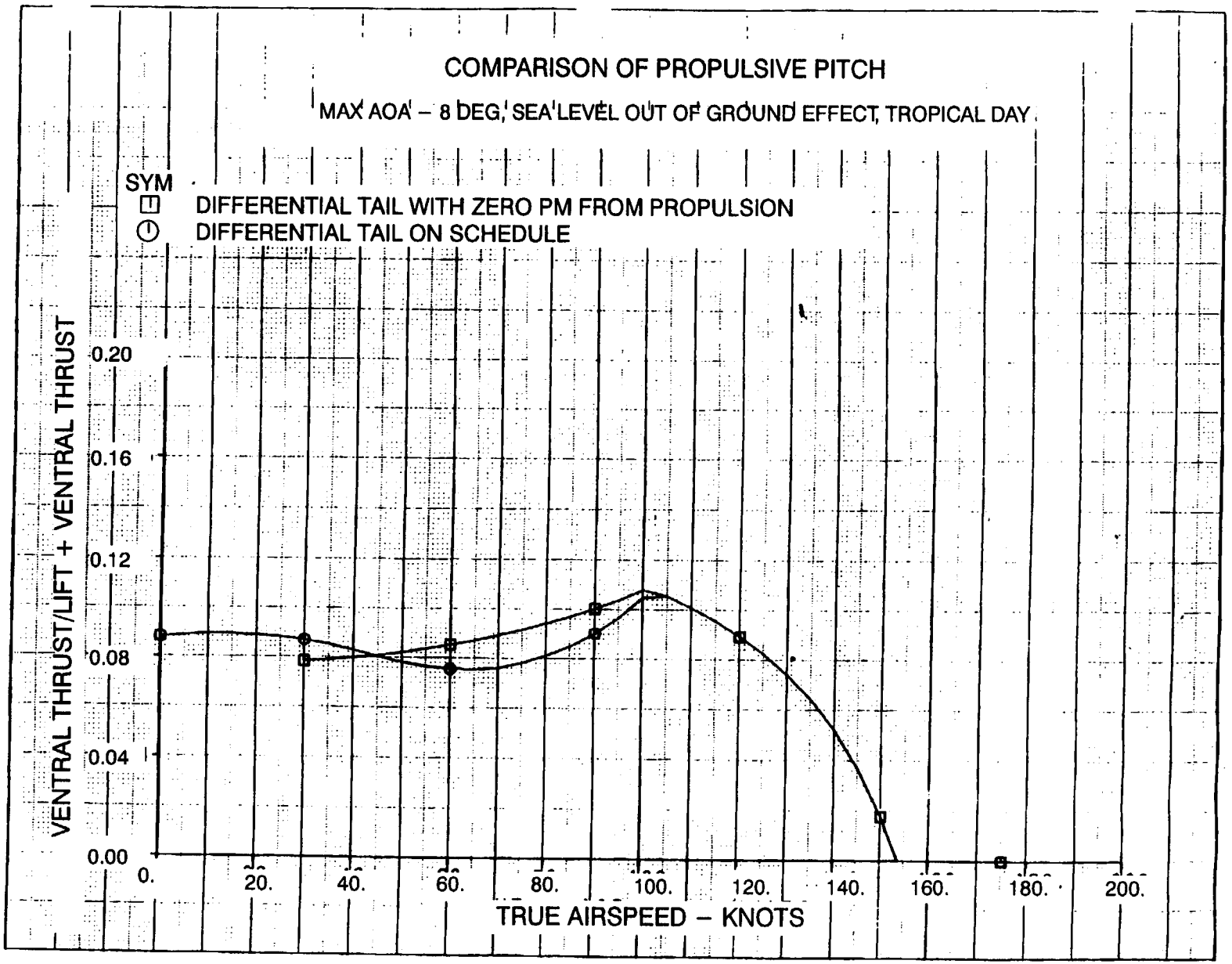

Figure 88. Comparison of Propulsive Pitch

The corresponding pitch axis mixer blending schedule is shown in Figure 89. The schedule blends the pitching moment command as a function of dynamic pressure from all propulsive at 5.4 lb/ft^2 (40 KEAS) to all aerodynamic at 33.8 lb/ft^2 (100 KEAS). This schedule results in a trimmed tail deflection which blends from −8 degrees at 100 knots to 0 degrees at 40 knots, Figure 87. Figure 88 shows the corresponding trimmed ratio of the ventral nozzle's thrust to the sum of the lift and ventral nozzles' thrusts. Figure 90 shows the pitching moment required to trim the aircraft, showing the reversal of required pitching moment to trim resulting from the ram drag forces dominating the basic aerodynamics. This figure also plots the pitch trim contributions of the aerodynamic and propulsive effectors, indicating the smooth and reasonable blend between these effectors.

The pitch axis dynamic pressure blending schedule is also used in the roll and yaw axes, since it provides a reasonable blend and results in simpler control laws. These schedules were analyzed using a steady level flight trim sweep along a maximum 8 degree pitch attitude profile in a 20 knot crosswind.

The yaw axis schedule blends collective tail deflection with differential lift nozzle pitch vectoring. Figure 91 shows the yawing moment required to trim the aircraft in a 20 knot crosswind. Note that the total required trim yawing moment also reverses around 40 knots, indicating that the trimmed collective tail surface deflection naturally tends to zero as airspeed decreases to 40 knots. Thus this dynamic pressure schedule results in low trimmed yawing moment required from the propulsive effectors. Figure 91 also shows the yawing moment contributions from the aerodynamic and propulsive effectors indicating the smooth and reasonable blend between these effectors.

The roll axis schedule blends differential aileron and trailing edge flap deflection with the thrust difference between the left and right lift nozzles. Figure 92 shows the rolling moment required to trim the aircraft in a 20 knot crosswind. Note that the required trimmed rolling moment not only includes contributions from basic aerodynamics and ram drag, but also includes rolling moments generated by the collective tail deflection and differential lift nozzle vectoring used to trim the yaw axis. Figure 92 also shows the rolling moment contributions from the aerodynamic and propulsive effectors, indicating the smooth and reasonable blend between these effectors.

3.4.2. Transition Envelope Sensitivity and Control Power Analyses

The analyses use the MODSDF aerodynamic analysis options which perform trim sweeps. The trim sweeps plot the trimmed aircraft states, surface deflections, nozzle thrusts, and nozzle vector angles, as a function of velocity ranging from 0 to 200 knots. In each analysis described in the subsequent subsections, the transition envelope is described using trim sweeps which vary a second flight condition parameter describing whether the aircraft is in a descending or ascending flight condition, in an accelerating or decelerating flight condition, or in a crosswind. The trimmed control effector positions are computed using the schedules described in Section 3.4.1.

All cases are for STOL flaps (leading and trailing edge flaps down 30 degrees, and ailerons down 15 degrees). Also the gears are down, LIDs are deployed, and both the main and secondary inlets are open. Gross weight is 25000 pounds with corresponding inertias of 97450, 11650, and 104775 in pitch, roll, and yaw, respectively. All flight conditions are for 50 feet (out of ground effect) and a MIL−STD−210A tropical day temperature (about 90°F at sea level).

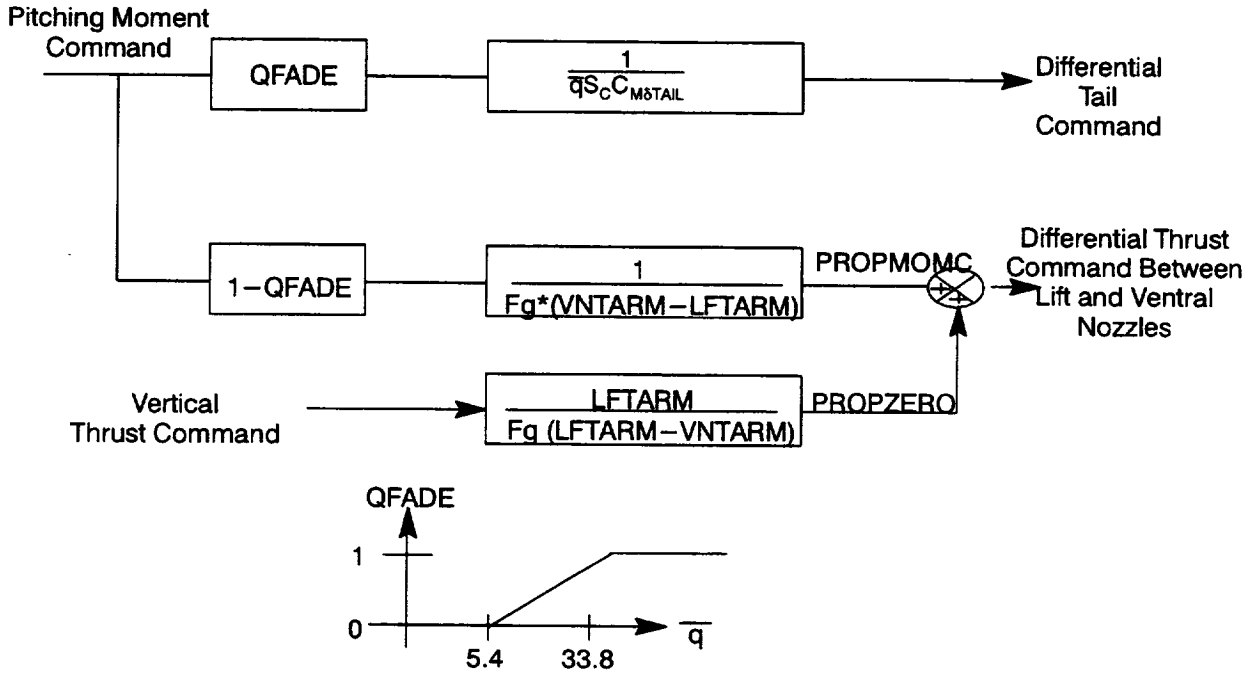

FG = Total Thrust
VNTARM = Moment Arm of Ventral Nozzle Thrust to cg
LFTARM = Moment Arm of Lift Nozzle Thrust to cg

Figure 89. Corresponding Pitch Axis Mixer Blending Schedule

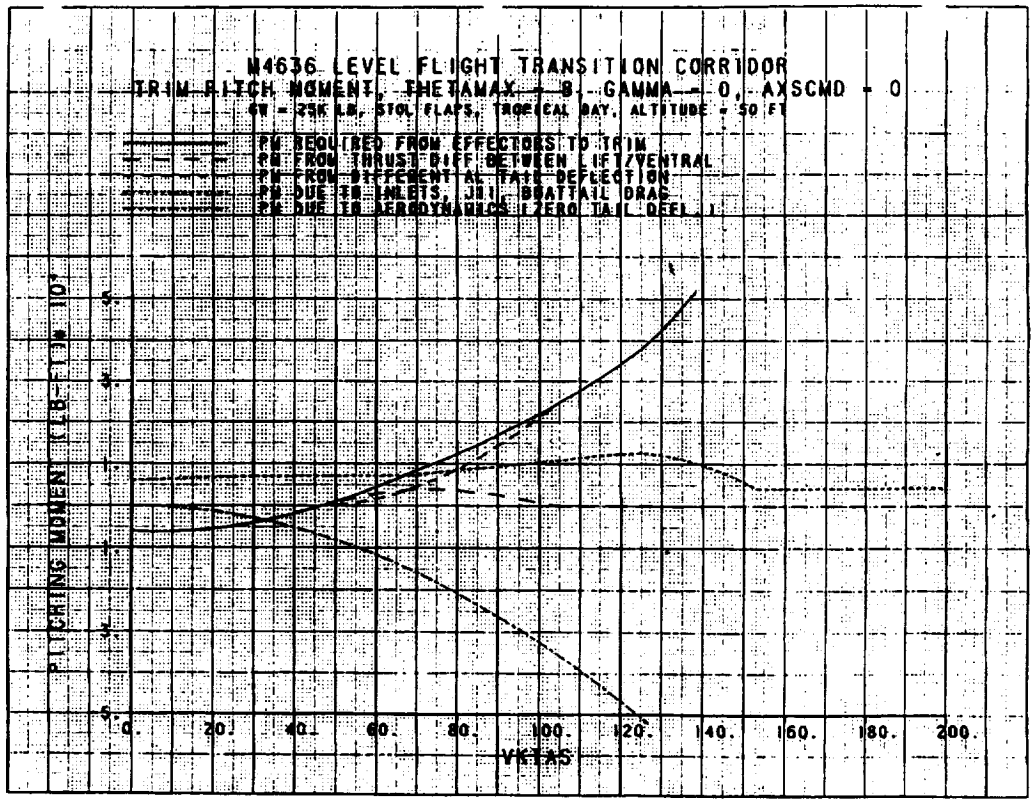

Figure 90. Trim Pitch Moment, Thetamax = 8, Gamma = 0, AXSCMD = 0

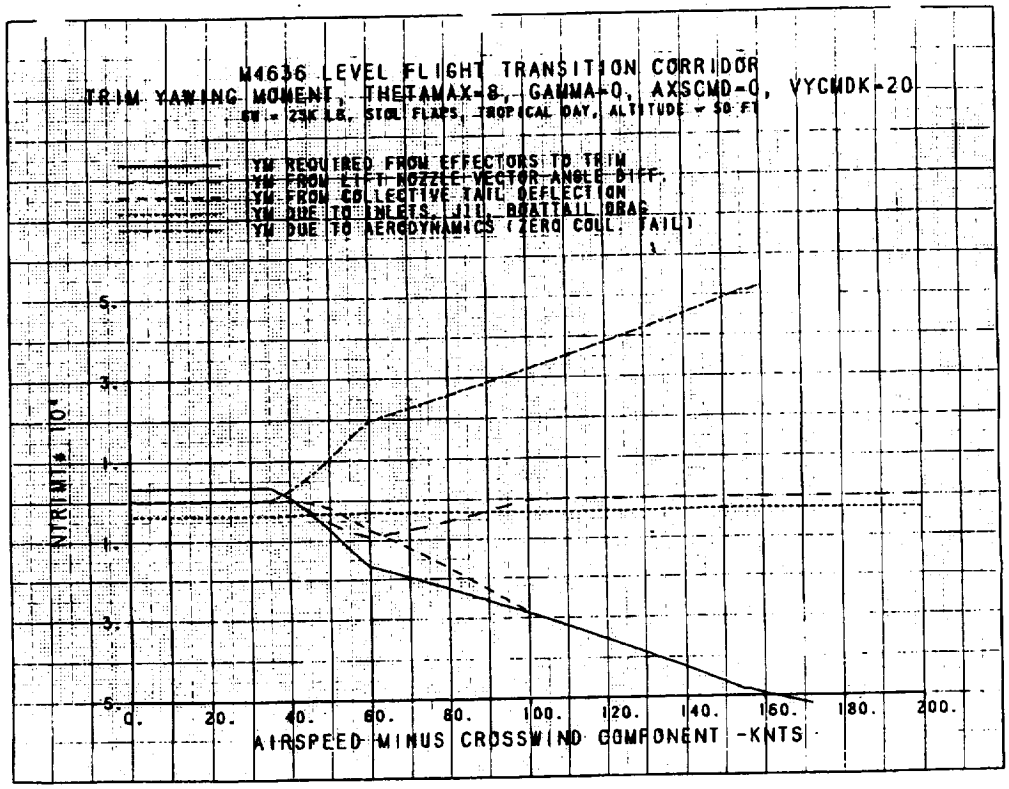

Figure 91. Trim Yawing Moment, Thetamax = 8, Gamma = 0, AXSCMD = 0, VYCMDK = 20

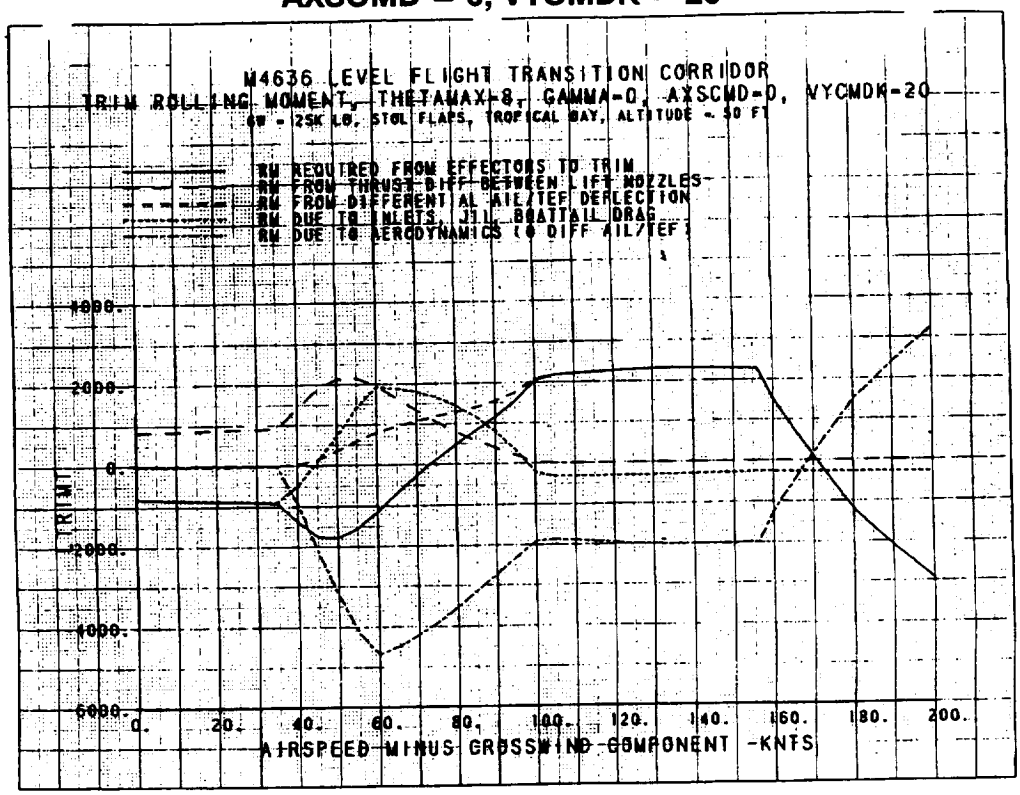

Figure 92. Trim Rolling Moment, Thetamax = 8, Gamma = 0, AXSCMD = 0, VYCMDK = 20

The control power capability is described as the pitch, roll, and yaw acceleration that results when the control effectors are abruptly moved from their trimmed settings to their limits. In hovering cases, normal force capability is described as the normal acceleration that results with an abrupt change to maximum engine power.

3.4.2.1. Transition Envelopes

This section describes the envelope of nonaccelerating flight conditions for which trimmed flight is possible during transition. These envelopes are described using plots of the envelope of achievable flight path elevation angles at various effective jet angles ranging from 0 to 90 degrees. Figure 93 describes the flight path/velocity envelope for an effective jet angle of 0 degrees. The lower limit from 200 knots down to about 120 knots is the trimmed flight path at idle engine power. The envelope then is limited by 16 degrees trim angle of attack down to about 55 knots where the maximum flight path angle of 74 degrees at 16 degrees angle of attack is reached (pitch attitude equals 90 degrees). The envelope is limited above by maximum engine power. An upper limit is reached here due to the high drag associated with having flaps down, gear down, and LIDs deployed. Figure 94 shows these same limits for an effective jet angle of ten degrees. For jet angles of 20, 30, and 40 degrees, the envelope limits come together as shown in Figure 95 to, Figure 97 illustrating that lower velocity flight conditions can only be reached at higher effective jet vector angles. Figure 98 through Figure 102 show the lower velocity flight conditions which can be achieved at these higher effective jet angles.

3.4.2.2. Transition Envelope Sensitivity to Maximum Allowable Pitch Attitude

This section describes the sensitivity of the steady level flight transition envelope to maximum allowable pitch attitude, and control power available at the trim points along the maximum pitch attitude profile. The trim sweep is steady level flight with varying limits on allowable pitch attitude from 6 to 16 degrees. Figure 103 plots the envelope of effective jet angles as a function of velocity, illustrating the sensitivity of the lower end to the maximum allowable pitch attitude. Figure 104 shows the effective jet thrust magnitude sensitivity to maximum pitch attitude. Figure 105 shows the corresponding trimmed pitch attitude. These figures verify that the reference 8 degrees maximum pitch attitude profile is near the center of the envelope and allows adequate margin to produce lift with angle of attack or engine power, while providing adequate line of sight for the pilot.

Figure 106 through Figure 111 show the pitch, roll, and, yaw acceleration capability for the trimmed flight conditions along the maximum pitch attitude profile. These figures show that the US/UK CEM pitch, roll, and yaw acceleration requirements below 35 knots are met, and increase sufficiently in transition to provide adequate control power using the primary effectors with no reaction controls utilized. Figure 112 plots the normal acceleration in aircraft body axes that results from an abrupt increase in engine power to maximum dry power, and exceeds 0.1 g in the lower speed regions. In higher speed regions sufficient normal acceleration is achieved through wing lift.

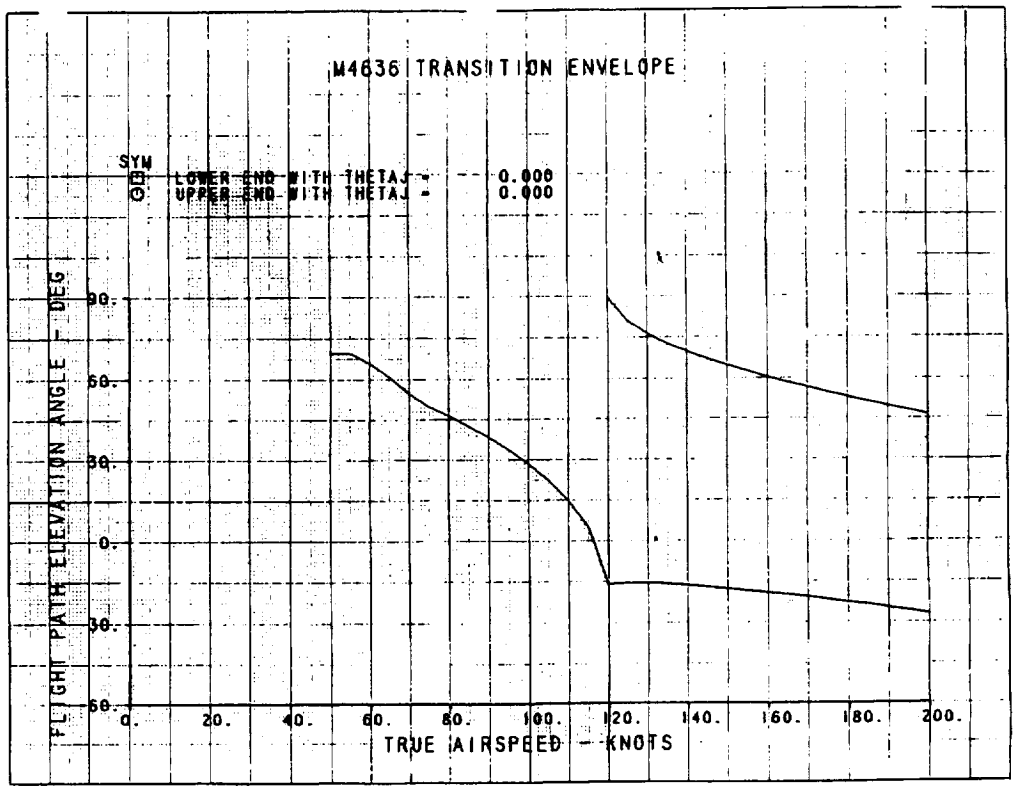

Figure 93. M4636 Transition Envelope, Jet Angle = 0°

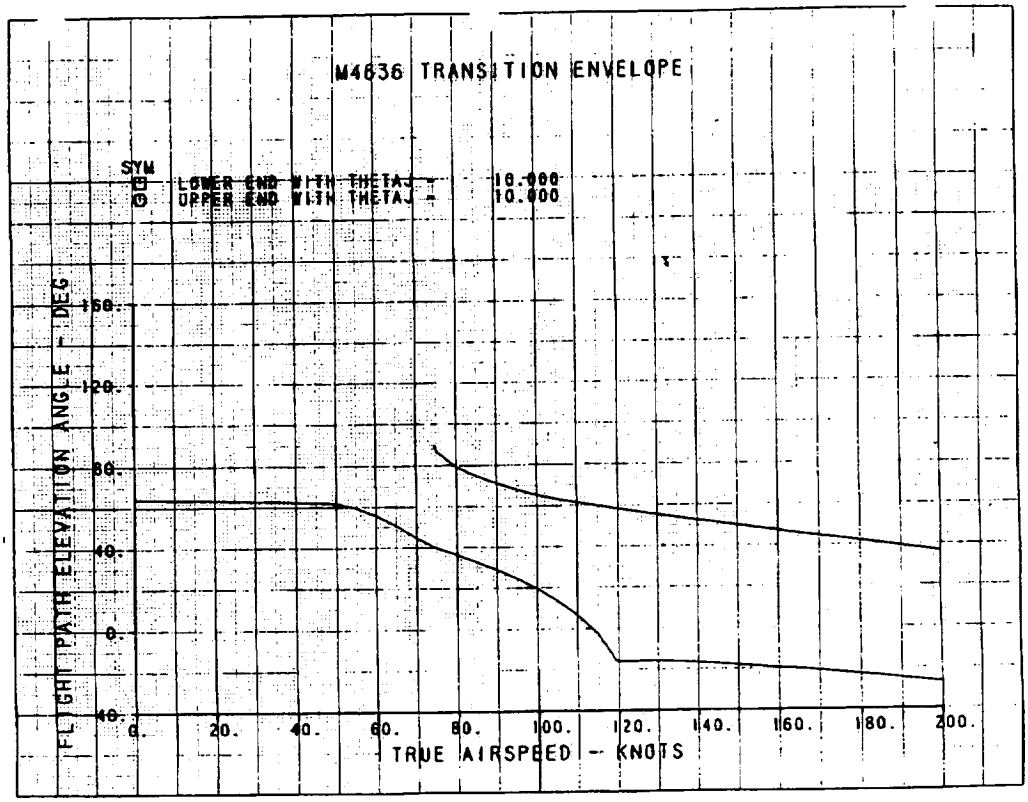

Figure 94. M4636 Transition Envelope, Jet Angle = 10°

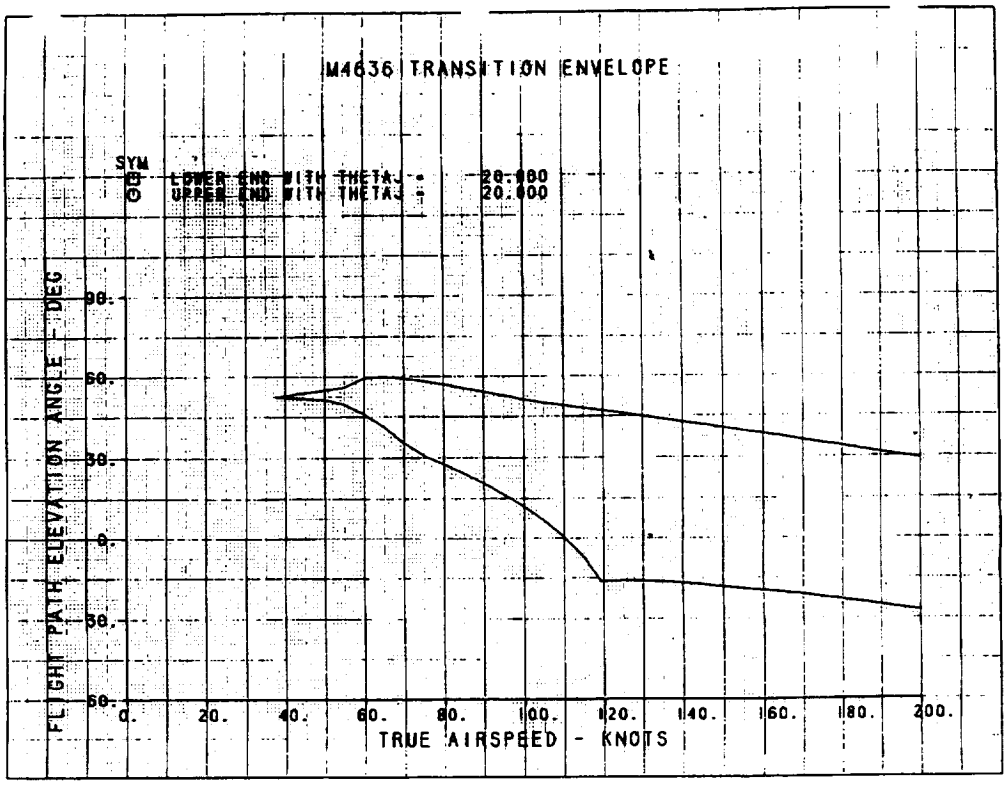

Figure 95. M4636 Transition Envelope, Jet Angle = 20°

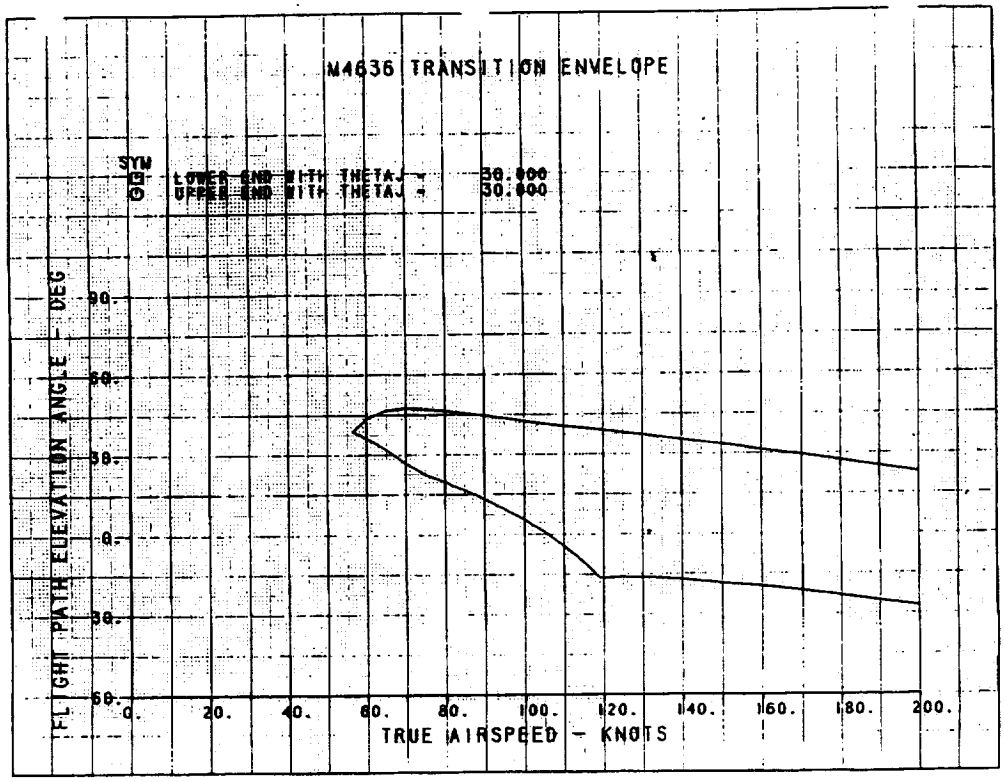

Figure 96. M4636 Transition Envelope, Jet Angle = 30°

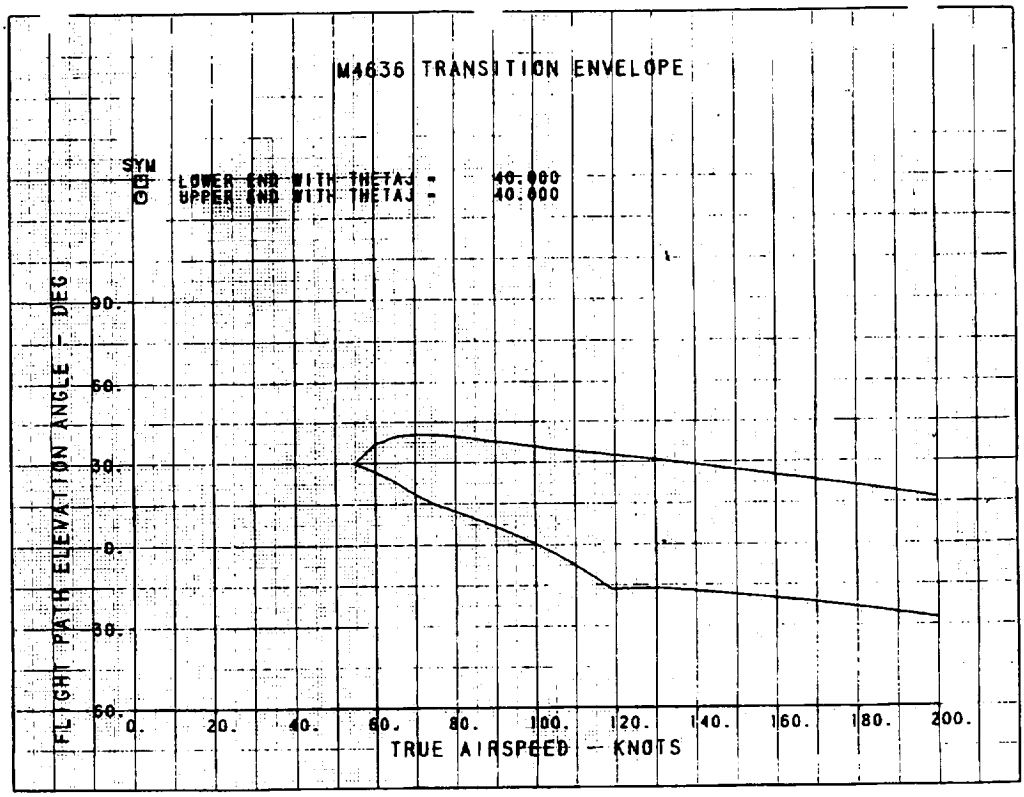

Figure 97. M4636 Transition Envelope, Jet Angle = 40°

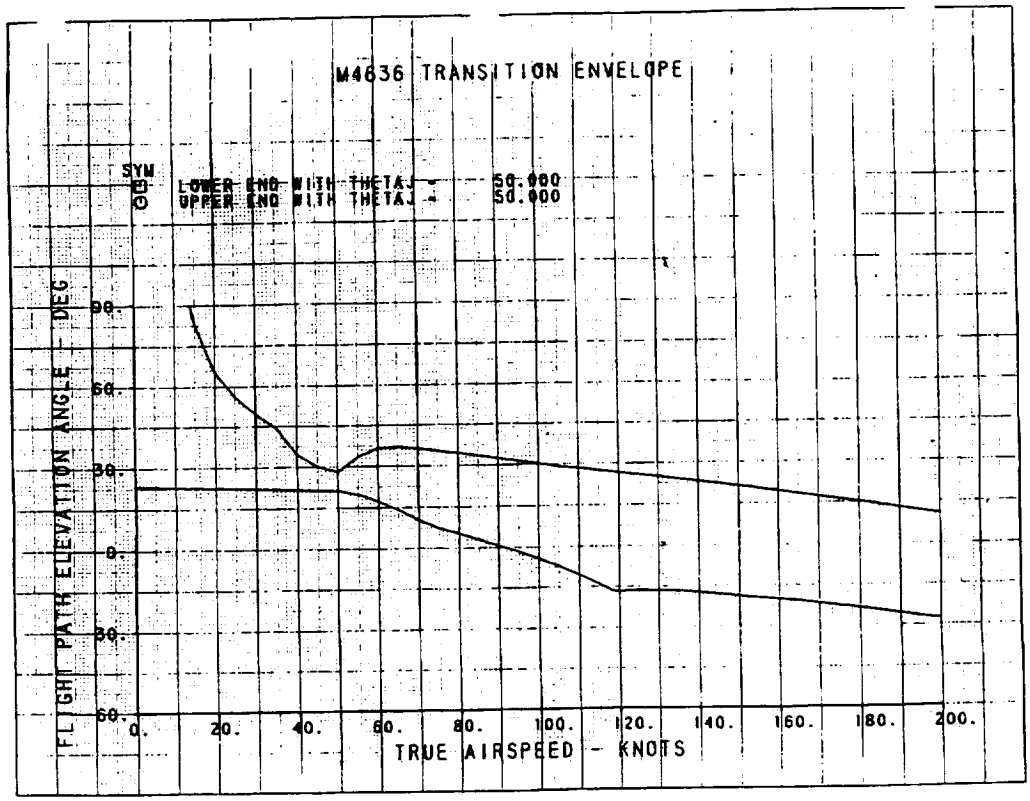

Figure 98. M4636 Transition Envelope, Jet Angle = 50°

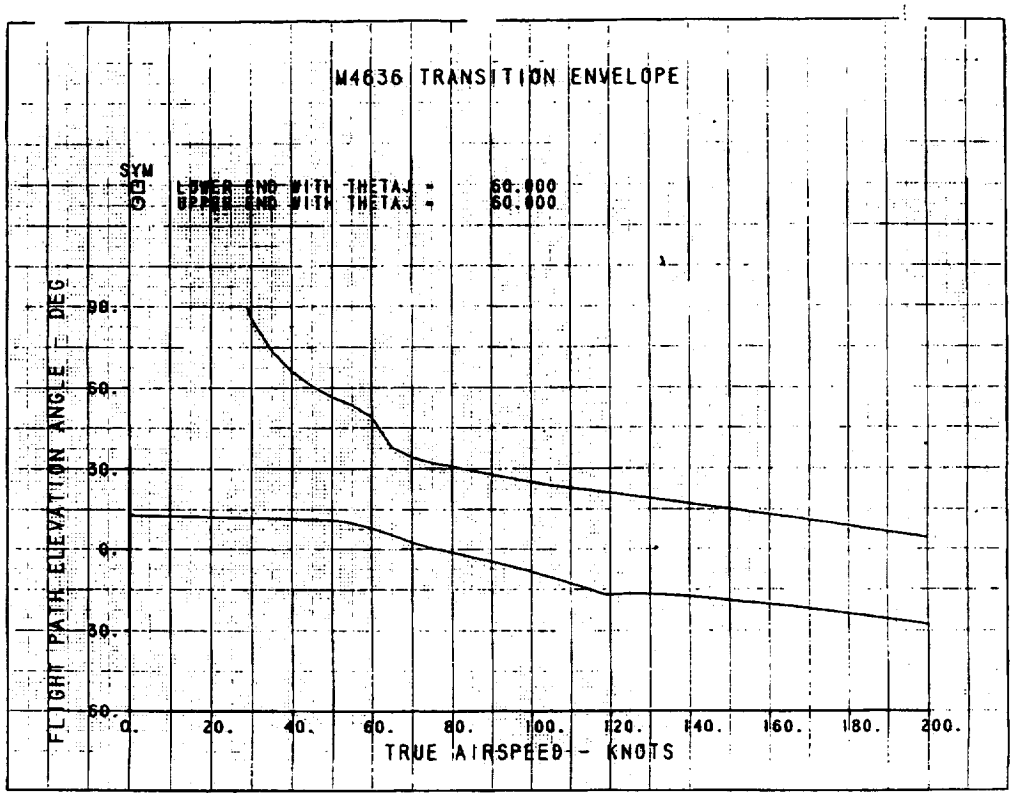

Figure 99. M4636 Transition Envelope, Jet Angle = 60°

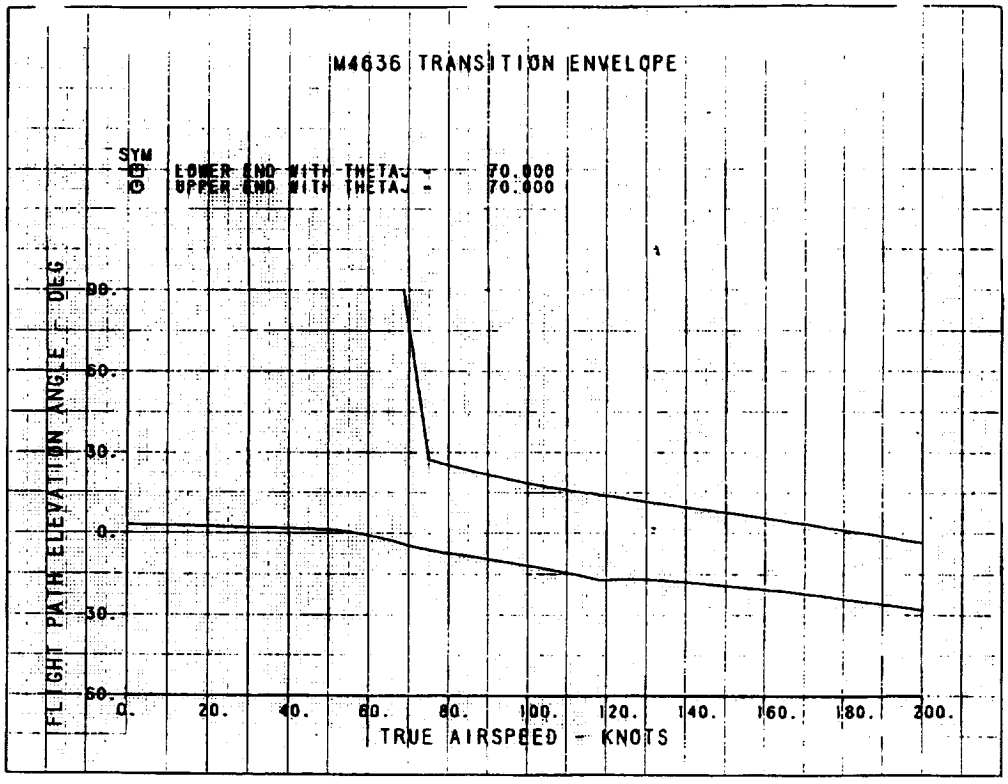

Figure 100. M4636 Transition Envelope, Jet Angle = 70°

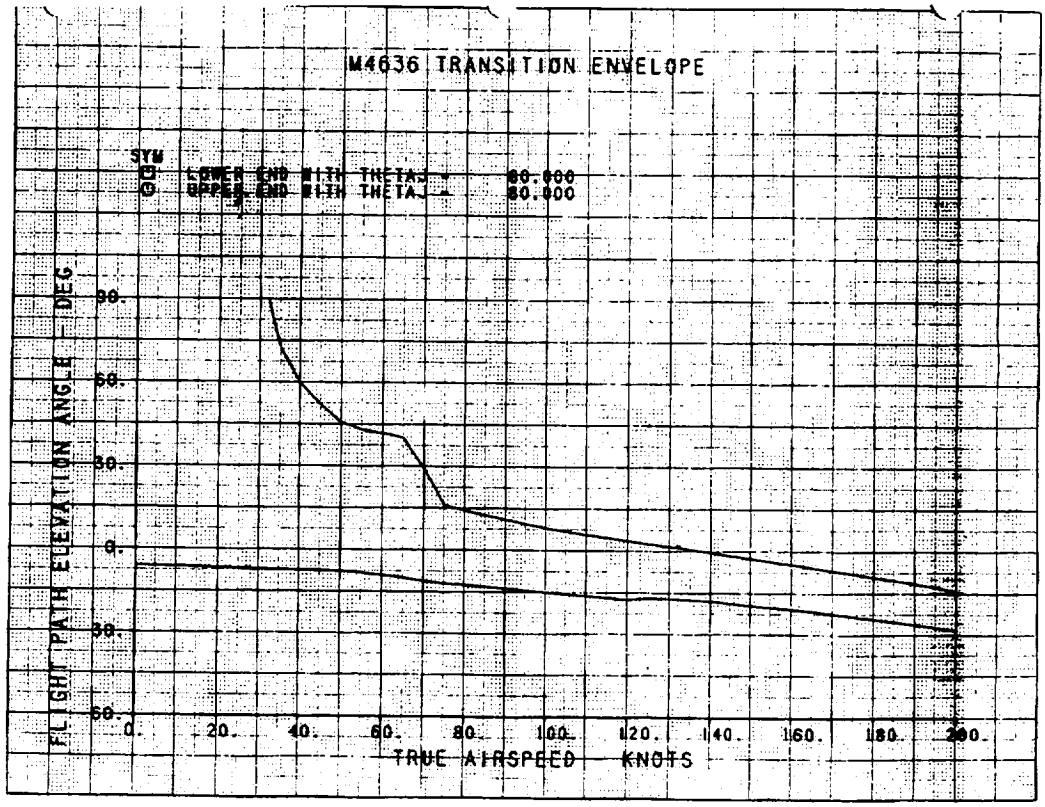

Figure 101. M4636 Transition Envelope, Jet Angle = 50°

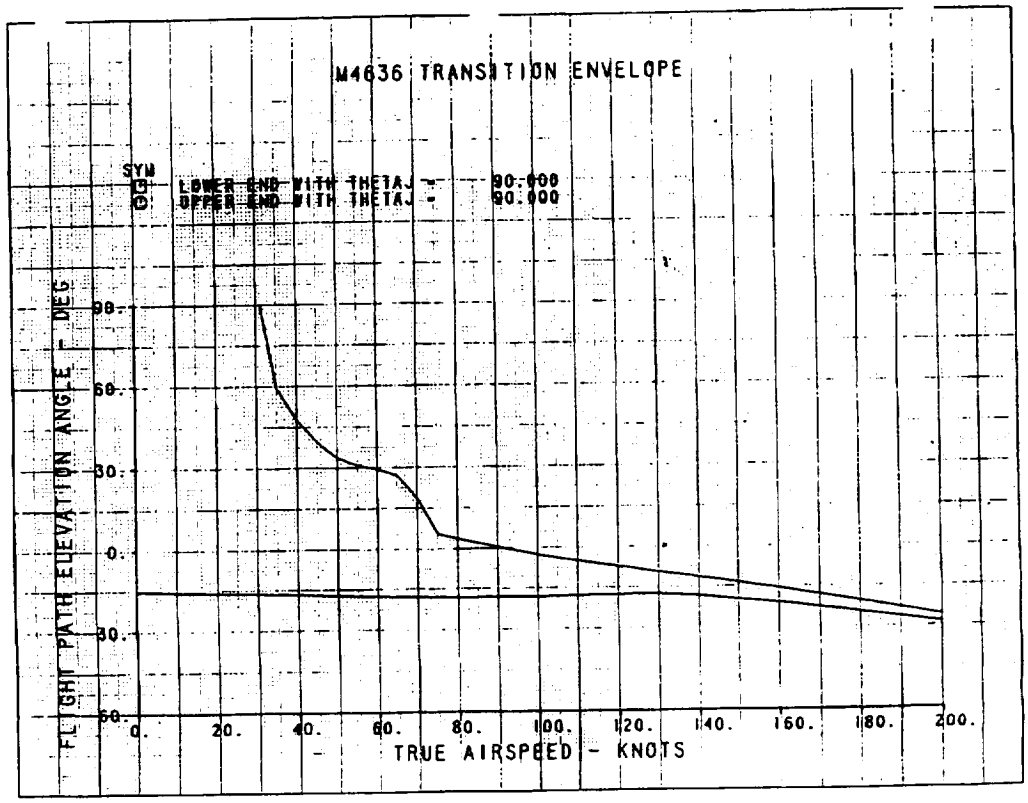

Figure 102. M4636 Transition Envelope, Jet Angle = 60°

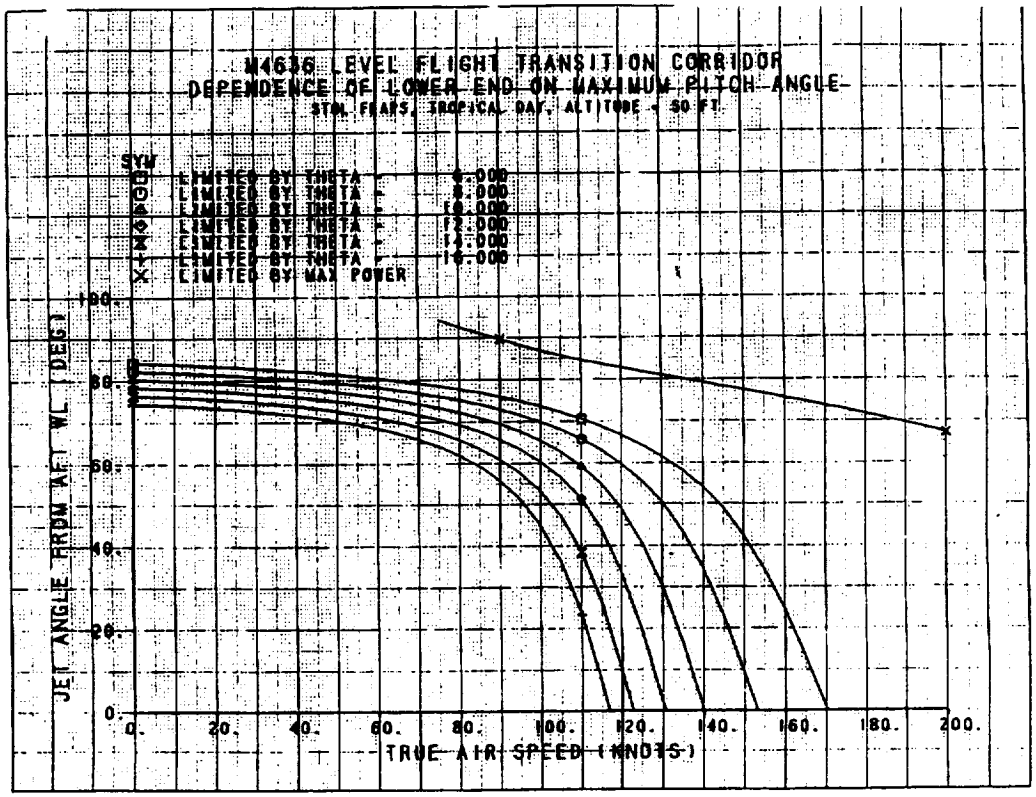

Figure 103. Jet Angle versus True Air Speed

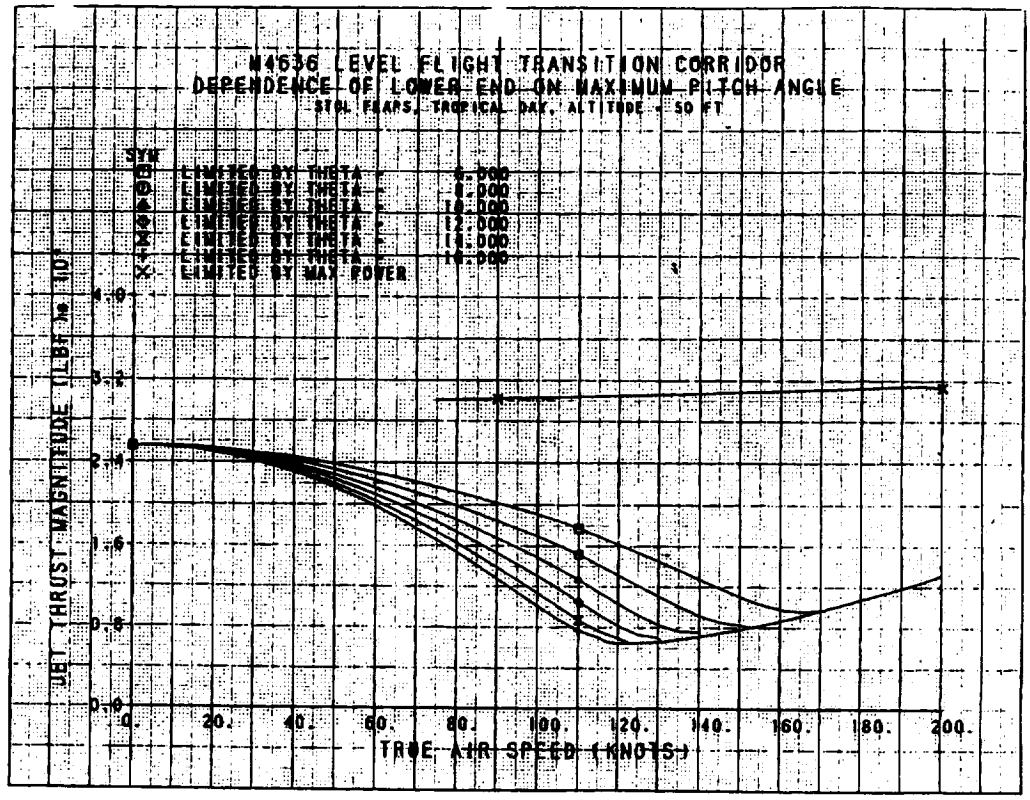

Figure 104. Thrust Magnitude versus True Air Speed

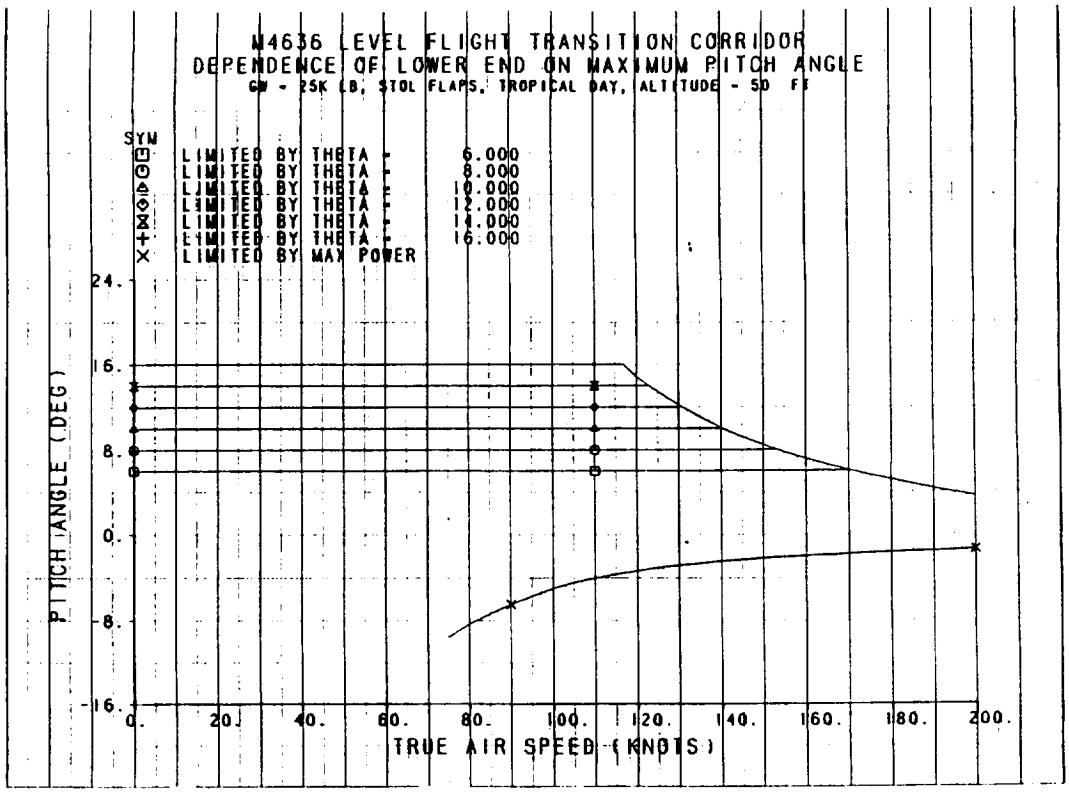

Figure 105. Dependence of Lower End on Maximum Pitch Angle

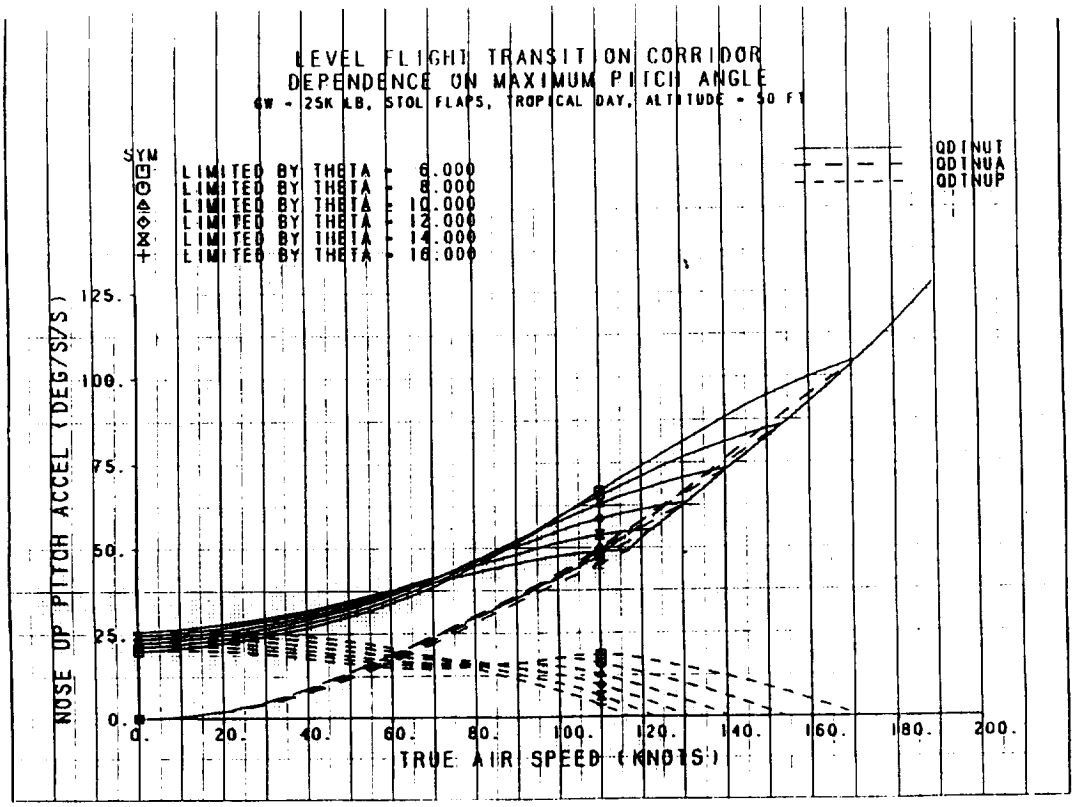

Figure 106. Dependence on Maximum Pitch Angle

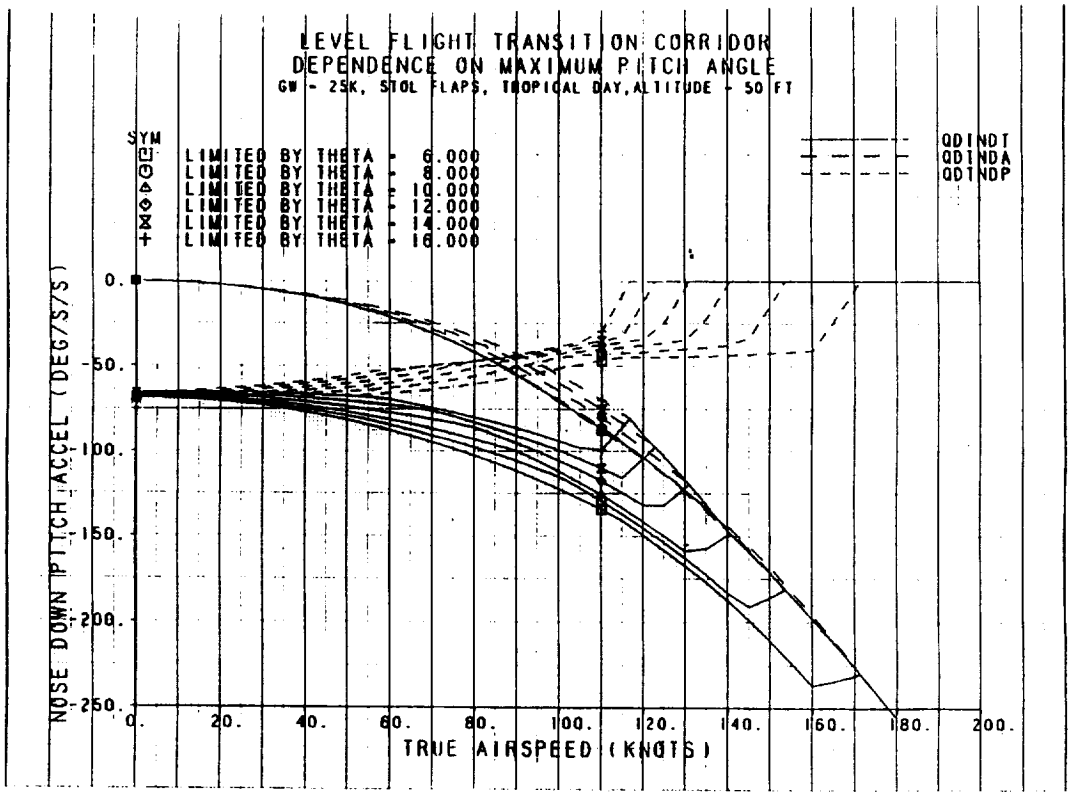

Figure 107. Dependence on Maximum Pitch Angle

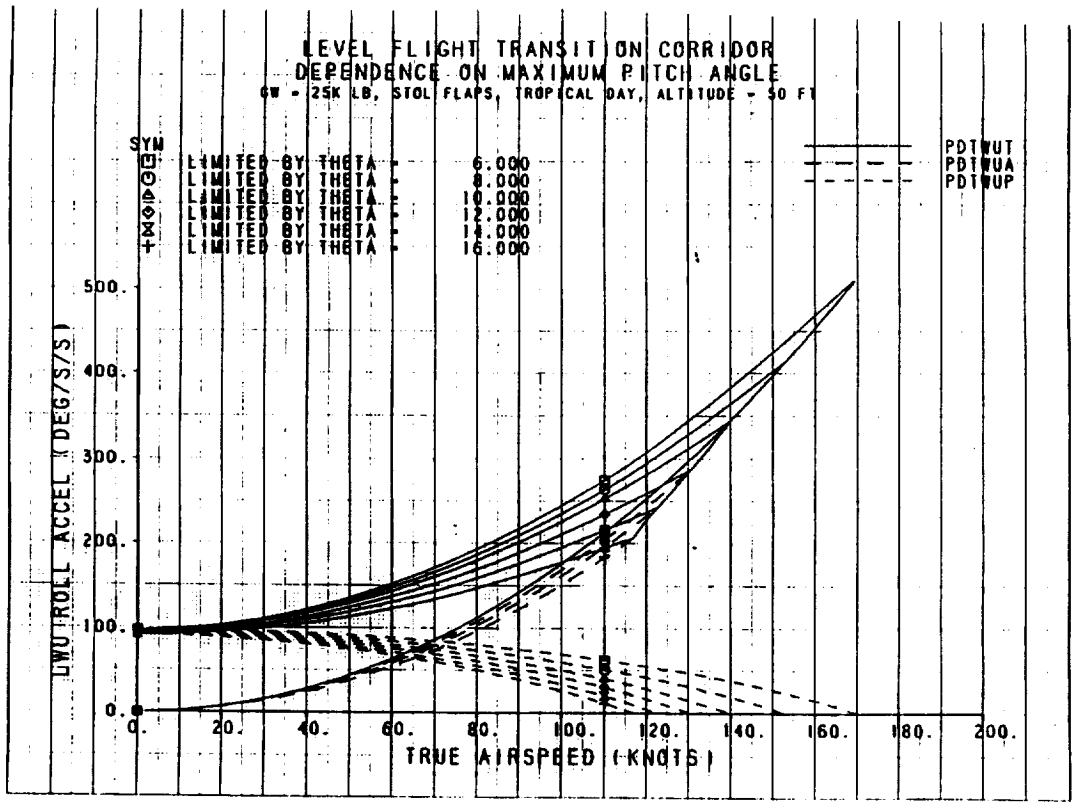

Figure 108. Dependence on Maximum Pitch Angle

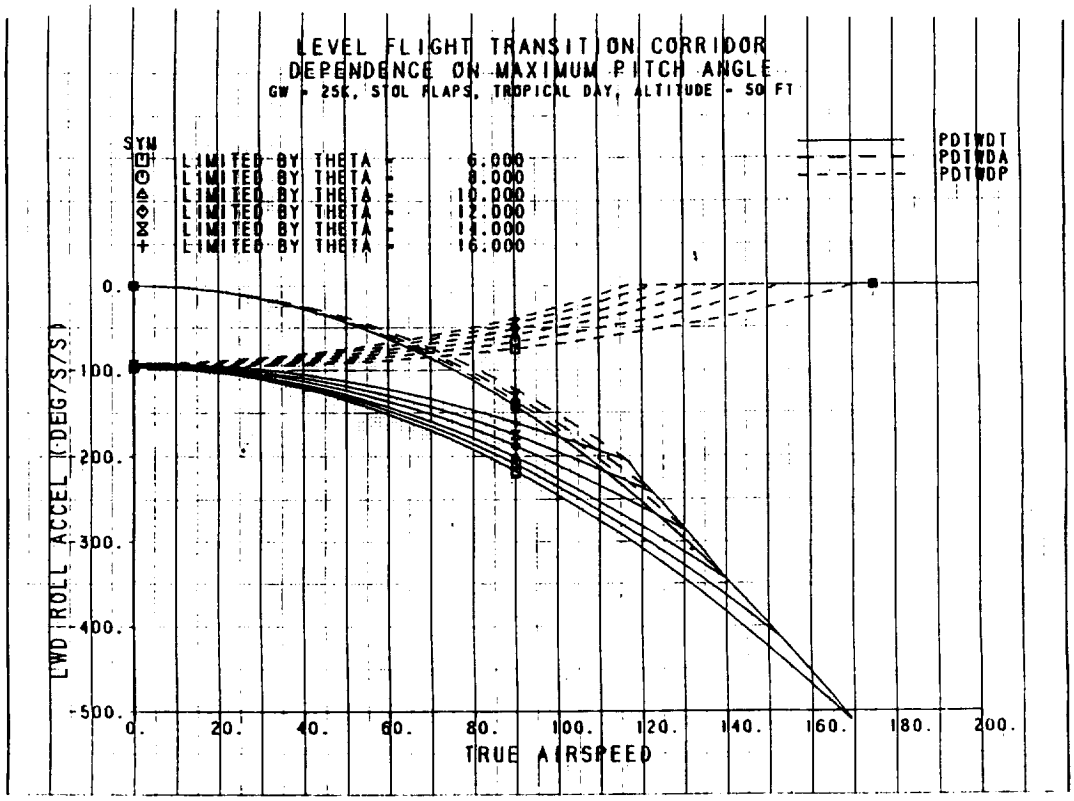

Figure 109. Dependence on Maximum Pitch Angle

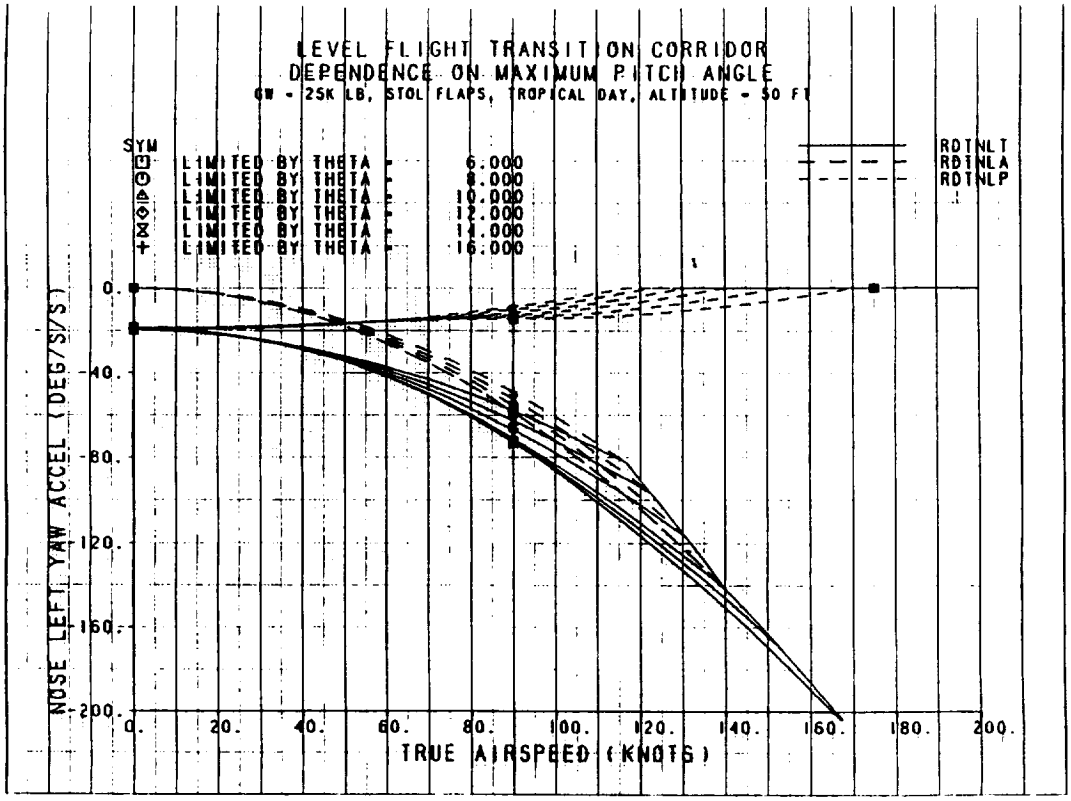

Figure 110. Dependence of Lower End on Maximum Pitch Angle

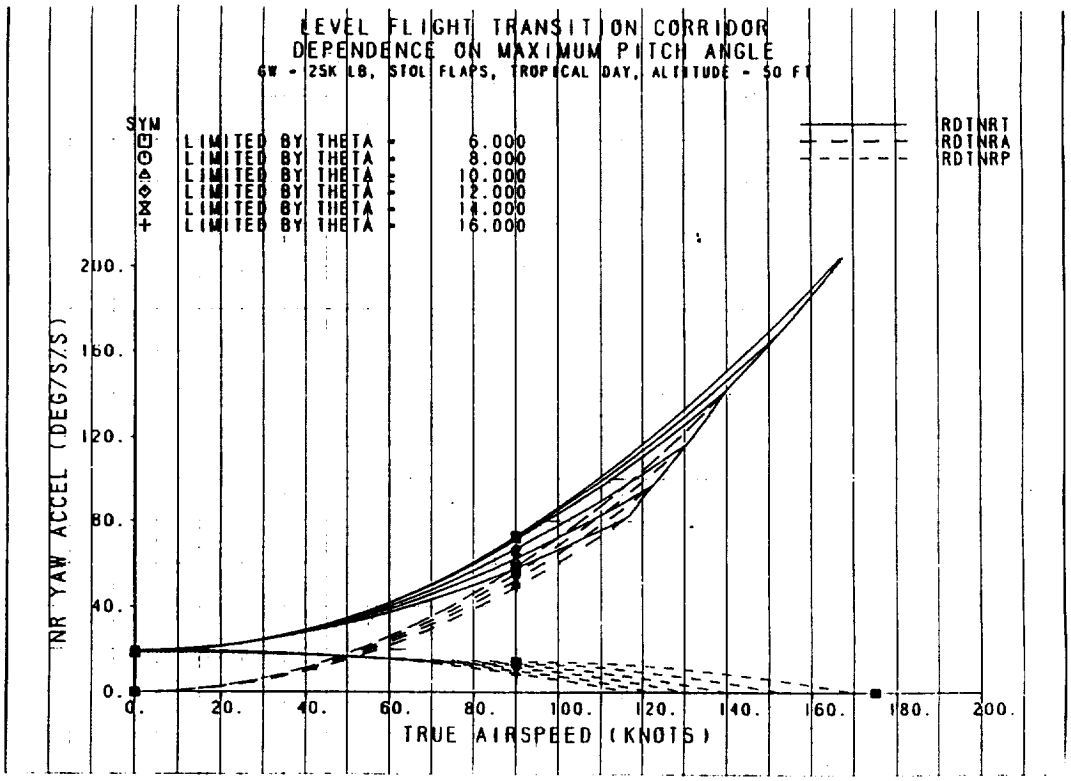

Figure 111. Dependence on Maximum Pitch Angle

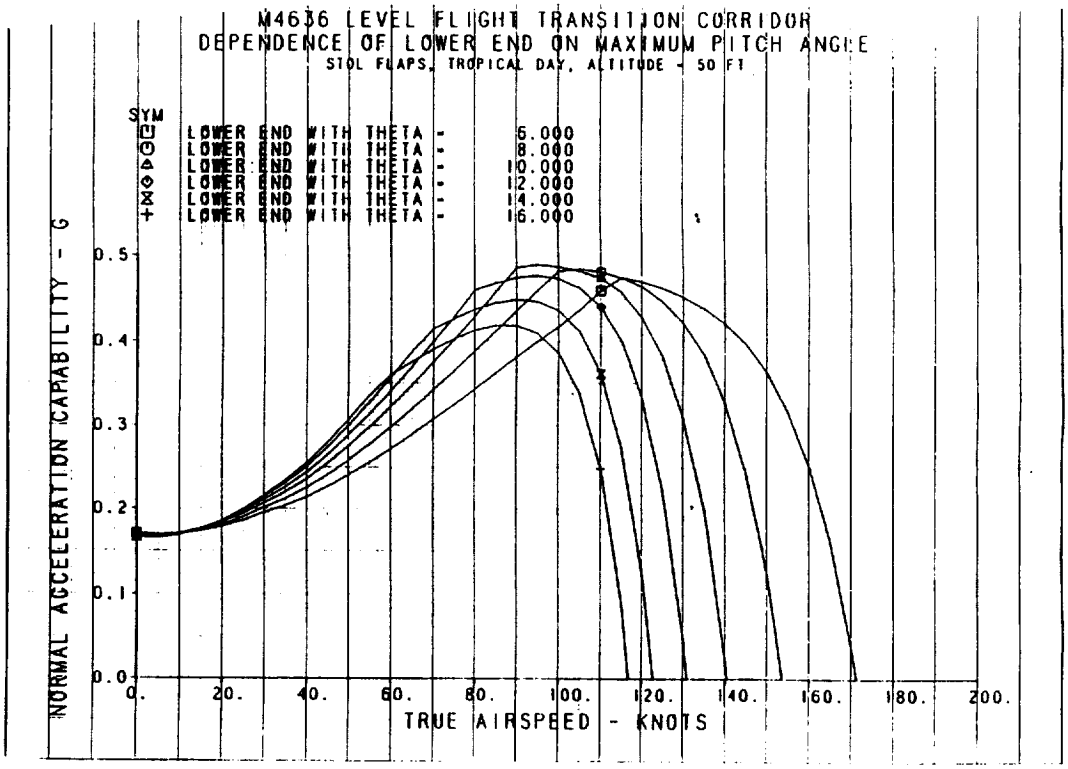

Figure 112. Dependence of Lower End on Maximum Pitch Angle

3.4.2.3. Level Flight Accelerating and Decelerating Transition Envelopes

This section describes the level flight decelerating and accelerating transition envelopes. The lower end of the effective jet angle envelopes were computed along the reference maximum 8 degree pitch attitude profile with acceleration along the flight path varying between −0.25 and +0.20 g's. A deceleration of −0.21 g's corresponds to the US/UK CEM requirement for a decelerating transition from 200 knots to hover in 50 seconds.

For decelerating transitions, Figure 113 and Figure 114 describe the envelopes of effective jet thrust vector angles and magnitudes. Note that a −0.20 g steady deceleration requires forward nozzle vectoring (greater than 82 degrees) below 123 knots airspeed. Also the maximum power envelope limit depends on the deceleration rate. Figure 115 shows the corresponding trimmed pitch attitude. These figures indicate that the aircraft satisfies the US/UK CEM requirement of 50 seconds to decelerate from 200 knots to hover. Figure 116 through Figure 121 show the pitch, roll, and, yaw acceleration capability for these trimmed flight conditions, indicating the adequate control power exists in level flight decelerating transitions along the reference 8 degree maximum pitch attitude profile. Figure 122 indicates that adequate normal acceleration capability from engine power exists in the lower end of the transition envelope.

Figure 123 through Figure 132 show similar plots for accelerating transitions, and show that adequate control power exists in accelerations.

3.4.2.4. Transition Envelope Sensitivity to Trimmed Flight Path Angle

This section describes the transition envelope limits in steady ascents and descents. The trim sweeps are steady descents along a maximum 8 degree pitch attitude profile with flight path varying between −9 and 0 degrees, and steady ascents along a maximum 8 degree angle of attack profile with flight path varying between 0 and 12 degrees.

Figure 133 and Figure 134 describe the effective jet thrust vector angles and magnitudes for steady descents. Note that the transition envelope widens as flight path elevation angle decreases. This is primarily due to the increase in allowable angle of attack along the 8 degree pitch attitude profile that results when the flight path is decreased. Figure 135 and Figure 136 show the corresponding trimmed pitch attitude and angle of attack. Figure 137 through Figure 142 show the pitch, roll, and yaw acceleration capability for these trimmed flight conditions, indicating that adequate control power exists in steady descents. Figure 143 indicates that adequate normal acceleration capability from engine power exists.

Figure 144 through Figure 154 show similar plots for steady ascents. As seen in Figure 144, the width of the jet angle/velocity envelope does not change significantly due to the fact that the trim sweep for the lower end is along a constant 8 degree angle of attack profile, with pitch attitude increasing with the flight path, as shown in Figure 146 and Figure 147. Again the figures show that adequate control power exists in steady ascents.

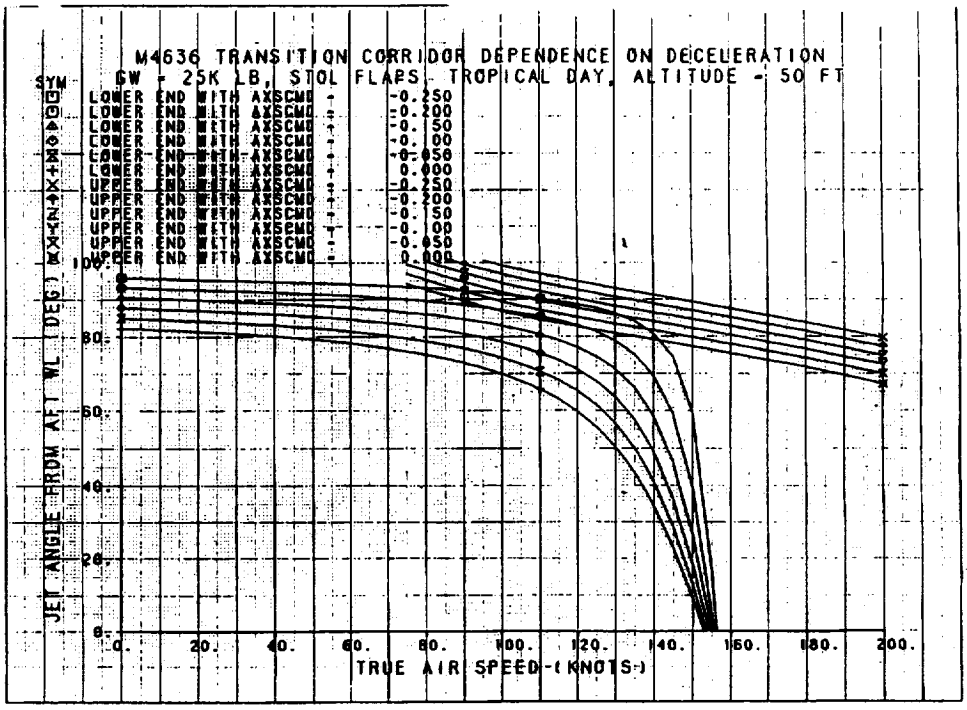

Figure 113. Transition Corridor Depending on Deceleration

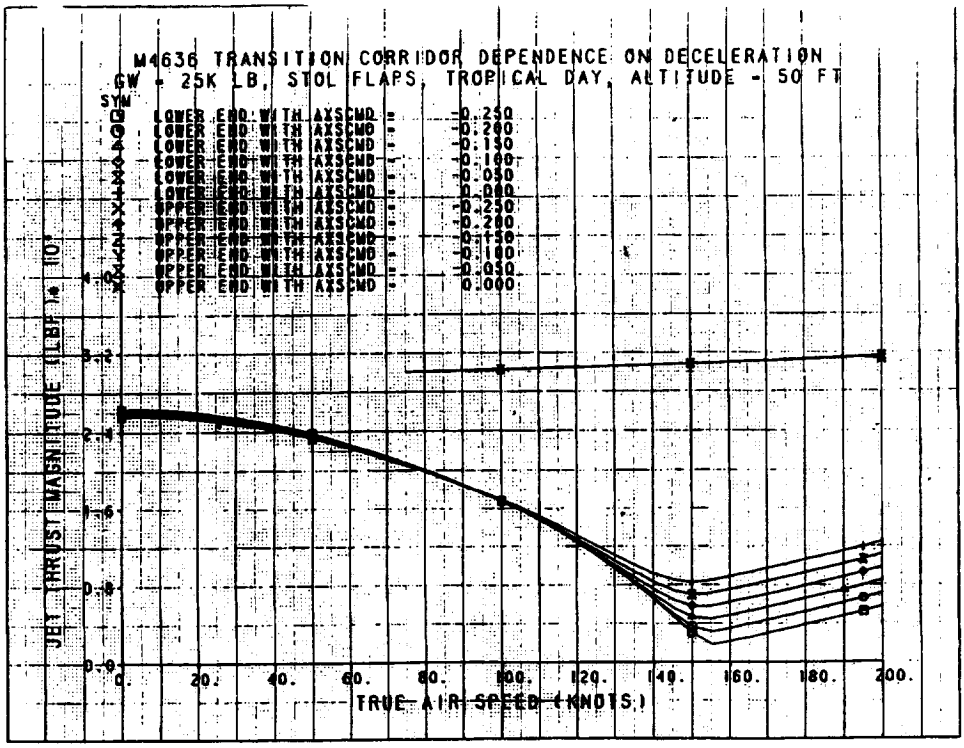

Figure 114. Transition Corridor Dependence on Deceleration

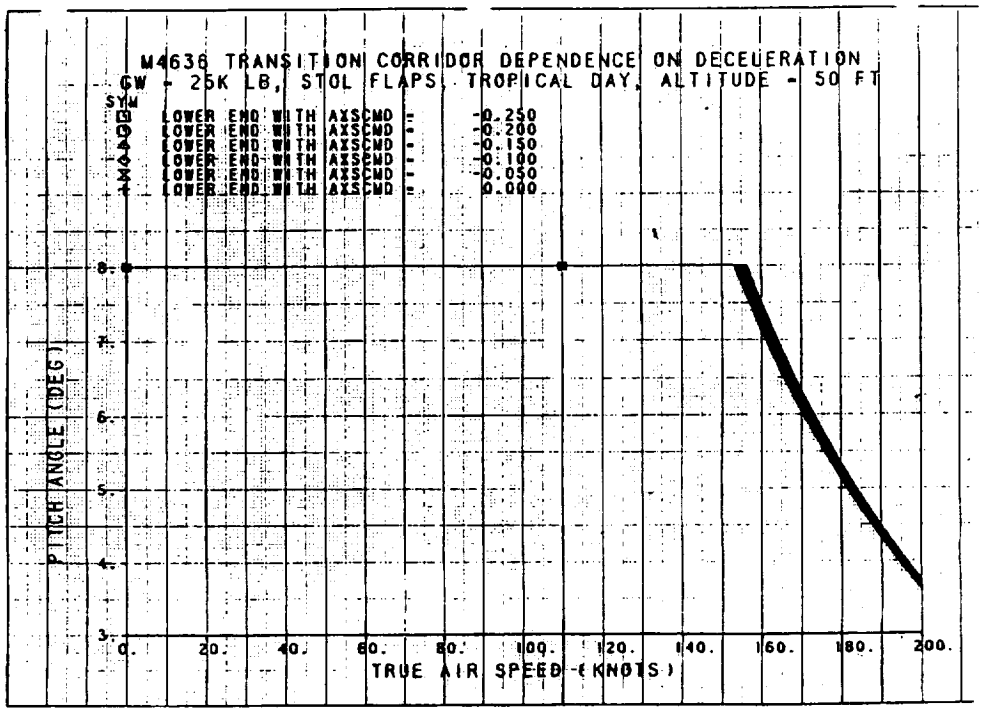

Figure 115. Transition Corridor Dependence on Deceleration

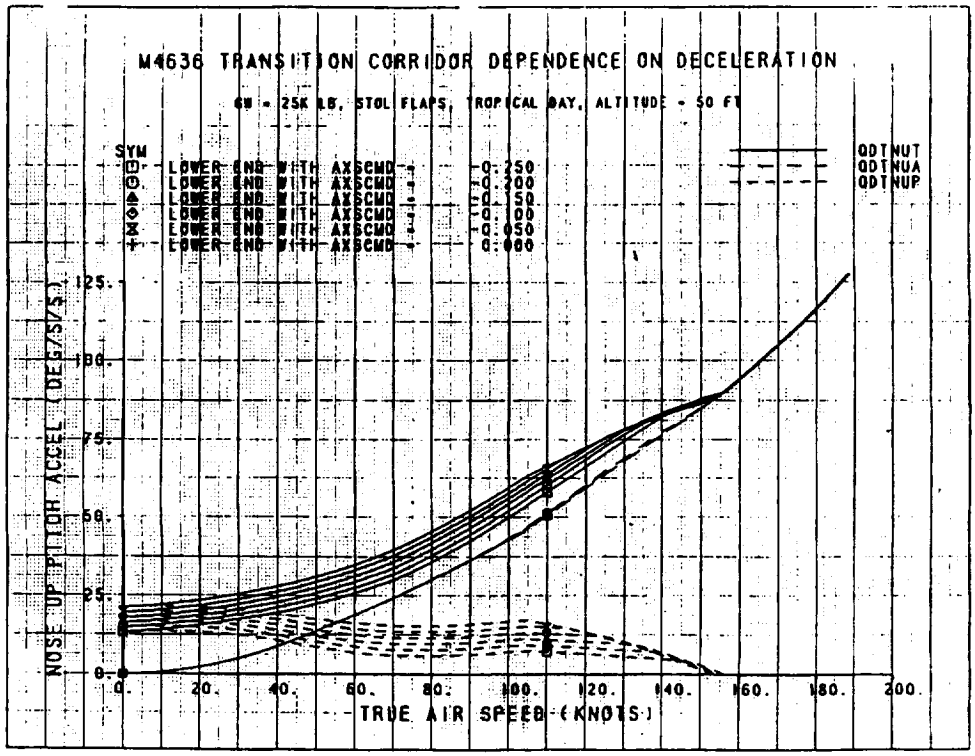

Figure 116. Transition Corridor Dependence on Deceleration

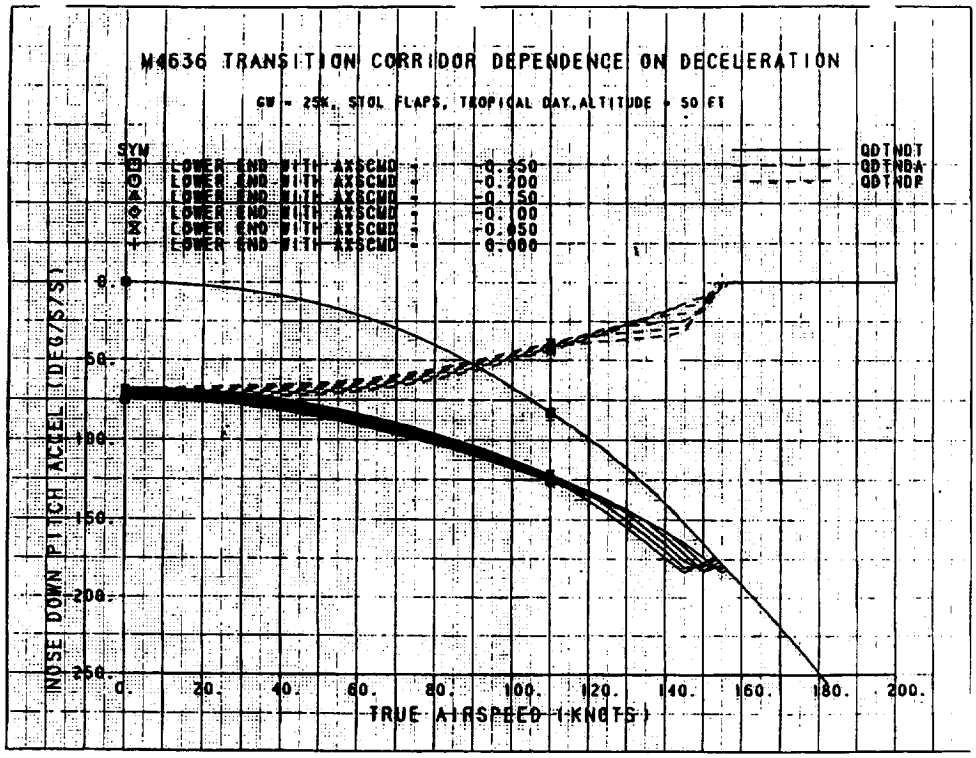

Figure 117. M4636 Transition Corridor Dependence On Deceleration

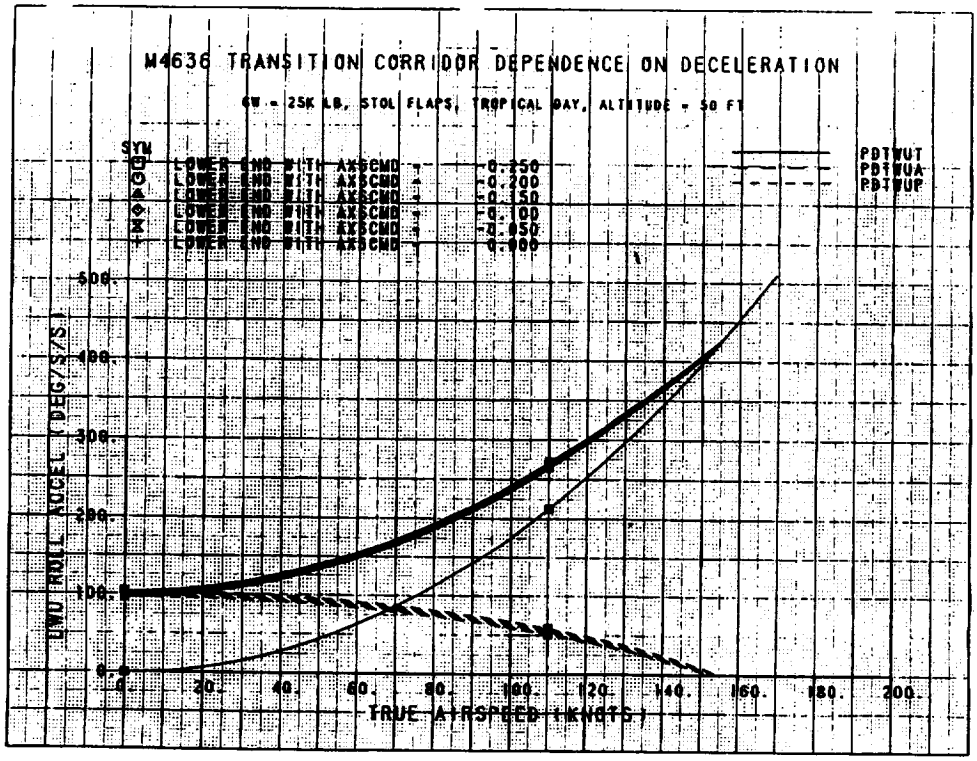

Figure 118. M4636 Transition Corridor Dependence On Deceleration

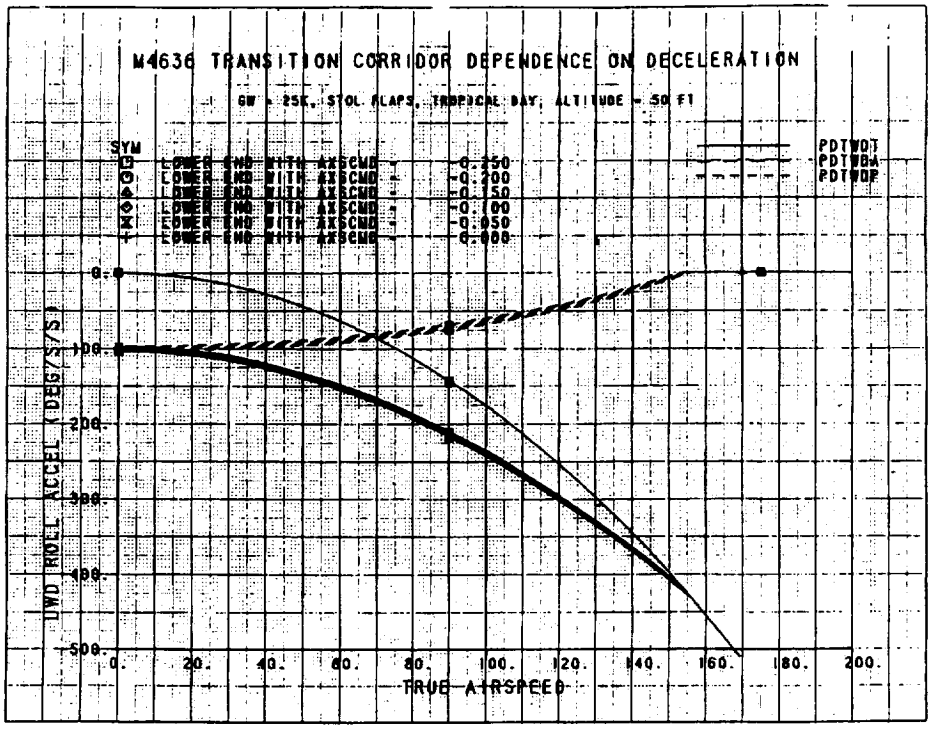

Figure 119. M4636 Transiton Corridor Dependence On Delceleration

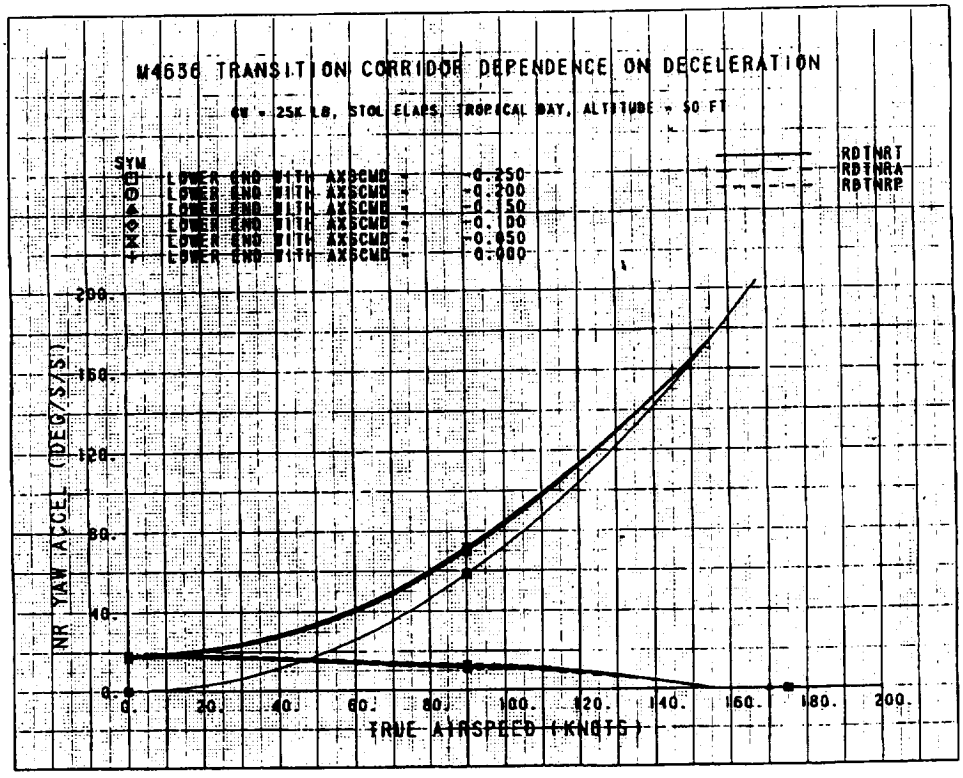

Figure 120. M4636 Transition Corridor Depencence On Deceleration

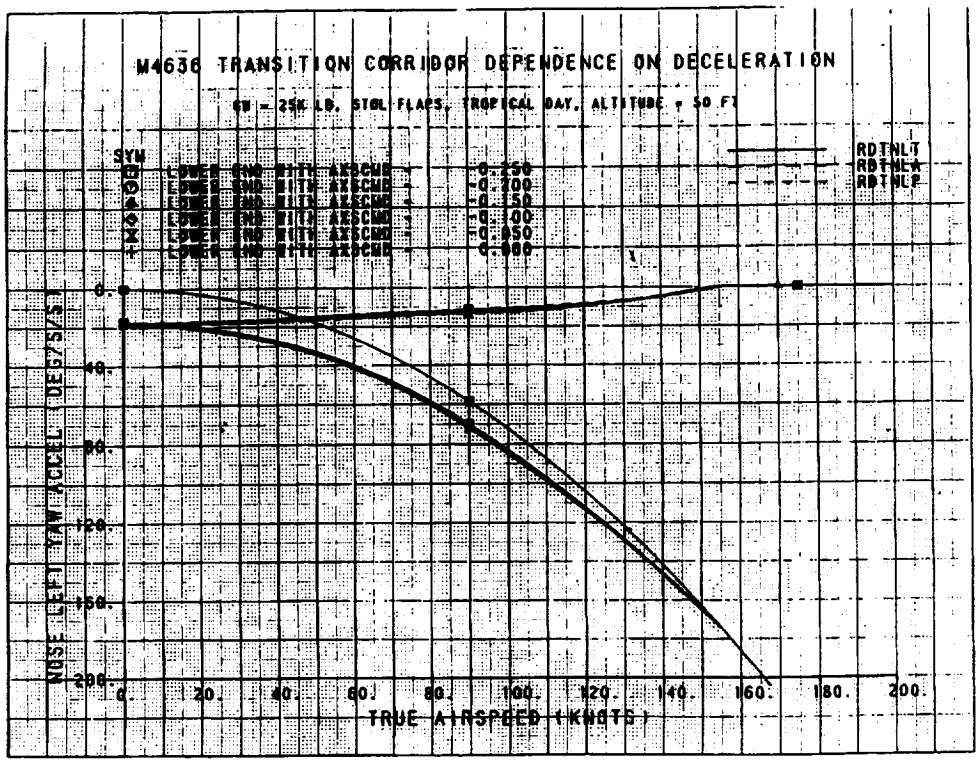

Figure 121. M4636 Transition Corridor Dependence On Deceleration

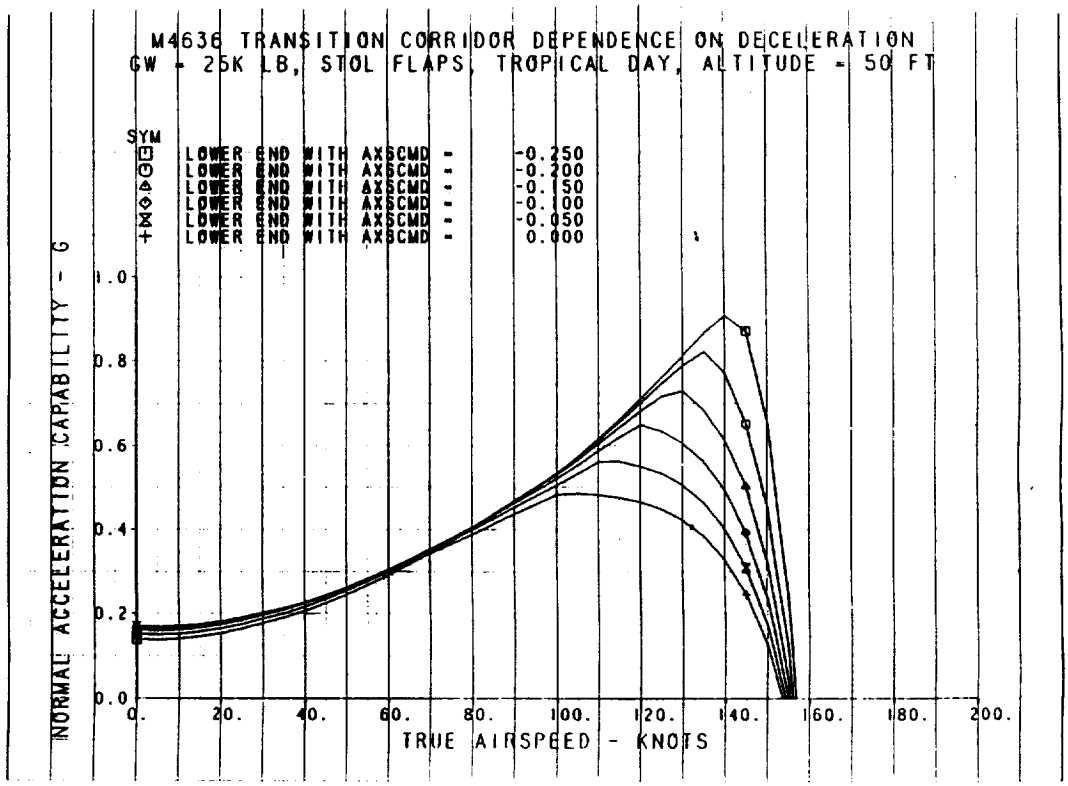

Figure 122. M4636 Transition Corridor Dependence on Deceleration

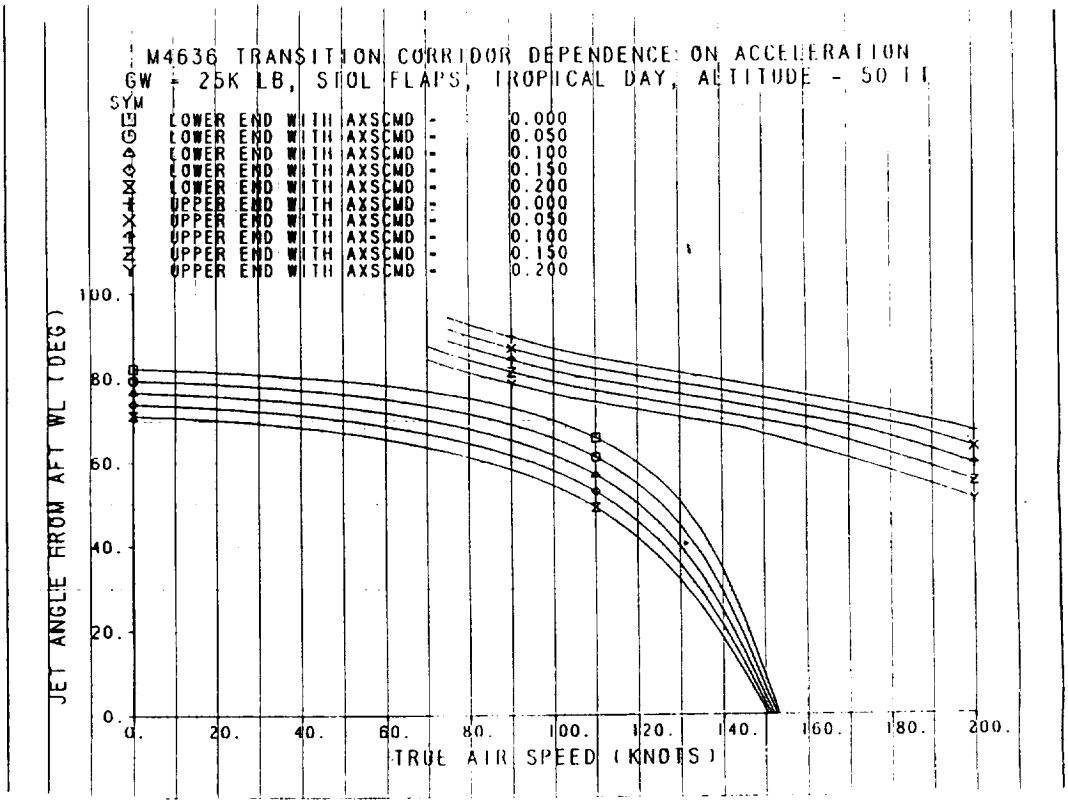

Figure 123. M4636 Transition Corridor Dependence on Acceleration

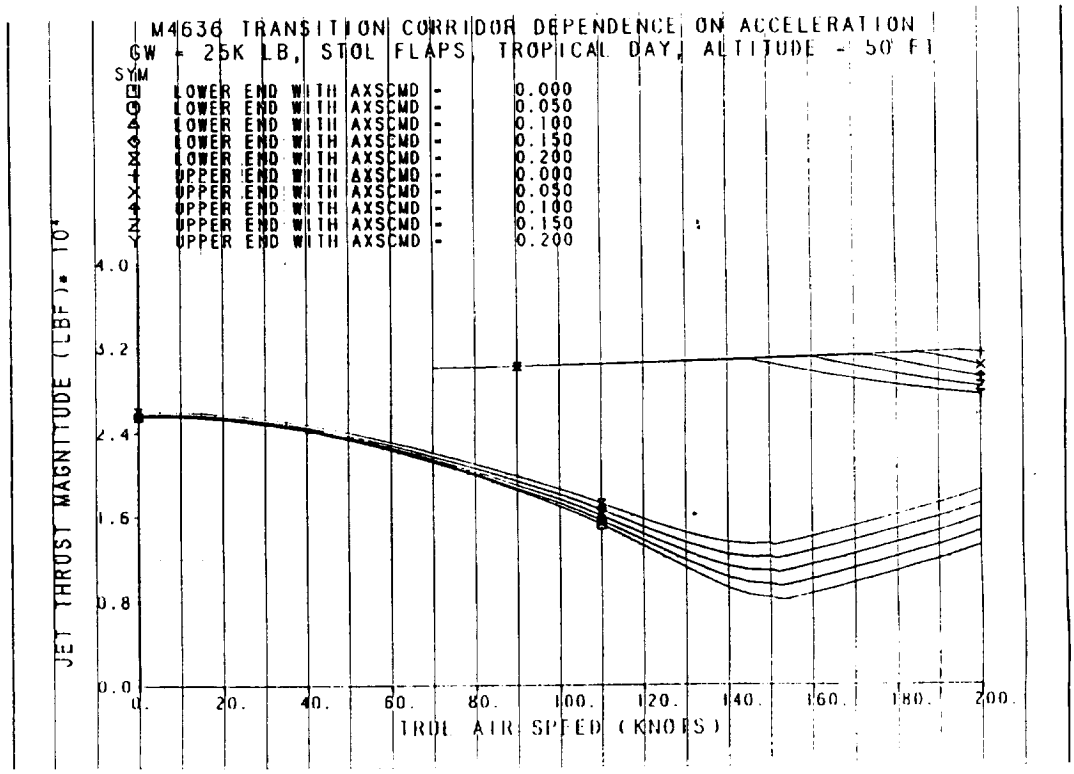

Figure 124. M4636 Transition Corridor Dependence on Acceleration

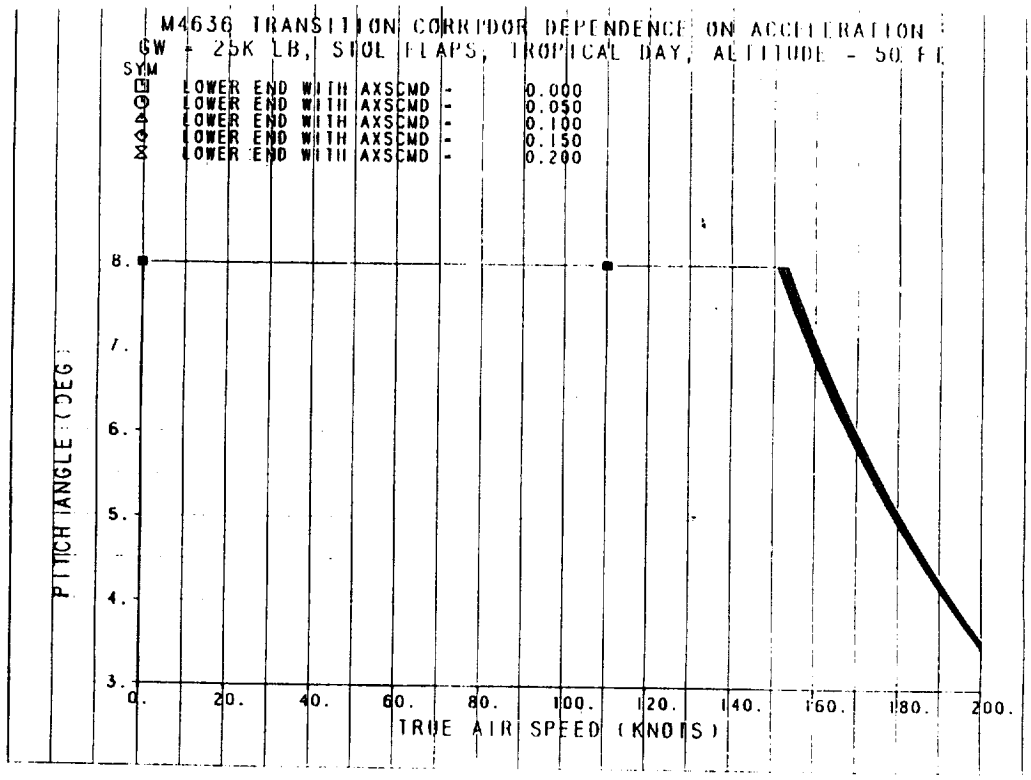

Figure 125. M4636 Transition Corridor Dependence on Acceleration

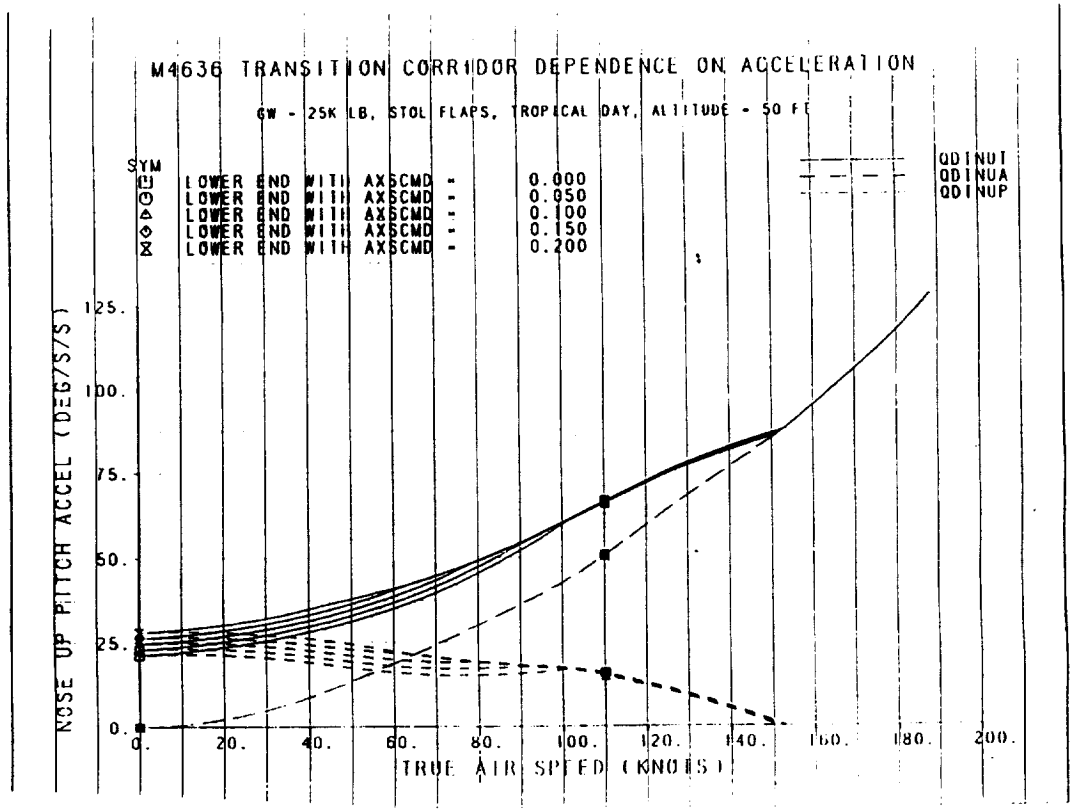

Figure 126. M4636 Transition Corridor Dependence on Acceleration

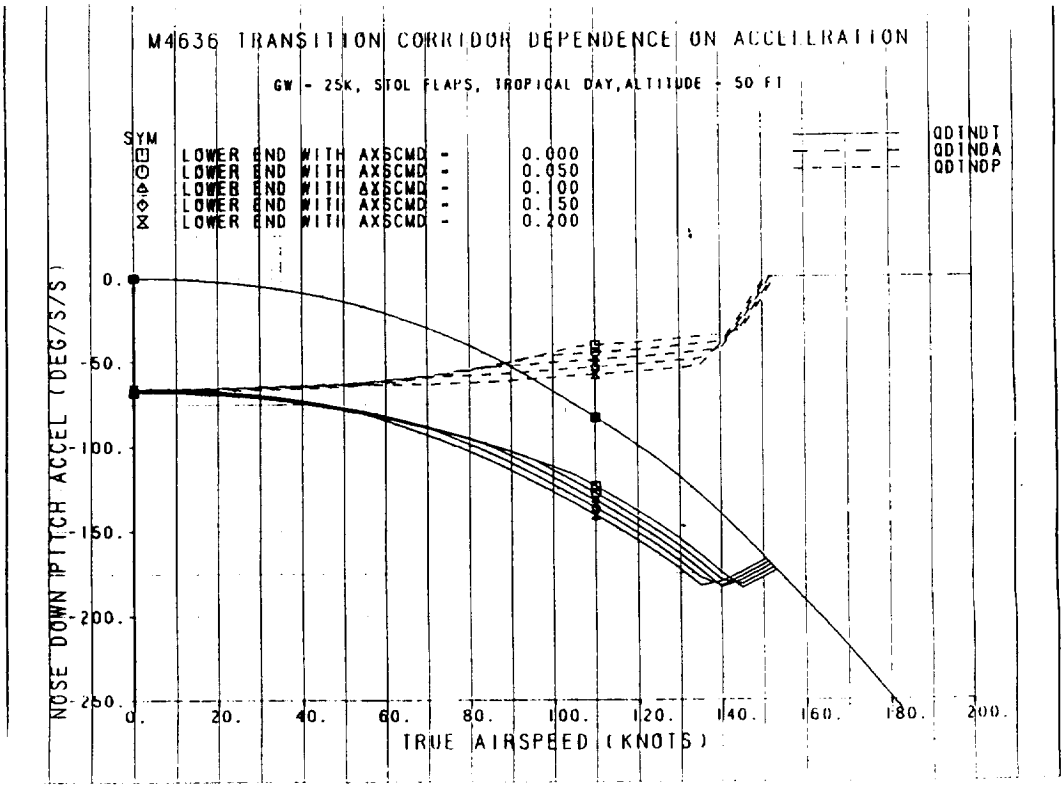

Figure 127. M4636 Transition Corridor Dependence on Acceleration

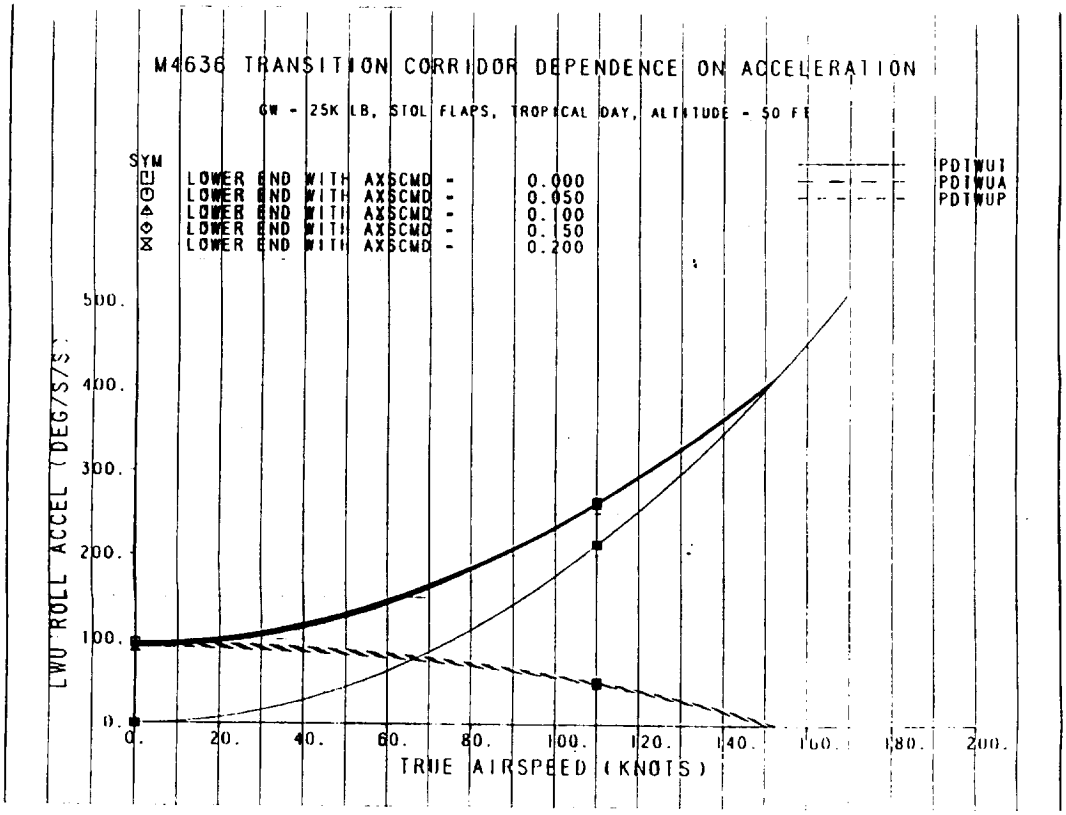

Figure 128. M4636 Transition Corridor Dependence on Acceleration

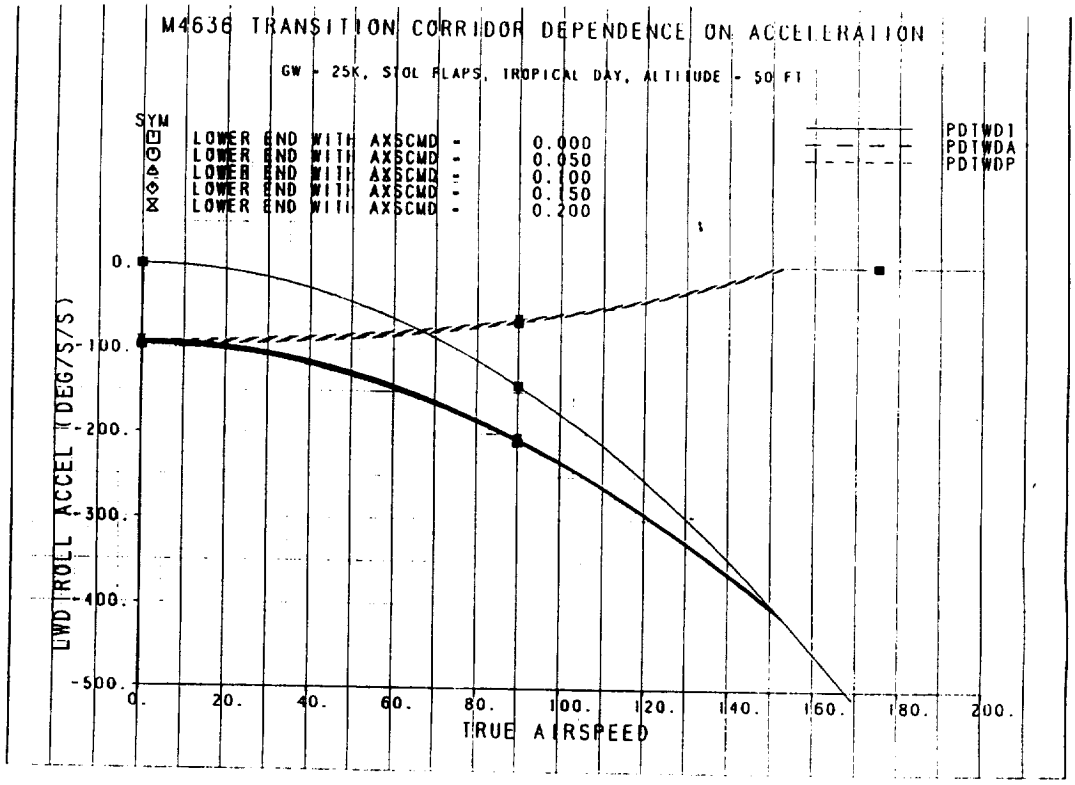

Figure 129. M4636 Transition Corridor Dependence on Acceleration

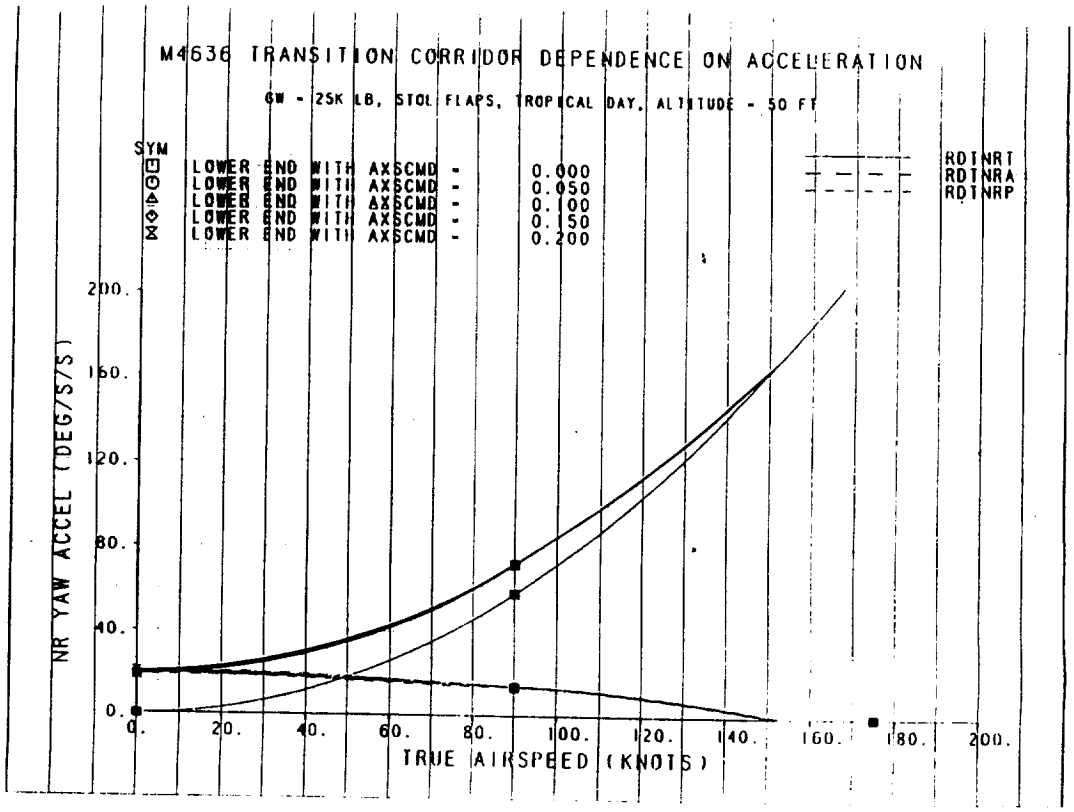

Figure 130. M4636 Transition Corridor Dependence on Acceleration

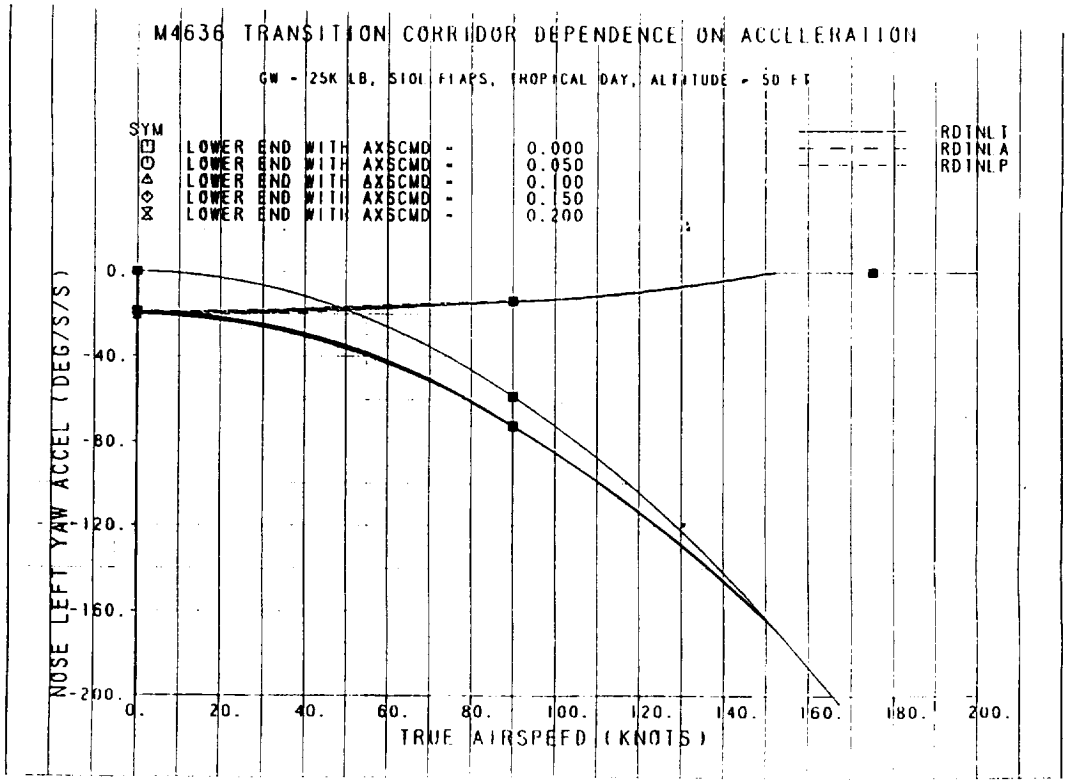

Figure 131. M4636 Transition Corridor Dependence on Acceleration

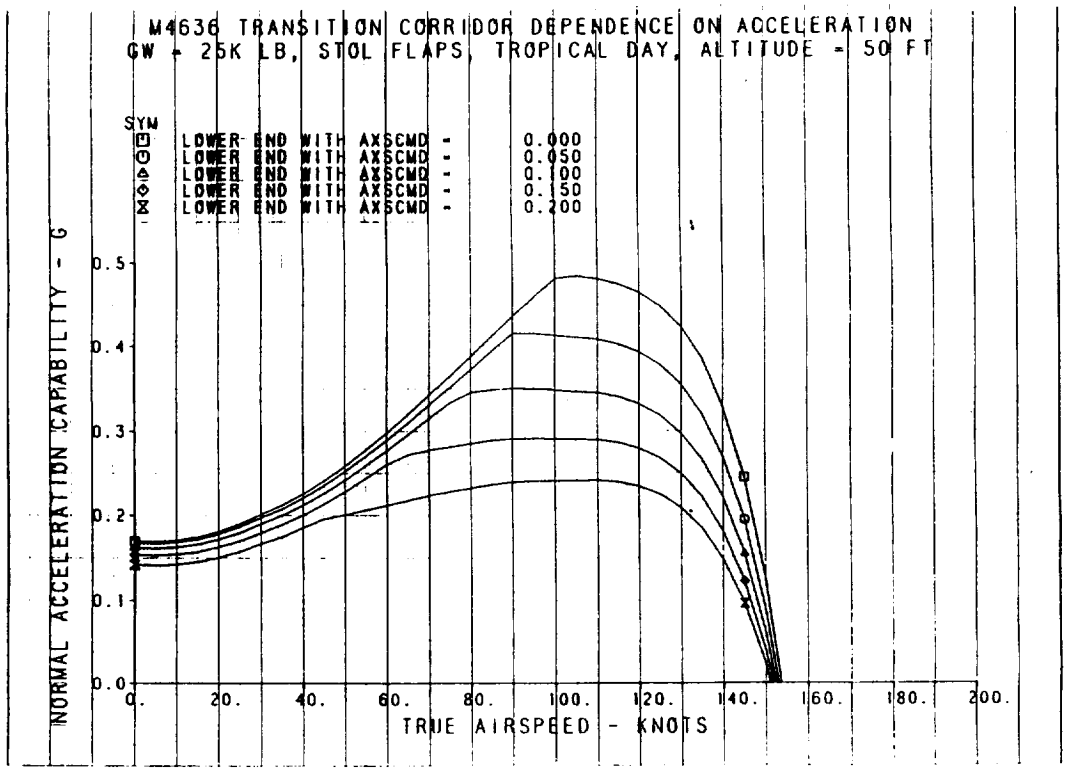

Figure 132. M4636 Transition Corridor Dependence on Acceleration

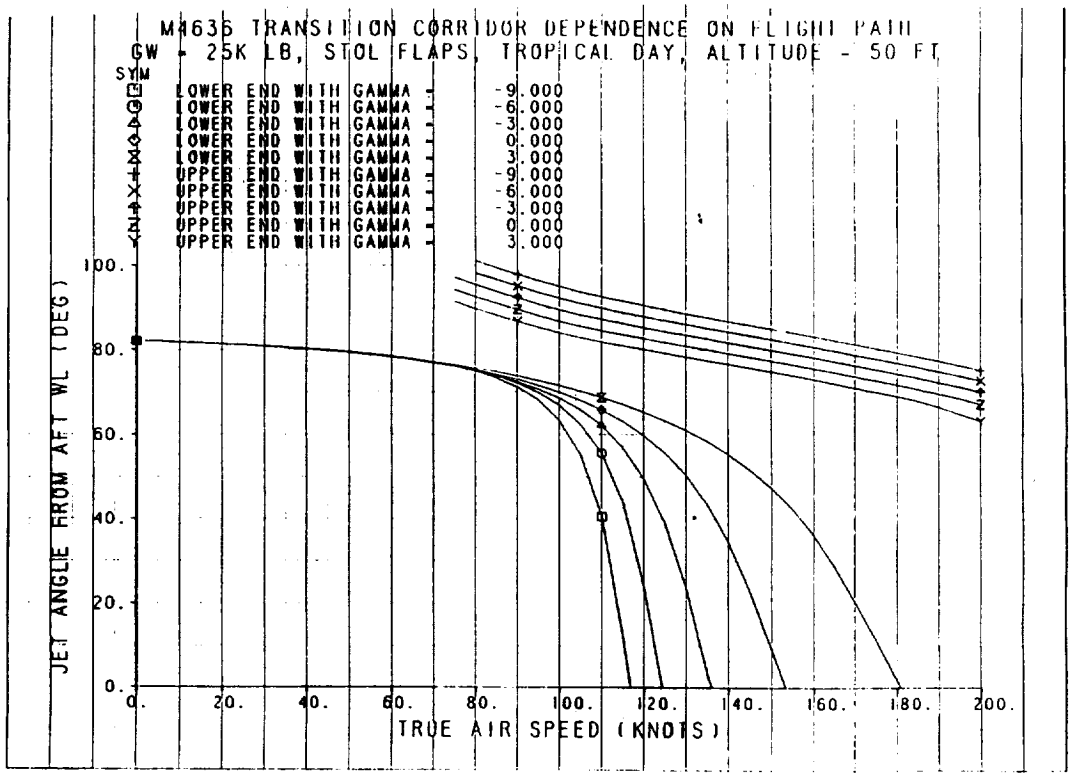

Figure 133. M4636 Transition Corridor Dependence on Flight Path

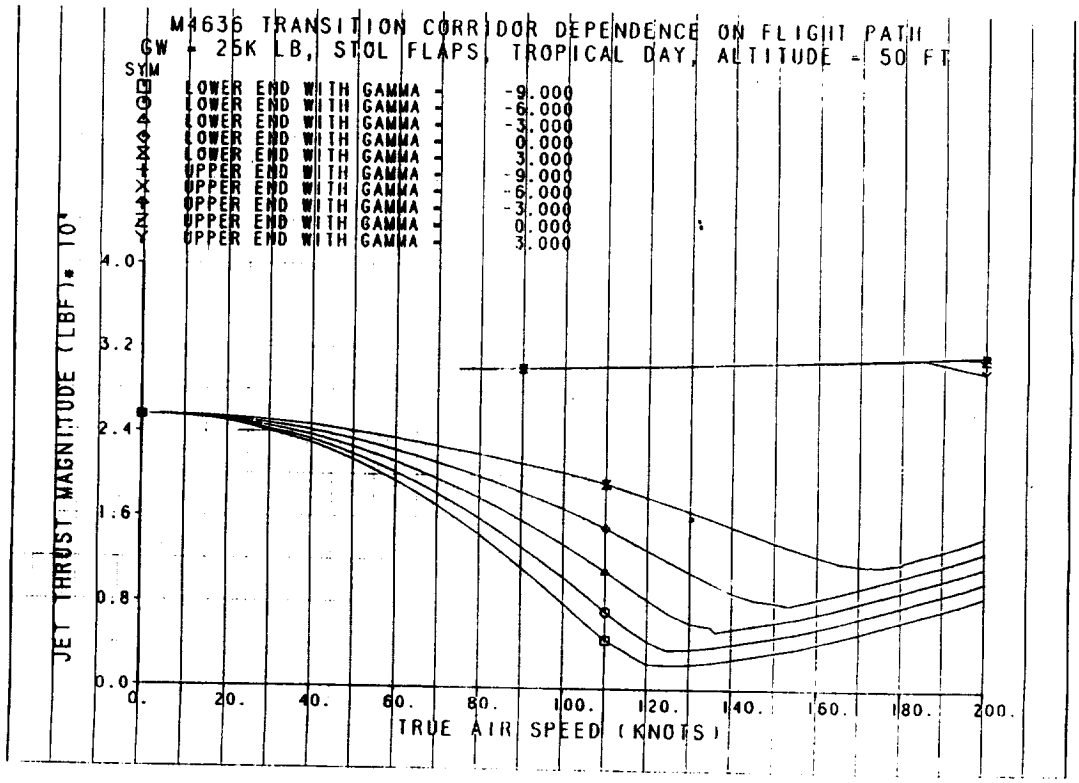

Figure 134. M4636 Transition Corridor Dependence on Flight Path

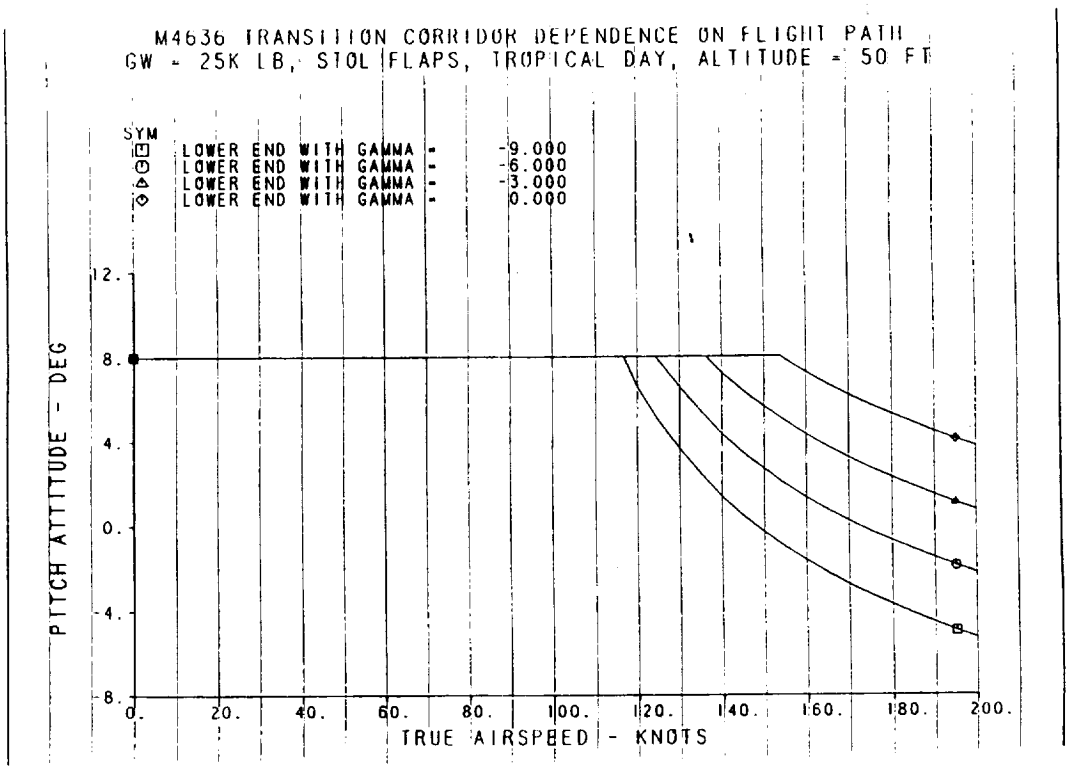

Figure 135. M4636 Transition Corridor Dependence on Flight Path

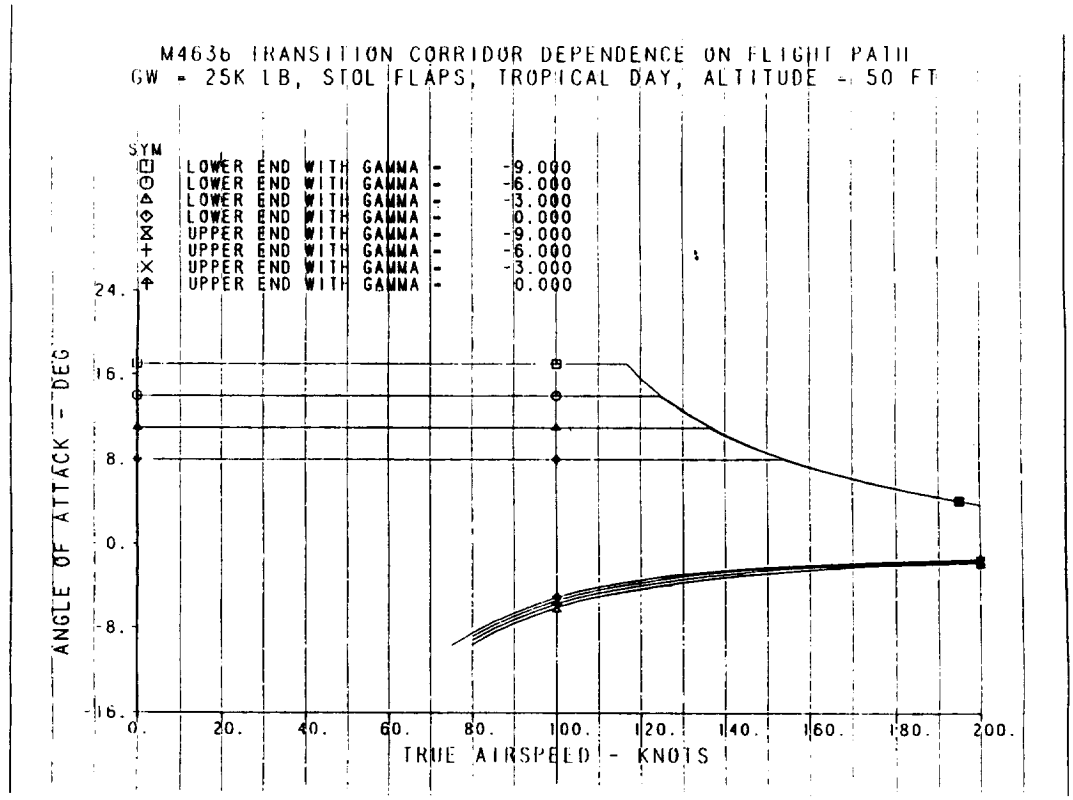

Figure 136. M4636 Transition Corridor Dependence on Flight Path

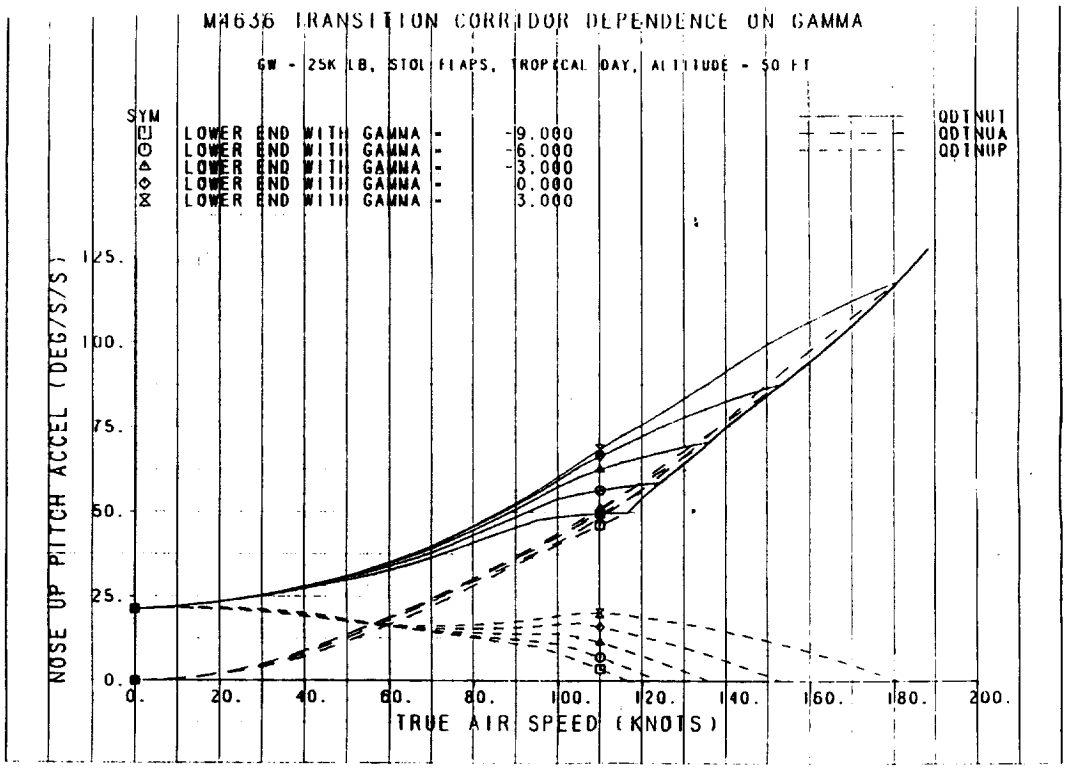

Figure 137. M4636 Transition Corridor Dependence on Gamma

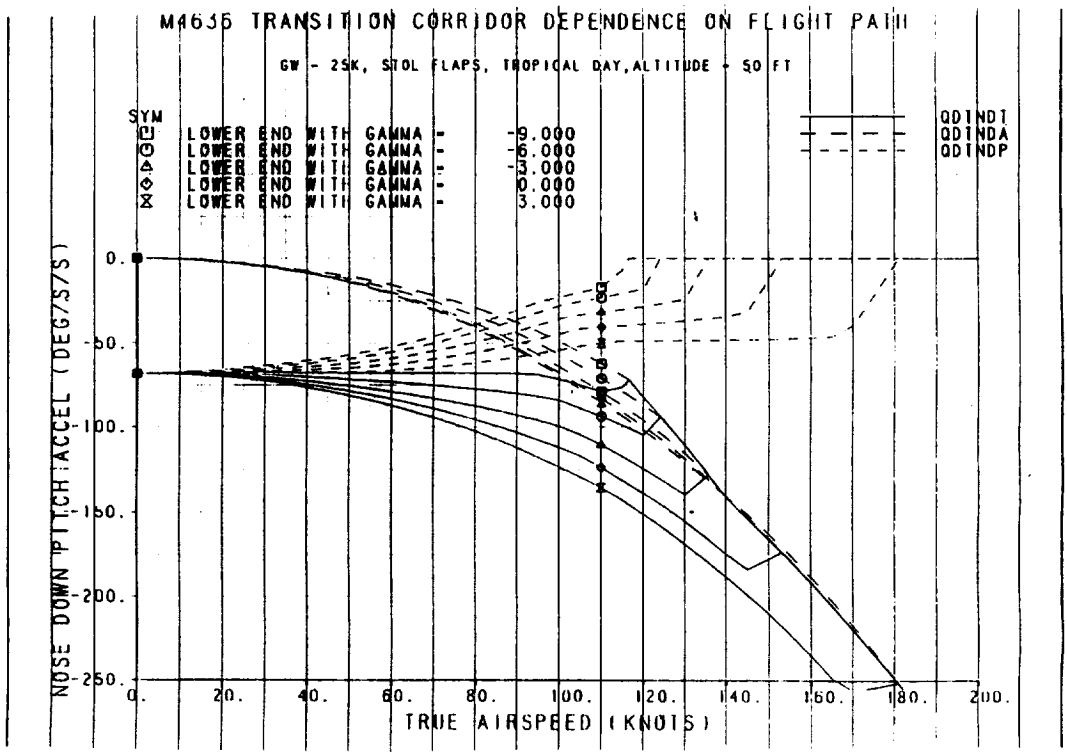

Figure 138. M4636 Transition Corridor Dependence on Flight Path

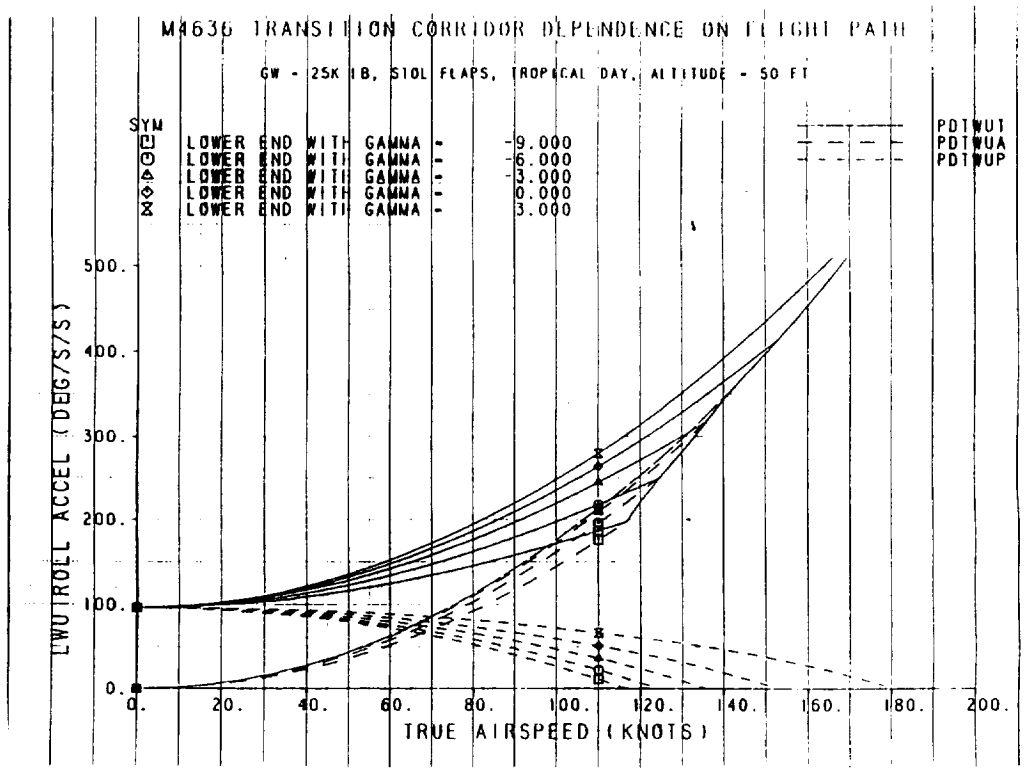

Figure 139. M4636 Transition Corridor Dependence on Flight Path

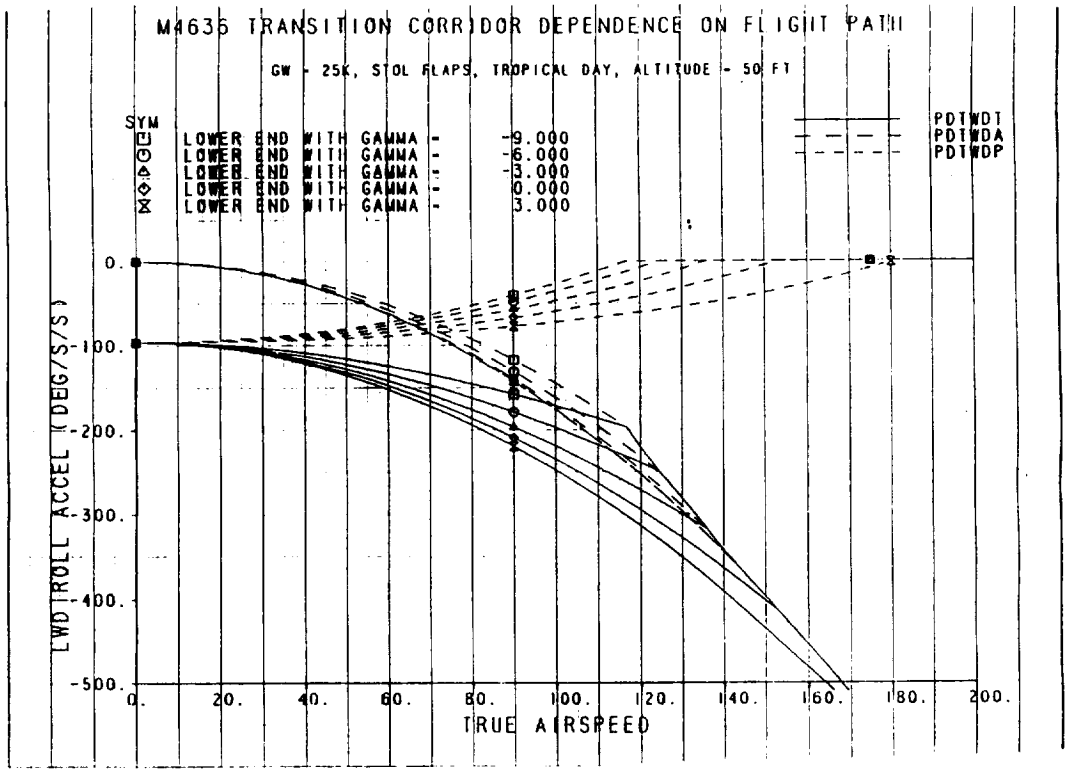

Figure 140. M4636 Transition Corridor Dependence on Flight Path

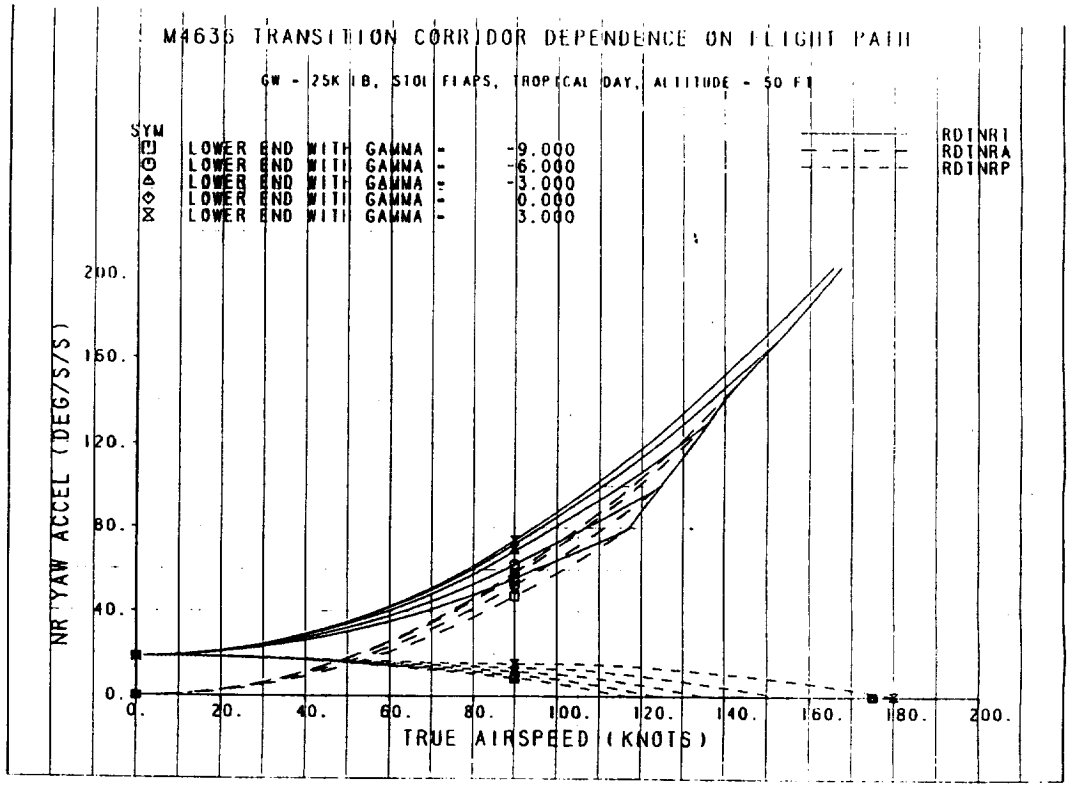

Figure 141. M4636 Transition Corridor Dependence on Flight Path

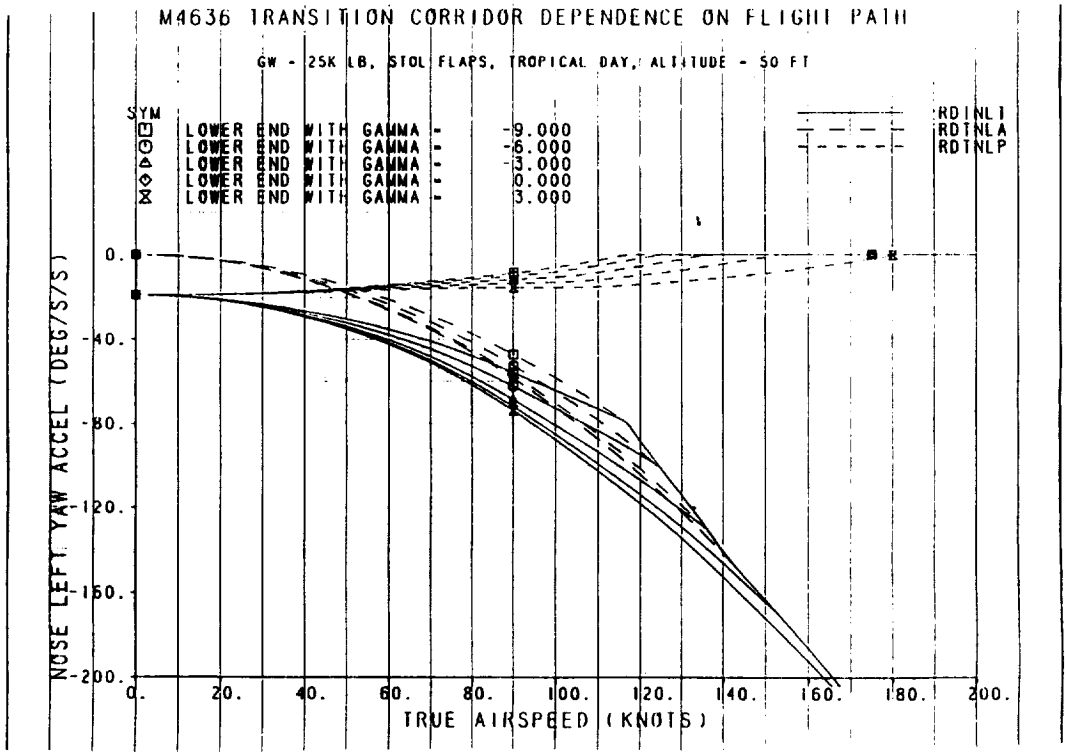

Figure 142. M4636 Transition Corridor Dependence on Flight Path

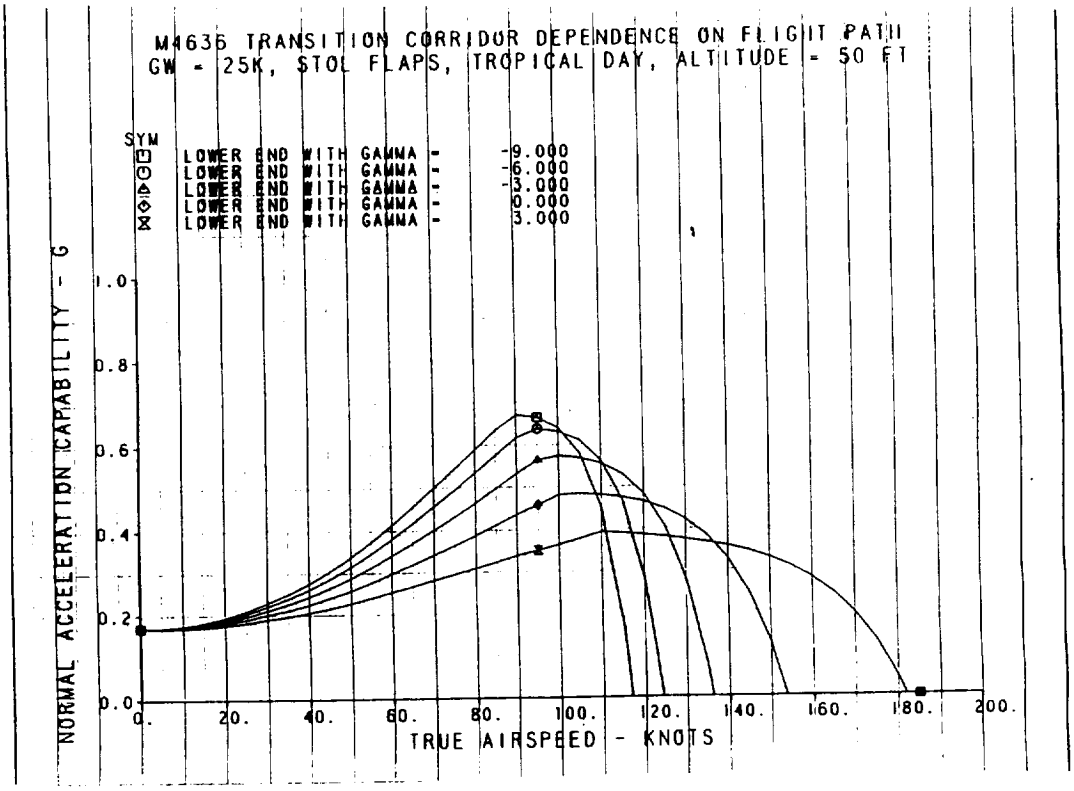

Figure 143. M4636 Transition Corridor Dependence on Flight Path

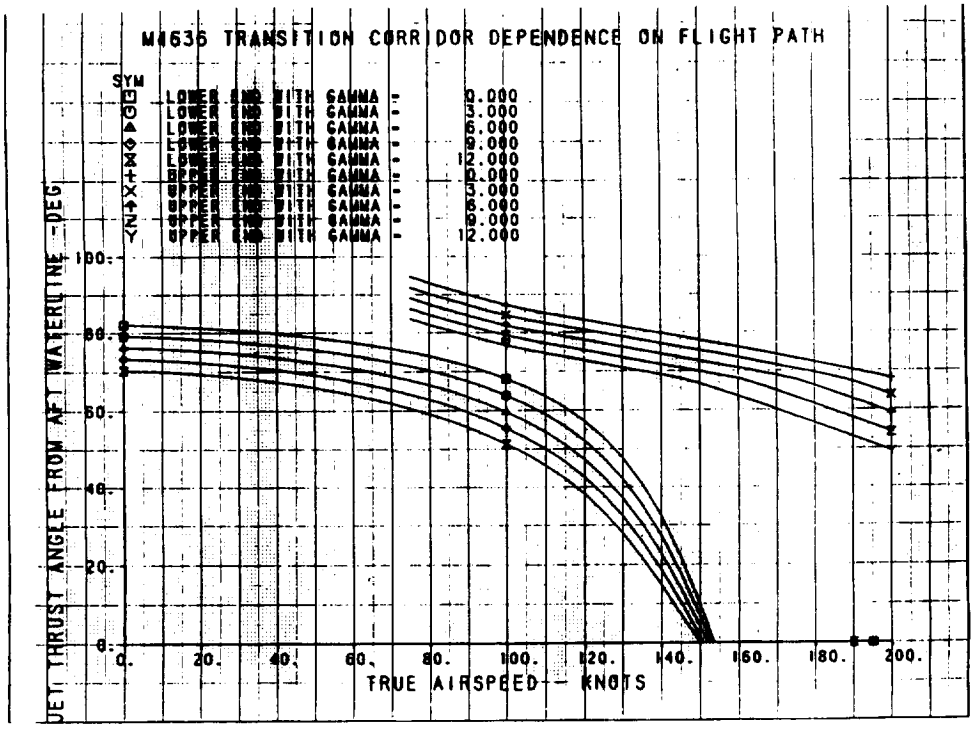

Figure 144. M4636 Transition Corridor Dependence on Flight Path

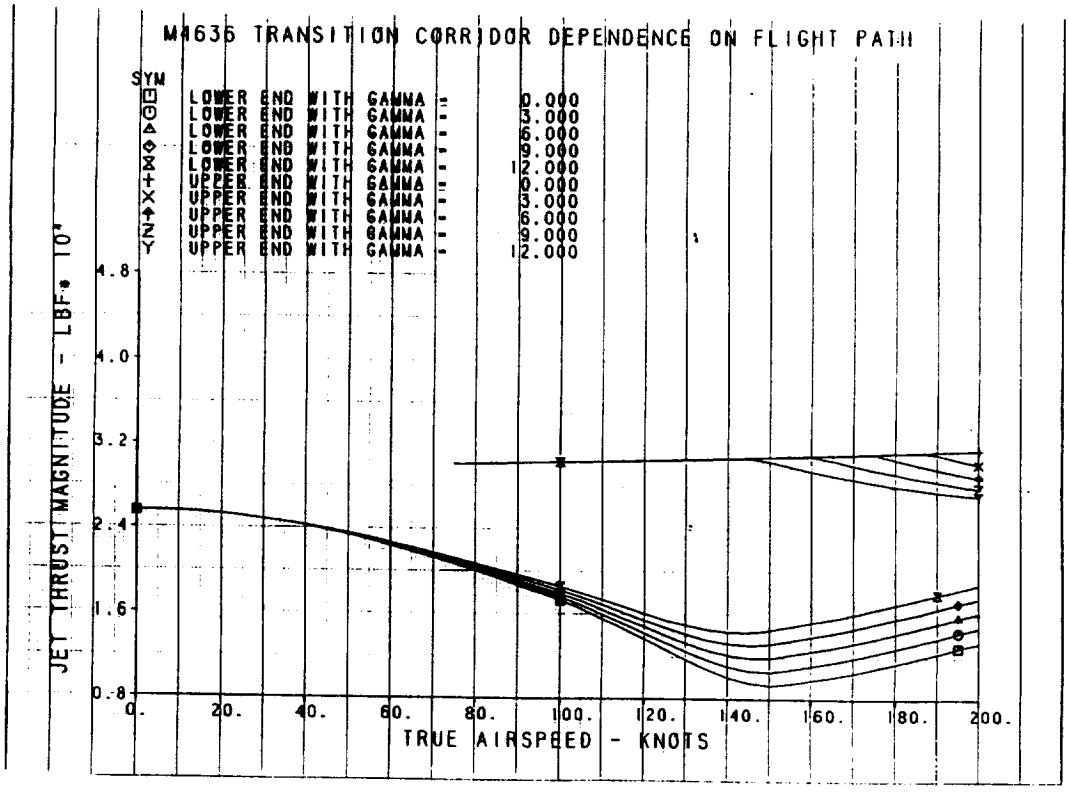

Figure 145. M4636 Transition Corridor Dependence on Flight Path

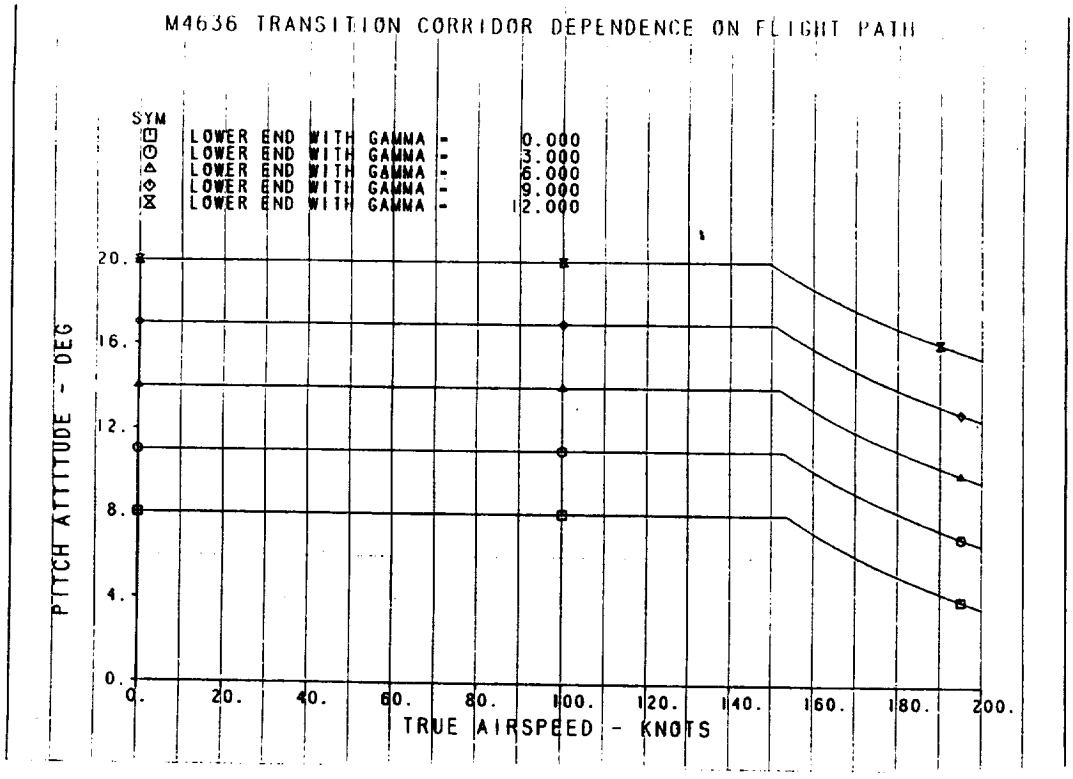

Figure 146. M4636 Transition Corridor Dependence on Flight Path

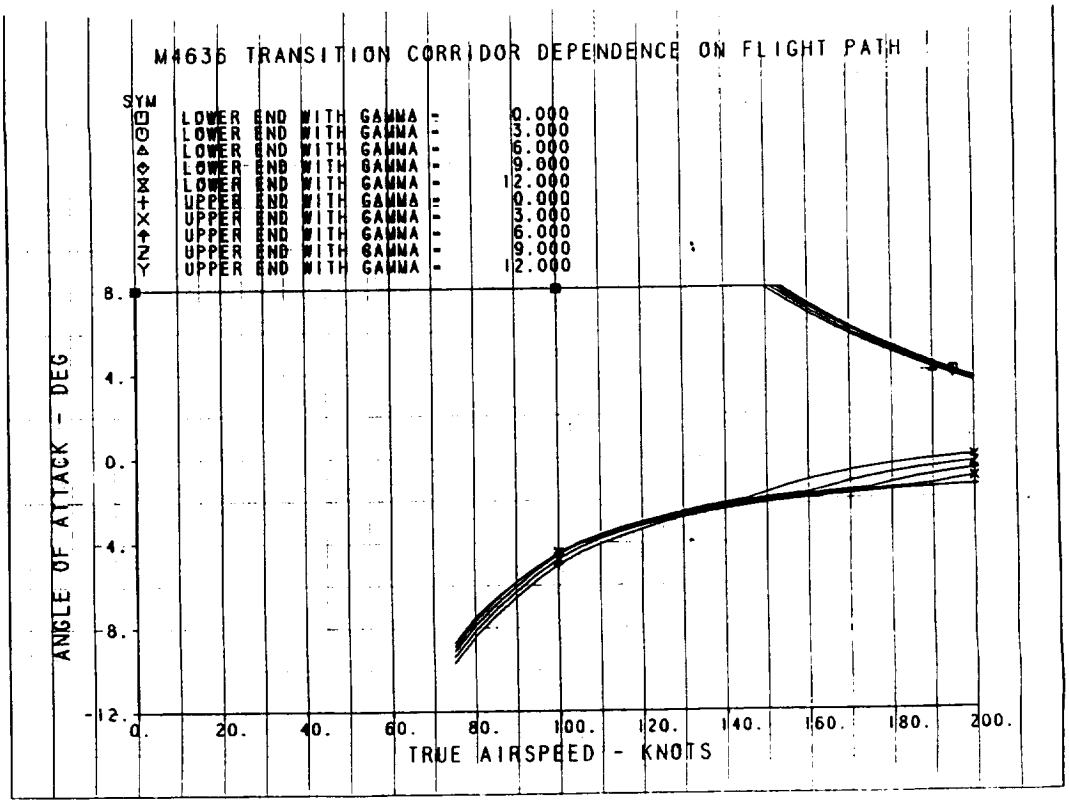

Figure 147. M4636 Transition Corridor Dependence on Flight Path

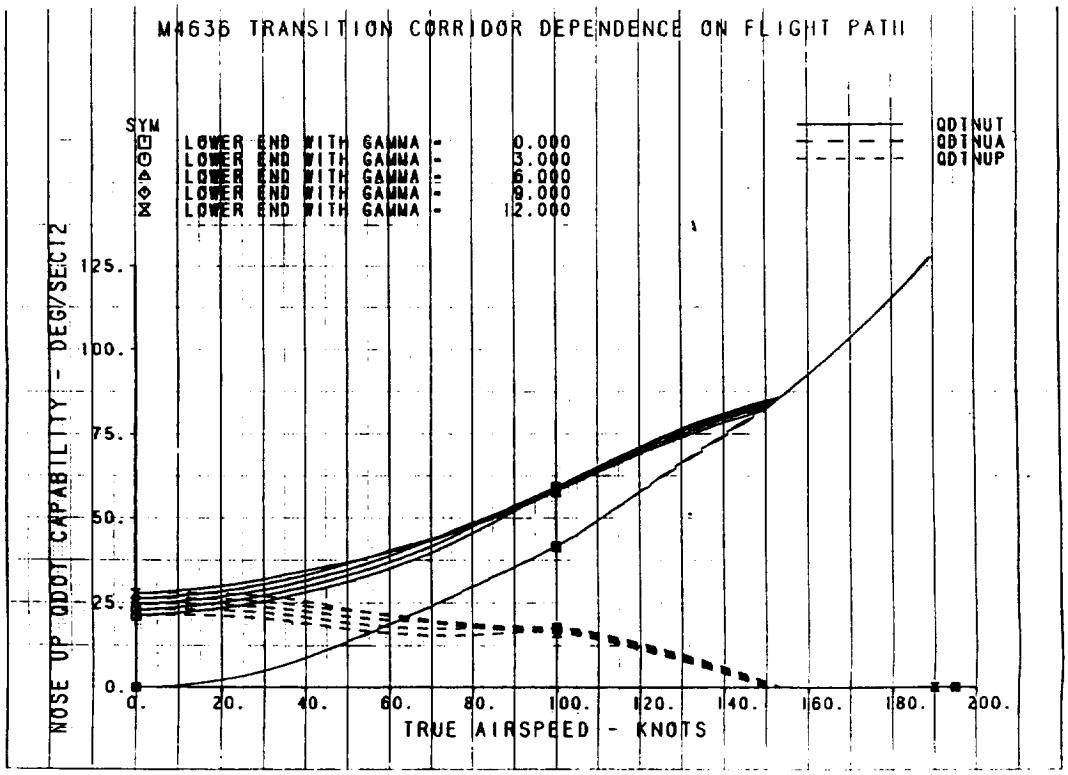

Figure 148. M4636 Transition Corridor Dependence on Flight Path

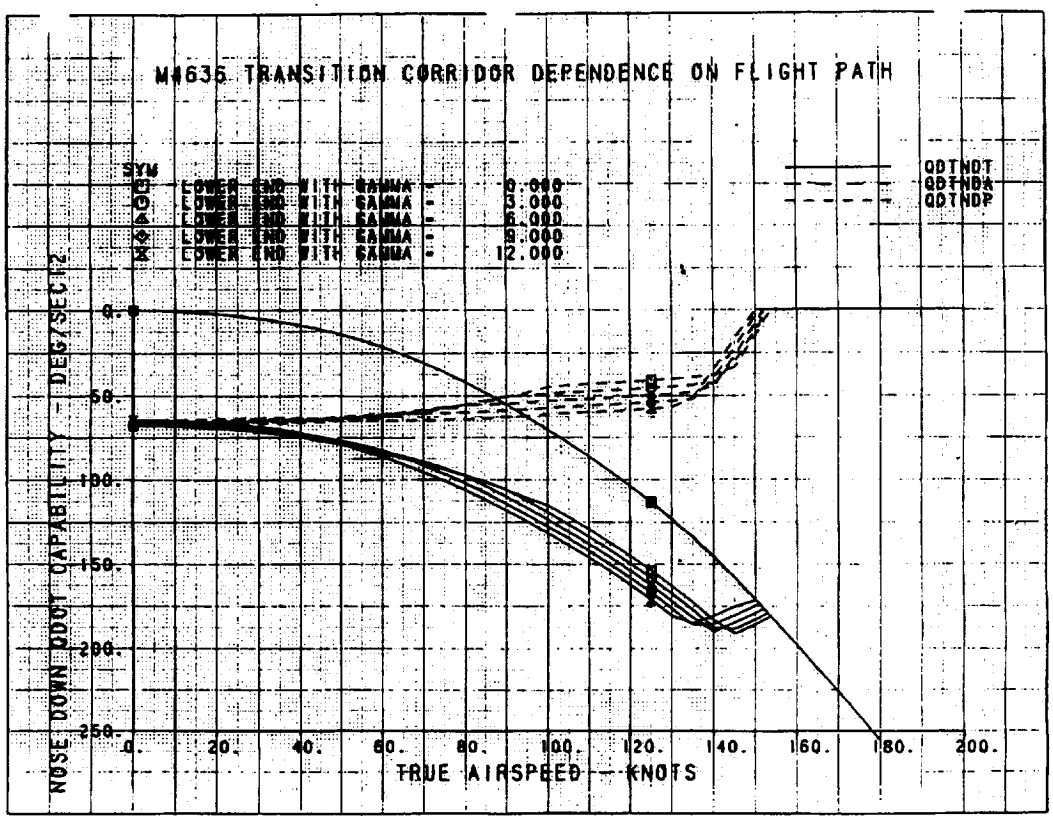

Figure 149. M4636 Transition Corridor Dependence on Flight Path

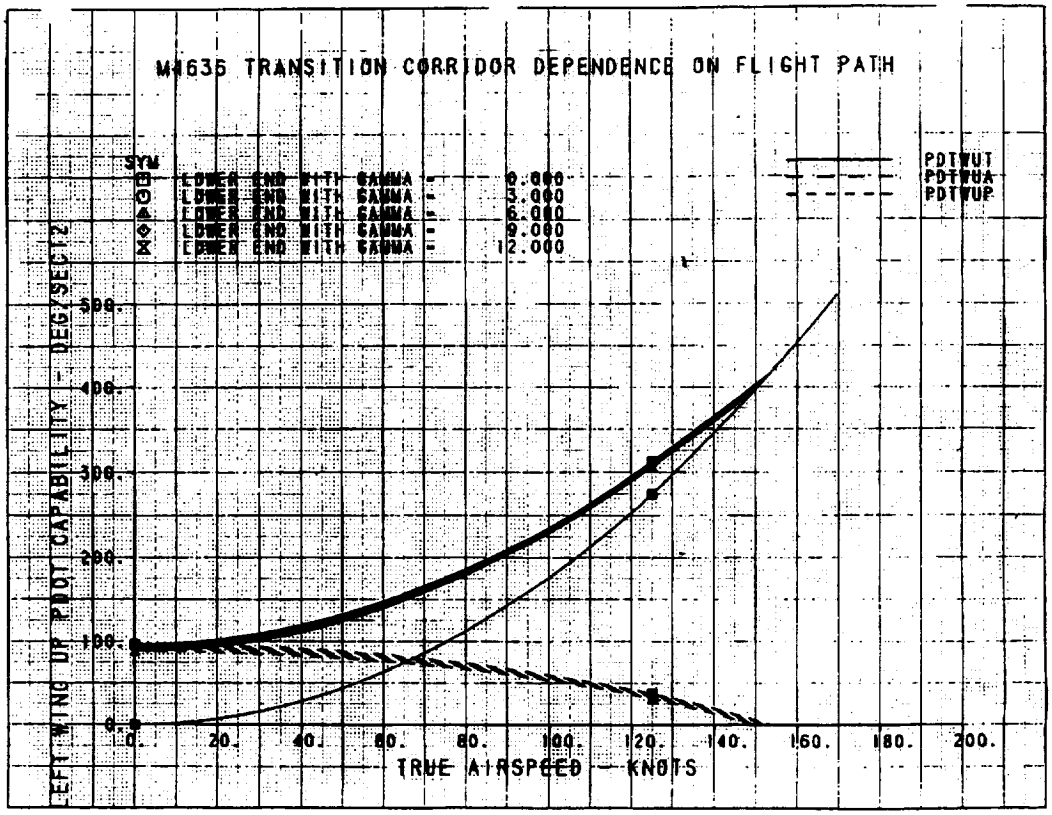

Figure 150. M4636 Transition Corridor Dependence on Flight Path

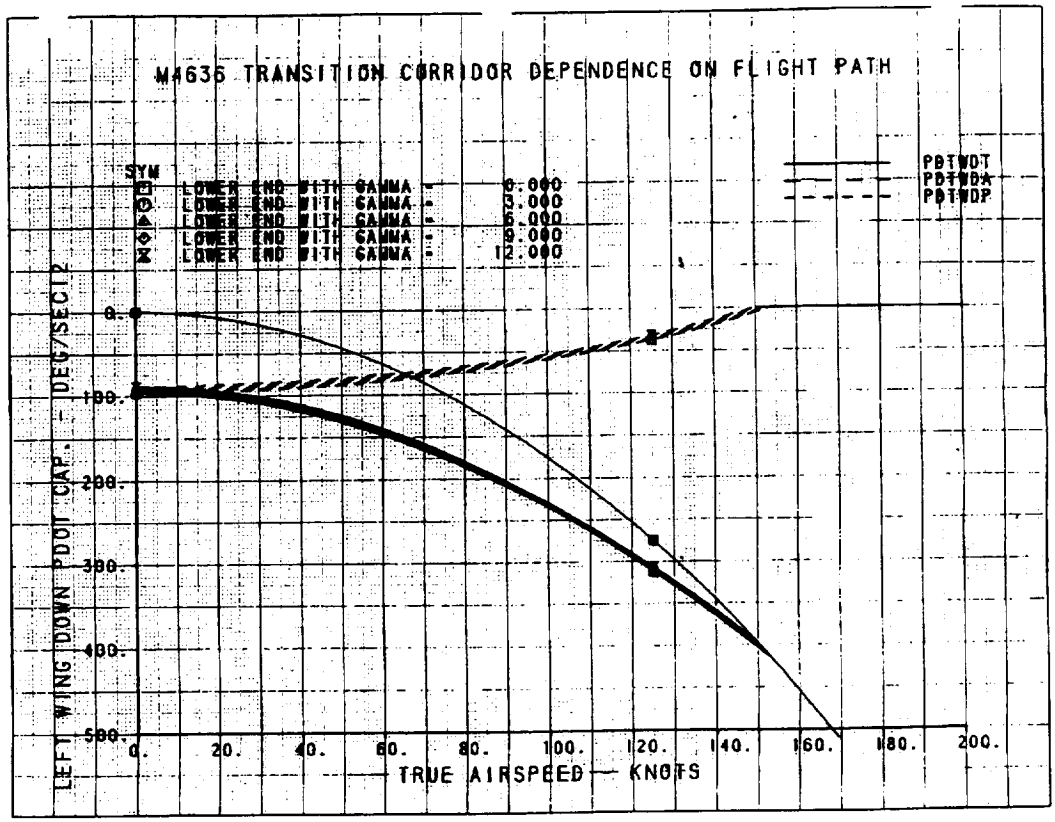

Figure 151. M4636 Transition Corridor Dependence on Flight Path

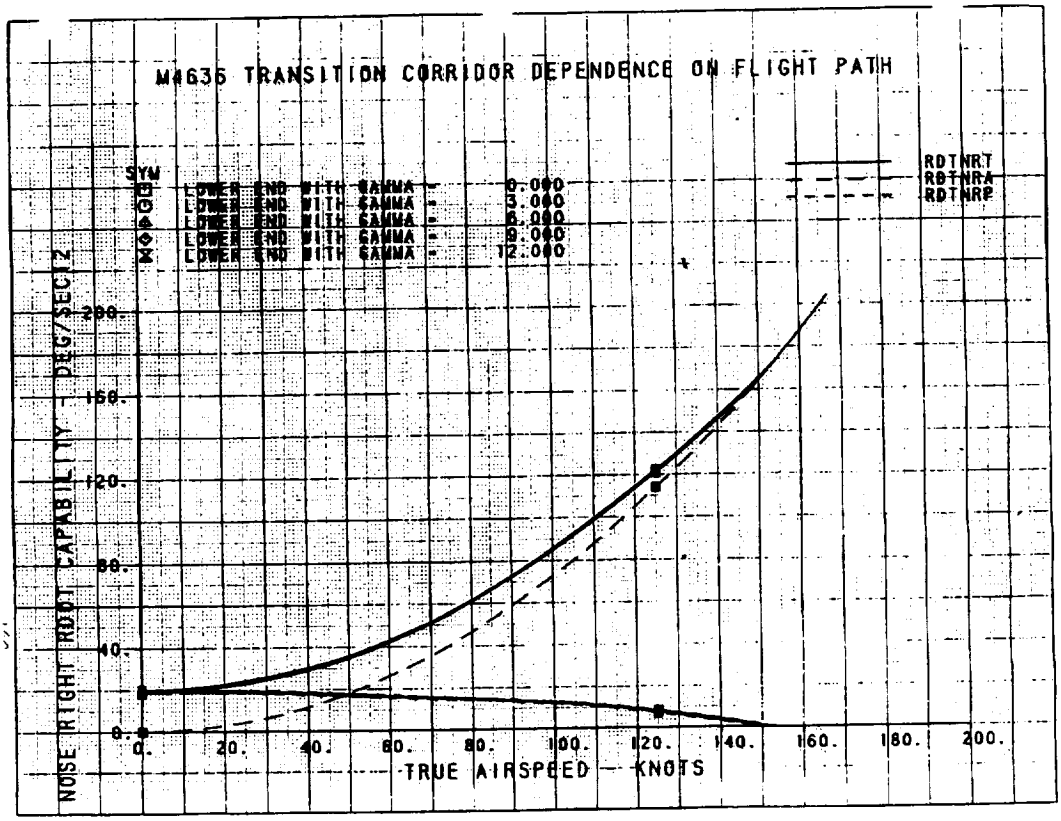

Figure 152. M4636 Transition Corridor Dependence on Flight Path

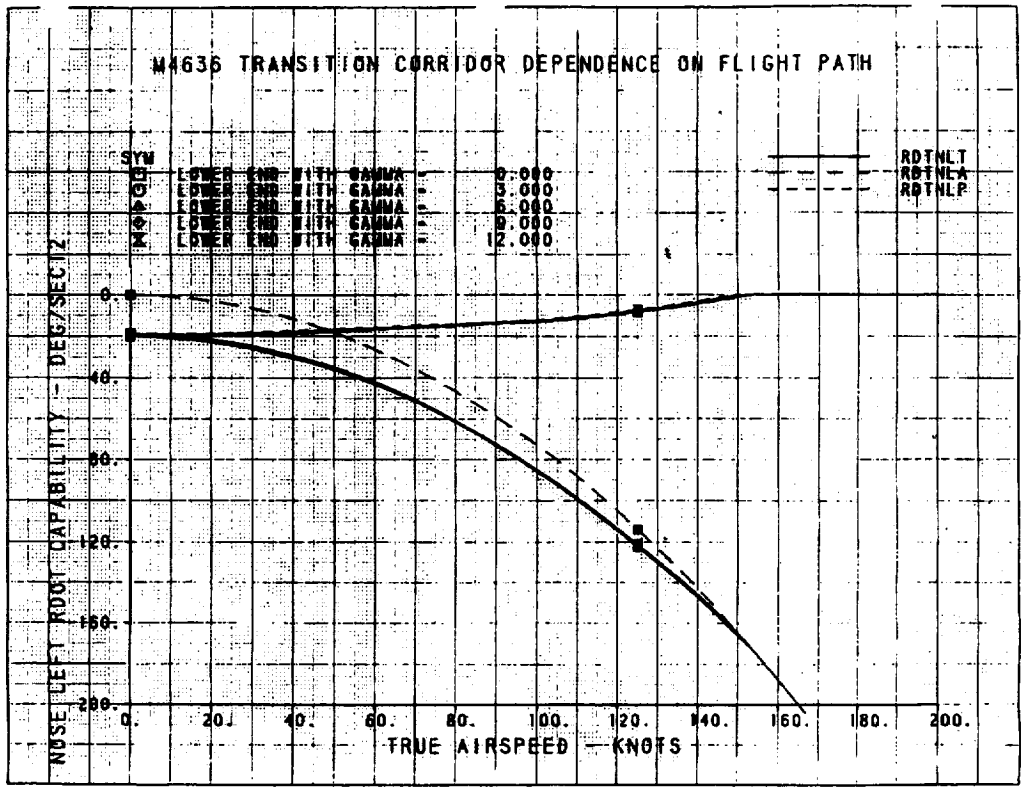

Figure 153. M4636 Transition Corridor Dependence on Flight Path

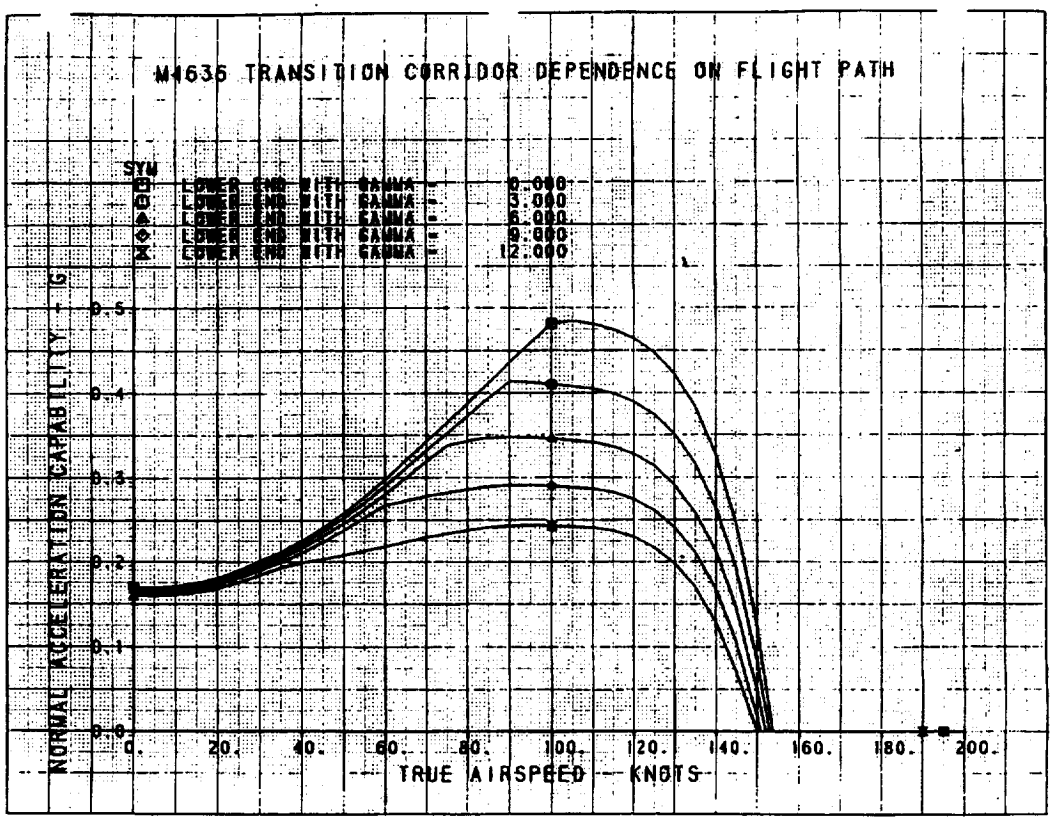

Figure 154. M4636 Transition Corridor Dependence on Flight Path

3.4.2.5. Transition Envelopes in Crosswinds

This section describes the steady level flight transition envelopes in crosswinds. The trim sweep is steady level flight along a maximum 8 degree pitch attitude profile in crosswinds ranging from 0 to 20 knots. The trim sweeps are plotted as a function of velocity with the crosswind component removed. Therefore, with the aircraft flying due North in a steady wind coming from due East, the x−axis represents North inertial aircraft velocity. Figure 155 and Figure 156 show that the jet angle and jet magnitude envelopes are not sensitive to crosswind velocity.

Figure 157 shows the trimmed pitch attitude profile and Figure 158 shows the increasing trimmed roll attitude as crosswind velocity increases. Figure 159 plots the flight path azimuth angle, which is the angle between the projection of the aircraft velocity vector onto the inertial horizontal plane and the North compass direction. (The aircraft nose is kept pointed North in these trim sweeps.) This angle approaches 90 degrees as the aircraft slows to 0 North inertial velocity (representing a hovering condition in a crosswind). Figure 160 and Figure 161 show the corresponding sideslip angles and angles of attack. The rightmost vertical line in the angle of attack plot is due to the plotting routine, which is attempting to draw a straight line between the trimmed angle of attack at 5 knots inertial North velocity and the trimmed angle of attack at 0 velocity in a pure crosswind (which is always −90 degrees).

Figure 162 through Figure 168 are the control power plots, indicating that adequate control power exists for steady level flight in a 20 knot crosswind. In particular, Figure 164 through Figure 168 show the sensitivity of the lateral/directional control power to crosswind velocity.

3.4.2.6. Transition Envelope Sensitivities to Center of Gravity

This section describes the sensitivity of the level flight transition envelope to shifts in center of gravity location. The trim sweep is steady level flight along a maximum 8 degree pitch attitude profile with center of gravity ranging between 37 and 43%. This range of center of gravity locations covers the expected center of gravity travel for the aircraft during all mission phases, as indicated in Figure 169 in Reference 1. Figure 169 through Figure 171 are plots of the jet angle envelopes, jet thrust magnitude envelopes, and the pitch attitude profiles, indicating that the transition envelope is not sensitive to center of gravity variations. Figure 172 and Figure 173 show the shift in pitch control power capability toward nose up which occurs as the center of gravity travels aft. This is due to the decreasing required trim pitching moment as shown in Figure 174. Figure 175 shows that normal acceleration capability from increasing the engine power is not sensitive to these center of gravity variations.

3.4.2.7. Transition Envelope Sensitivities to Predicted Ram Drag

This section describes the sensitivity of the level flight transition envelope to variations in predicted ram drag. The trim sweep is steady level flight along a maximum 8 degree pitch attitude profile with ±20% variation in ram drag. The ram drag was varied by adding a percentage scale factor to the calculated air massflow into the inlets when that massflow was used for the ram drag calculations in MODSDF. Figure 176 shows the effective jet angle envelope with the ram drag at 80% and 120% of its calculated value, and indicates that the transition envelope is not sensitive to variations in ram drag.

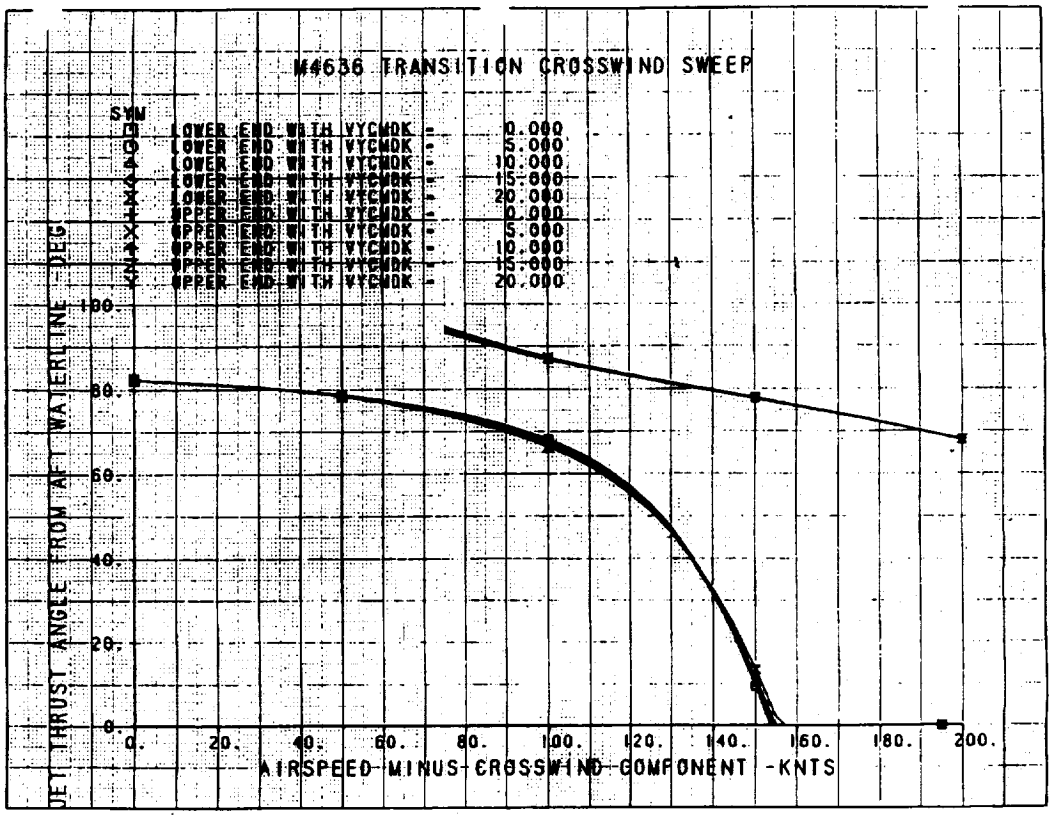

Figure 155. M4636 Transition Crosswind Sweep – Jet Angle

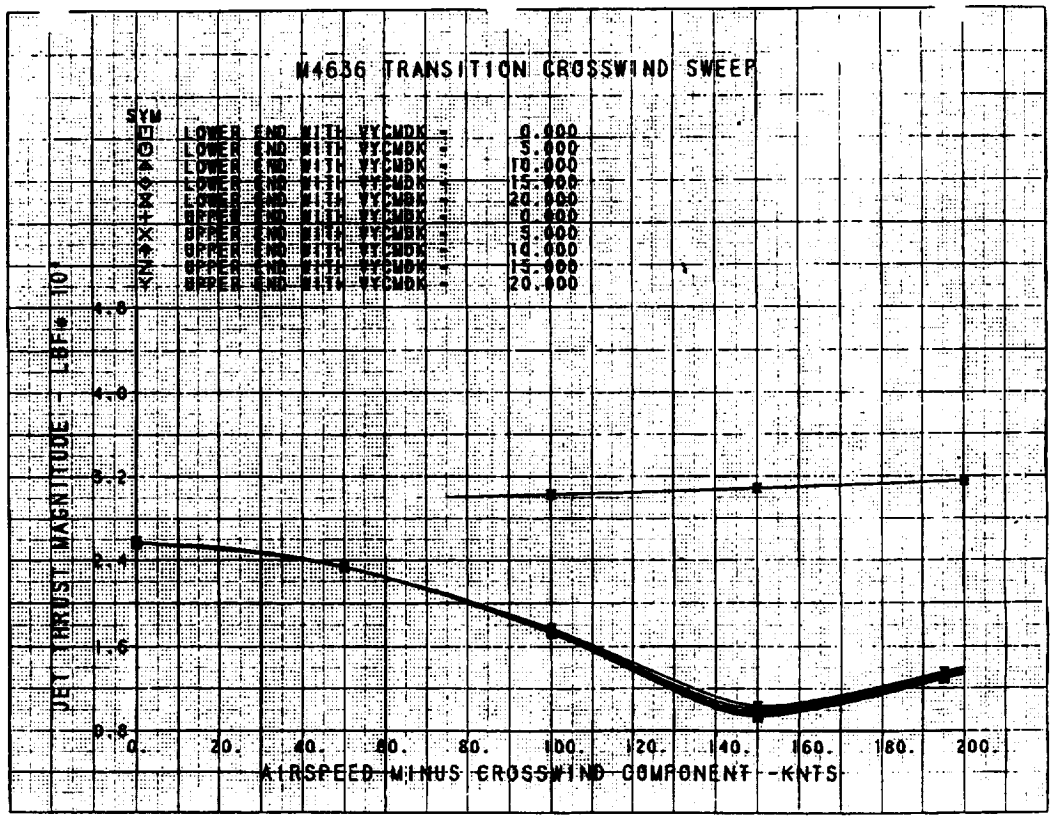

Figure 156. M4636 Transition Crosswind Sweep – Thrust Magnitude

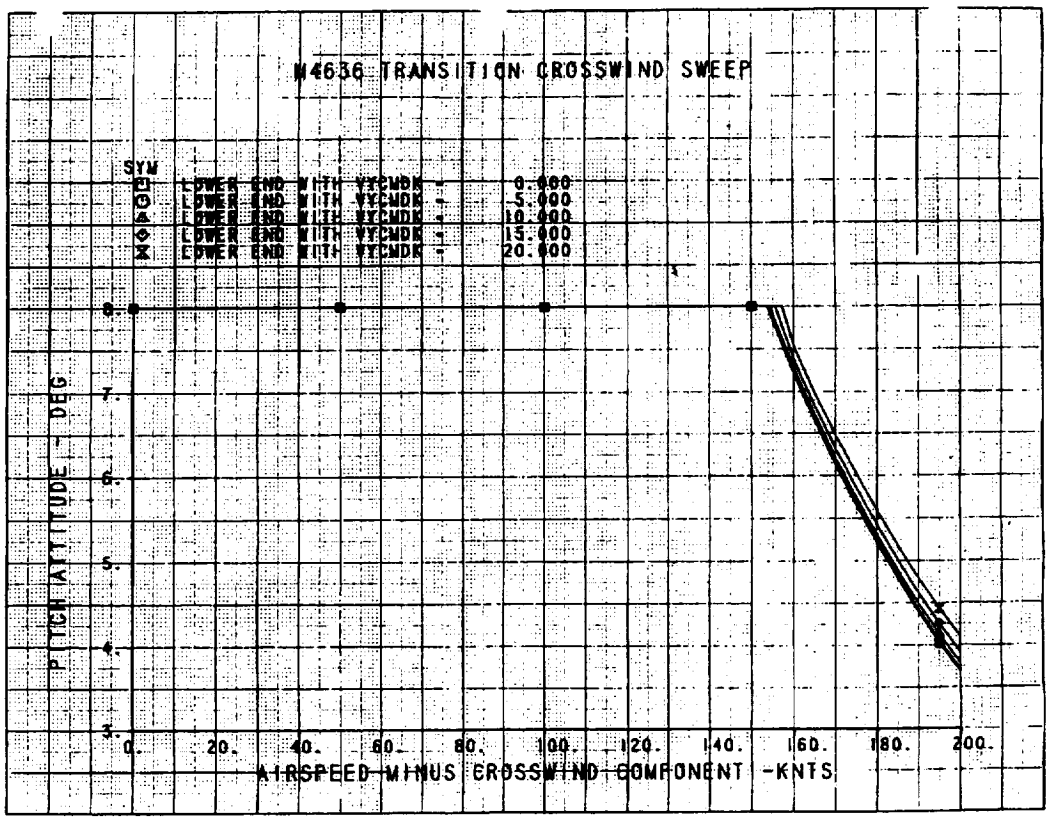

Figure 157. M4636 Transition Crosswind Sweep, Pitch Attitude

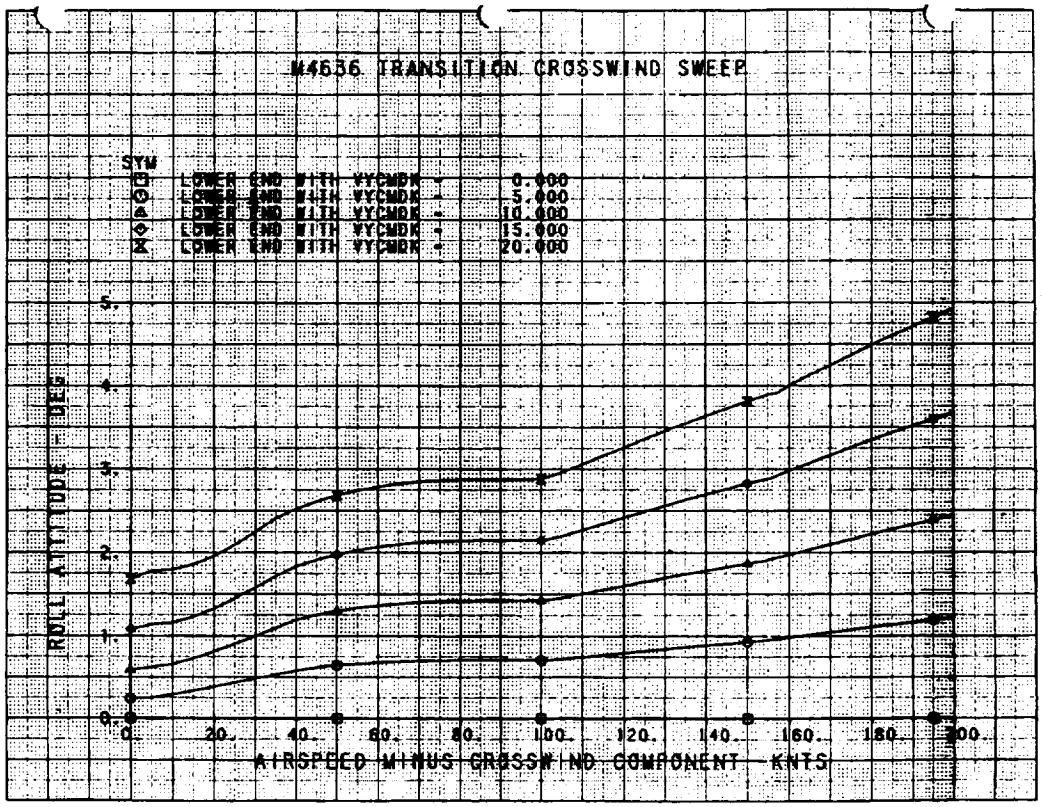

Figure 158. M4636 Transition Crosswind Sweep, Roll Attitude

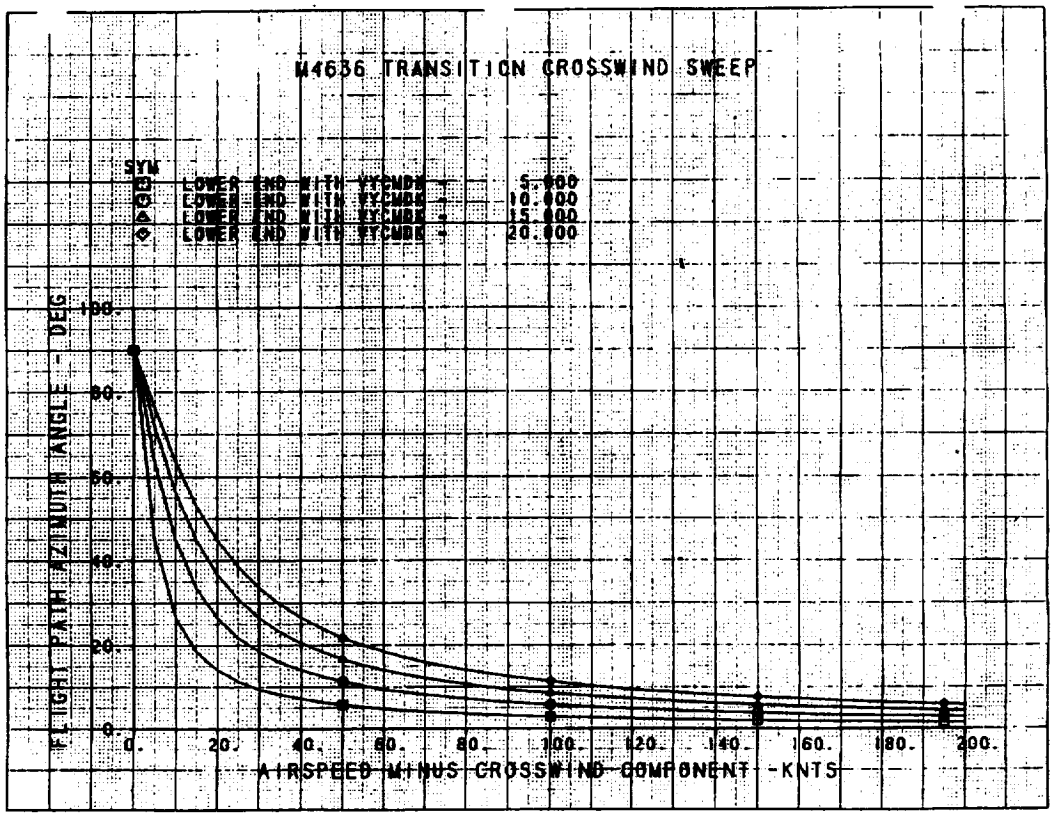

Figure 159. M4636 Transition Crosswind Sweep, Azimuth Angle

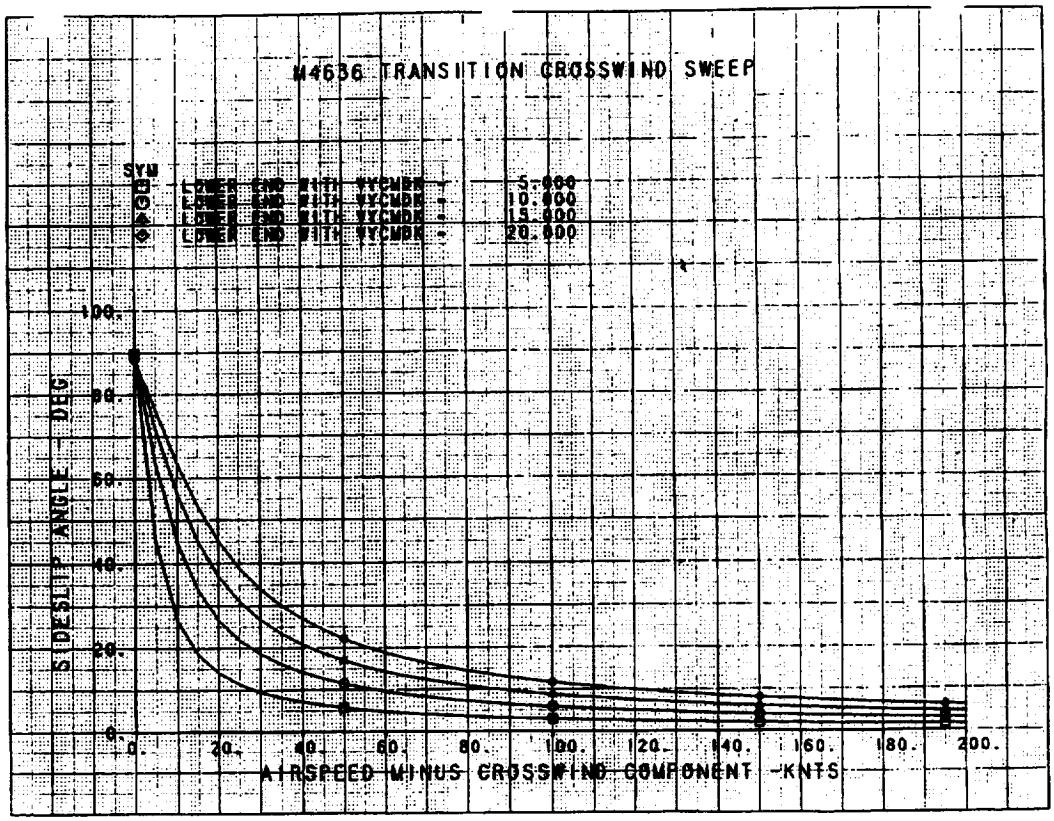

Figure 160. M4636 Transition Crosswind Sweep, Sideslip Angle

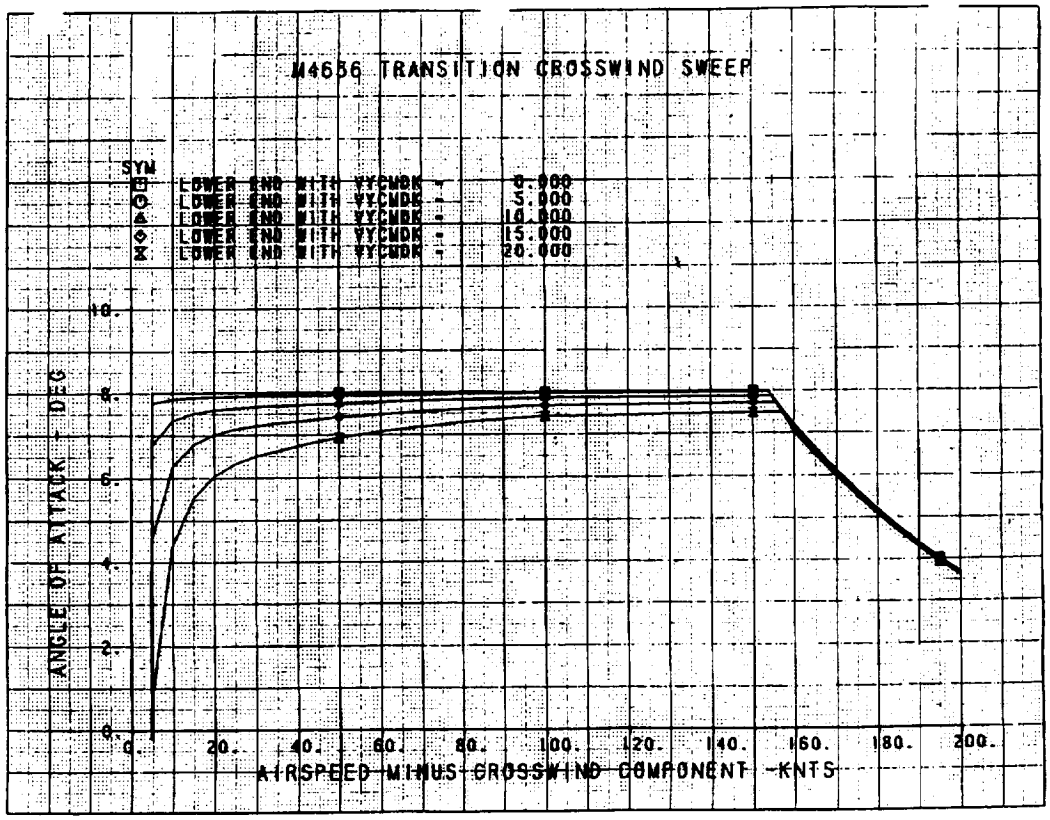

Figure 161. M4636 Transition Crosswind Sweep, Angle of Attack

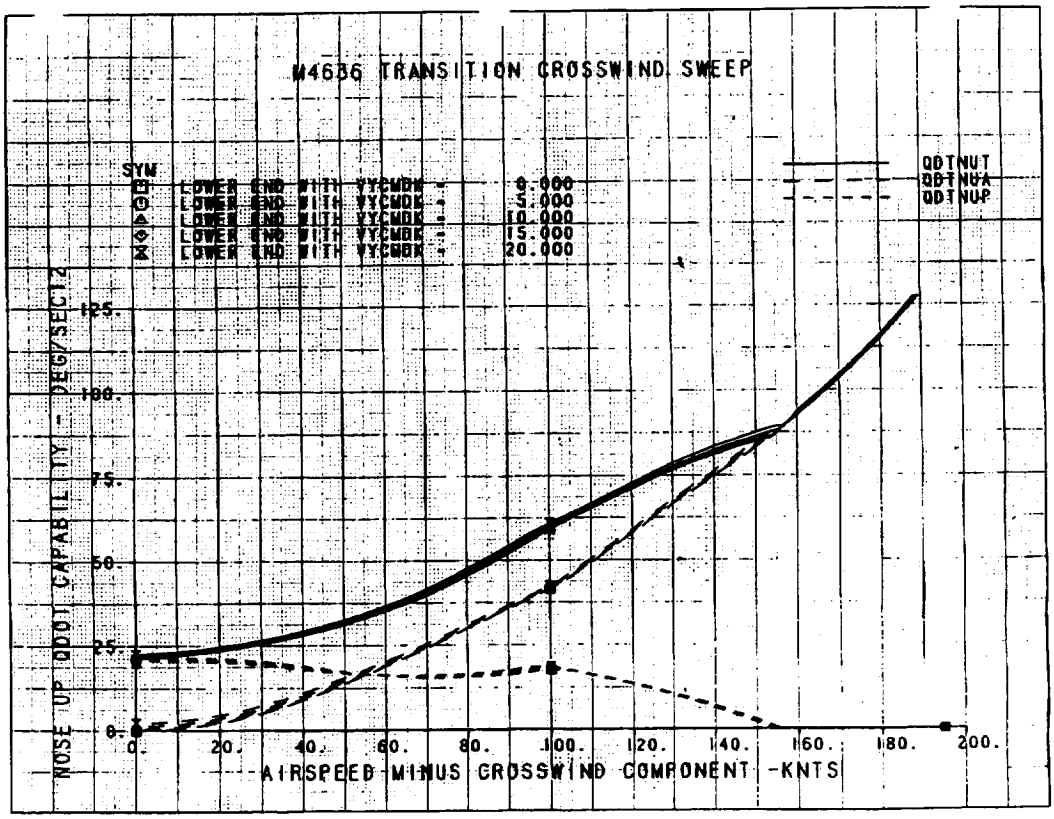

Figure 162. M4636 Transition Crosswind Sweep, Nose Up Qdot

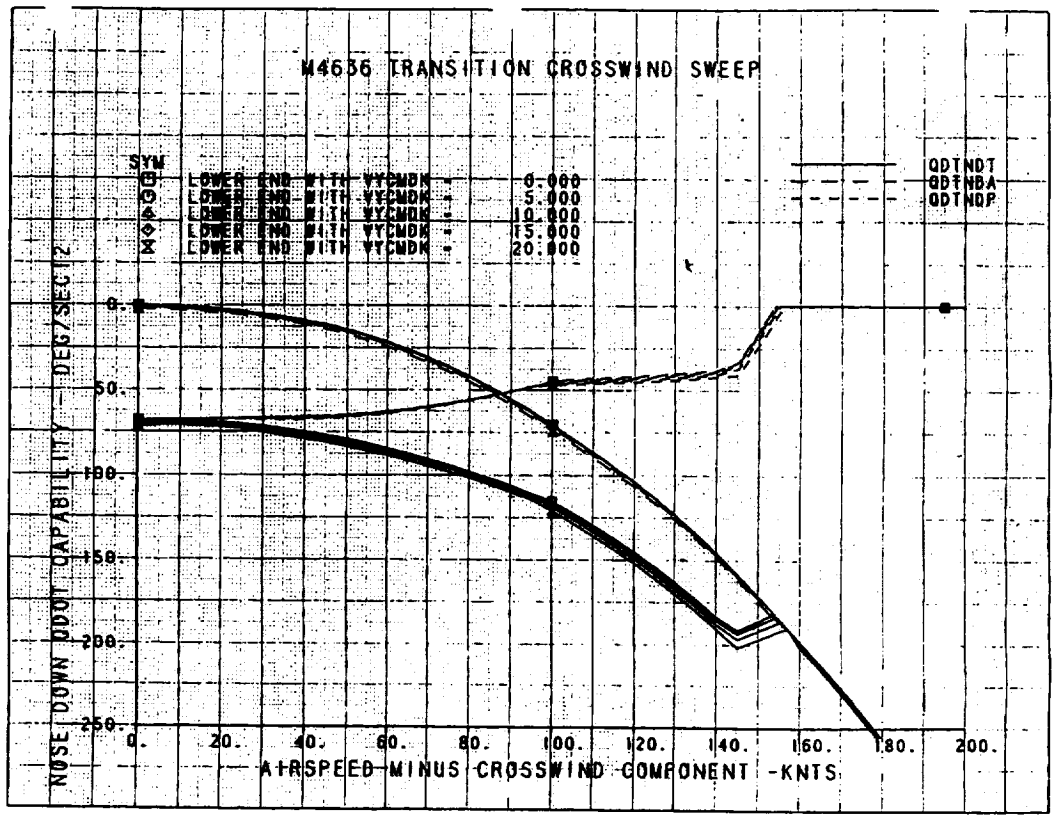

Figure 163. M4636 Transition Crosswind Sweep, Nose Down Qdot

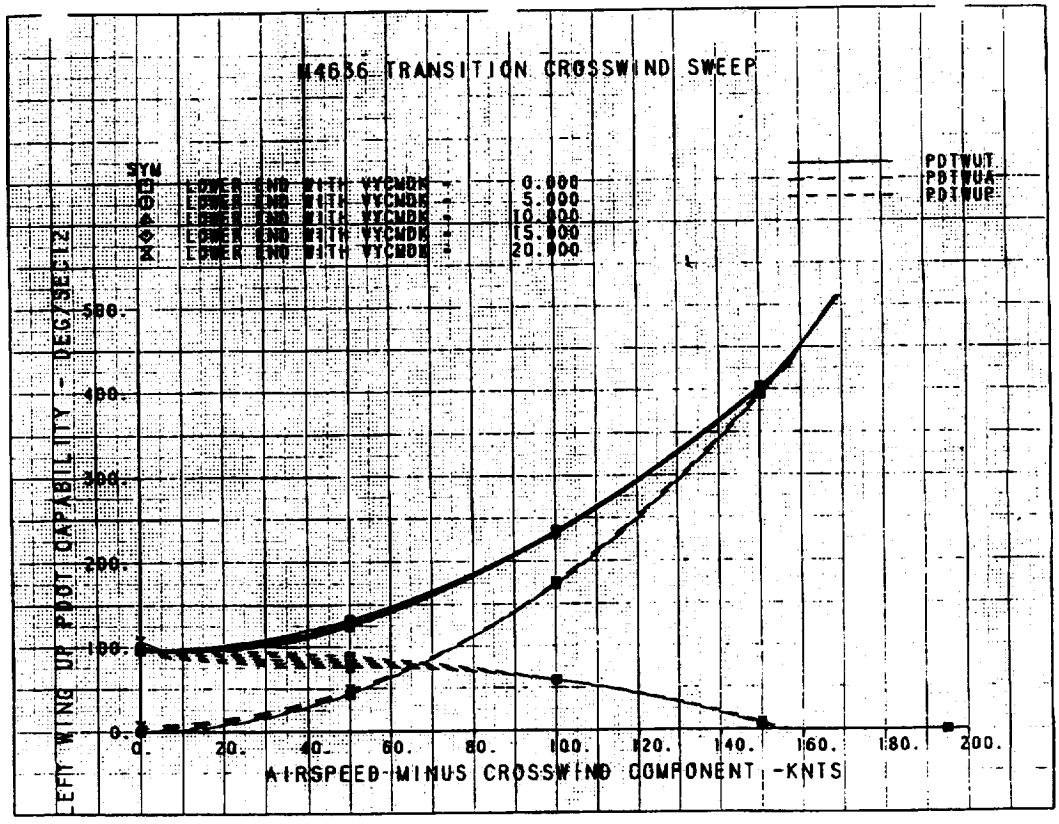

Figure 164. M4636 Transition Crosswind Sweep, Left Wing Up Pdot

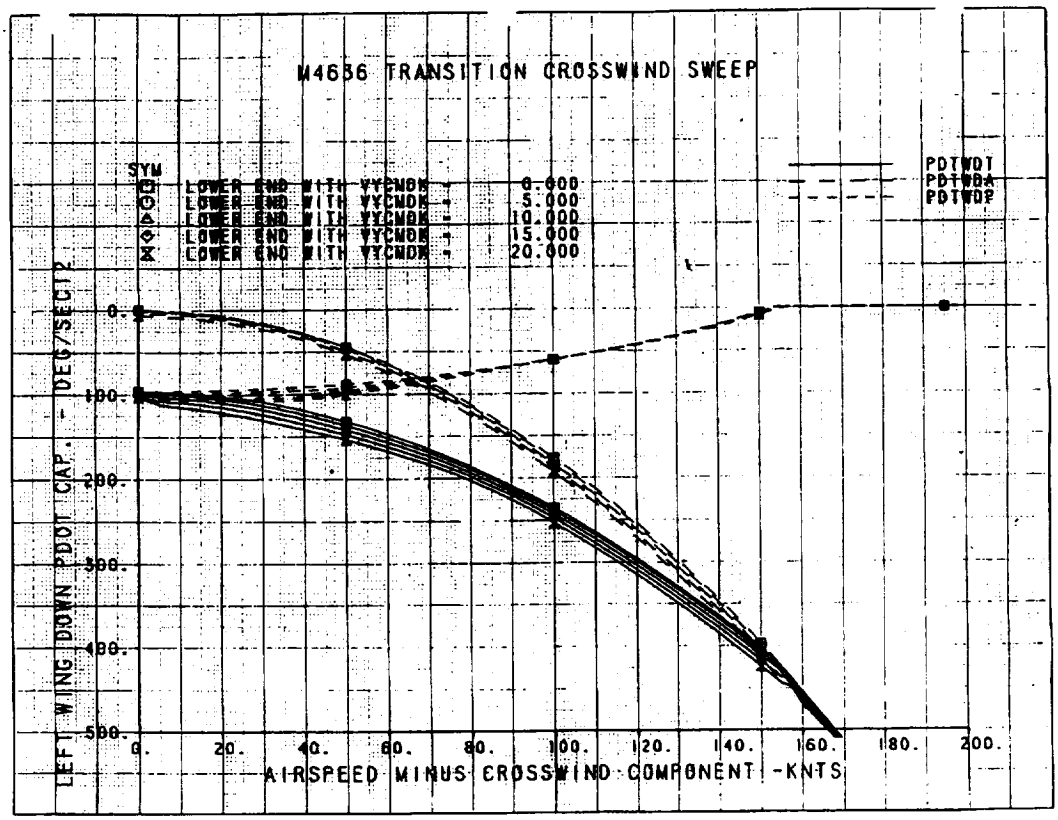

Figure 165. M4636 Transition Crosswind Sweep, Left Wing Down Pdot

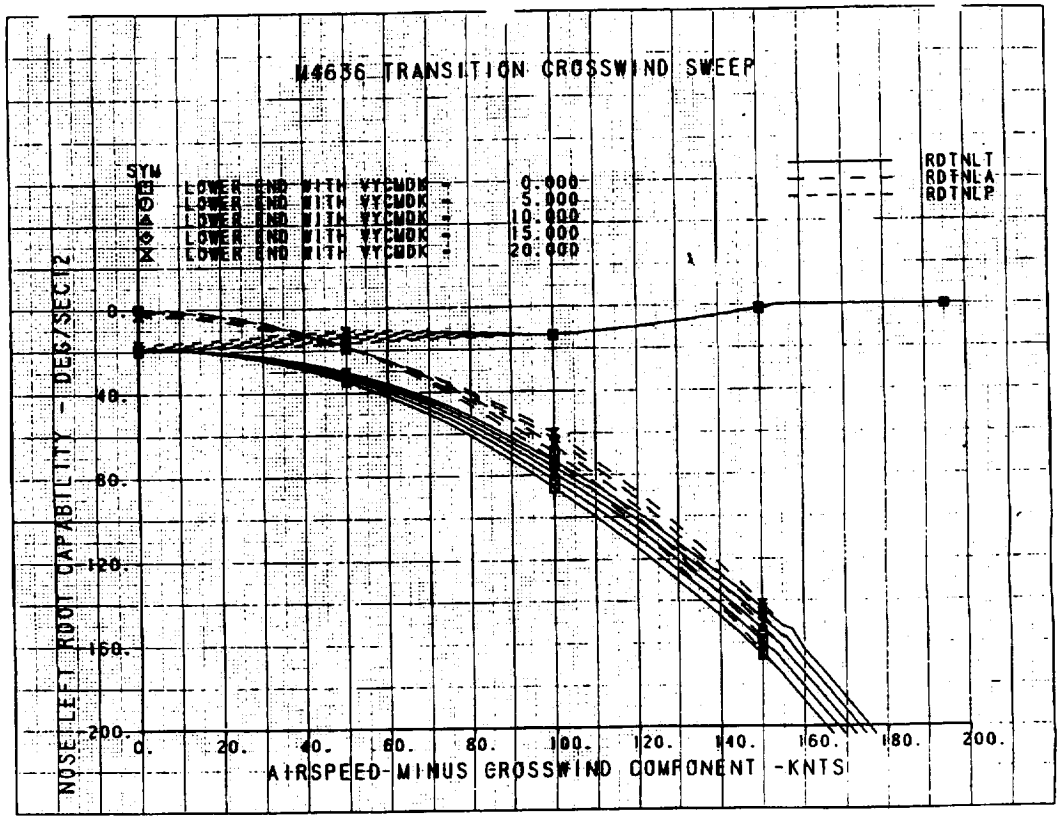

Figure 166. M4636 Transition Crosswind Sweep, Nose Left Rdot

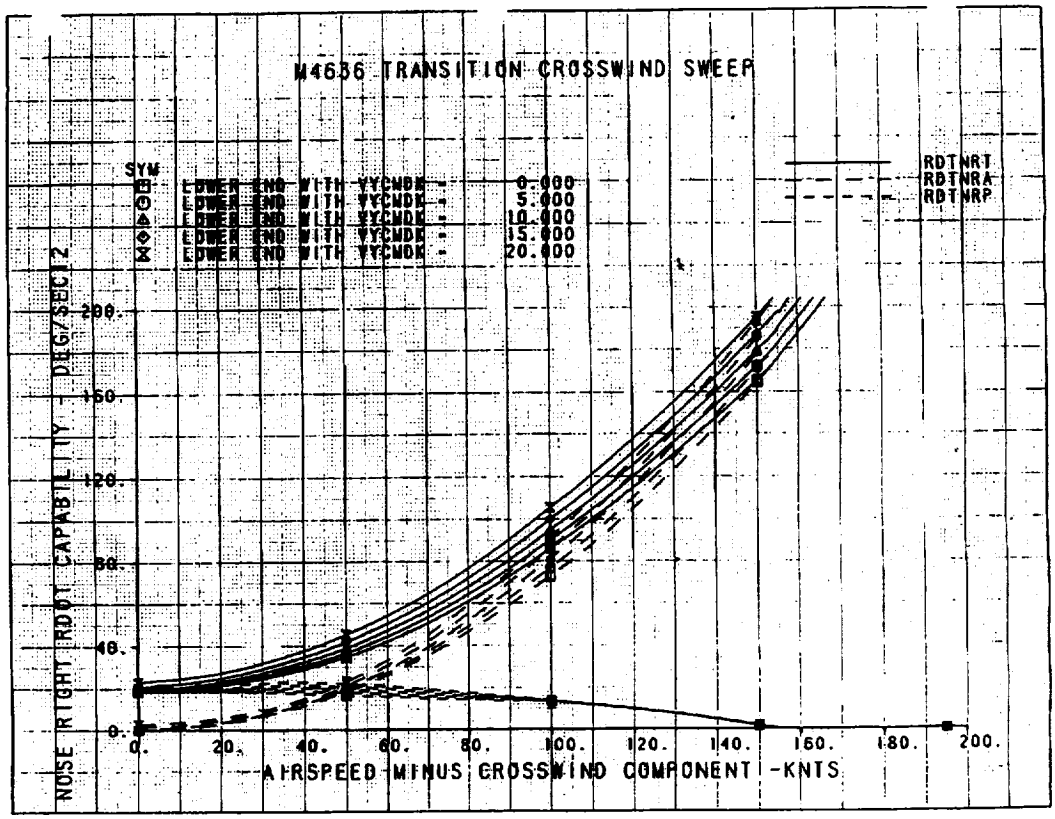

Figure 167. M4636 Transition Crosswind Sweep, Nose Right Rdot

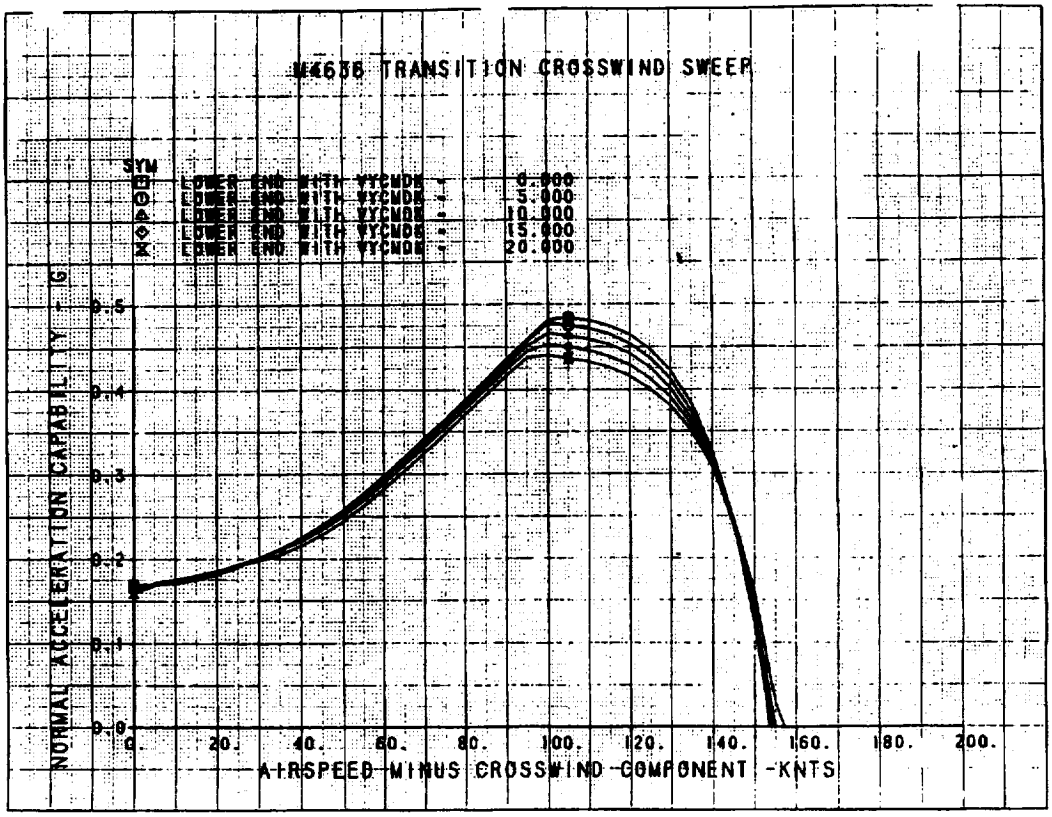

Figure 168. M4636 Transition Crosswind Sweep, Normal Acceleration

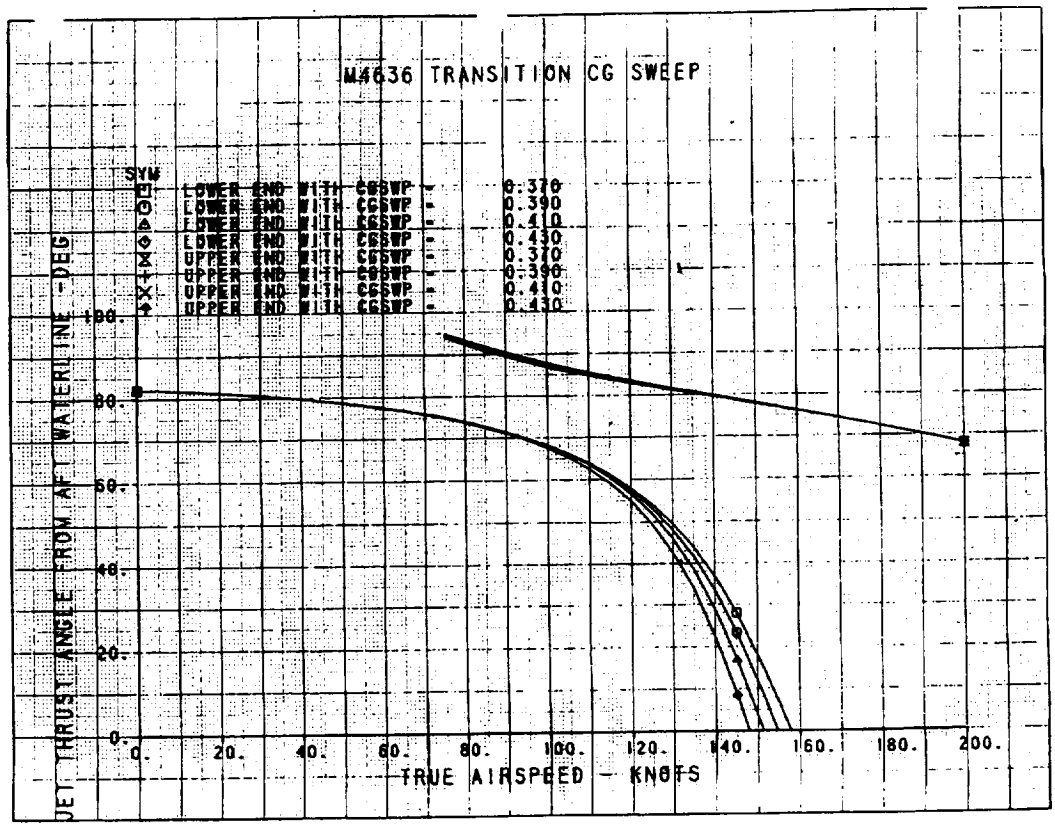

Figure 169. M4636 Transition CG Sweep, Jet Angle

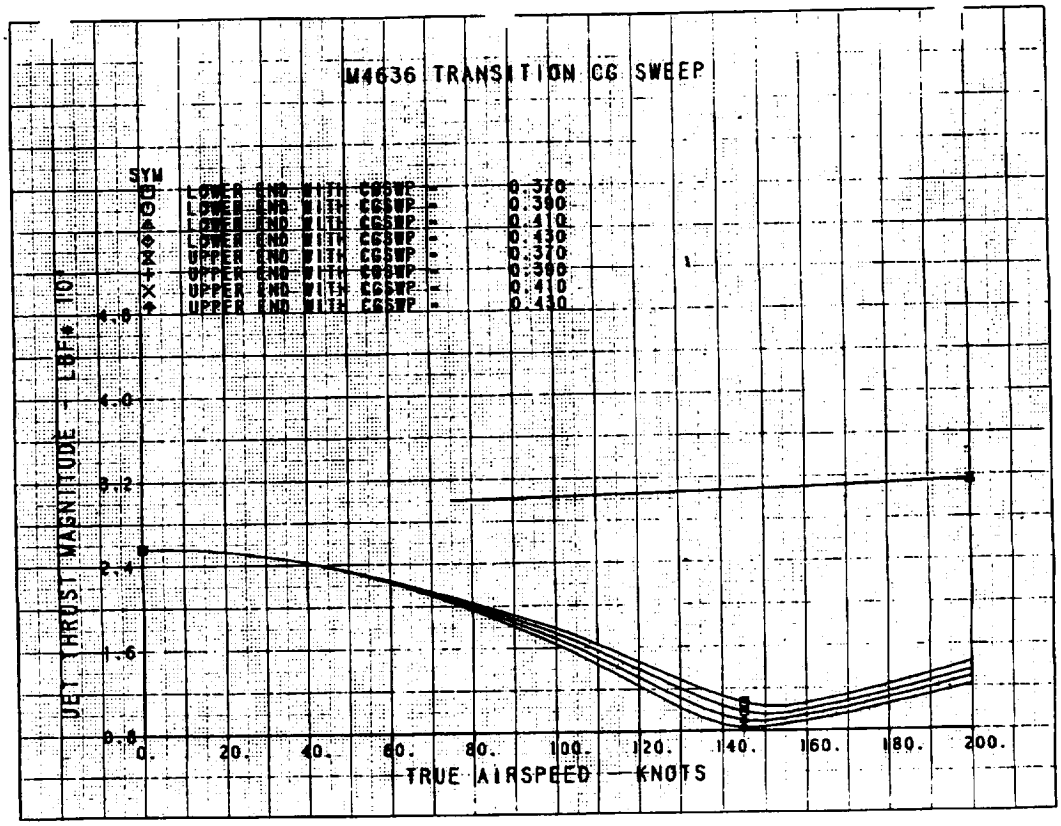

Figure 170. M4636 Transition CG Sweep, Thrust Magnitude

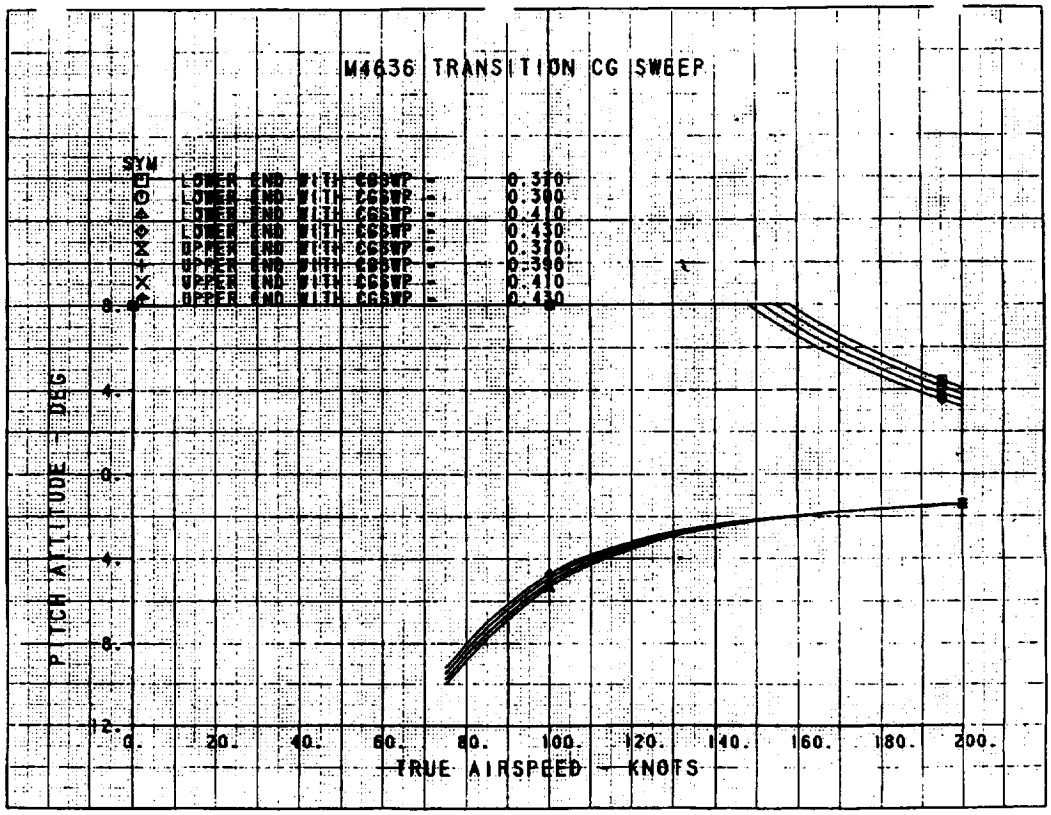

Figure 171. M4636 Transition CG Sweep, Pitch Attitude

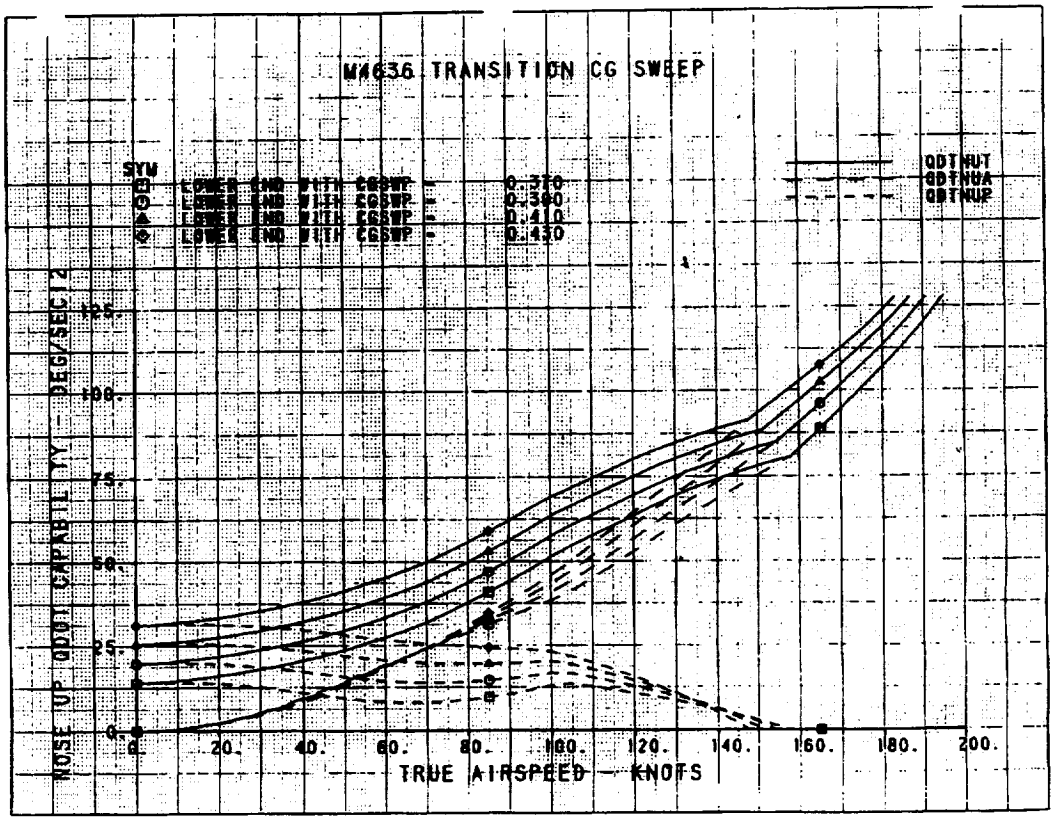

Figure 172. M4636 Transition CG Sweep, Nose Up Qdot

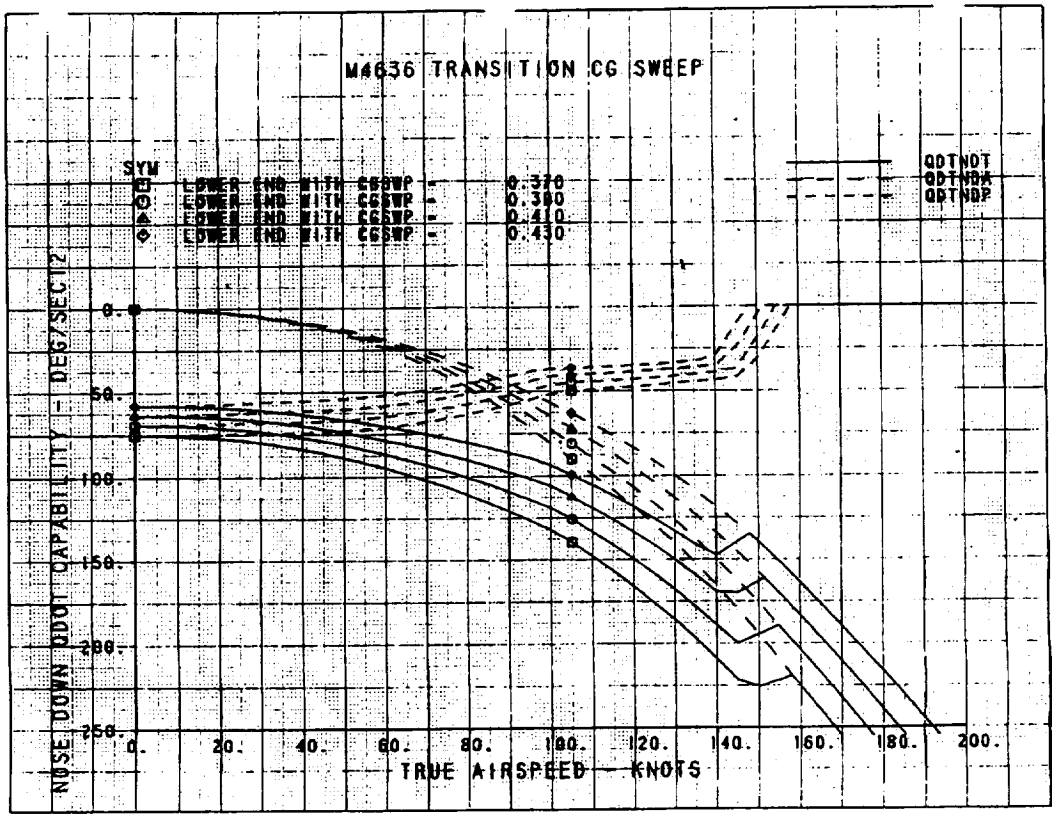

Figure 173. M4636 Transition CG Sweep, Nose Down Qdot

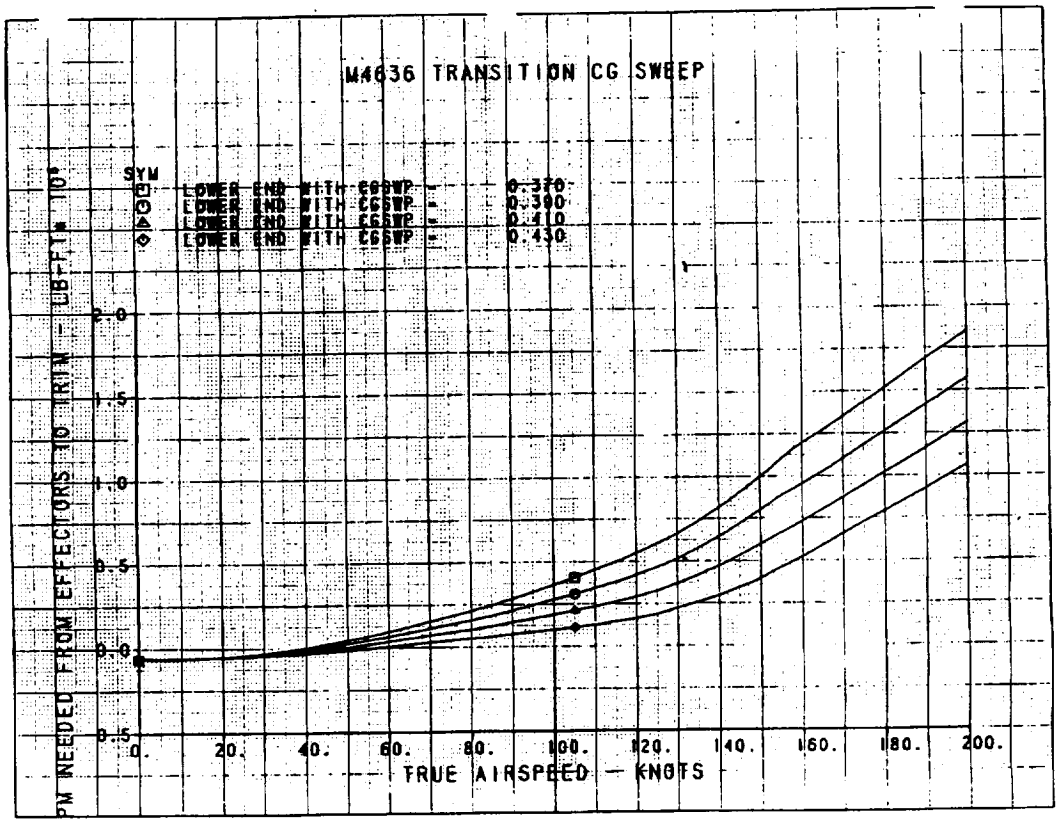

Figure 174. M4636 Transition CG Sweep, Trim Pitching Moment

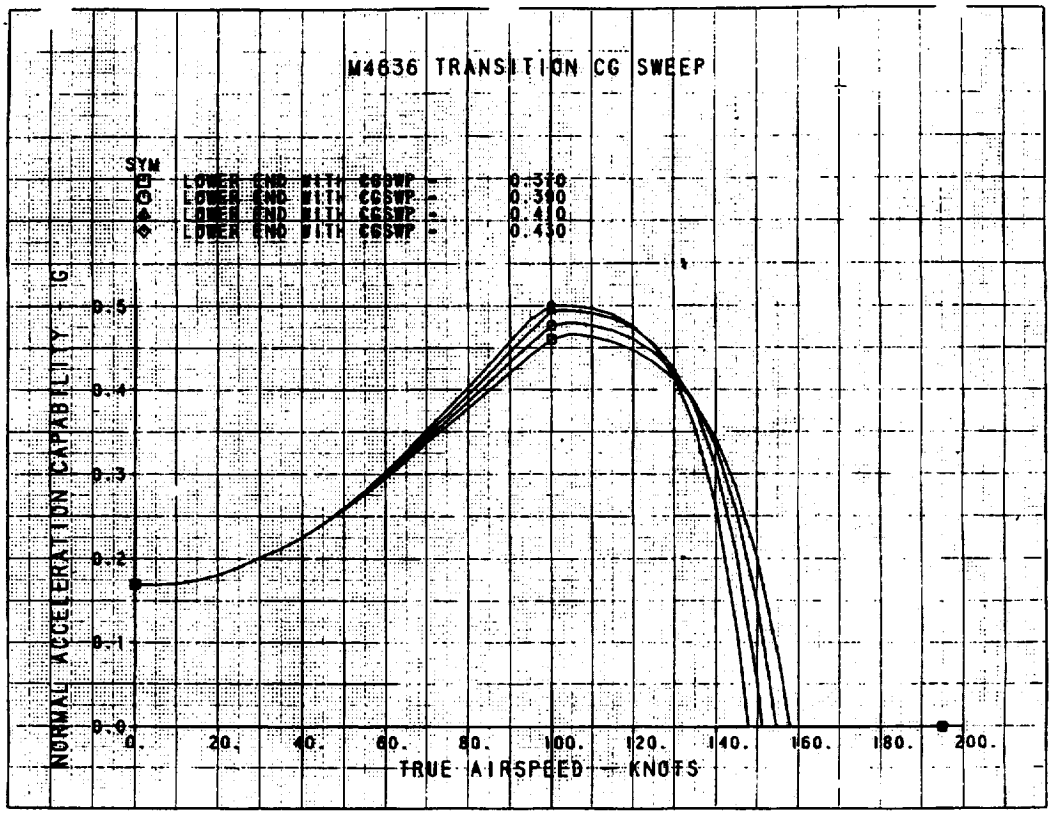

Figure 175. M4636 Transition CG Sweep, Normal Acceleration

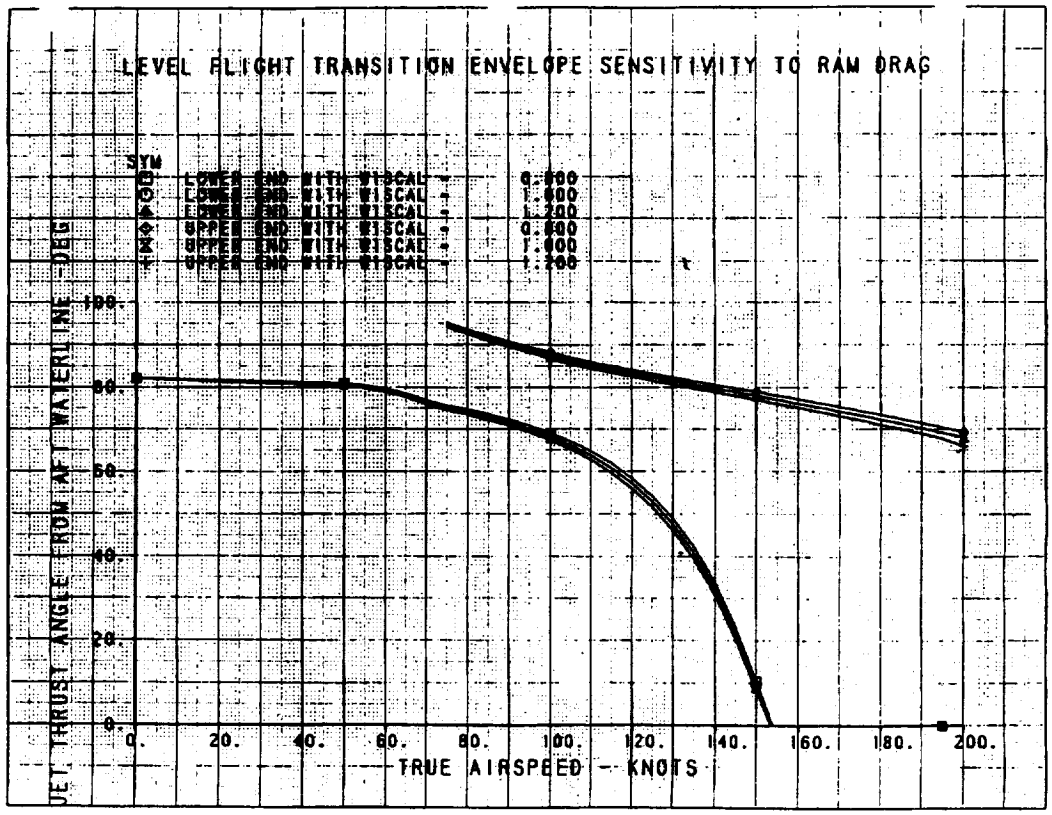

Figure 176. Level Flight Transition Envelope Sensitivity to Ram Drag

3.4.3. Hover Control Power Analyses

This section describes the control power available in hovering flight. The trim sweep is trimmed hover for velocity azimuth angles from −180 to 180 degrees and velocities ranging from 10 to 40 knots. This sweep represents either hovering flight in any direction with airspeeds up to 40 knots, or hovering flight over a ground reference point in a horizontal wind up to 40 knots from any horizontal direction. In all cases the aircraft nose is pointed North. Figure 177 is a plot of trimmed roll attitude versus trimmed pitch attitude for lines of constant velocity, forming a closed plot as the wind direction is varied from −180 to 180 degrees. This figure shows that the MIL−STD−83300 requirement for trimmed attitude variations of less than 10 degrees in a 35 knot wind are satisfied for this aircraft. Figure 178 shows the jet thrust magnitude required (the equivalent jet angle was kept at 82 degrees).

The trimmed pitching moment required from the ventral nozzle for these flight conditions are shown in Figure 179, along with the aerodynamic and propulsive contributions. Since the ventral nozzle is used exclusively to trim pitching moment in these cases, the plot of pitching moment due to the ventral nozzle overlaps the solid plot of the total pitching moment required to trim. Figure 180 through Figure 185 show the control power available in the pitch, roll, and yaw axes, indicating that the US/UK CEM requirements are met.

The normal acceleration capability is shown in Figure 186, with a capability above .13 g's incremental normal acceleration in crosswinds up to 40 knots. Figure 187 shows the normal acceleration capability in ground effect (gear contact occurs at an altitude of 6.42 feet). The plot indicates that the minimum normal acceleration capability is at 15.42 feet, but actually the minimum occurs at 14.42 feet. Figure 188 shows the sensitivity of the normal acceleration to descent rate at this altitude of 14.42 feet, and shows that the capability is above the 0.1 g requirement.

3.5. Simulation Test

A simulation test of the SCIP aircraft was conducted on a fixed−base simulator at NASA−ARC from March 15 to April 23 1993. The simulation objectives were to evaluate the integrated flight propulsion control system, including the benefits of different levels of control augmentation under the influence of varying environments during both field and shipboard operations.

To evaluate the IFPC system, flying qualities were evaluated for specific tasks through pilot comments and Cooper−Harper (Reference 24) ratings. The benefits of different levels of control augmentation were studied by investigating five transition modes and four hovering modes. The influence of different environmental conditions was studied by evaluating flying qualities for both VFR and IFR conditions and various turbulence levels ranging from calm to severe conditions. The influence of both field operations and shipboard operations was studied by performing vertical landings at an airfield, an LHA class ship and on a destroyer class ship in various sea states ranging from calm seas to sea state five.

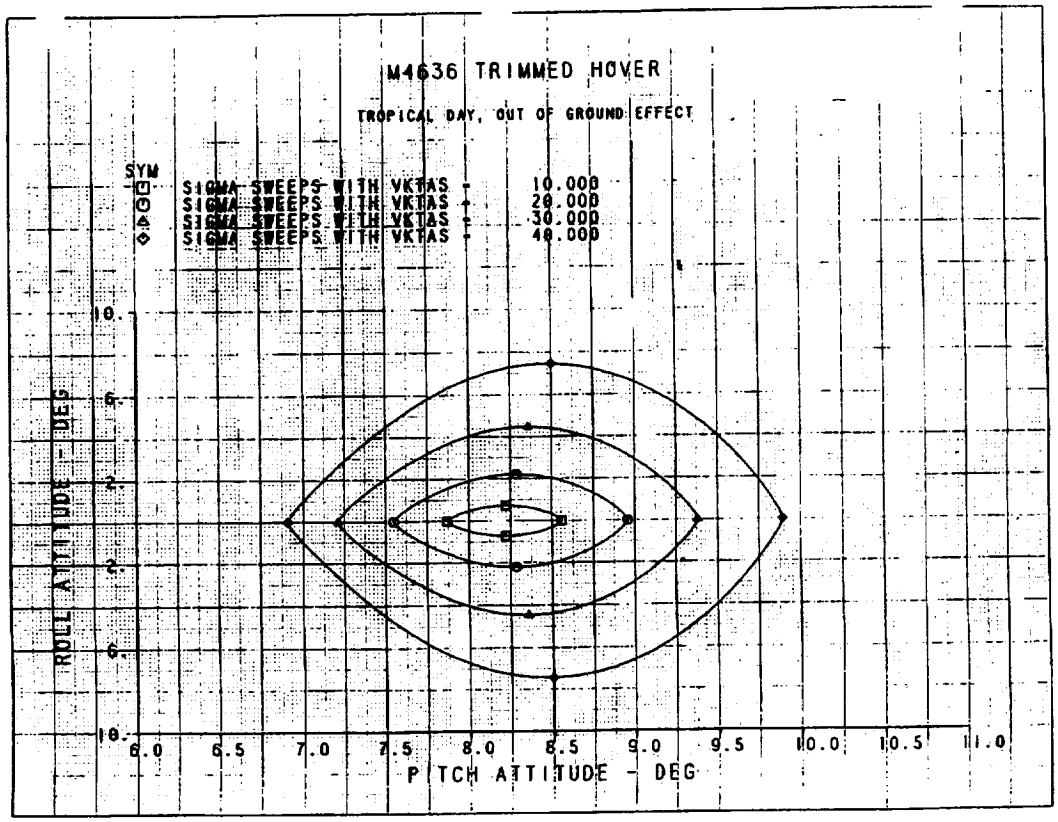

Figure 177. M4636 Trimmed Hover, Roll Attitude vs Pitch Attitude

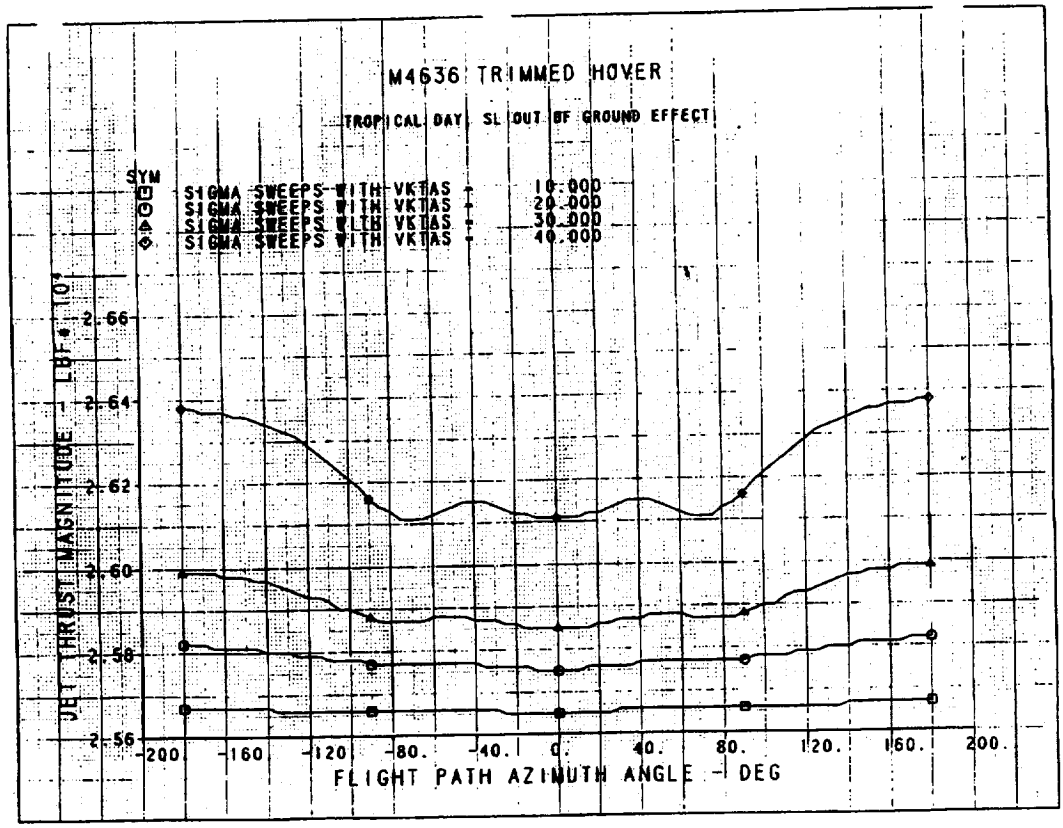

Figure 178. M4636 Trimmed Hover, Thrust Magnitude

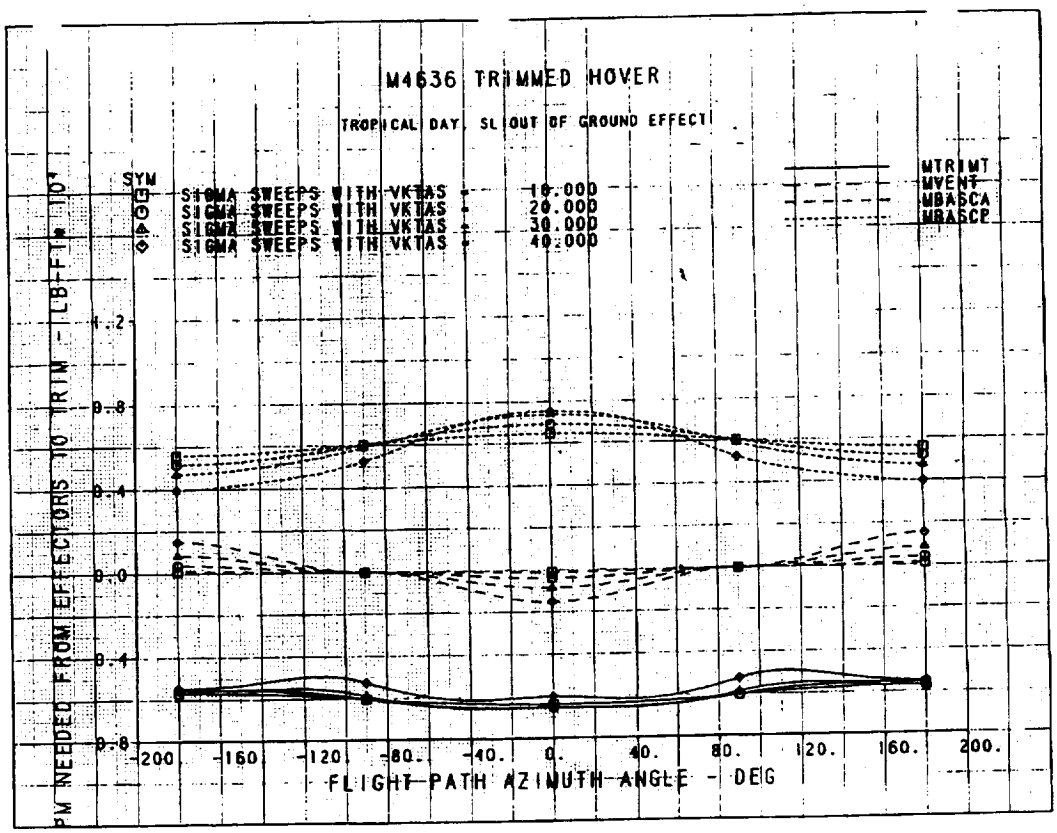

Figure 179. M4636 Trimmed Hover, Trim Pitching Movement

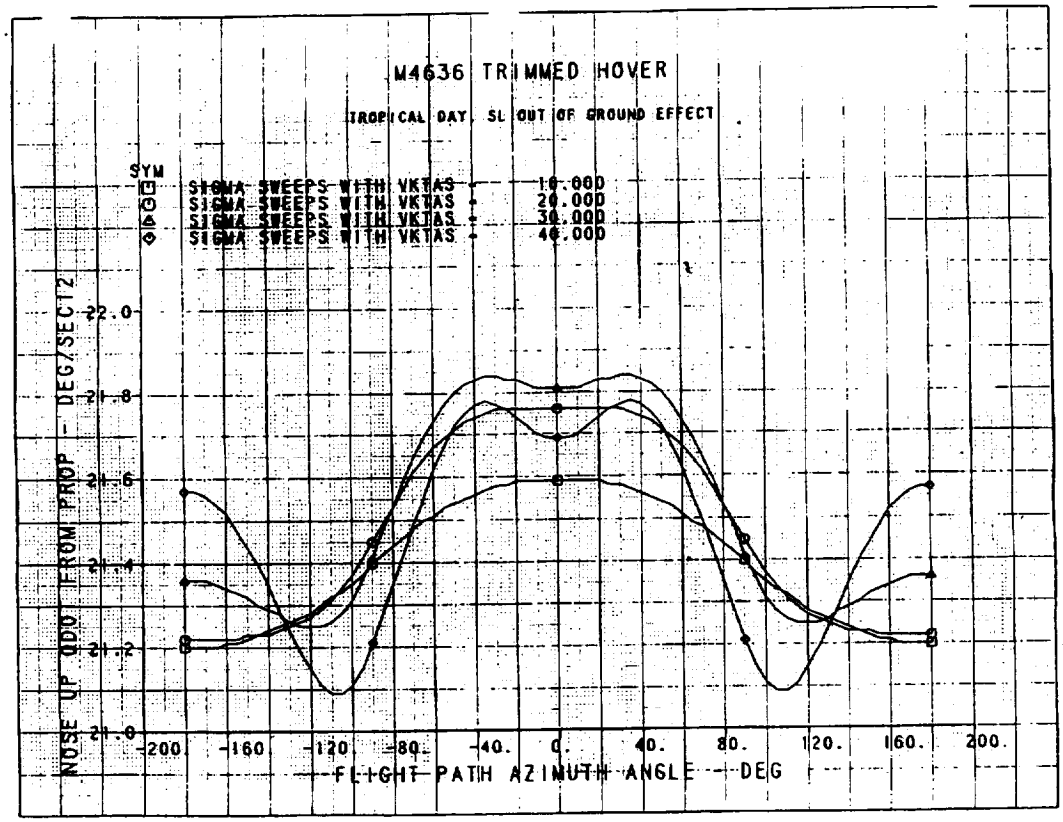

Figure 180. M4636 Trimmed Hover, Nose Up Qdot

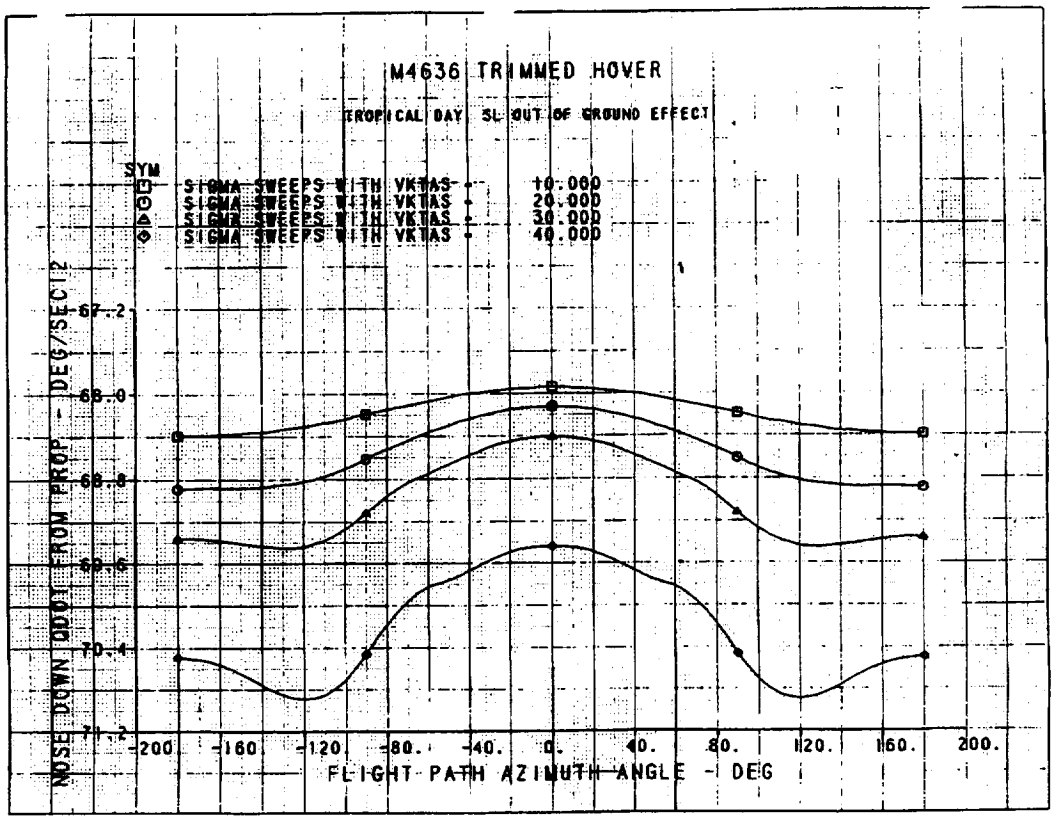

Figure 181. M4636 Trimmed Hover, Nose Down Qdot

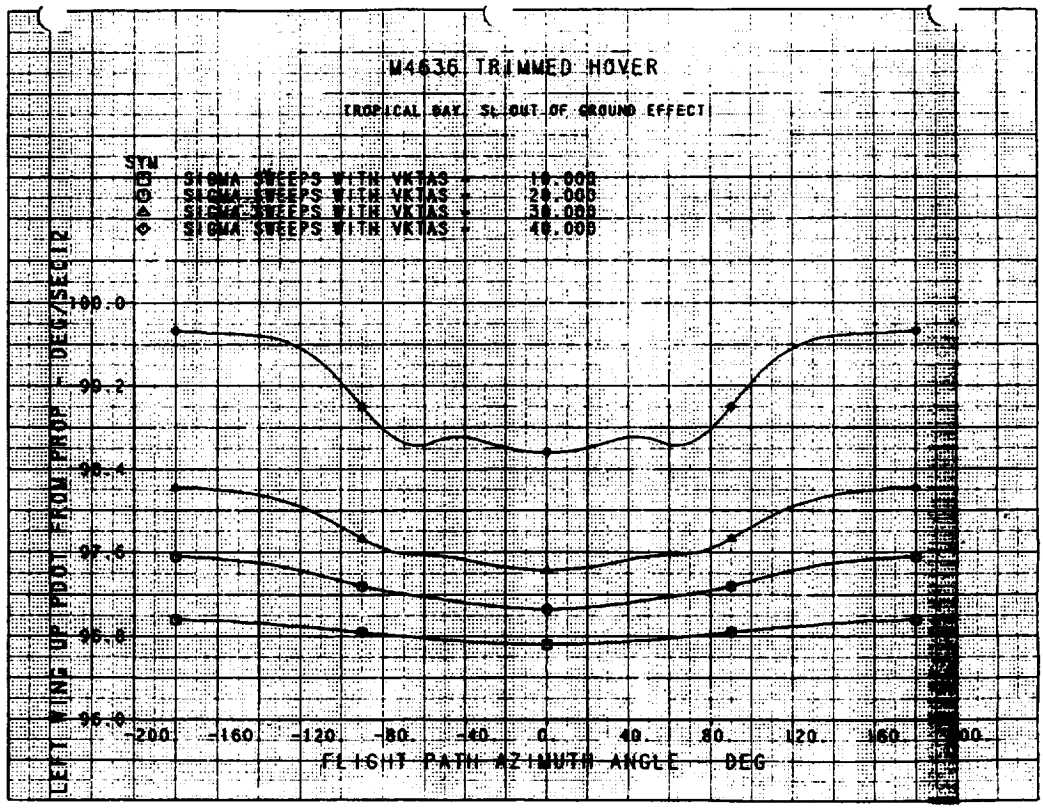

Figure 182. M4636 Trimmed Hover, Left Wing Up Pdot

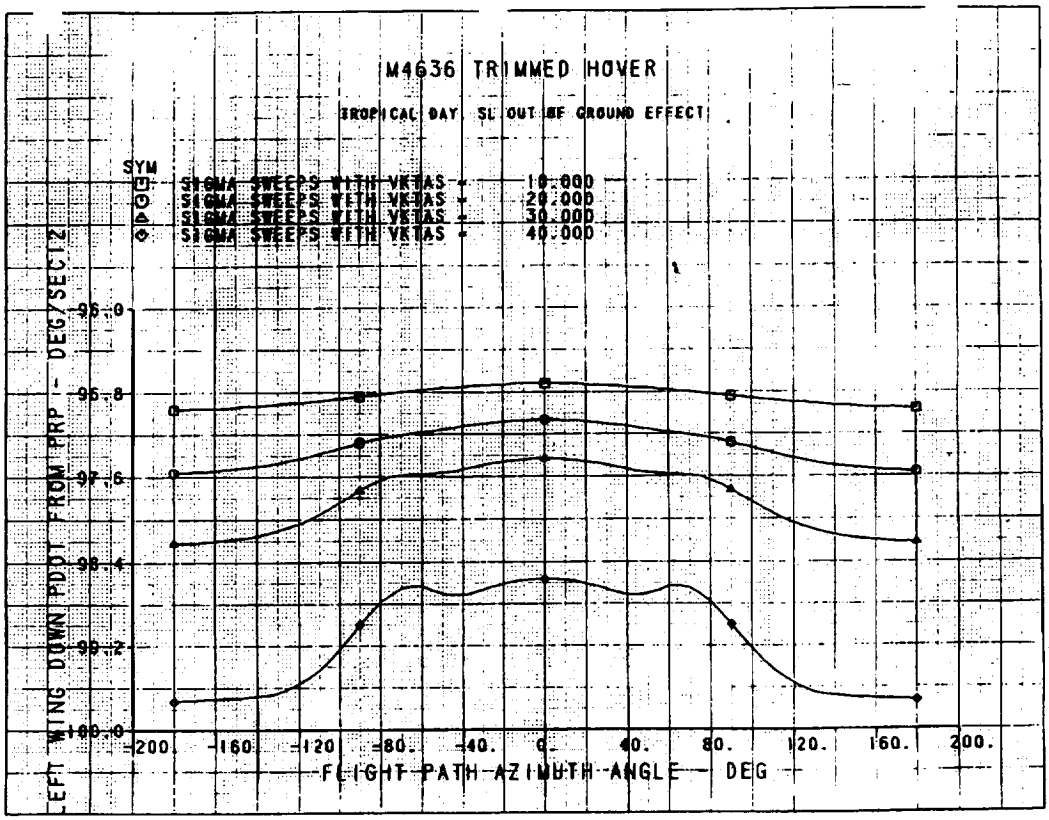

Figure 183. M4636 Trimmed Hover, Left Wing Down Pdot

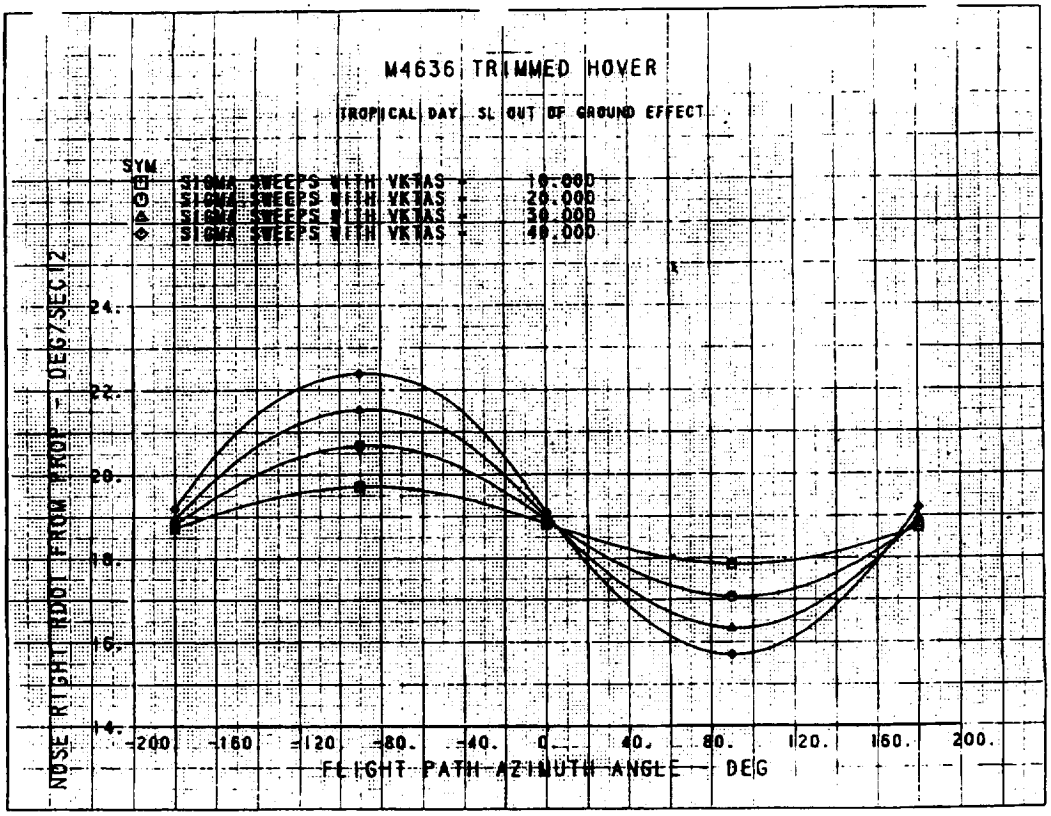

Figure 184. M4636 Trimmed Hover, Nose Right Rdot

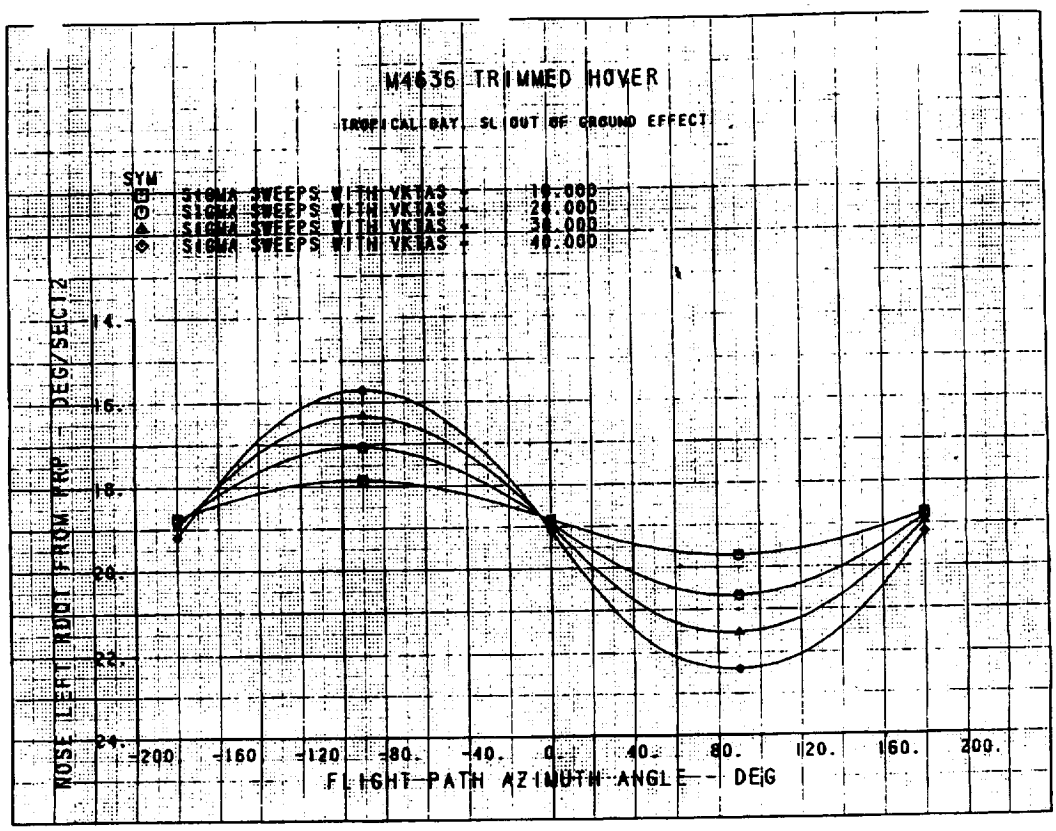

Figure 185. M4636 Trimmed Hover, Nose Left Rdot

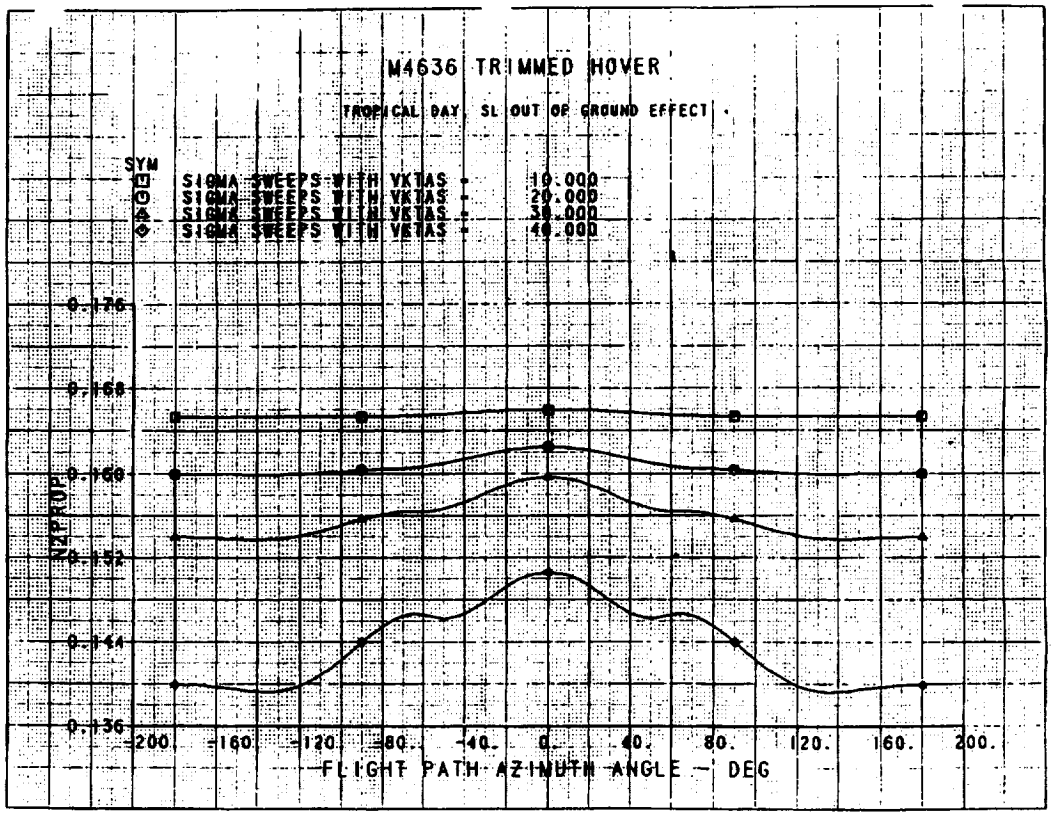

Figure 186. M4636 Trimmed Hover, Normal Acceleration in Crosswinds

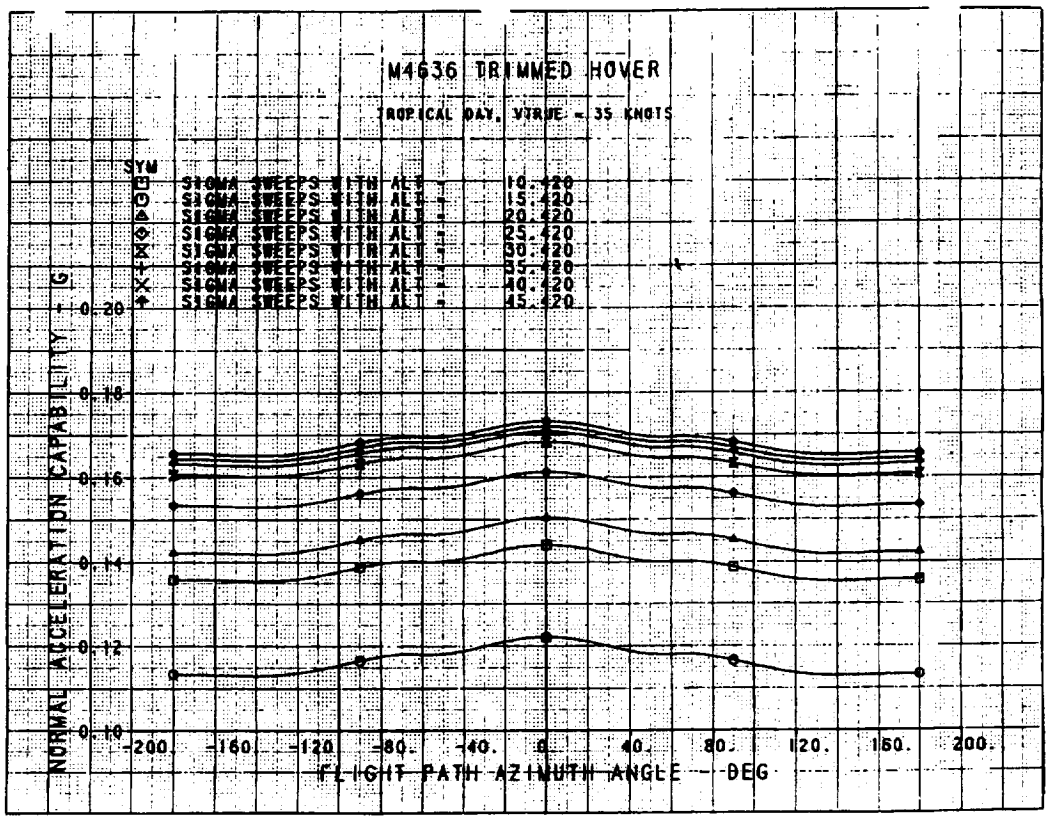

Figure 187. M4636 Trimmed Hover, Normal Acceleration in Ground Effect

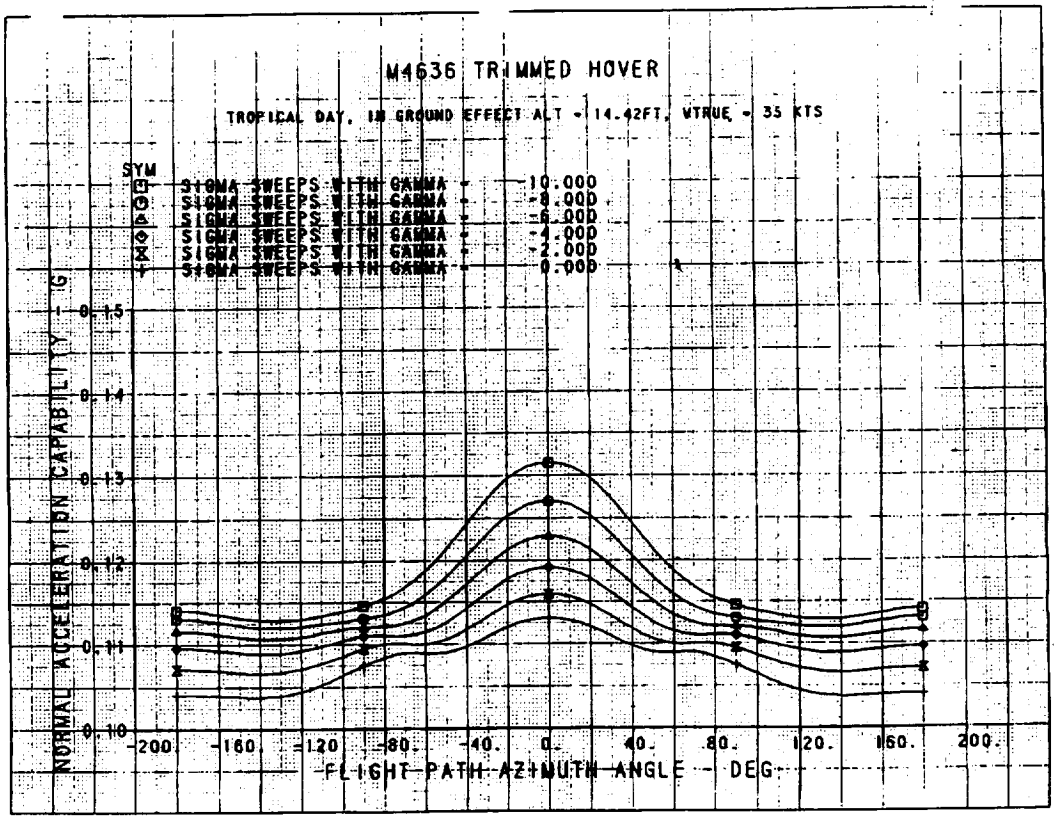

Figure 188. M4636 Trimmed Hover, Normal Acceleration in Ground Effect

Another objective of the simulation was to study the coordination of the aerodynamic and propulsive effectors in transition and to study the propulsion system performance. The simulation had the ability to run the propulsion controls in three different modes: 1) no RCS controls, lift and ventral nozzle vectoring used for attitude control; 2) RCS controls used for control of attitude, no lift or ventral nozzle vectoring; 3) both RCS and nozzle vectoring used for attitude control. Different conditions requiring a range of propulsion system performance were generated by changing the day type for different temperature levels, and aircraft weight for different thrust levels.

Section 3.5.1 gives a description of the simulation, including the evaluation tasks performed by the pilots. Section 3.5.2 presents the pilot evaluations and summarizes the pilot comments. Section 3.5.3 summarizes the control power used during the various tasks in terms of the amount of pitch, roll, and yaw acceleration generated by the controls. Section 3.5.4 describes result fan analysis of the propulsion system data from the piloted simulation.

3.5.1. Simulation Description

The SCIP simulation was conducted on a fixed-base, single-seat flight simulator at NASA-ARC. Pilot controls include a center stick, rudder pedals and a Harrier-type throttle/nozzle lever quadrant. Both the stick and the nozzle lever were modified with thumbwheels for use in the ACT-MT and ACT-AT modes, either the stick thumbwheel or the throttle thumbwheel could be used to command deceleration.

A three window computer-generated imaging system provided the external view. This system presented either a view of an airfield representing the Seymore-Johnson airfield with STOL runway markings, a ship scene modeling an LHA class ship (LPH-2), or a ship scene modeling a Spruance class destroyer (DD-963) with a 40- by 70-ft landing pad. Various visibility conditions can also be generated.

An overhead optical-combining glass projected the HUD for the pilot. The HUD displays in this simulation used a format employed in several previous NASA V/STOL simulations at Ames, References 8 and 9. The HUD formats are described in detail in Reference 19.

3.5.2. Test Results-Pilot Comments and Ratings on Flying Qualities

The approach and landing tasks described in Section 3.5.1 were evaluated as three specific tasks: 1) Decelerating Transition (DT), this is the initial phase of the approach; 2) Hover Acquisition (HA), the final phase where the hover point is acquired; and 3) Vertical Landing (VL), done on either the field or one of the two ships. The approaches were done in both VMC and IMC conditions. Approach profiles to the runway and destroyer are shown in Figure 189. The pilot rating summaries are plotted versus mode, a table of the modes is in Figure 190.

The pilot ratings for DT are shown in Figure 191 and Figure 192, for VMC and IMC conditions, respectively. TURB is the root mean square atmospheric turbulence in feet/sec. In calm conditions, the manual throttle modes were Level 1. Adding RCAH to the TRAN mode improved the ratings slightly (TRAN vs. TRAN-RCAH), and adding the thumbwheel command again improved the ratings further (ACT-MT vs. TRAN-RCAH).

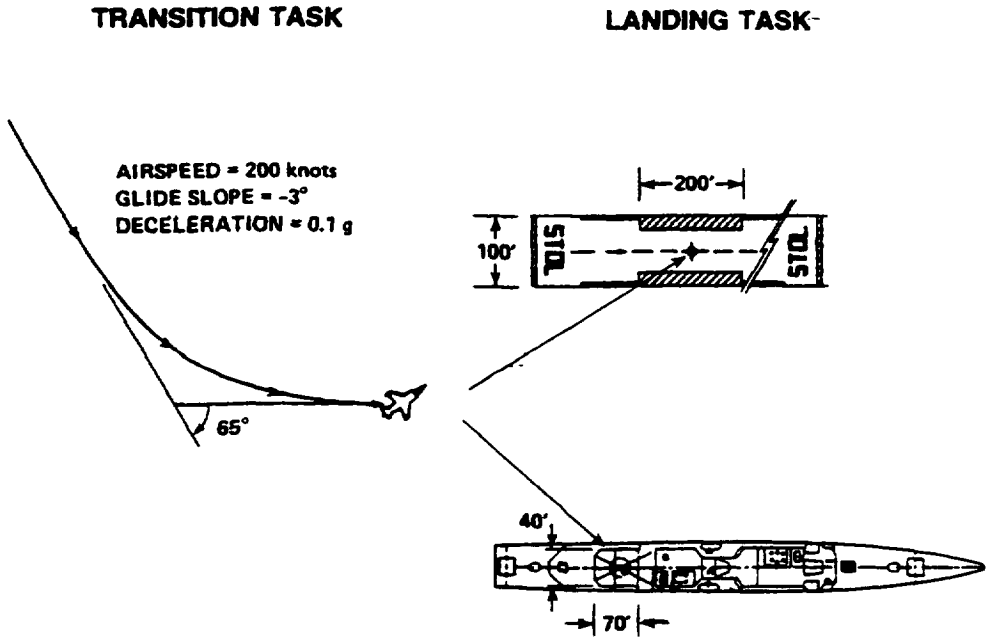

Figure 189. Approach Profile to Runway or DD–963 Destroyer

Transition Cases		Vertical Landing Cases		Control Power Cases	
Value	**Mode**	**Value**	**Mode**	**Power**	**Data Type**
1	TRAN	1	TRAN	1	Maximum
2	TRAN–RCAH	2	ACT–AT	2	Mean + Std. Dev.
3	ACT–MT	3	TRC–MT	3	Mean
4	ACT–AT	4	TRC–AT	4	Mean – Std. Dev.
5	VET			5	Minimum
				6	Std. Dev.

Figure 190. Case Numbers and Control Modes

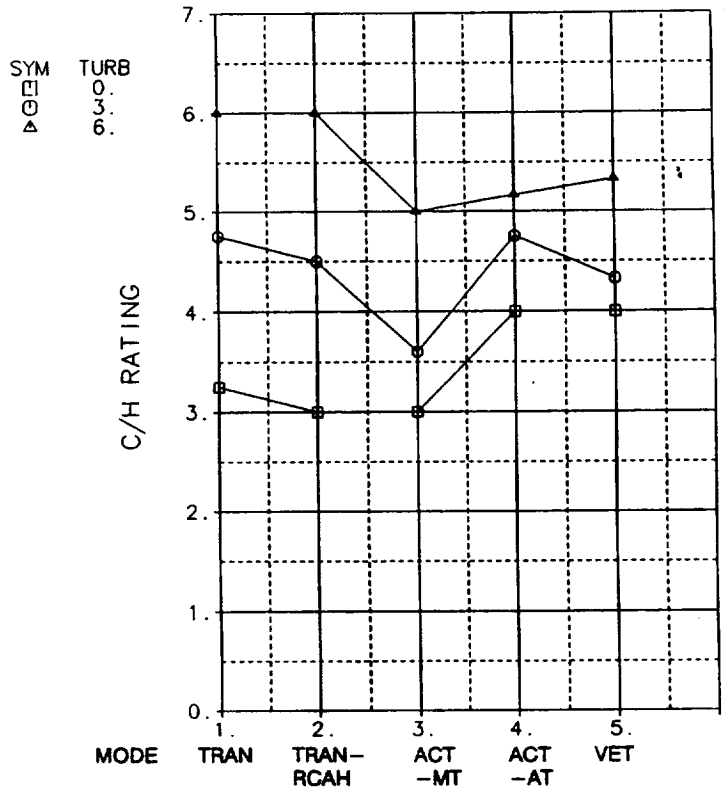

Figure 191. Pilot Ratings for VMC Decelerating Transition

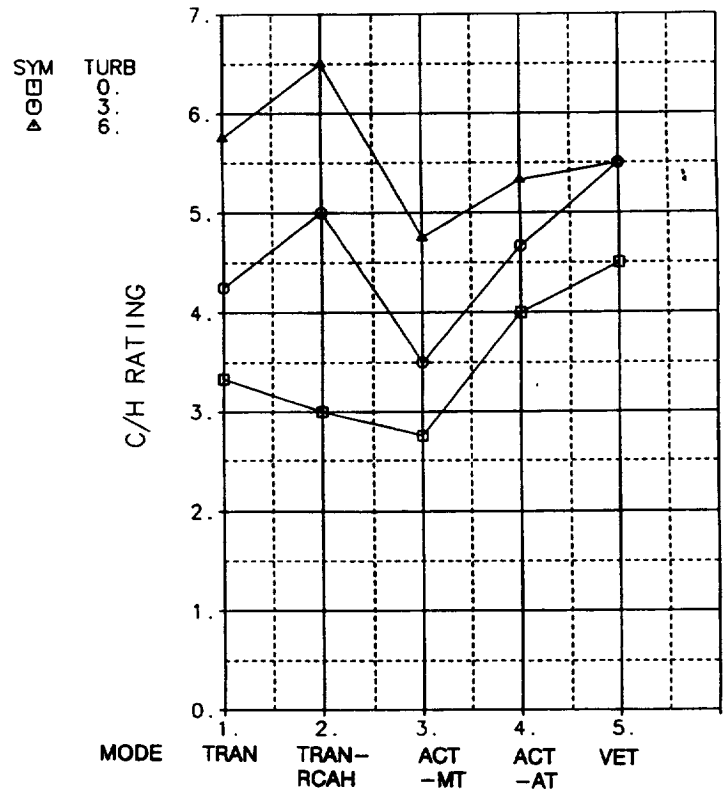

Figure 192. Pilot Ratings for IMC Declerating Transition

In calm conditions, the ratings for the autothrottle modes increase into Level 2 category. The main deficiency was that the autothrottle response dynamics and the pitch stick response dynamics were not properly matched. With flight path being controllable with either the throttle or the stick, and the dynamics not being well matched, the pilot could command both controls out of phase making it easy to PIO the flight path response. Also the thrust response during the initial vectoring down to hold angle of attack was momentarily oscillatory, creating about a ten knot range where the pilot had to decelerate through rapidly. Another comment was that, when setting the autothrottle, the handle had to be moved through a large travel to a new location, during which time no thrust response was apparent. Although this was the proper operation of the autothrottle, some pilots found moving the throttle with no thrust response a little disconcerting.

In turbulent conditions, all ratings increased into Level 2 category. This was due mainly to poor gust response caused by very light wing loading (42 lb/sq ft), making precise flight path response difficult. Again ratings for ACT–MT were the best, and the autothrottle ratings are similar to the manual throttle modes. The similarity between manual and autothrottle is due to the ratings being dominated by the light gust response. ACT–AT received better ratings because the thumbwheel control allowed the pilot to accurately control deceleration while also being able to fly with hands on throttle and stick.

Note that rating did not vary much between VMC and IMC conditions. This was true mainly because the tasks were flown with the approach guidance on. The approach guidance thus was able to make the IFR approach as easy as the VFR approach.

The pilot rating summaries for HA are in Figure 193 and Figure 194. Most of the same conclusions for the DT task applies in HA. As speed decreased, the autothrottle response improved dramatically as the control laws blended to an inertially referenced command system and as the natural coupling between pitch rate and angle of attack went away.

The pilot ratings for VLs on the airfield are in Figure 195. The rating were Level 1 in all cases. For all the modes the turbulence level was not apparent to the pilot below about 45 knots. Differences in pilot ratings at different turbulence conditions were due to differences in the steady wind speed, where the pilot was required to vane the aircraft into the wind prior to landing, creating a slightly higher workload task. Note that the TRC modes were generally rated 0.5 to 1 point better, putting the ratings solidly into Level 1 for all conditions.

Also the ACT–AT mode, which translated forward/aft with the throttle thumbwheel was considered to be more difficult than TRAN mode where forward/aft translations were controlled using pitch attitude commanded by the stick. This was mainly due to a perception that controlling horizontal velocity with a single one hand controller was easier than with two hands on different controllers. A few qualitative flights were performed to see if this effect was improved by using the thumbwheel on the stick. The comments were that the thumbwheel on the stick improved things, but that translations by pitch and roll attitude commands was preferred.

The ratings for landing on the LPH–2 ship are in Figure 196. Again, in calm seas, the attitude command system (TRAN) was preferred to commanding forward/aft translations with the thumbwheel (ACT–AT). THe TRC mode received the best ratings. The difference between TRC–MT and TRC–AT is that the autothrottle provides full authority altitude rate command, making precise control of sink rate in ground effect just prior to touchdown

much easier. Ratings for all modes fall into Level 2; this was because the ground effect was severe enough so that the pilots could not consistently achieve the <5 ft/sec sink rate criterion for satisfactory performance. All pilots emphasized that without this deficiency the TRC command system would be rated much higher, and that it is a much easier task with TRC.

The ratings for landing on the DD–963 ship are shown in Figure 197. The conclusions for the LPH case apply here. Note that the average rating for the TRC mode with autothrottle is below 2, because one pilot gave a rating of C/H 1.

3.5.3. Test Results–Control Usage

During each simulation run, the pitch, roll and yaw acceleration time histories were processed to compute statistical data on the pitch, roll and yaw accelerations produced by the controls. These data are cataloged using a variable called POWER, as shown in Figure 190, and include the maximum, minimum, mean, and standard deviation of the pitch, roll, and yaw accelerations produced by the control during each run. These data were then averaged or correlated with similar data from other runs where the same mode and task were flown.

These data were compiled for each task segment and each mode. Data are shown in Figure 198 thru Figure 218. The variable TURB corresponds to 0, 3, and 6 ft/sec rms turbulence in the transition and field vertical landing cases, otherwise, TURB represents sea state. The figure numbers showing control usage data for each task are in the following table:

Task	Pitch	Roll	Yaw
VMC Decelerating Transition	198	199	200
VMC Hover Acquisition	201	202	203
IMC Decelerating Transition	209	205	206
IMC Hover Acquisition	207	208	209
Field Vertical Landing	210	211	212
LPH–2 Vertical Landing	213	214	215
DD–963 Vertical Landing	216	217	218

A few general conclusions may be drawn. One is that the pitch and yaw accelerations produced by the controls generally fell within the US/UK Concept Evaluation Model (CEM) requirements of 0.3 and 0.2 rad/sec, but the roll usage was generally higher than the 0.6 rad/sec requirement from the CEM, especially seen in severe turbulence. Also, control requirements generally increased with turbulence level.

Trends between modes can be drawn by looking at the standard deviation of the control power used as a function of control mode. Figure 219 and Figure 220 show the results for pitch, roll and yaw acceleration for the VMC and IMC DT tasks. Pitch, roll, and yaw control usage was less for TRAN–RCAH than for TRAN mode. In the other modes, the control usage was comparable. Figure 221 and Figure 222 show the results for VMC and IMC HA. Again the control power usage for TRAN–RCAH was less than for TRAN mode, with usage in other modes being comparable. Figure 223, Figure 224, and Figure 225 show the results for vertical landings. These results show that the control power utilized in the TRC modes was higher than the other modes, especially apparent on the shipboard tasks.

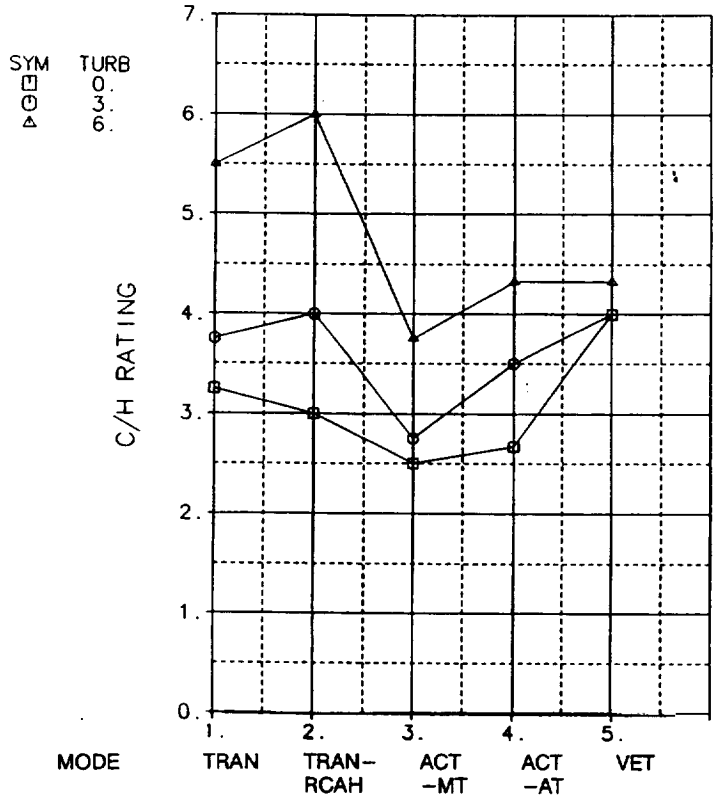

Figure 193. VMC Hover Acquisition

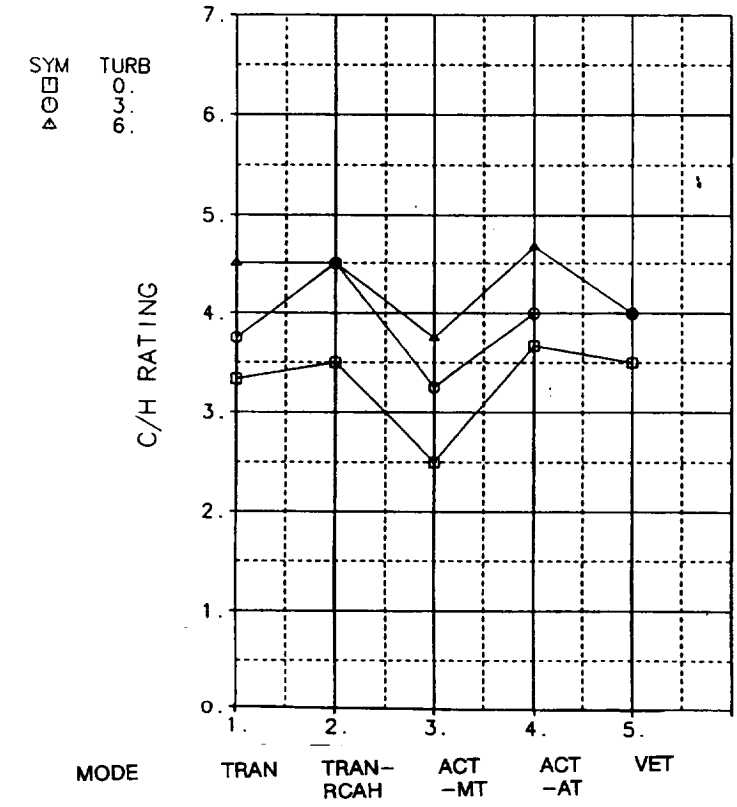

Figure 194. IMC Hover Acquisition

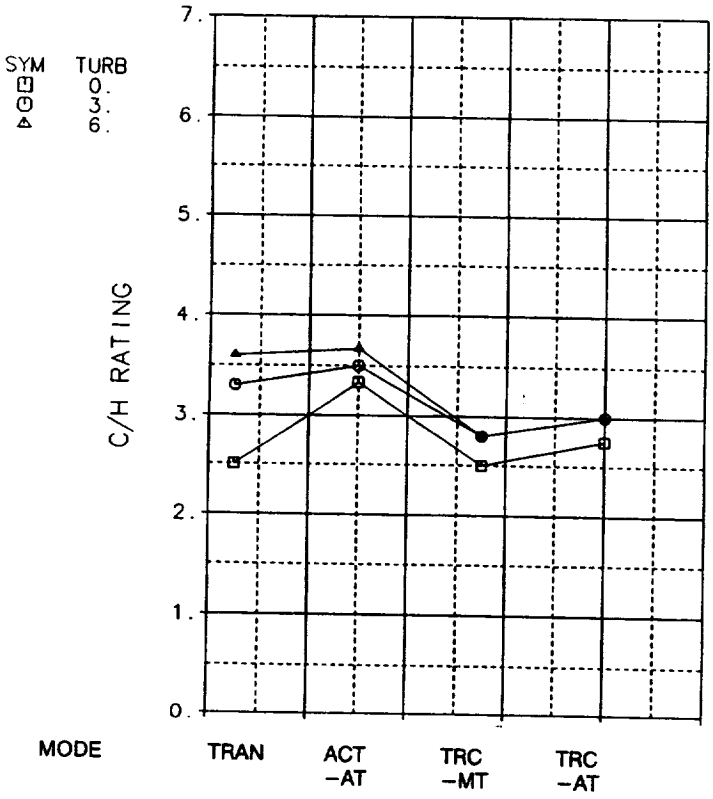

Figure 195. Field Vertical Landing

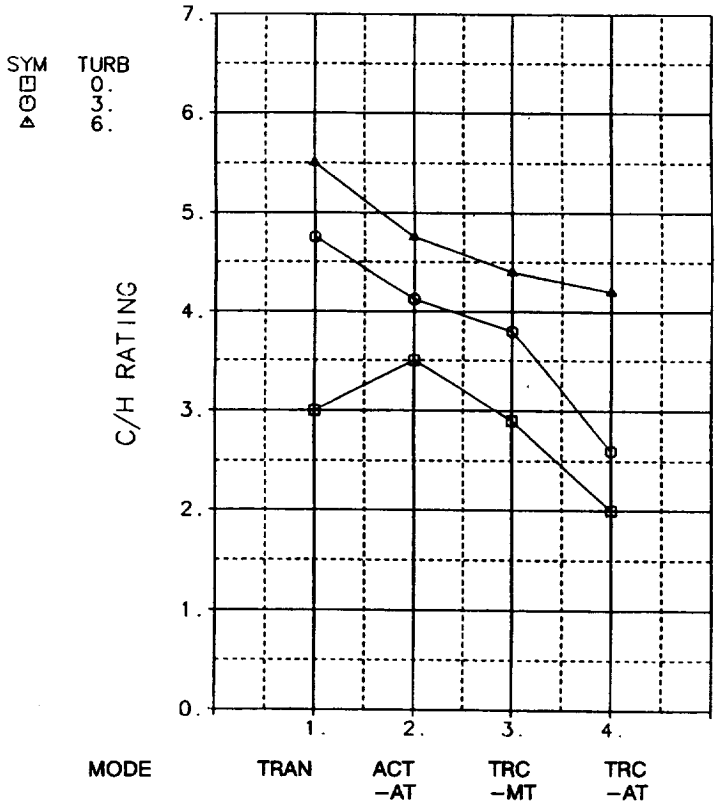

Figure 196. LPH Vertical Landing

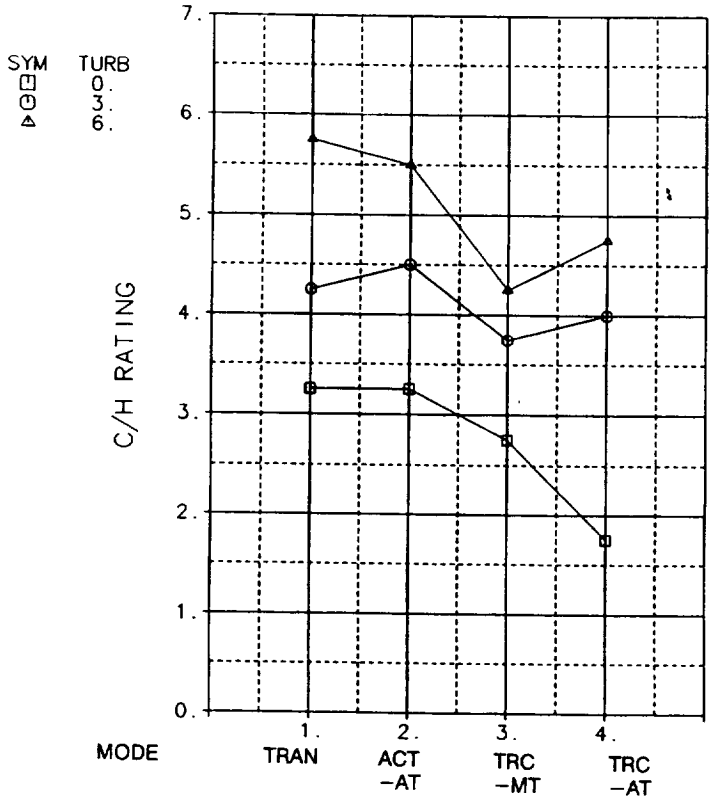

Figure 197. DD-963 Vertical Landing

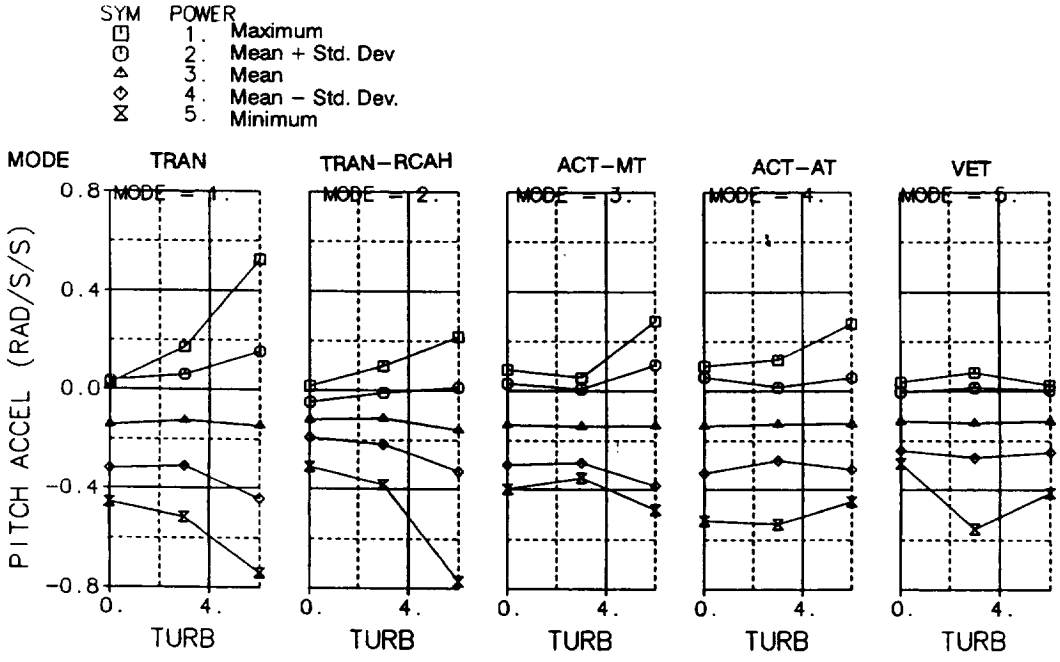

Figure 198. VMC Decelerating Transition

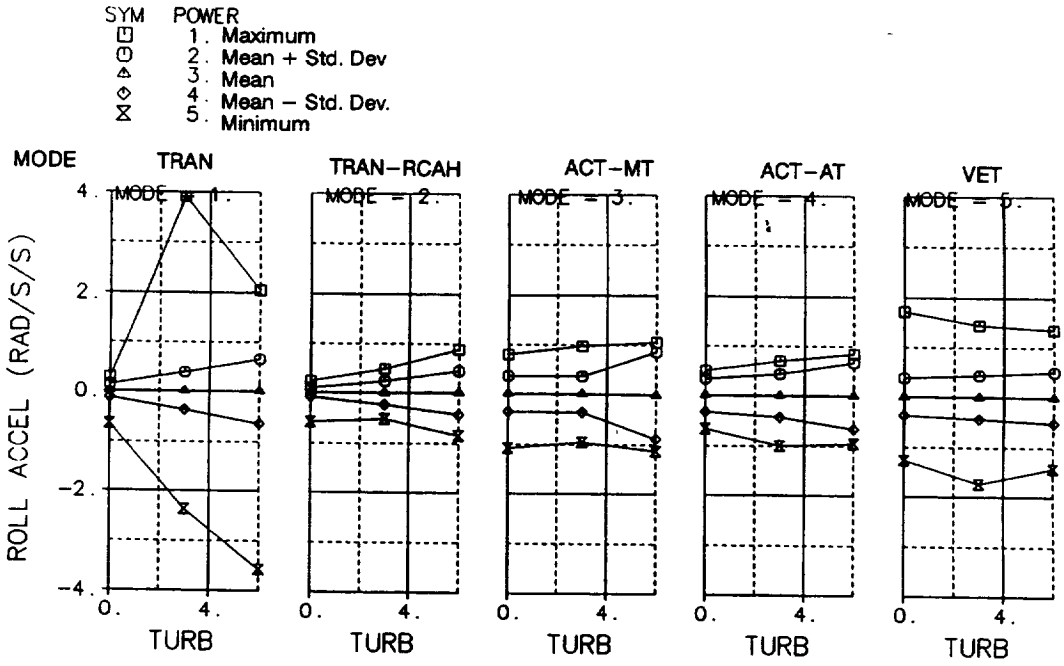

Figure 199. VMC Decelerating Transition

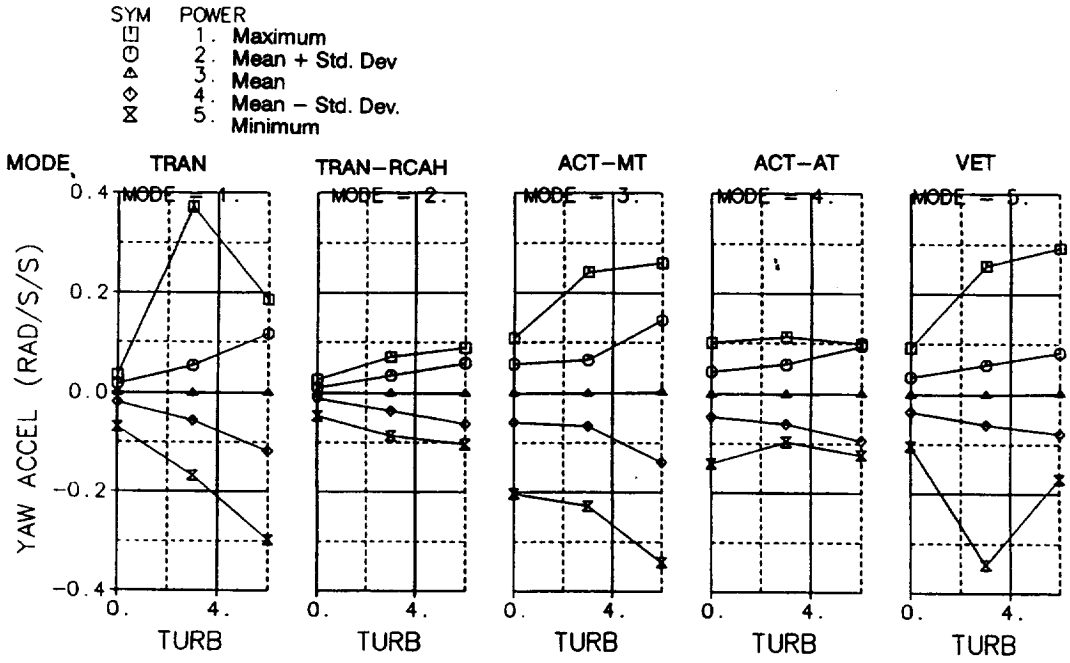

Figure 200. VMC Decelerating Transition

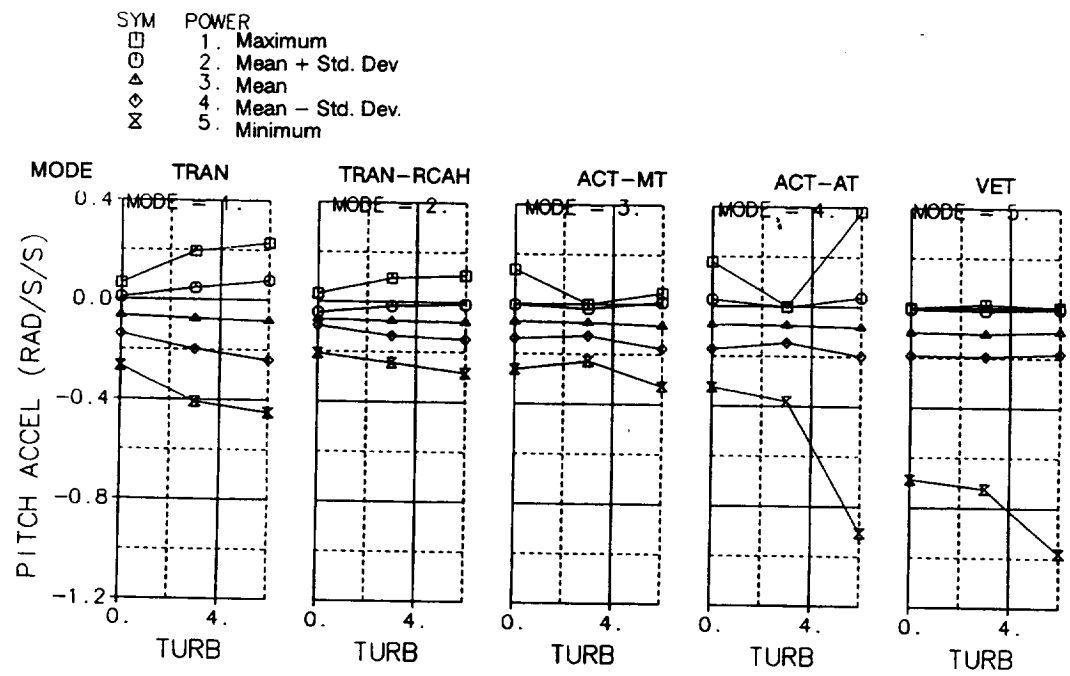

Figure 201. VMC Hover Acquisition

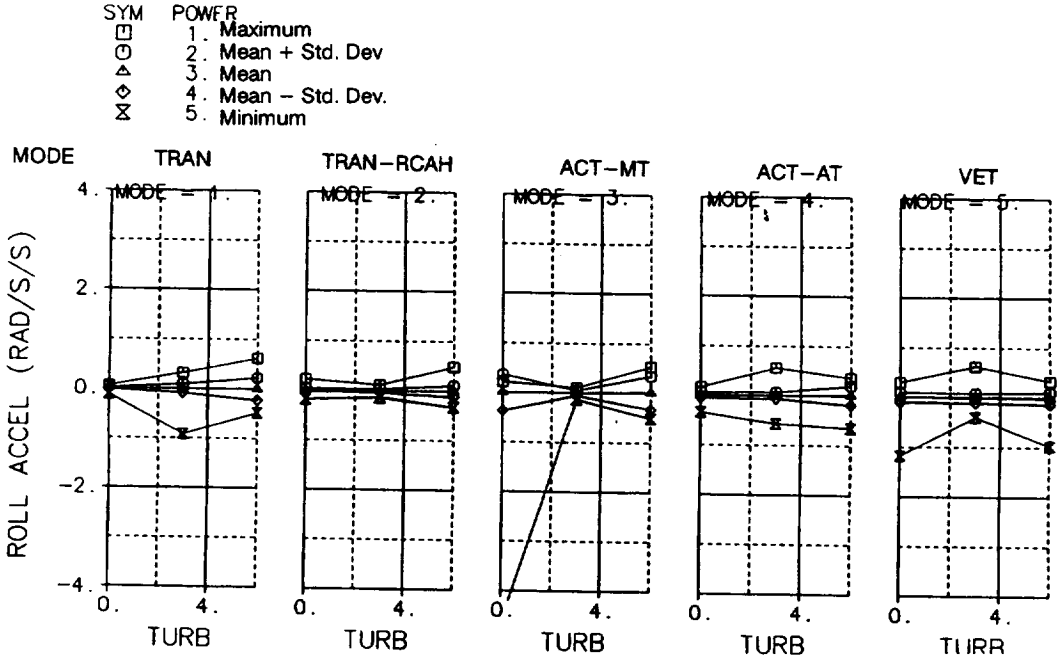

Figure 202. VMC Hover Acquisition

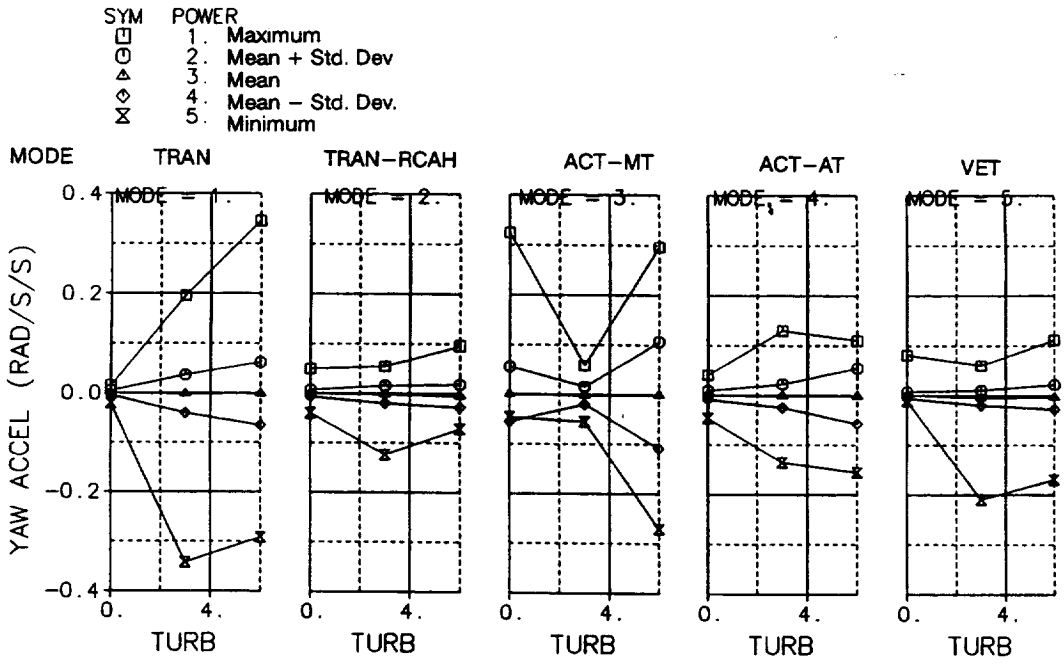

Figure 203. VMC Hover Acquisition

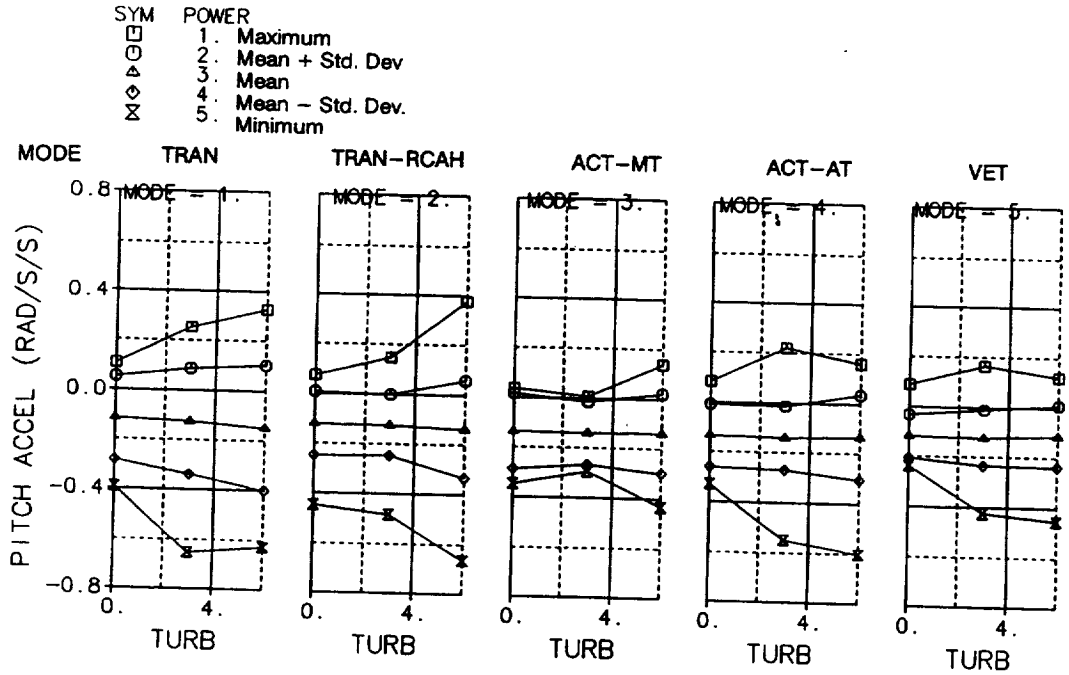

Figure 204. IMC Decelerating Transition

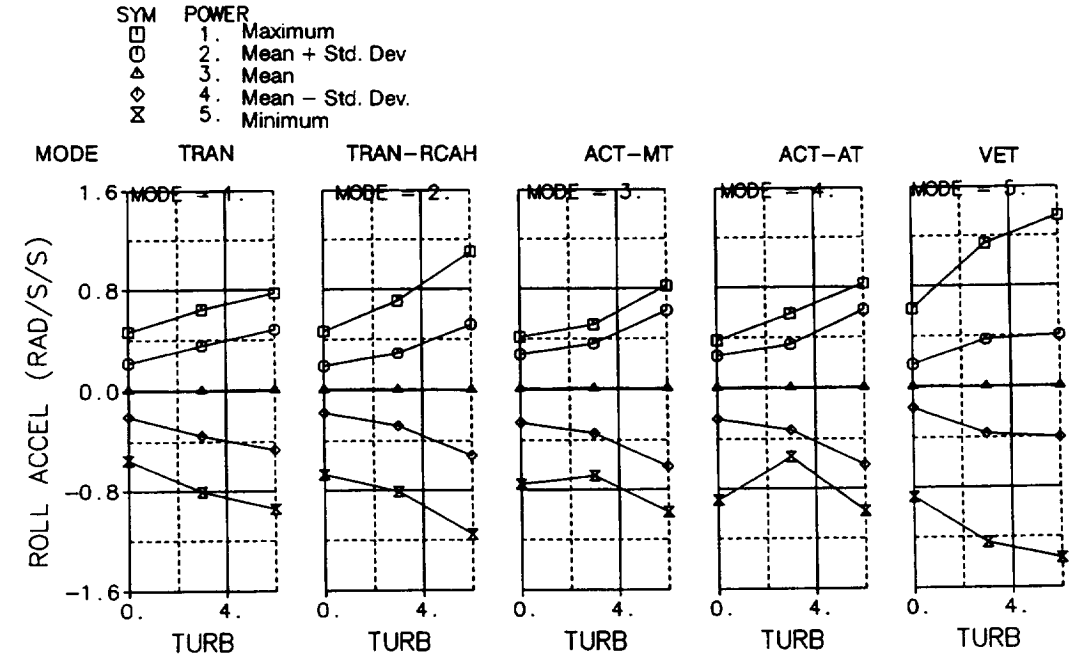

Figure 205. IMC Decelerating Transition

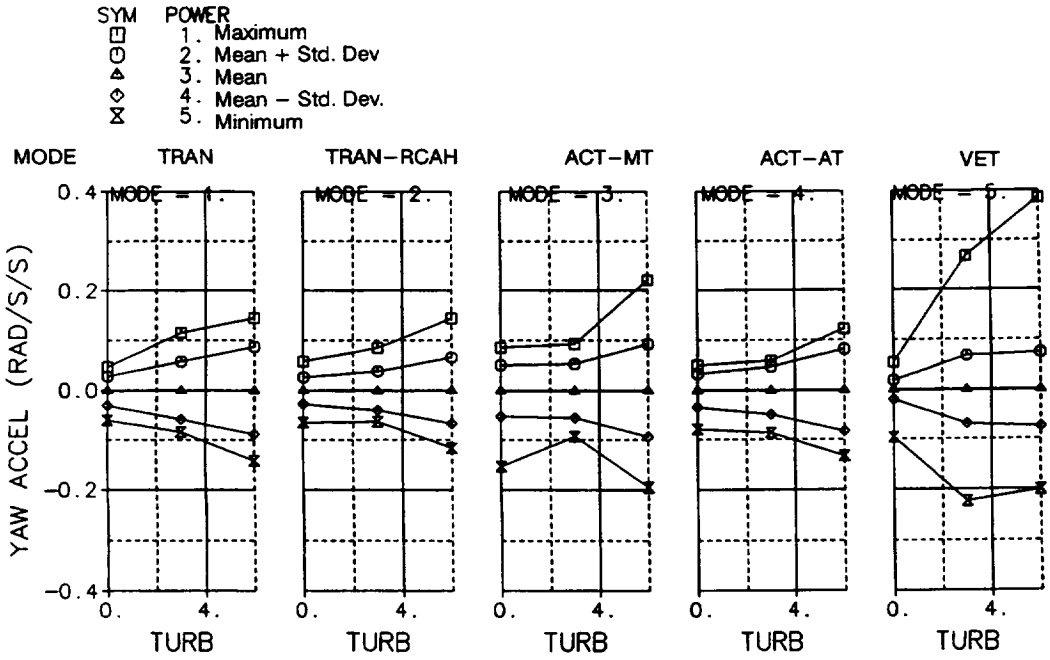

Figure 206. IMC Deceleration Transition

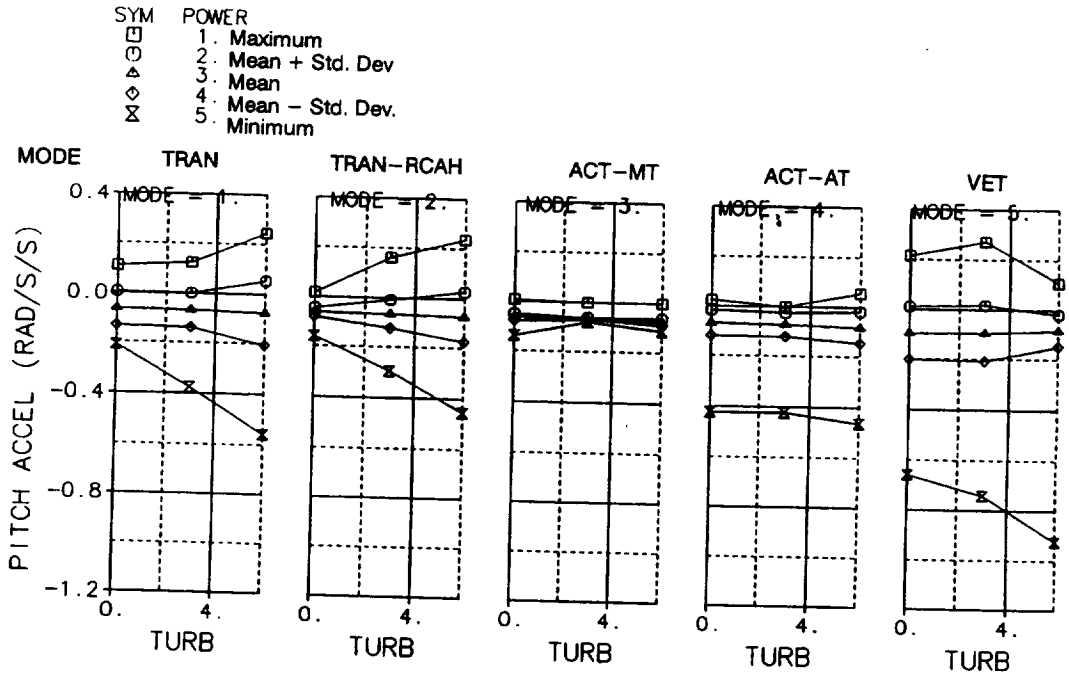

Figure 207. IMC Hover Acquisition

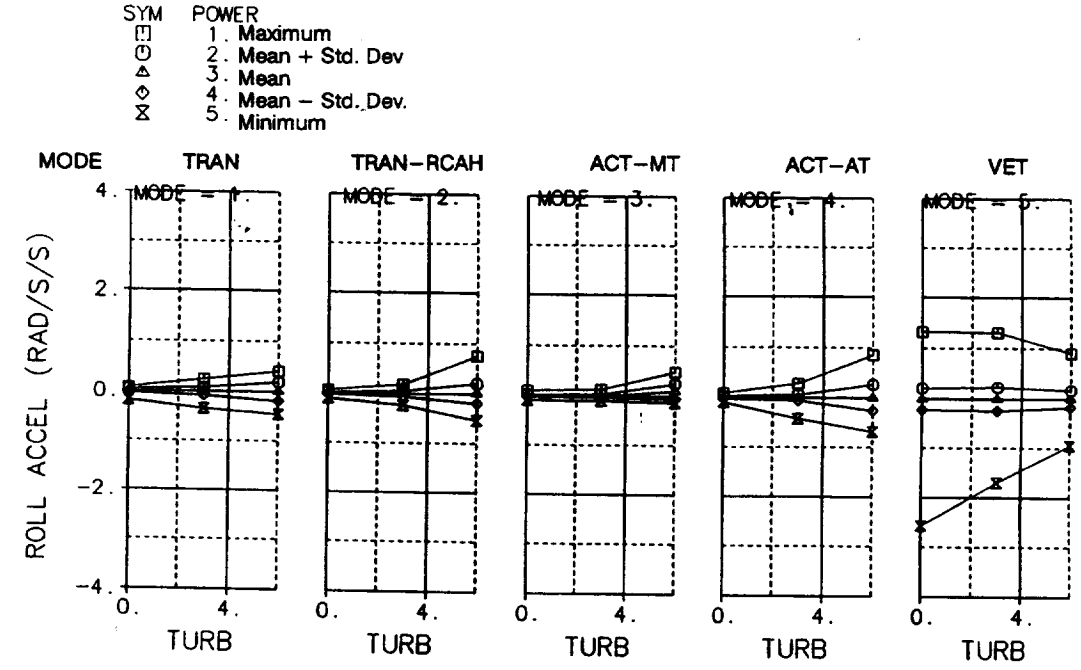

Figure 208. IMC Hover Acquisition

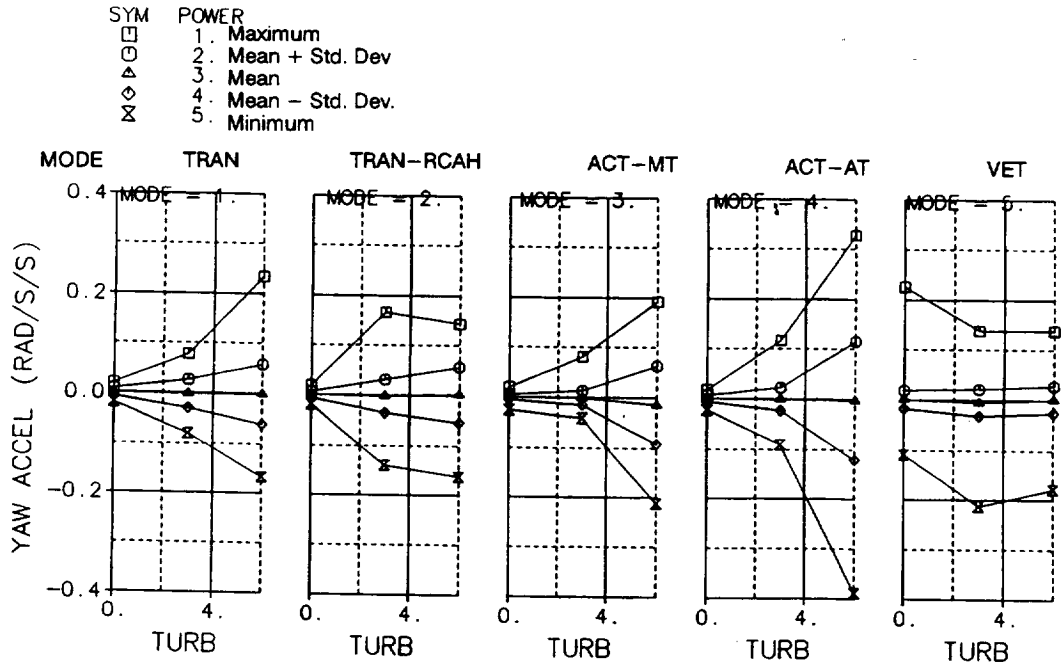

Figure 209. IMC Hover Acquisition

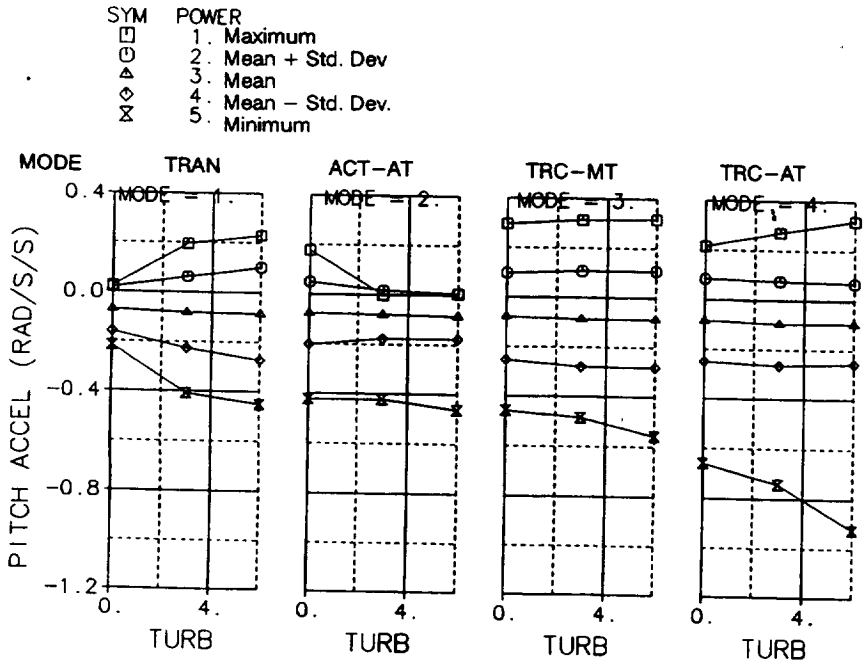

Figure 210. Field Vertical Landing

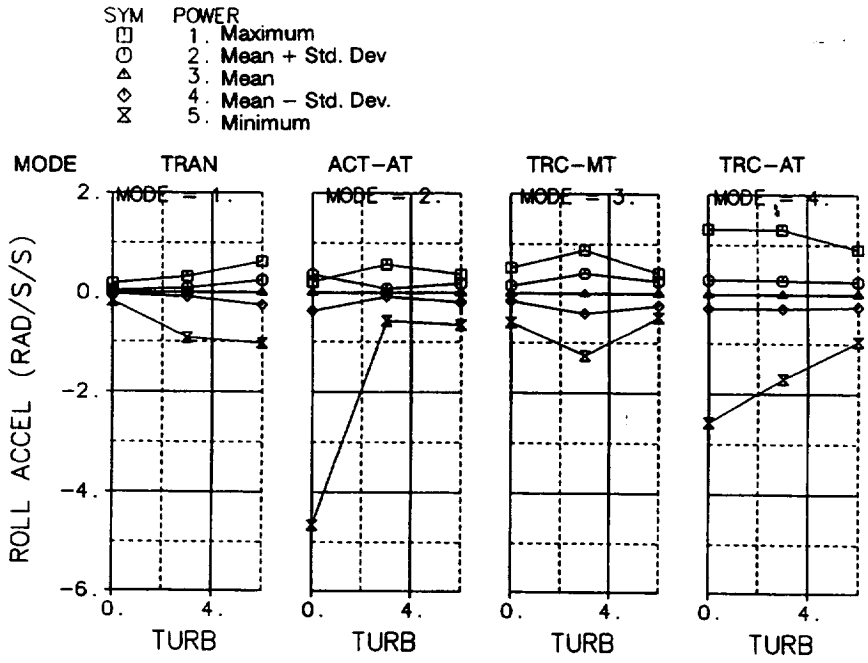

Figure 211. Field Vertical Landing

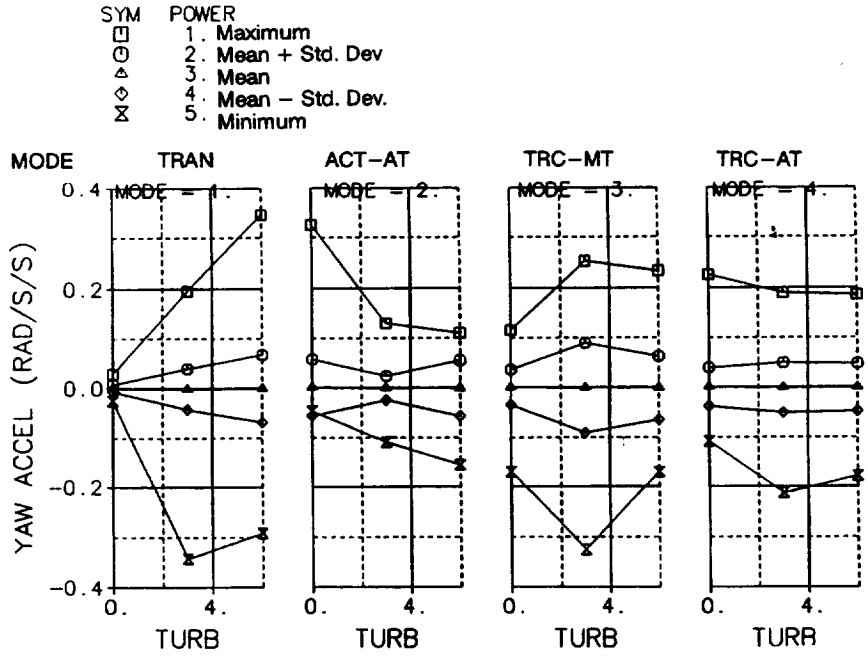

Figure 212. Field Vertical Landing

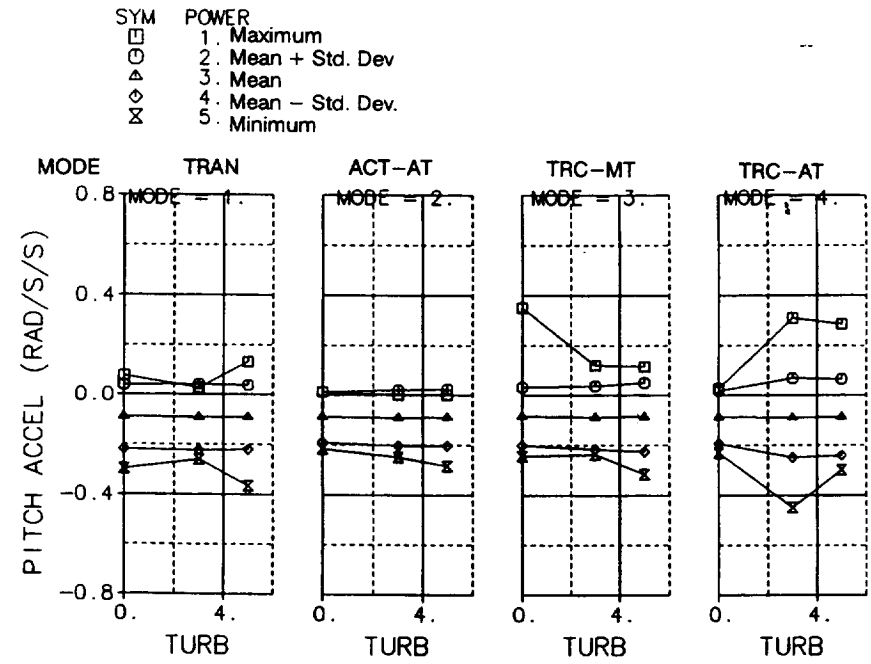

Figure 213. LPH Vertcial Landing

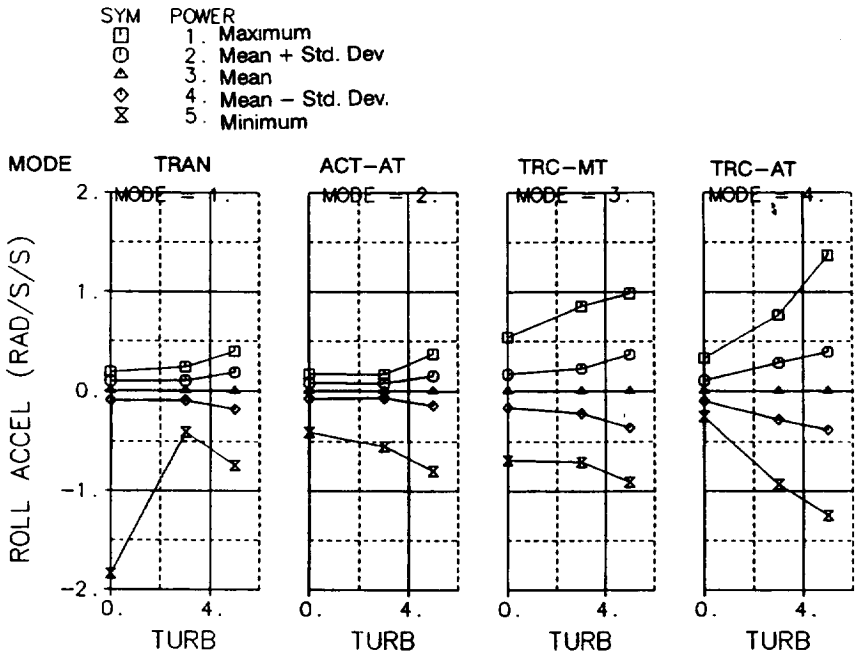

Figure 214. LPH Vertical Landing

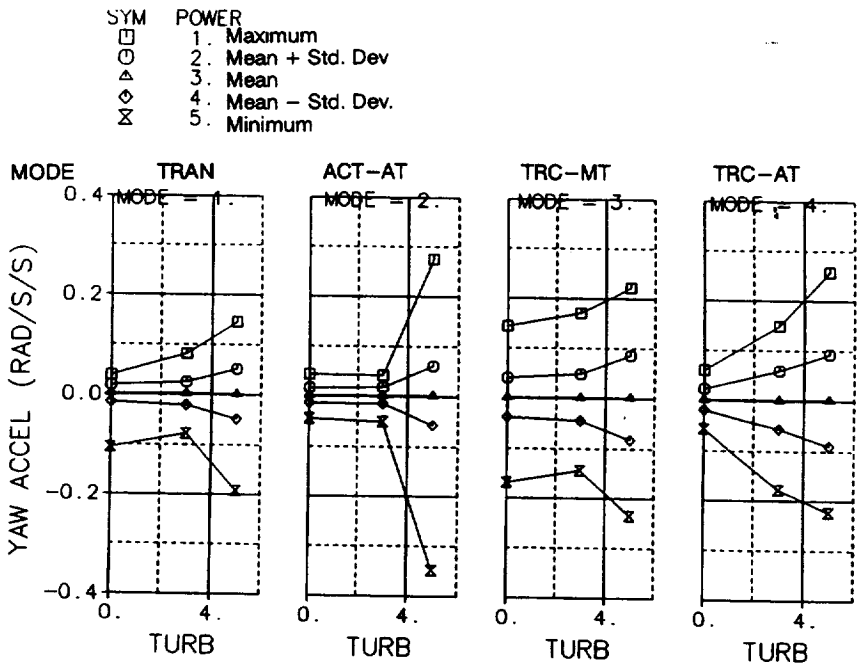

Figure 215. LPH Vertical Landing

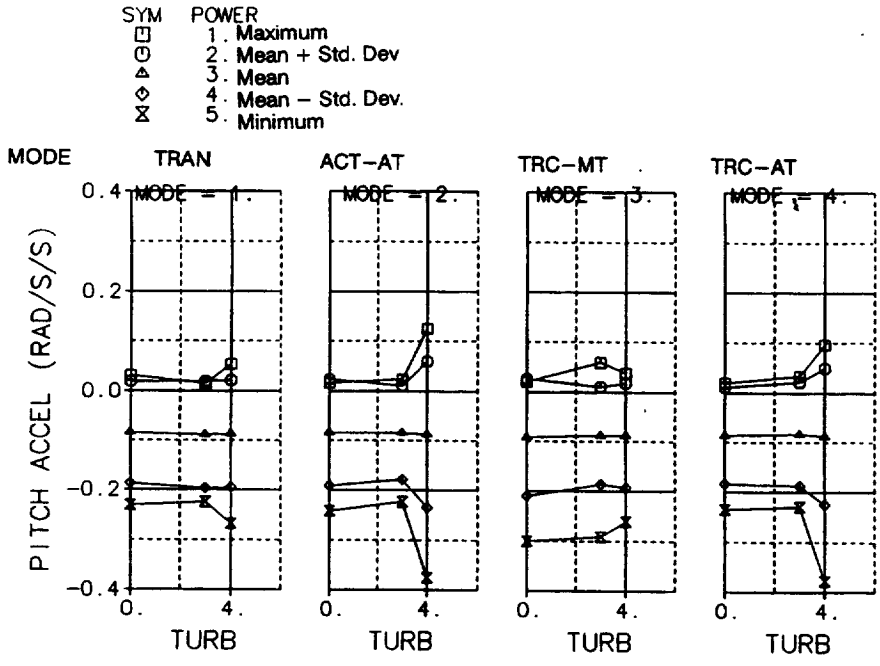

Figure 216. DD−963 Vertical Landing

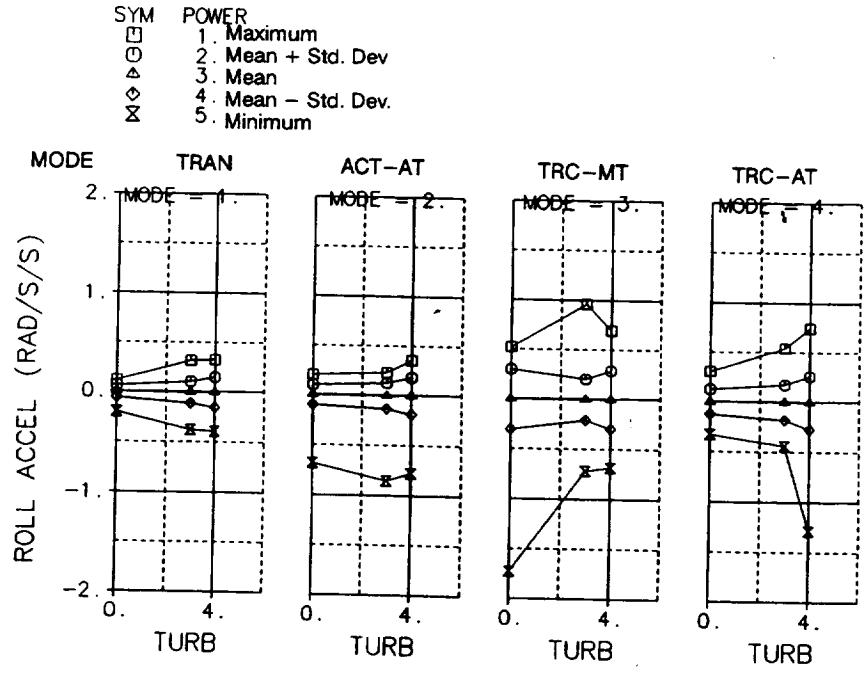

Figure 217. DD–963 Vertical Landing

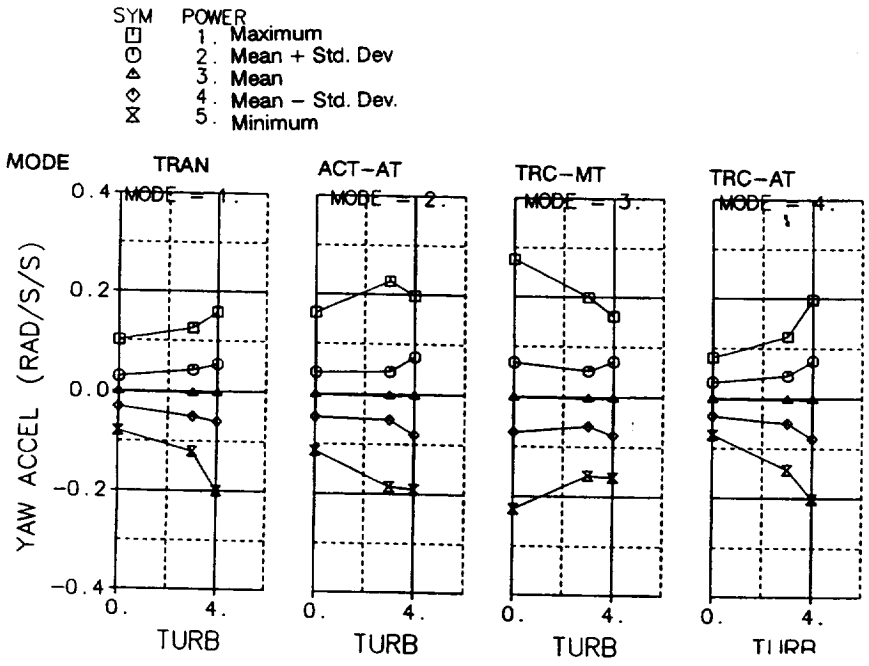

Figure 218. DD–963 Vertical Landing

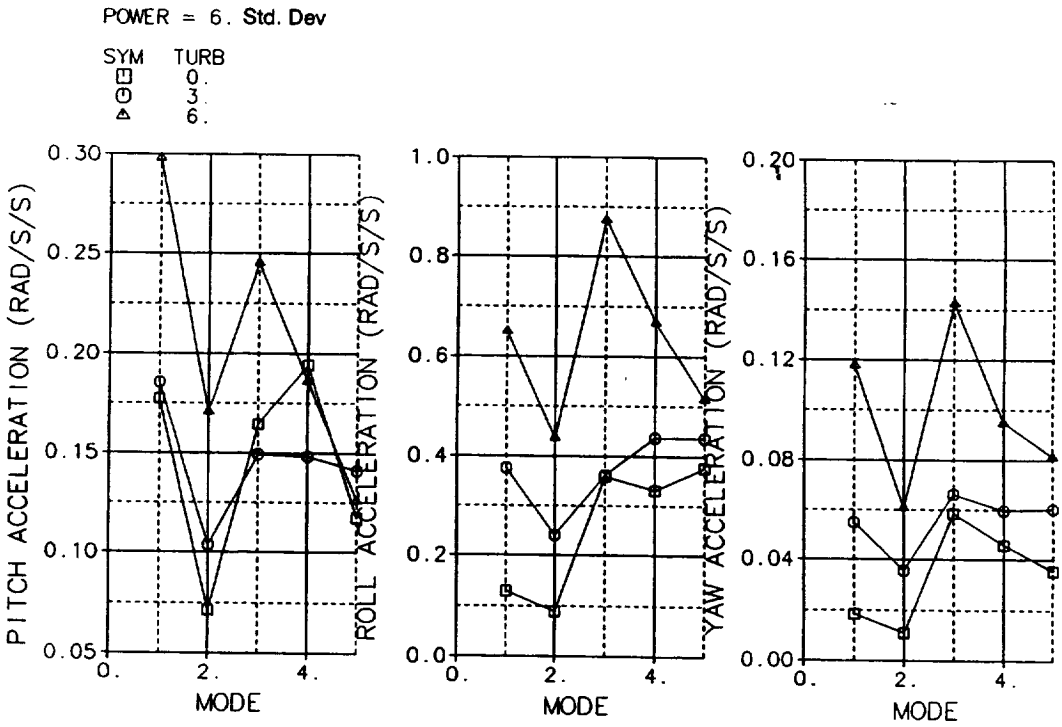

Figure 219. VMC Decelerating Transition

Value	Mod
1	TRAI
2	TRAN–F
3	ACT–I
4	ACT–
5	VET

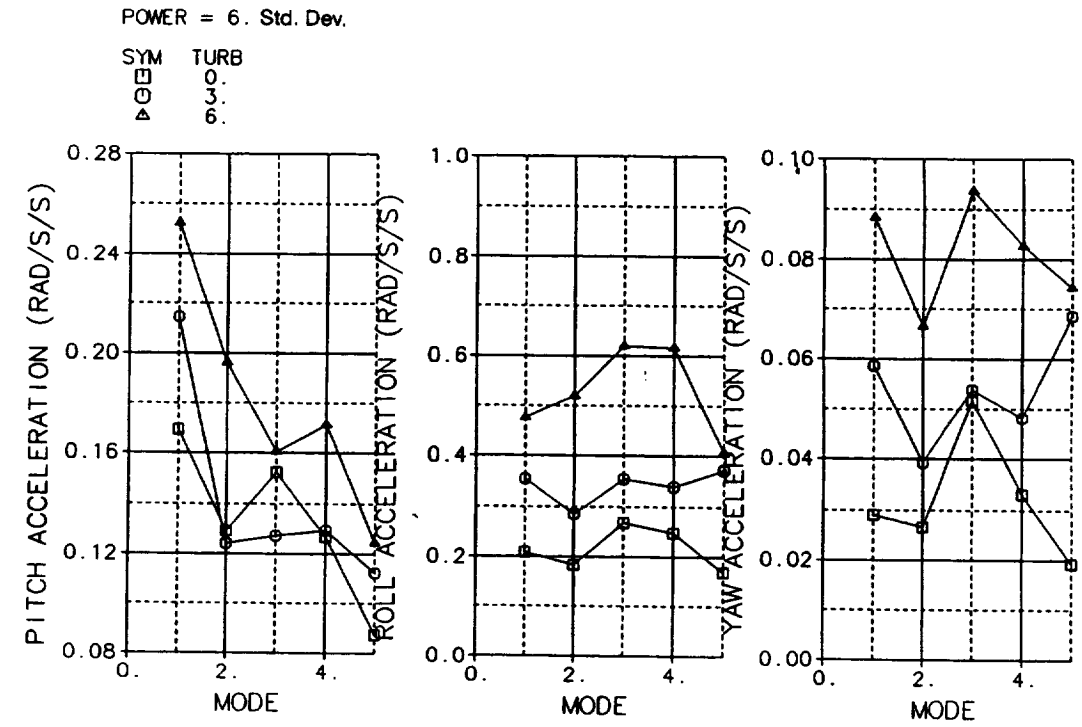

Figure 220. IMC Decelerating Transition

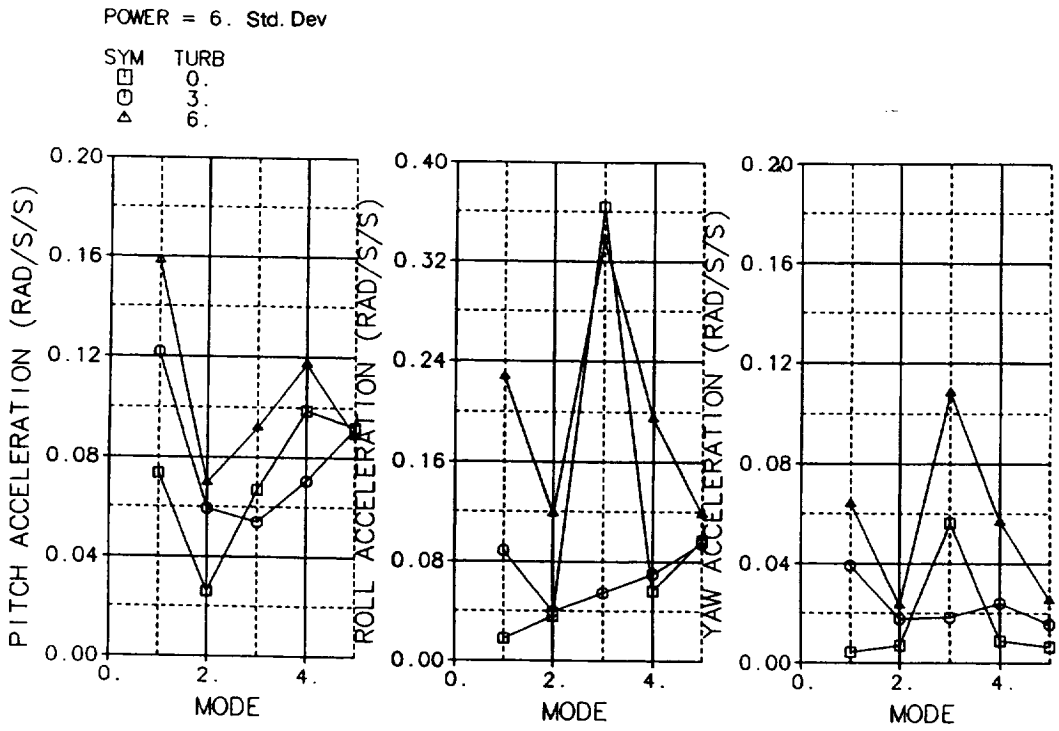

Figure 221. VMC Hover Acquisition

Value	Mode
1	TRAN
2	TRAN–RCAH
3	ACT–MT
4	ACT–AT
5	VET

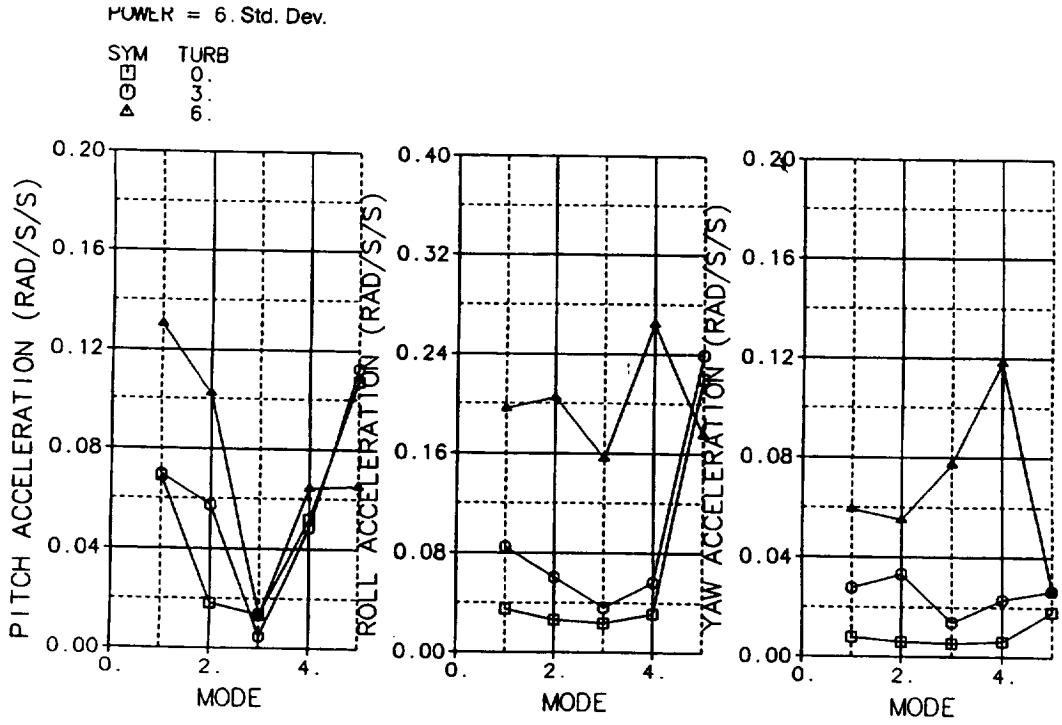

Figure 222. IMC Hover Acquisition

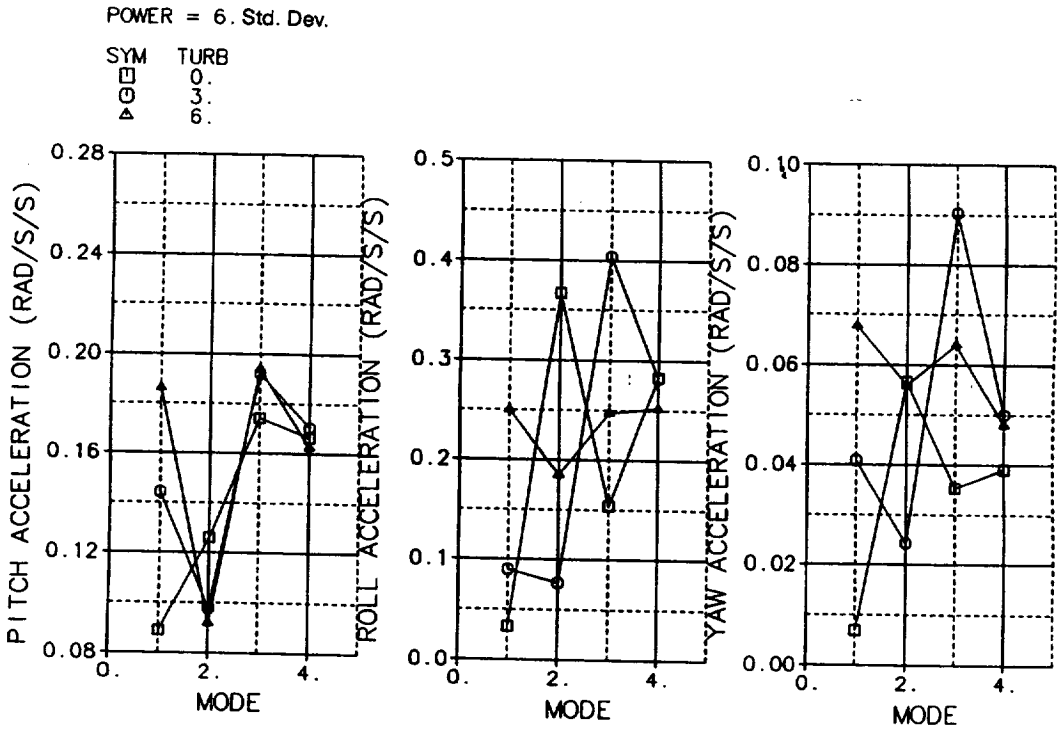

Figure 223. Field Vertical Landing

Value	Mode
1	TRAN
2	ACT–A
3	TRC–A
4	TRC–A

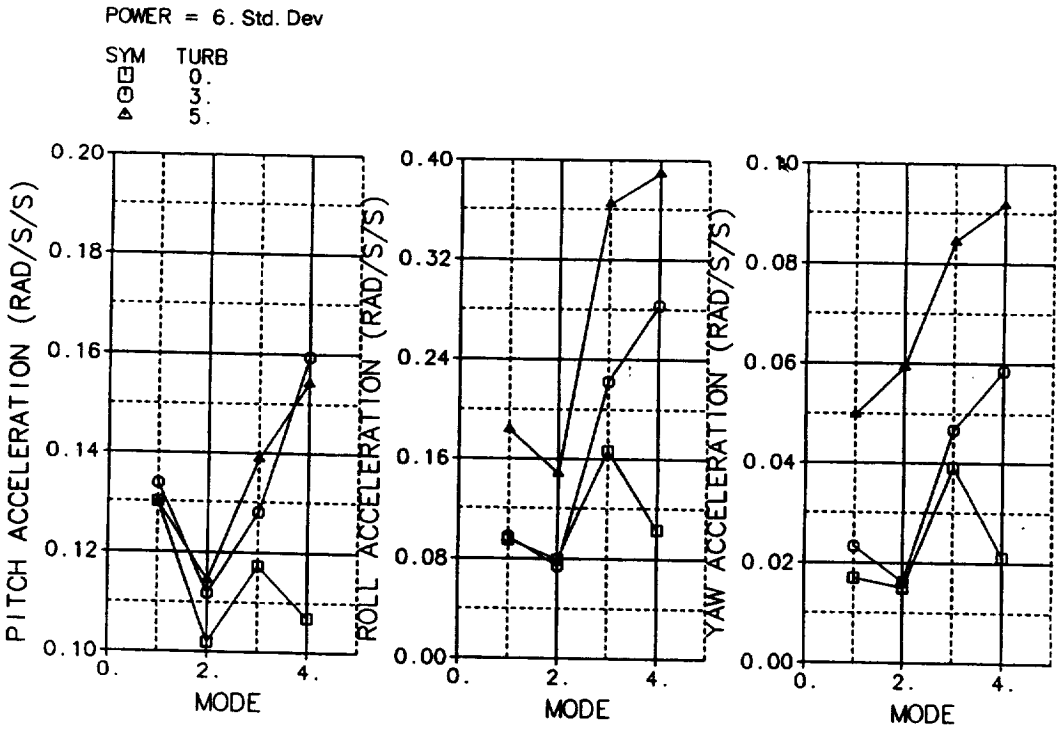

Figure 224. LPH–2 Vertical Landing

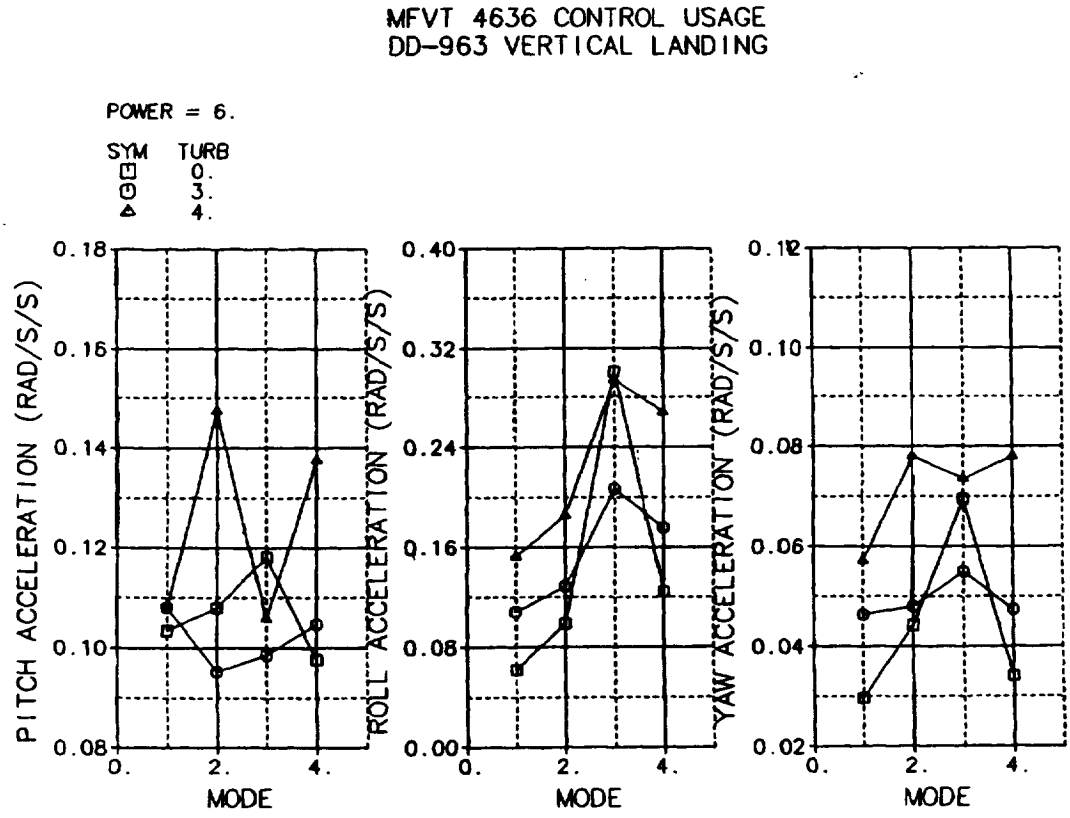

Figure 225. DD−963 Vertical Landing

3.5.4. Propulsion System Test Results

The integrated vehicle and propulsion system underwent five weeks of testing in a real time piloted simulation at NASA Ames. The simulator testing concentrated on the flight control modes with an emphasis on the flight regime of transition from wing borne flight (axial propulsive thrust) to powered lift mode (lift and trim flap nozzle thrust), concluding with vertical landing. In general Pilot comments were very favorable for the fully integrated system. Pilot's comments and suggestions were implemented onsite and flight control modes were retested following the suggested modifications. Analysis of propulsion system data provides insight into how the propulsion will be used for future STOVL applications. For the specific MFVT design, the data can be categorized into two separate areas: engine response and exhaust nozzle system response.

Engine response is defined by the magnitude and frequency of the total thrust request from the flight control. Analysis of the test data verifies the preliminary studies suggesting a 10 radian/second closed loop thrust response was adequate for vehicle control.

It should be noted that the acceleration requirements were not taxed in this flight regime during manual (Pilot controlled) flight. Computer controlled throttle was not a primary concern of the flight control designer and no attempts were made to modify the mode because the manual throttle mode provided adequate vehicle control.

It should also be noted that the flight control design resulted in no RCS bleed use during powered lift mode. Use of RCS bleed would have resulted in more activity in the total thrust control loop.

Figure 226 shows the closed loop frequency response of the thrust request and the thrust. This frequency response was obtained from using a time histories recursive maximum likelihood system identification. Analysis of the spectral content of the total thrust request, Figure 227, indicates that the propulsion system response requirements should be limited to 2 hertz.

Exhaust nozzle response is obtained from analyzing the flight control request for thrust split and nozzle vector angle. As previously stated, during powered lift the exhaust nozzles are flight control surfaces and should respond accordingly. The thrust split is defined as the four percentage thrust requests from the flight control for the spherical convergent flap main nozzle, the left and right nozzles, and the trim flap. The left and right nozzles and the trim flap nozzle, are of primary interest during the transition and attaining hover. Together these exhaust nozzles provide the total thrust, thrust lifting force, pitch, roll and yaw control. The flight control request for total thrust, thrust splits, and nozzle vector angles and the geometric configuration of the propulsion system, were used to calculate equivalent pitch, roll and yaw moment commands. The propulsion system feedbacks for thrust split, nozzle vector angles and the geometric configuration of the engine are used to calculate the pitch, roll and yaw feedbacks from the propulsion system response. The pitch, roll and yaw moment commands and resulting moment command and pitch moments were again analyzed using the maximum likelihood recursive method to provide the frequency response. Figure 228 shows the frequency response of the pitch moment command and pitch moment. The roll and yaw moment commands and resulting moments show similar results. The pitch, roll and yaw request and feedback loops generally have a two and one half hertz bandwidth (20 radian/second).

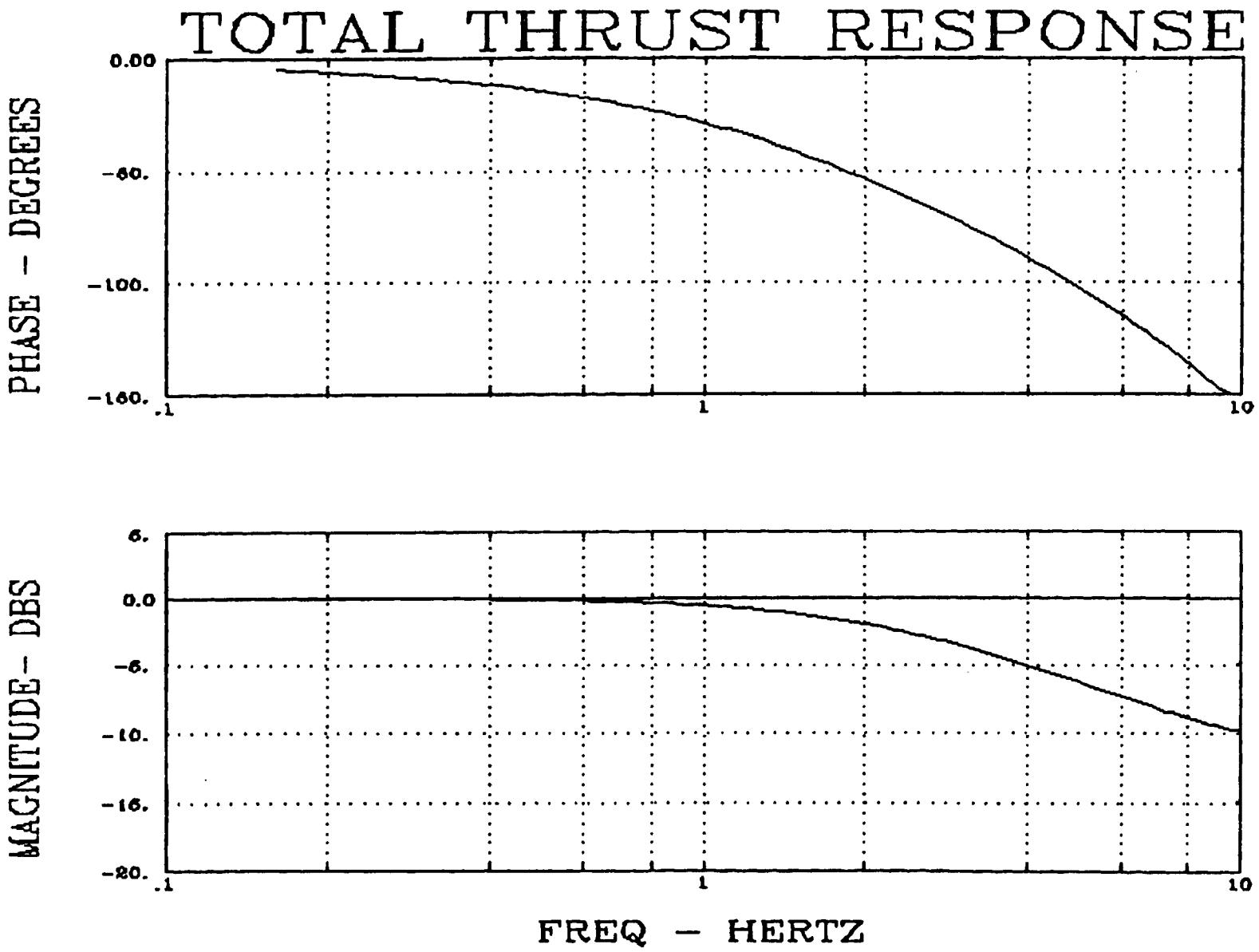

Figure 226. Thrust Frequency Response

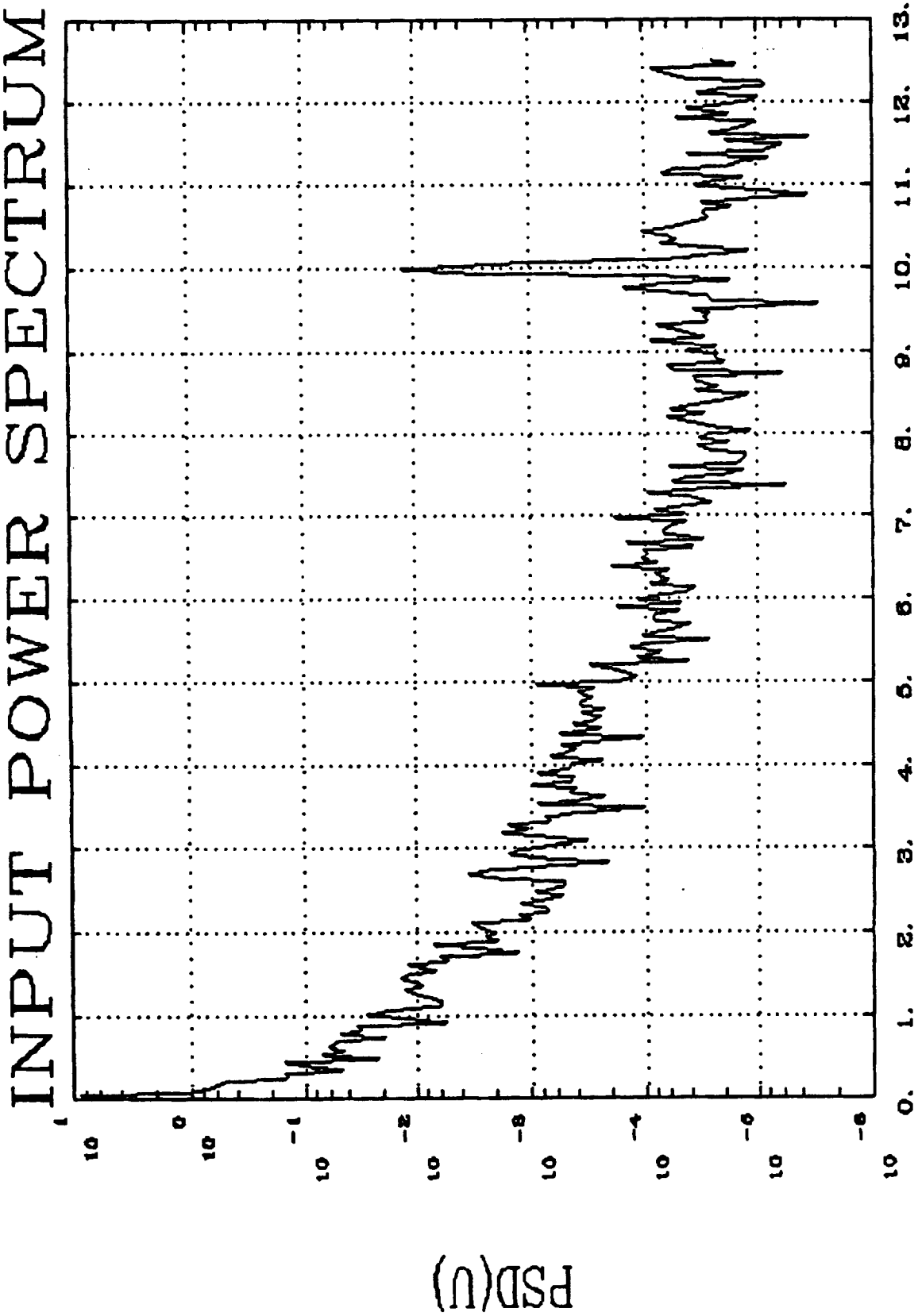

Figure 227. Thrust Request Spectral Content

C-3

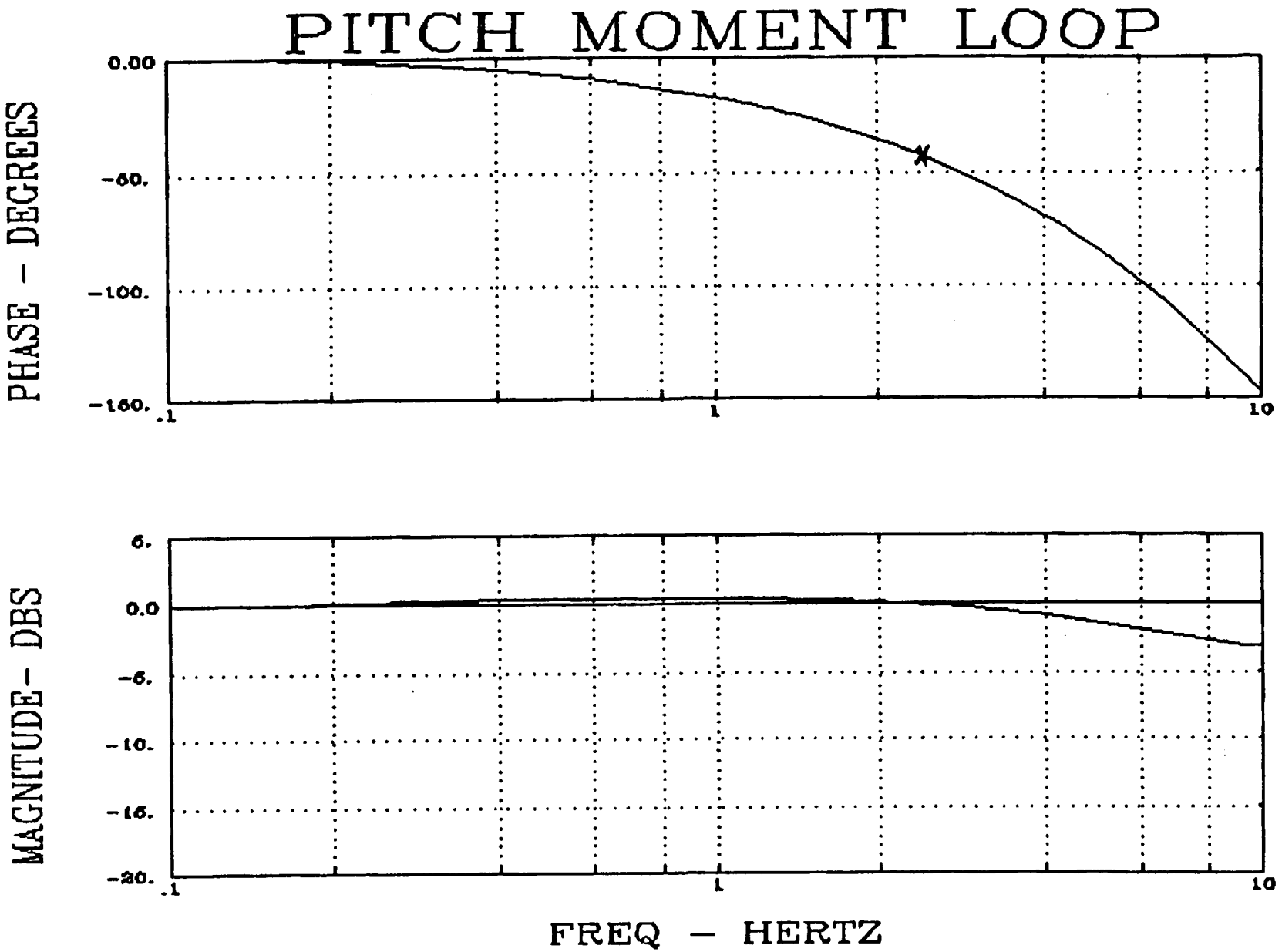

Figure 228. Pitch Moment Frequency Response

The pitch, roll and yaw commands were also reviewed for their content. Figure 229 shows a typical spectral response for the calculated flight control commands. The data indicates that flight control request are bounded at approximately 4 hertz.

The propulsion system requirements specify a 10000. lb/second (100 percent roll control power) thrust modulation for roll control, while the propulsion system was designed to provide 20000.0 lb/second thrust modulation for control to be ± 16500.0 lb/second (165 percent roll control power) and the normal usage was between ± 6000.0 lb/second (60 percent roll control power), both within the propulsion system control design.

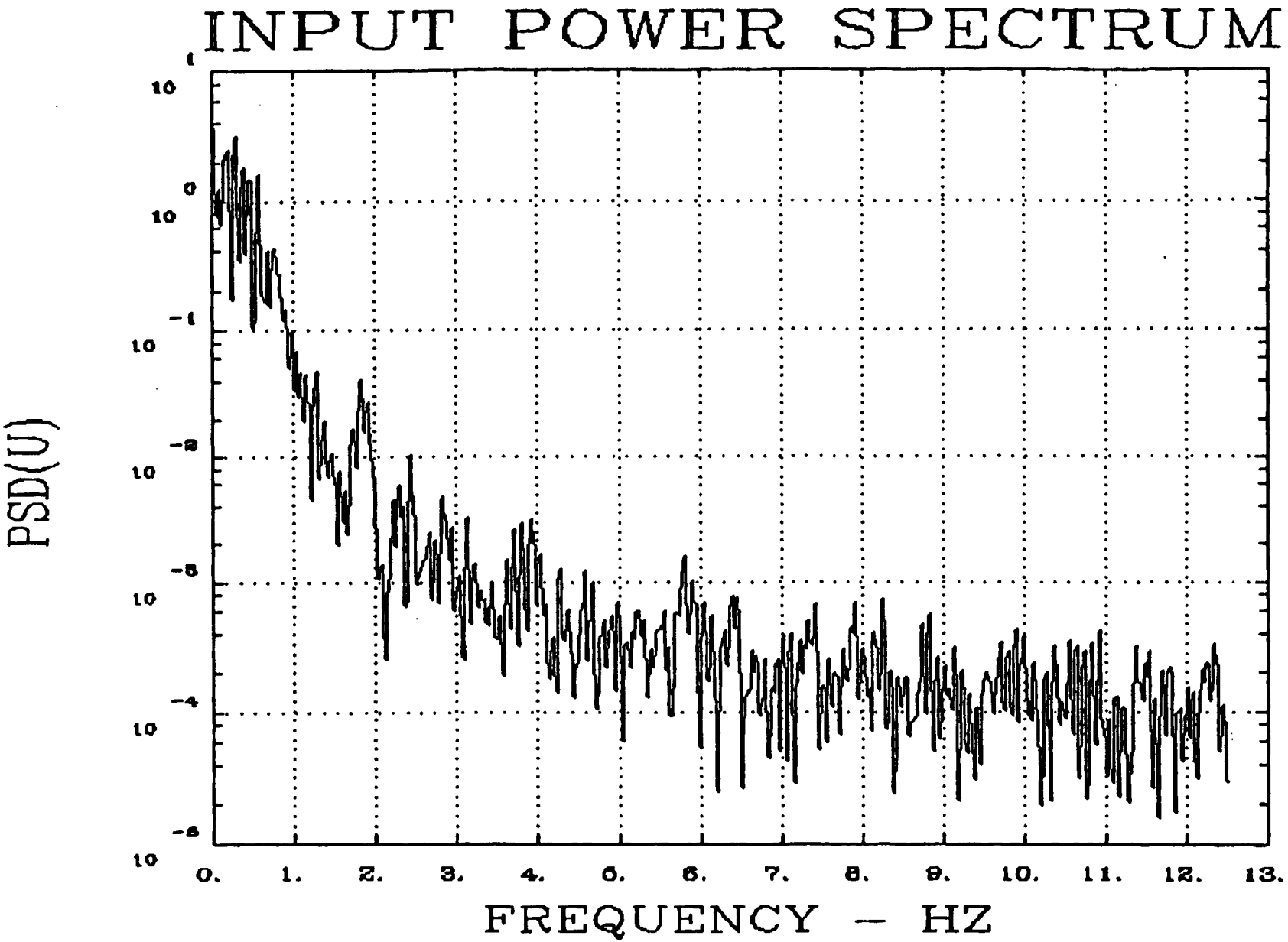

Figure 229. Spectral Content of Calculated Flight Control Commands

4. SUMMARY AND CONCLUSIONS

The STOVL Control Integration Program developed Integrated Flight/Propulsion Control (IFPC) technologies for STOVL aircraft by developing technologies for integrated control systems, and also by developing integrated processes for the design and development of IFPC systems.

We developed methods for partitioning control functions and assigning responsibility for those functions among design teams. The functional partitioning process feeds into the hardware architecture design process, where functions are assigned to different processing centers and actuation systems.

We also developed processes for establishing and continuing tight and frequent communications between design teams. One process was the use of the General Actuator Model (GAM) for communicating propulsion system performance and response requirements. The GAM was also very useful in the preliminary design of the flight control laws early in the design process, allowing early testing of the operation of the propulsion system in closed loop flight control, and allowing changes to the propulsion system requirements via changes to the GAM. This process lowers design risk by helping to prevent costly design fixes later in an aircraft/propulsion system development program. The GAM was also used by the propulsion design team as a design goal model for the propulsion system control law design.

Another process we used to communicate design information was the use of interface control documents to define the interfaces between the various components of the IFPC system. This process is a well established process in IFPC integration, and successfully established a clear understanding of the interfaces to each design team.

We also developed processes for control law design for STOVL applications. The process we used involved a decentralized approach where the propulsion control laws were designed as a separate function under the command of the flight control function. The fight controls were also defined such that the flight controls were very tolerant to differences in true propulsion system response relative to predicted response.

The simulation demonstrated the successful application of this design philosophy for this particular STOVL aircraft. The simulation contained detailed models of the aircraft, the propulsion system, and the IFPC system, and demonstrated good integration of flight control and propulsion control functions for transitioning and hovering powered lift assisted flight. The simulation results showed that total system performance was good with the aerodynamic and propulsive control effectors properly coordinated. The results also showed that the aircraft could be controlled successfully without the reaction controls.

The simulation also demonstrated the benefits of advanced control modes relative to an AV–8B type command and control system. Six pilots evaluated 5 transition modes and 4 hover modes over five weeks of testing, including 717 evaluation flights. The 5 transition modes represented a methodical build–up to higher levels of control augmentation, from an AV–8B type system (with improved handling qualities) up to full authority flight path and speed command systems.

The simulation demonstrated these benefits in the context of both land based and sea based operations aboard both LH class ships and destroyer class ships which are equipped with a helicopter pad. Evaluations included approaches and vertical landings

to a runway and to the ships. Approaches were taken in both VFR and IFR conditions and in levels of wind ranging from 0 to 35 knots, and turbulence ranging from calm air to MIL–STD–8785C severe turbulence. Ship board landings were performed in sea states ranging from calm seas to sea state 5. The evaluations showed that the benefits in improved handling qualities and pilot workload allow operations in more severe conditions than is currently done with the AV–8B.

The SCIP program has provided a firm foundation for integrated control system design processes and technologies for application in future STOVL aircraft programs. The SCIP program developed integrated processes for the design of these IFPC systems, thus lowering risk in design efforts for future programs. The SCIP program also showed the benefits in high control integration for STOVL applications, not only in the cost, weight, risk, and reliability of the control system, but also in the increased ability to provide pilot relief modes, thus allowing safer and more effective aircraft operations in harsh environments.

References

1. McDonnell Aircraft Company, "Airframe Concept Evaluation Study for the US/UK ASTOVL Aircraft Technology Program," NASA CR–177519, Feb. 1989
2. Tillman, K.D., et al., "Design, Development, and Demonstration Plan –PROLIFIC Task 1," WL–TR–91–2114, Jan. 1992
3. Carpenter, C. G., & Hodgkinson, J., "V/STOL Equivalent Systems Analysis," NADC–79141–60, May 1980
4. Carpenter, C. G., "V/STOL Low Speed and Transition Equivalent Systems Analysis," NADC–81104–60, Dec. 1982
5. Carpenter, C. G. "Handling Quality Analysis of Translational Rate Command Systems for Hover and Low Speed Flight through Ground–Based Simulation," MDC Report A7171 Rev. B, Aug 1984
6. Krekeler, G. C., and Ehlers, J. C., "Simulation Studies of Translational Rate Command Control Systems for Hover and Low Speed Flight," MDC Report A9604, Aug. 1986
7. Foster, J. D., et al., "Integrated Control and Display Research for Transition and Vertical Flight on the NASA V/STOL Research Aircraft (VSRA)," NASA TM–100029, 1987
8. Franklin, J. A., et al., "Simulation Evaluation of Transition and Hover Flying Qualities of the E–7A STOVL Aircraft," NASA TM–101015, 1988
9. Franklin, J. A., et al., "Simulation Evaluation of Transition and Hover Flying Qualities of a Mixed–Flow Remote–Lift STOVL Aircraft," NASA TM–102274, Feb. 1990
10. Hoh, R. H., & Ashkenas, I. L., "Development of VTOL Flying Qualities Criteria for Low Speed and Hover," NADC–77052–30, Dec. 1979
11. Radford, R. C., et al., "An Experimental Investigation of VTOL Flying Qualities Requirements for Shipboard Landings," NADC–77318–60, Aug. 1981
12. Miller. D. P., & Vinje, E. W., "Fixed–Base Flight Simulator Studies of VTOL Aircraft Handling Qualities in Hovering and Low Speed Flight," AFFDL–TR–67–152, Jan. 1968
13. Vinje, E. W., & Miller, D. P., "Analytical and Flight Simulator Studies to Develop Design Criteria for VTOL Aircraft Control Systems," AFFDL–TR–68–165, Apr. 1968
14. McCormick, R. L., "VTOL Handling Qualities Criteria Study through Moving–Base Simulation," AFFDL–TR–69–27, Oct. 1969
15. "Military Specification – Flying Qualities of Piloted V/STOL Aircraft," MIL–F–83300, Dec. 1970
16. Chalk, C. R., et al., "Background Information and User Guide for MIL–F–83300 – Military Specification – Flying Qualities for V/STOL Aircraft," AFFDL–TR–70–88, Nov. 1971
17. Hoh, R. H., & Mitchell, D. G., "Proposed Revisions to MIL–F–83300 V/STOL Flying Qualities Specification," NADC–82146–60, Jan 1986

18. "V/STOL Handling," AGARD Report No. 577, Dec. 1970

19. Merrick, V. K., & Farris, G. G., "A Head–Up–Display Format for Application to V/STOL Approach and Landing," NASA TM–102216, 1990

20. "Design Methods for Integrated Control Systems," AFWAL–TR–88–2061, Jun. 1988

21. McDowell, P. H., "Control Logic and Simulation Delivery and Piloted Simulation Support for a STOVL Aircraft (SCIP 3)," Aug. 1992

22. Thomas, R. W., "Analysis of Aircraft Stability and Control Design Methods," AFWAL–TR–84–3038, May 1984

23. Bland, M., et al., "Alternative Guidelines for Pitch Tracking," AIAA 87–2289, Aug. 1987

24. Cooper, G. E., & Harper, R. P. Jr., "The Use of Pilot Rating in the Evaluation of Aircraft Handling Qualities," NASA TN D–5153, Apr. 1969

REPORT DOCUMENTATION PAGE

Form Approved
OMB No. 0704-0188

1. AGENCY USE ONLY (*Leave blank*)	2. REPORT DATE	3. REPORT TYPE AND DATES COVERED
	July 1994	Final Contractor Report

4. TITLE AND SUBTITLE

STOVL Control Integration Program

5. FUNDING NUMBERS

WU–505–68–32
C–NAS3–25194

6. AUTHOR(S)

C. Weiss, P. McDowell, and S. Watts

7. PERFORMING ORGANIZATION NAME(S) AND ADDRESS(ES)

Pratt & Whitney
P.O. Box 109600
West Palm Beach, Florida 33410–9600

8. PERFORMING ORGANIZATION REPORT NUMBER

E–9023

9. SPONSORING/MONITORING AGENCY NAME(S) AND ADDRESS(ES)

National Aeronautics and Space Administration
Lewis Research Center
Cleveland, Ohio 44135–3191

10. SPONSORING/MONITORING AGENCY REPORT NUMBER

NASA CR–195358

11. SUPPLEMENTARY NOTES

C. Weiss and S. Watts, Pratt & Whitney, P.O. Box 109600, West Palm Beach, Florida 33410–9600; P. McDowell, McDonnell Douglas Aerospace East, St. Louis, Missouri. Project Manager, Sanjay Garg, Instrumentation and Control Technology Division, NASA Lewis Research Center, organization code 2550, (216) 433–2355.

12a. DISTRIBUTION/AVAILABILITY STATEMENT

Unclassified - Unlimited
Subject Categories 63, 08 and 07

12b. DISTRIBUTION CODE

13. ABSTRACT ***(Maximum 200 words)***

An integrated flight/propulsion control for an advanced vector thrust supersonic STOVL aircraft, was developed by Pratt & Whitney and McDonnell Douglas Aerospace East. The IFPC design was based upon the partitioning of the global requirements into flight control and propulsion control requirements. To validate the design, aircraft and engine models were also developed for use on a NASA Ames piloted simulator. Different flight control implementations, evaluated for their handling qualities, are documented in the report along with the propulsion control, engine model and aircraft model.

14. SUBJECT TERMS

STOVL; IFPC; ASTOVL; Piloted simulation; Propulsion control; Flight control; Vectored thrust; Control partitioning

15. NUMBER OF PAGES

202

16. PRICE CODE

A10

17. SECURITY CLASSIFICATION OF REPORT	18. SECURITY CLASSIFICATION OF THIS PAGE	19. SECURITY CLASSIFICATION OF ABSTRACT	20. LIMITATION OF ABSTRACT
Unclassified	Unclassified	Unclassified	